Inaugural dissertation

for

obtaining the doctoral degree

of the

Combined Faculty of Mathematics, Engineering and Natural Sciences

of the

Ruprecht - Karls - University

Heidelberg

Presented by

M.Sc. Alaa Abdelghani Mohamed Madi

born in: Al-Madinah Al-Munawarah, Saudi Arabia

Oral examination: January 17th, 2023

Development and homeostasis of memory CD8+ T cells and implications for cancer immunotherapy

Referees

Prof. Dr. Ralf Bartenschlager

Dr. Guoliang Cui

“And [He] has taught you that which you did not know. And ever has the favour of Allah upon you been great”

The Qur’an, 4:113

Acknowledgements

The brain, unlike the immune system, is actively trying to erase memories[1]. There are some moments in my PhD journey that I really would not mind forgetting. However, at the end of it all, I find myself overwhelmed with gratitude.

I want to thank my supervisor, Dr. Guoliang Cui. I clearly remember the first time I listened to one of his talks. After almost six years, I am still in awe (and a little bit envious) of his intelligence and drive. I am truly grateful for his support, patience, and trust. I know it is ambitious, but I really want to be like him when I 'grow up'.

I additionally would like to thank my thesis advisory committee members, Prof. Dr. Ralf Bartenschlager and Prof. Dr. Alexander Dalpke, for their invaluable advice and constructive input throughout the course of my PhD work. I am also grateful to Prof. Dr. Nina Papavasiliou for her participation in my examination committee.

My sincere thanks go to previous and current members of the T cell metabolism lab, Dr. Jingxia Wu, Dr. Sicong Ma, Dr. Nina Weisshaar, Dr. Yanan Ming, (soon-to-be) Dr. Alessa Mieg, Ferdinand Zettl, and Nora ten Bosch. It has been an exciting journey and I have learned so much from all of them. I especially want to thank Marvin Hering for the stimulating discussions and Kerstin Mohr for saving my life on countless occasions.

To my dear friend Menattallah Elserafy: thank you for believing in me and for always motivating me to just keep pushing. That I started a PhD at all is partially the fault of Reham Ramadan, Youssef George, and Sara Osman. Yours has been the purest of friendships and I forgive you for putting me on this path.

I also want to thank the mice I directly and indirectly used during my work. None of this would have been possible without your ultimate sacrifice.

And last, my biggest thanks go to my family.

إلى أعز الناس و أقربهم إلى قلبي إلى أمي الغالية و أبي العزيز اللذين كانا و لا زالا عونًا و سندًا لي: تعجز الكلمات عن التعبير عن شكري و امتناني لكما و عرفاني بالجميل، جزاكما الله عني خير الجزاء و لا حرمني دعائكما. إلي إخوتي رانيا و محمد و أحمد: كنتم لي محبةً لا تنضب و دعمًا مستمرًا و مصدرًا للزن المتواصل و خير صحبة. إلى كريم صانع البهجة الحقيقي: آسفة لمصيرك الزملكاوي.

و قبل كل شيء و بعد كل شيئ: الحمد لله الذي بنعمته تتم الصالحات.

[1] L. Gravitz, *Nature* **571**, S12–S12 (2019)

Abstract

The defining feature of the adaptive immune system is the development of long-lived memory cells that are able to respond more vigorously upon recurrent pathogen encounters. Based on their recirculation potential, memory CD8+ T cells are categorised into central memory T (TCM), effector memory T (TEM), and resident memory T (TRM) cells. Compared to effector CD8+ T cells, TCM cells are more adept at controlling tumour growth when used for adoptive T cell therapy (ACT). However, transferred memory cells eventually develop functional exhaustion, and durable responses to ACT are observed in, at best, 50% of patients with solid malignancies.

Here, I show that elevated CD8 levels in TCM cells could be harnessed to improve the antitumour function of adoptively transferred, memory-like CD8+ T cells in a mouse melanoma model. CD8α ligation with an agonistic antibody activated proximal TCR signalling and induced a hybrid effector/memory differentiation state. CD8-ligated cells displayed enhanced proliferation, cytotoxicity, and glycolysis without compromising memory cell-like persistence and oxidative phosphorylation. Effector cytokine production in CD8-ligated cells was dependent on rewired glucose and glutamine metabolism. Expansion of memory-like CD8+ T cells in presence of this agonistic antibody significantly enhanced their tumoricidal function *in vivo*. Furthermore, agonistic CD8 Fab′ partially rescued T cell dysfunction, induced the proliferation of progenitor exhausted T cells, and significantly reduced tumour burden. These findings establish CD8 as an immunotherapeutic target that does not require prior knowledge of the patients' TCR repertoire.

Interleukin (IL) 15 is required for survival and homeostatic turnover of all memory CD8+ T cell subsets, but its cellular source remains undefined. Using a mouse model of acute infection with lymphocytic choriomeningitis virus (LCMV), I demonstrate that in spite of IL-15 being widely expressed, different memory T cell subsets rely on distinct IL-15 sources for maintenance. Terminal TEM (tTEM) cells in particular are significantly depleted in mice with CD4+ regulatory T (Treg) cell-specific *Il15* deletion. These results show that Treg cells play a direct role in supporting the diversity of the memory immune response.

Finally, I provide preliminary evidence that signal transducer and activator of transcription (Stat) 6 activation downstream of IL-4 signalling controls the infiltration of circulating T cells into non-lymphoid tissues and their subsequent development into TRM cells. Using

mouse models of infection with LCMV and influenza, I show that CD8+ T cell-intrinsic Stat6 signalling induces the migration of T cells into liver and lung, respectively, possibly by modulating the expression of the chemokine receptor C-X-C Motif Chemokine Receptor 6 (CXCR6).

Together, the data presented here explore different aspects of all memory T cell subsets and provide insights into the development of TRM cells, the homeostatic requirements of TEM cells, and the transferability of TCM biology to the field of tumour immunotherapy.

Zusammenfassung

Das entscheidende Merkmal des adaptiven Immunsystems ist die Entwicklung von langlebigen Gedächtniszellen, die bei erneuten Begegnungen mit Krankheitserregern energischer reagieren können. CD8+ Gedächtnis-T-Zellen können, basierend auf ihrer Fähigkeit wieder zu zirkulieren, in zentrale T-Gedächtniszellen (TCM), Effektor-T-Gedächtniszellen (TEM) und residierende T-Gedächtniszellen (TRM) unterteilt werden. Für den Einsatz bei einer adoptiven T-Zell-Therapie (ACT) eignen sich TCM-Zellen im Vergleich zu Effektor CD8+ T-Zellen besser zur Kontrolle des Tumorwachstums. Allerdings kommt es bei den transferierten Gedächtniszellen letztlich zu einer funktionellen Erschöpfung und dauerhafte Reaktionen auf ACT werden bestenfalls bei 50% der Patienten mit soliden Malignomen beobachtet.

Hier zeige ich, dass erhöhte CD8-Werte in TCM-Zellen genutzt werden können, um die Anti-Tumor-Funktion von adoptiv übertragenen gedächtnisähnlichen CD8+ T-Zellen im Maus-Melanom-Model zu verbessern. Die Ligation von CD8α mit einem agonistischen Antikörper aktivierte die proximale TCR-Signalübertragung und induzierte einen hybriden Effektor-/Gedächtnis-Differenzierungszustand. CD8-ligierte Zellen zeigten erhöhte Proliferation, Zytotoxizität und Glykolyse ohne dabei in ihrer Gedächtniszell-ähnlichen Persistenz und oxidativen Phosphorylierung beeinträchtigt zu sein. Die Produktion von Effektor-Zytokinen in CD8-ligierten Zellen war von einem umgestellten Glukose- und Glutaminstoffwechsel abhängig. Die Expansion von gedächtnisähnlichen CD8+ T-Zellen in Gegenwart dieses agonistischen Antikörpers verstärkte deren Anti-Tumor-Funktion in vivo erheblich. Darüber hinaus verhinderte der agonistische CD8-Fab′ teilweise die T-Zell-Dysfunktion, induzierte die Proliferation von erschöpften Vorläufer-T-Zellen und reduzierte die Tumorlast erheblich. Diese Ergebnisse etablieren CD8 als immuntherapeutisches Ziel, ohne dass das TCR-Repertoire der Patienten bekannt sein muss.

Interleukin (IL) 15 ist für das Überleben und den homöostatischen Umsatz aller CD8+ Gedächtnis-T-Zell-Untergruppen erforderlich, jedoch bleibt der zelluläre Ursprung bislang unklar. Anhand eines Mausmodells für eine akute Infektion mit dem lymphozytären Choriomeningitis-Virus (LCMV) zeige ich, dass, obwohl IL-15 stark exprimiert wird, verschiedene Gedächtnis-T-Zell-Untergruppen für ihre Aufrechterhaltung auf unterschiedliche IL-15 Quellen angewiesen sind. Insbesondere terminale TEM-Zellen (tTEM) sind bei Mäusen mit einer Il15-Deletion, die spezifisch für CD4+ regulatorischen T-Zellen (Treg-Zellen) ist, depletiert. Diese

Ergebnisse zeigen, dass Treg-Zellen eine direkte Rolle für die Vielfalt der Gedächtnisfunktion einer Immunantwort spielen.

Abschließend liefere ich vorläufige Beweise dafür, dass die Aktivierung von „Signal Transducer and Activator of Transcription (Stat)“6, der dem IL-4-Signalweg nachgeschaltet ist, die Infiltration zirkulierender T-Zellen in nicht-lymphoides Gewebe und ihre anschließende Entwicklung zu TRM-Zellen steuert. Unter Verwendung von Mausmodellen für Infektionen mit LCMV und Influenza zeige ich, dass CD8+ T-Zell-intrinsische Stat6 Signalwege die Migration von T-Zellen in die Leber bzw. die Lunge, möglicherweise durch Modulation der Expression des Chemokinrezeptors C-X-C-Motiv-Chemokinrezeptor 6 (CXCR6), induzieren.

Zusammengenommen untersuchen die hier vorgestellten Daten verschiedene Aspekte aller Gedächtnis-T-Zell-Untergruppen und bieten Einblicke in die Entwicklung von TRM-Zellen, die homöostatischen Anforderungen von TEM-Zellen und die Übertragbarkeit der TCM Biologie auf den Bereich der Tumorimmuntherapie.

Table of contents

List of Figures

List of Tables

1 Introduction

In 1958, working in a refurbished mansion, Jacques Miller was pursuing his doctoral degree in one of the satellite facilities of the Chester Beatty Research Institute in London, the United Kingdom [1, 2]. In a repurposed horse stable, which served as his animal holding facility, Miller performed groundbreaking experiments. His work revealed that the thymus is not a vestigial organ, but was important for immune competence as the source of what we now know as T (for thymus-derived) cells [3–7]. By 1965, he was already mentoring his first doctoral student, Graham Mitchell [1]. They would soon publish two back-to-back papers confirming previous observations made by Max Cooper and his colleagues [8], and showing that T cells are distinct from bone marrow-derived lymphocytes (B cells), yet the interaction between the two populations was required for an optimal antibody response [9, 10]. Presenting his work at a scientific conference in 1969, Miller was accused of unnecessarily complicating immunology [11].

1.1 T cell development

T cells are small lymphocytes that, together with B cells, represent the cellular component of the adaptive immune system [12]. As mentioned, they develop in the thymus, but they originate from bone marrow-derived common lymphoid progenitors (CLPs) [13]. Notch signalling in the thymus commits CLPs to the T cell lineage [14, 15]. During thymic development of αβ T cells, nascent thymocytes sequentially express chemokine receptors that guide them to distinct microenvironments [16]. In this journey, CD4CD8 double negative (DN) cells rearrange their T cell receptor β (TCRb) chain in-frame, rapidly proliferate, and transition to the CD4+CD8+ double positive (DP) stage, where they proceed to rearrange their TCR α (TCRa) chain [17–19]. Only 3 - 5% of developing thymocytes mature to the point where they become single positive (SP) cells [20]. The basis of this positive selection is their ability to engage in low-affinity interactions with self-peptides presented on the surface of cortical thymic epithelial cells (cTECs) in the context of self major histocompatibility complex (MHC) class I (for CD8 SP cells) or class II (for CD4 SP cells) [21–24]. Cells that cannot recognise self MHC-I/II die by neglect, and cells that bind self peptide-MHC (pMHC) complexes with high affinity are negatively selected [24–26]. As a result, MHC-restricted T cells with a highly diverse TCR repertoire are, largely, self-tolerant.

Unlike the somatically rearranged TCR, CD4 and CD8 co-receptors are germline encoded. CD4 is an integral membrane protein with four immunoglobulin (Ig)-like domains [27, 28], whereas CD8 is commonly expressed as a disulfide-linked dimer of two CD8α chains (CD8αα) or, more commonly, one CD8α and one CD8β chain (CDαβ) [29, 30]. CD8αα is also expressed by a subset of dendritic cells (DCs), natural killer (NK) cells, and intraepithelial lymphocytes (IELs), and is thought to inhibit TCR signalling [31–35]. Both co-receptors interact with non-variant regions in their respective MHC partners while their cytoplasmic tails non-covalently bind the Src family tyrosine kinase Lck [36–40], which plays a vital role in TCR signal transduction [41–43]. Broadly, CD4+ and CD8+ T cells are referred to as helper and cytotoxic T cells, respectively [12].

1.2 Naive T cell homeostasis

New thymic emigrants persist in the periphery for 6 - 10 weeks in mice and between 6 and 10 years in humans [44]. In the absence of antigenic stimulation, two factors are essential for naive T cell maintenance; tonic TCR signalling and interleukin 7 (IL-7) stimulation [45–48]. Tonic TCR signalling refers to the transient interaction between TCR and self peptides presented in the context of MHC-I/II in the periphery [49]. MHC-I-deficient mice that fail to provide such a signal quickly lose naive CD8+ T cells [46]. The same happens, albeit at much slower kinetics, for CD4+ T cells in MHC-II-knockout (KO) mice [50].

Like MHC deficiency, loss of IL-7 signalling compromises naive CD4+ and CD8+ T cell survival and limits lymphopenia-induced proliferation [45, 48, 51, 52]. IL-7 induces the expression of the anti-apoptotic proteins B-cell lymphoma 2 (Bcl-2) and myeloid cell leukaemia 1 (Mcl-1), and inhibits the expression of several pro-apoptotic factors, thus maintaining T cell longevity [52]. Administration of IL-7 induces basal proliferation of T cells, especially CD8+ T cells, without significantly changing their activation status [53, 54]. Therefore, competition for the limiting IL-7 concentration provides a theoretical ceiling for the number of naive T cells in the periphery [55]. However, access to IL-7 is equitable because IL-7 suppresses transcription of the IL-7 receptor α subunit (IL-7Rα; encoded by *Il7r*) [56]. Consequently, cells that have already received IL-7 signalling no longer compete for the remaining cytokine and cells that did not receive the signal upregulate *Il7r* and are more sensitive to IL-7.

1.2.1 Integration of tonic TCR and IL-7 signalling

Naive CD8+ T cells integrate information from IL-7 signalling and self antigen recognition to maintain their quiescence in what is known as 'co-receptor tuning' [57]. One of the CD8 enhancer elements, namely $E8_I$, has a binding site for Stat5, which is activated downstream of IL-7 binding. Thus, IL-7 signalling induces the upregulation of *Cd8a* and enhances TCR signalling in response to low-affinity self antigens. In contrast, TCR signalling blocks *Il7r* transcription and causes a downregulation of surface CD8 levels, therefore limiting CD8 expression as well as sensitivity to both IL-7 and self peptides [57] (Fig. 1).

In principle, CD8 and IL-7R share a similar regulatory mechanism to ensure peripheral maintenance of naive T cells. IL-7 signalling induces the downregulation of IL-7Rα to limit IL-7 sensitivity [56] and, in the same fashion, cells that receive strong tonic TCR signalling express lower levels of CD8, which prevents weak self antigens from accidentally activating T cells [57, 58]. Thus, in naive mice, CD8 surface expression acts as a rheostat to achieve survival without autoreactivity.

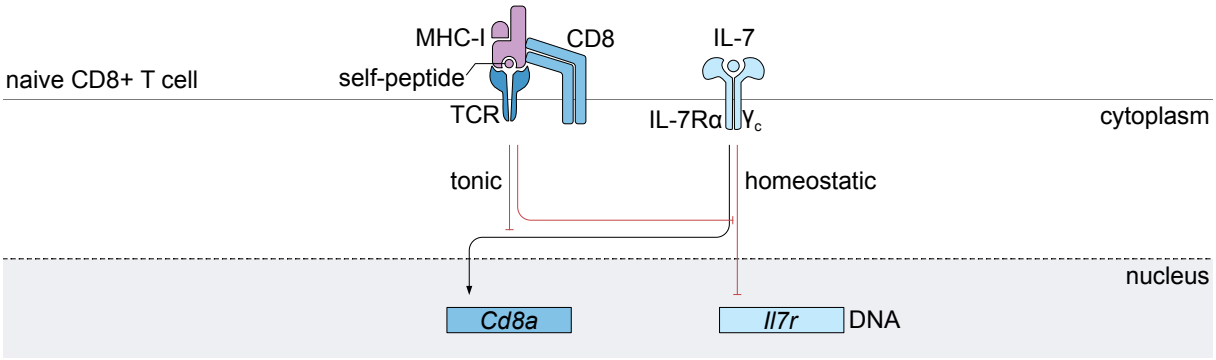

Figure 1: Mutual regulation of tonic TCR and IL-7 signalling

The co-receptor tuning model refers to how naive T cells maintain long-term survival without overt autoimmunity. IL-7 limits the expression of its own receptor but enhances T cell sensitivity to self peptides by inducing *Cd8a* transcription. In turn, strong tonic TCR signalling limits IL-7 sensitivity and reduces surface CD8 expression. This mutual regulatory mechanism balances T cell response to tonic and homeostatic signalling and is required for naive T cell peripheral maintenance.

1.3 T cell activation

In contrast to physiological recognition of self antigens, foreign antigen presentation induces a three-phase program that characterises response to acutely resolved infections; 1) T cell

activation, clonal expansion, and the execution of effector functions, 2) apoptotic cell death of the majority of effector cells, and 3) persistence of long-lived memory cells after pathogen clearance [59]. Notably, naive T cells maintain a state of 'preparedness', where quiescence is actively instructed through proteins with very short half-lives [60]. This strategy ensures that these proteins disappear once a cell is activated and their transcription is silenced. On the other hand, many mRNAs encoding effector proteins are translationally repressed, allowing for their rapid translation following activation.

Three signals are required for quiescence exit and optimal T cell activation; antigen recognition, co-stimulation, and cytokine signalling [61]. Immature DCs patrol non-lymphoid tissues (NLTs) and routinely sample their environment through phagocytosis, pinocytosis, and receptor-mediated endocytosis [62–64]. Recognition of conserved pathogen-associated molecular patterns (PAMPs) as well as inflammatory cues induce the maturation of DCs [64, 65], which are the only antigen-presenting cells (APCs) capable of activating naive T cells [64].

1.3.1 Proximal TCR signalling

Naive T cells express the lymphoid homing receptors CD62L and C-C chemokine receptor type 7 (CCR7) [66, 67]. This allows T cells to migrate to secondary lymphoid organs (SLOs), where they might encounter antigen-loaded APCs. Importantly, mature DCs in SLOs express the CCR7 ligand CCL19, which helps attract naive T cells from the circulation [68].

αβ TCRs have very short cytoplasmic tails and themselves do not undergo any conformational change when bound to their cognate antigen [69]. The signal is instead transduced through the accessory molecules bound electrostatically and hydrophobically to the TCR chains [70–72]. These include one CD3γ chain, one CD3δ chain, two CD3ε chains, and two CD3ζ chains [72, 73]. Together, TCRαβ and the associated CD3 chains are known as the TCR complex. In essence, TCR signal transduction is dependent on a phosphorylation cascade that creates multiprotein platforms for enzyme-substrate interactions. This eventually culminates in the activation of transcription factors, changing the metabolic status of the cell, proliferation, increasing the adhesion strength to endothelial and target cells, and effector protein synthesis [74–76].

Collectively, the TCR complex contains a total of 10 immunoreceptor tyrosine-based activation motifs (ITAMs) [77, 78], each of which has two tyrosine residues, which are targeted

for phosphorylation through the co-receptor-bound, Src-family tyrosine kinase Lck [36, 79, 80]. Another tyrosine kinase, ζ-chain-associated protein kinase 70 (ZAP70), is able to bind through its tandem Src-homology 2 (SH2) domains to the phosphorylated ITAMs and is itself phosphorylated by Lck [80–83]. Activated ZAP70 phosphorylates linker for activation of T cells (LAT) and SLP76 [84, 85], which when bridged with the linker Gads form an adaptor complex that binds signalling proteins many of which are Lck substrates [84]. From this node, several downstream signalling pathways are initiated.

1.3.2 Co-receptor function

Because co-receptors interact with both MHC and Lck, their role in TCR signal initiation has been extensively studied. Although several models were proposed to provide a mechanistic explanation for this effect [86], recent structural and kinetic evidence suggests that the formation of a stable pMHC::TCR ternary complex proceeds through four steps (Fig. 2). First, the TCR contacts MHC-I/II complex regardless of the bound peptide [87], but peptide recognition stabilises this initial interaction [88]. Second, although the conformation of the TCR itself does not change [69], the signal is somehow transmitted to CD3ε, revealing the receptor kinase motif. This motif is proline-rich and is able to recruit freely diffusing Lck through the SH3 domain [89]. Third, Lck phosphorylates ITAMs in the CD3 complex, recruiting the Lck-bound co-receptors through the SH2 domain [90]. Co-receptors then interact with invariable MHC-I/II domains and further stabilise the entire complex [91], eventually leading to stable downstream signal transmission. Therefore, the TCR must bind pMHC with a 'canonical' orientation to position the cytoplasmic components of the TCR complex in a conformation accessible to the CD8-bound Lck [92]. In summary, co-receptors act to stabilise pMHC::TCR interactions, amplify the signal, and enhance the overall functional avidity of the TCR.

1.3.3 Distal TCR signalling

As mentioned, an important consequence of proximal TCR signalling is the generation of protein scaffolds that alter the subcellular localisation of several downstream targets. LAT is an important components of these scaffolds [93], which were recently reported to support more than 360 unique protein interactions [94]. After ZAP70-mediated phosphorylation, LAT becomes involved in two multiprotein complexes; LAT-Gads-SLP76 and LAT-Grb2-SOS [84, 95]. SOS is a GTP exchange factor (GEF) and activates the small G protein Ras [95], which activ-

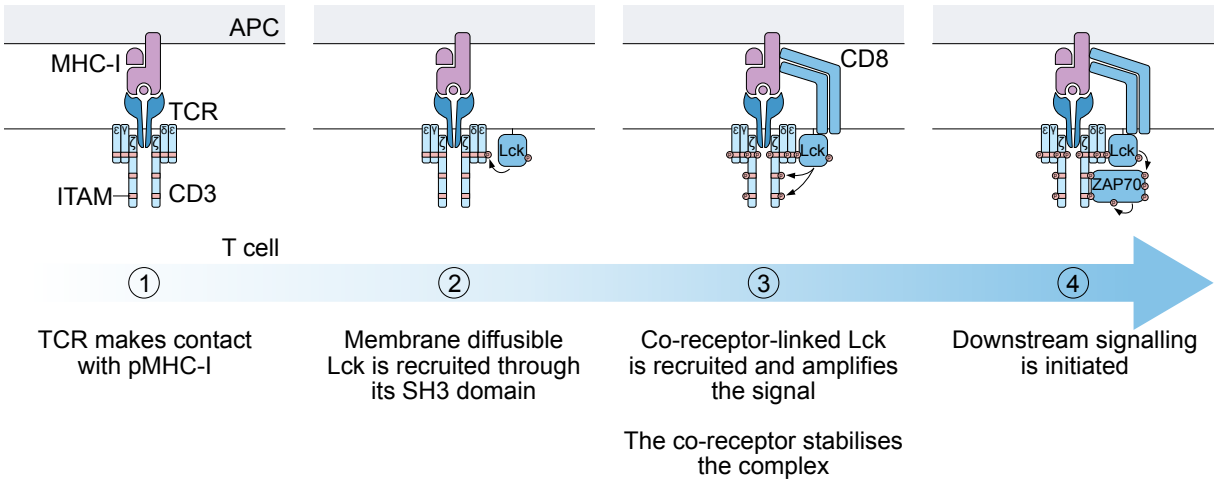

Figure 2: Early events in TCR signal initiation

This four-step model describes the sequence of interactions following cognate antigen recognition. Peptide recognition stabilises initial interaction between the TCR and peptide-MHC complexes, leading to a conformational change in the CD3ε chain, and allows it to interact with the SH3 domain of Lck freely diffusing in the membrane. Phosphorylation of immunoreceptor tyrosine-based activation motifs (ITAMs) domains then recruits a second pool of Lck that is bound to co-receptors (CD8 in this example). By binding to MHC-I, CD8 further stabilises the complex, while its bound Lck amplifies the signal, eventually initiating downstream phosphorylation cascades. Arrows refer to phosphorylation events. APC, antigen-presenting cell.

ates the lipid kinase Phosphatidylinositol-3-OH kinase (PI3K) [96]. PI3K phosphorylates inositol groups in membrane phospholipids to generate Phosphatidylinositol 3,4,5-triphosphate (PIP3) [97]. Pleckstrin-homology domain (PH)-containing proteins, including phospholipase Cγ (PLCγ), are recruited to membrane PIP3 [98]. PLCγ additionally binds the LAT-Gads-SLP76 complex through its SH2 domain and is thus brought in proximity to its kinase ITK [84]. Activated PLCγ is an important signalling node in T cells as it initiates the activation of three key transcription factors; nuclear factor of activated T cells (NFAT), nuclear factor-κB (NF-κB), and activator protein 1 (AP-1) [99] (Fig. 3).

PLCγ cleaves membrane phospholipids into inositol 1,4,5-triphoshpate (IP3) and diacylglycerol (DAG) [99]. IP3 diffuses into the cytoplasm and is able to increase cytosolic calcium ion (Ca^{2+}) concentrations. Ca^{2+} induces a conformational change in its receptor, calmodulin, and the Ca^{2+}-calmodulin complex binds and activates the protein phosphatase calcineurin. As a result, cytoplasmic NFAT is dephosphorylated and is able to translocate to the nucleus, where it binds to target sequences in the *Il2* promoter [100]. While IP3 is soluble, DAG remains

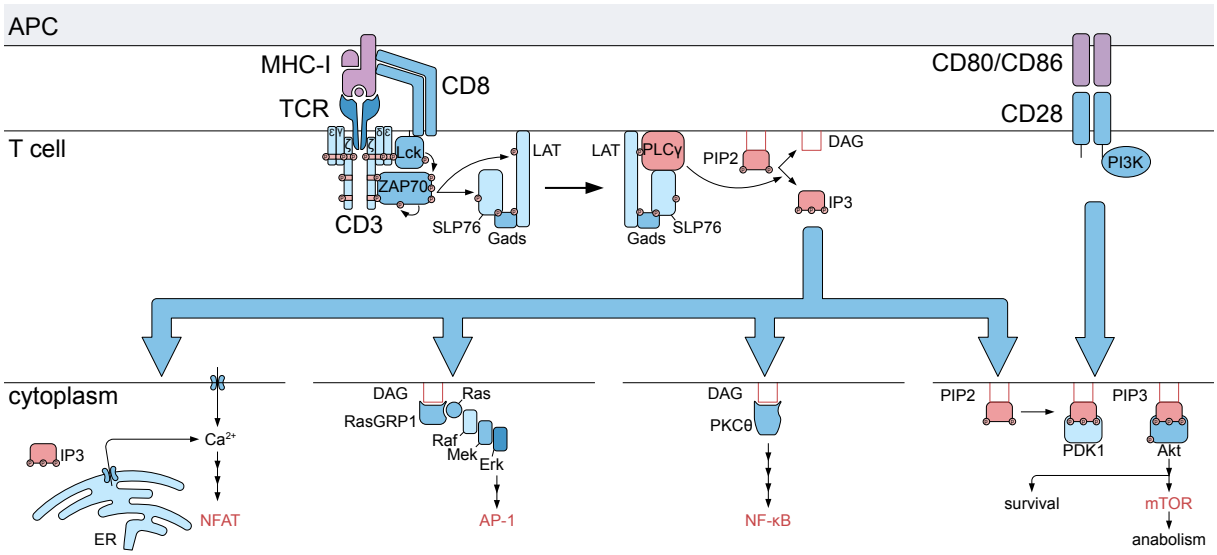

Figure 3: Overview of major distal TCR signalling pathways

Following Lck mediated- and auto-phosphorylation, ZAP70 is activated and is able to phosphorylate the adaptor protein linker for activation of T cells (LAT), which creates a docking platform for several enzymes. Shown here is phospholipase Cγ (PLCγ)-mediated signalling. PLCγ catalyses the conversion of membrane phosphatidylinositol 4,5-bisphosphate (PIP2) into inositol 1,4,5-triphoshpate (IP3) and diacylglycerol (DAG). Soluble IP3 binds its receptor in the endoplasmic reticulum (ER) membrane to initiate calcium ion (Ca^{2+}) release from the ER as well as uptake from the extracellular space. This axis eventually leads to the activation of nuclear factor of activated T cells (NFAT) and allows its translocation to the nucleus. On the other hand, membrane bound DAG recruits Ras guanyl-releasing protein 1 (RasGRP1) to initiate the mitogen-activated protein kinase (MAPK) pathway culminating in the generation and activation of the activator protein 1 (AP-1) complex. In the third axis, DAG binds protein kinase C θ (PKCθ) to eventually lead to the stabilisation and nuclear translocation of the nuclear factor-κB (NF-κB) complex. Ras signalling combined with co-stimulatory signalling lead to the activation of phosphatidylinositol-3-OH kinase (PI3K), which converts membrane PIP2 into PIP3 to act as a docking site for phosphoinositide-dependent kinase-1 (PDK1) and its substrate protein kinase B (also known as Akt). Akt then initiates a signalling cascade, involving mammalian target of rapamycin (mTOR) to induce anabolic metabolism and cell survival. Not depicted in this figure are signalling cascades inducing cytoskeletal rearrangements and enhancing T cell adhesion. APC, antigen-presenting cell.

in the membrane and recruits two C1-domain-containing proteins; protein kinaseθ (PKCθ) and Ras guanyl-releasing protein 1 (RasGRP1) [101–103]. PKCθ activation generates another adaptor complex that eventually leads to the degradation of the NF-κB inhibitor IκB and the translocation of the NF-κB heterodimer to the nucleus, where it also binds the *Il2* promoter

[104, 105]. Like SOS, the other C1-domain protein RasGrp1 is a Ras GEF and together they activate the mitogen-activated protein kinase (MAPK) cascade. Three main groups of MAPKs have been identified; extracellular signal–regulated protein kinase (Erk), c-Jun N-terminal kinase (Jnk), and p38 [106]. Activated Erk induces the transcription of *Fos* and Jnk activates the transcription factor c-Jun, which dimerises with Fos to form the AP-1 complex [61, 107]. AP-1 is the third key transcription factor required for initiating *Il2* transcription [108, 109].

The LAT-Gads-SLP76 complex additionally recruits and activates small G proteins that function to enhance cell adhesion and actin polymerisation [85, 110], while PI3K-generated PIP3 initiates a signal to modify metabolism. Both phosphoinositide-dependent kinase 1 (PDK1) and its substrate protein kinase B (also known as Akt) have PIP3-binding PH domains and when brought in proximity, PDK1 phosphorylates and activates Akt, which in turn activates mammalian target of rapamycin (mTOR) [111–113]. Akt signalling increases cell size, nutrient uptake, protein synthesis, survival, and proliferation [114, 115].

Despite engaging several transcriptional, metabolic, and adhesion modules, TCR signalling alone is not enough to initiate effector differentiation [116]. To fully acquire the effector cell program, T cells need co-stimulation and cytokine signalling [61, 117].

1.3.4 T cell co-stimulation

Purified CD8+ T cells cultured *in vitro* with agonistic anti-CD3 antibodies are not activated. Paradoxically, they become resistant to antigenic stimulation [116]. *In vivo*, some immature DCs are able to migrate to SLOs and to present self-antigens [118, 119]. These cells, however, do not express co-stimulatory molecules and do not activate T cells. Instead, naive T cells that bind self antigens strongly in the absence of co-stimulation are anergic and fail to respond to subsequent TCR stimulation [120, 121]. Such tolerogenic antigen presentation is important for elimination of the few autoreactive T cell clones that escaped thymic negative selection [118, 119]. This also underscores the importance of co-stimulation for an optimal immune response.

The protoctypical, but not the only, co-stimulatory signal is provided through the interaction between CD80 and/or CD86 on the surface of APCs and T cell CD28 [114, 122]. Ligated CD28 is phosphorylated and is able to interact with and sustain Lck activation [123, 124]. In addition, the cytoplasmic tail of CD28 binds PI3K and initiates all signalling downstream of

PIP3 generation [111] (Fig. 3). Further, optimal positioning of PKCθ in close proximity to the TCR complex is dependent on CD28 [125]. As a result, pronounced activation of the 3 key transcription factors is not achieved in the absence of CD28 signalling [126–128]. Besides supporting IL-2 transcription, CD28 signalling is also required for the expression of the high affinity IL-2 receptor IL-2Rα (also known as CD25) [129]. Although no unique signalling pathway is induced after co-stimulation, CD28 signalling strongly potentiates almost all pathways downstream of TCR activation and is indeed required for cell cycle entry [130, 131].

1.3.5 Cytokines license T cell effector functions and memory potential

The third fundamental signal required by T cells for full acquisition of effector function is delivered by the cytokine milieu. IL-2 is a downstream target of TCR and CD28 signalling and is the first cytokine produced by naive T cells after activation [12]. Although IL-2 is a staple in *in vitro* T cell expansion protocols [132–134], it is not required for initial T cell division *in vivo* [135, 136], but rather for sustained CD8+ T cell proliferation and survival, particularly in non-lymphoid tissues [137, 138]. Effector CD8+ T cells that sustain CD25 expression during the early course of acute lymphocytic choriomeningitis virus (LCMV) infection are more proliferative and cytotoxic compared to $CD25^{low}$ cells. However, $CD25^{high}$ cells are short-lived and contribute little to long term protective immunity [139, 140]. In addition to IL-2, IL-12 and type I interferons (IFNα and IFNβ) play an important role in the initial expansion of CD8+ T cells and their propensity to develop into long-lived memory cells [141]. CD8+ T cells deficient for type I IFN receptor (IFN1R) show a modest or severe reduction in primary expansion, depending on the infection model [142, 143]. In one study, IFN1R signalling was shown to be required for the survival, not proliferation, of antigen-specific cells [144]. Similarly, the effect of IL-12 on CD8+ T cell function seems to be model-specific [142, 145, 146]. IL-12 is particularly important in the context of infection with the intracellular bacteria *Listeria monocytogenes* (*L. monocytogenes*), where IL-12 supports the expression of the transcription factor T box expressed in T-cells (T-bet) and the differentiation of cytotoxic effector cells rather than memory precursor cells [145, 146]. Therefore, while inflammation supports CD8+ T cell cytotoxic function, it can compromise long term protective immunity [147]. Cytotoxic CD8+ T cell differentiation also relies on their sensitivity to IFNγ, whose receptor is upregulated early after acute LCMV infection [148]. However, unlike IL-12 and type 1 IFN signalling, IFNγ enhances the differentiation of memory CD8+ T cells post antigen elimination [149].

In contrast to CD8+ T cells, there is some plasticity in the range of effector functions acquired by CD4+ T cells. Several distinct CD4+ T cell helper (T_H) subsets have been identified, whose functions match the nature of the pathogen they first recognised. This synchrony is orchestrated by a network of innate immune cells and their cytokines [150, 151]. Importantly, T_H subsets represent [largely] stable differentiation lineages, with distinct epigenetic and transcriptional signatures and unique cytokine profiles [152]. However, with the advent of sensitive and single-cell analyses, new subsets are being proposed while the distinctions between recognised T_H lineages are becoming increasingly blurry [151, 153, 154].

1.4 Signal termination and T cell contraction

During effector cell differentiation and expansion, the expression of IL-7Rα is lost by the great majority of T cells [45, 155]. In addition, with successful antigen elimination, T cells lose TCR signalling and subsequent IL-2 release. This cytokine withdrawal limits T cell survival and induces intrinsic apoptosis [156, 157]. Cells that retain CD25 expression are particularly sensitive to apoptosis following viral clearance [139]. Furthermore, intrinsic and extrinsic negative feedback mechanisms act to terminate TCR signalling and induce the death of 90 - 95% of antigen-specific cells following pathogen clearance [59, 158, 159].

T cell death is linked to effector function. For example, CD4+ and CD8+ T cells lacking IFNγ expression do not experience a contraction phase and neither do effector T cells expanding in the absence of inflammation [160–162]. Additionally, activated T cells express several inhibitory receptors downstream of TCR activation. These 'checkpoint' proteins include programmed cell death protein 1 (PD-1), which is induced within 3 days of acute infection [163, 164]. PD-1 binds ligands from the same protein family as CD80/CD86, namely PD-1 ligand 1 (PD-L1) and PD-L2 [165, 166]. PD-L2 is widely expressed in non-lymphoid tissues, and IFNγ induces the expression of both ligands in APCs [165, 166]. PD-1 inhibits TCR signalling at consecutive steps. It inhibits CD8-induced cooperativity in pMHC::TCR interactions thus attenuating antigen recognition [167]. Intracellularly, PD-1 has immunoreceptor tyrosine-switch motif (ITSM) and immunoreceptor tyrosine-inhibitor motif (ITIM) that associate with SH2-containing phosphatase-1 (SHP-1) and SHP-2 [168, 169]. When PD-1 is ligated, it colocalises with the TCR and CD28 bringing SHP-1 and SHP-2 in close proximity to the phosphorylated domains in the TCR complex and CD28 cytoplasmic tail. Dephosphorylation of CD28 as well as proximal TCR components effectively terminates TCR and co-stimulatory sig-

nalling and blocks T cell proliferation and cytokine release [165, 166, 169–174].

Cytotoxic T-lymphocyte-associated protein 4 (CTLA-4) is another prototypical checkpoint receptor. It is translocated from the endosomal compartment to the cell surface following Lck-mediated phosphorylation [175, 176]. CTLA-4 is structurally similar to CD28 and maps to the same chromosome in mice and humans [175]. Importantly, CTLA-4 binds CD80/CD86 with a higher affinity than CD28, and CTLA-4-expressing cells trans-endocytose CD80/CD86 from the surface of APCs and induce their degradation in a process known as trogocytosis [177–181]. Thus, CTLA-4 deprives T cells of the survival effects induced by co-stimulation and acts to inhibit lethal lymphoproliferative diseases [182].

1.4.1 Treg cells usher immune memory

Helper CD4+ T cells activate immune resistance mechanisms in response to different pathogens [152]. One distinct CD4+ T cell lineage, regulatory T (Treg) cells, uses several strategies to suppress immune responses, thus preventing immunopathology and contributing to peripheral tolerance [183]. Treg cell expansion exhibits a delay compared to effector CD4+ and CD8+ T cells. For example, in mice infected with *L. monocytogenes*, Treg cells peak 7 days post infection (dpi) [184]. Therefore, the functional prime of Treg cells coincides with the contraction phase of the immune response. Treg cells suppress effector T cell function and expansion either by targeting effector T cells themselves or targeting APCs [183] (Fig. 4). Treg cells express the transcription factor forkhead box protein P3 (FoxP3), which induces the constitutive transcription of the high affinity IL-2 receptor CD25 [185]. Therefore, Treg cells strongly compete for IL-2 with effector cells [186–188]. Furthermore, FoxP3 induces the expression of CTLA-4 [185, 189, 190], and as a result, Treg cells terminate co-stimulatory signalling. Additionally, Treg cells secrete suppressive cytokines including IL-10, TGFβ, and IL-35 that act to inhibit DC function and maturation, T cell proliferation, and downregulate CD28 expression, respectively [191–195]. Further, both IL-10 and IL-35 induce PD-1 expression in CD8+ T cells [196]. In addition to producing immuno-inhibitory metabolites [197] and directly transferring them to effector cell cytoplasm through gap junctions [198], Treg cells secrete perforin and granzyme A to induce effector cell cytolysis [199]. Therefore, Treg cells directly contribute to effector cell contraction and foster an anti-inflammatory state that enhances the transition between the effector and memory phases of the immune response. Whether Treg cells have a direct effect on memory cells is unclear.

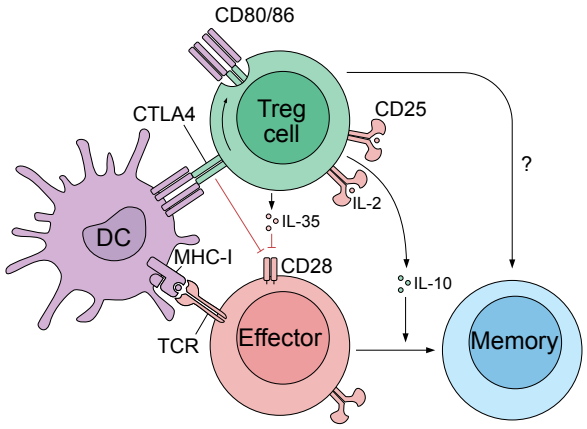

Figure 4: Overview of major Treg cell-mediated inhibitory mechanisms

FoxP3+ regulatory T (Treg) cells contribute to the contraction phase of the immune response by inhibiting denritic cell (DC) function and directly limiting effector T cell activation. Treg cells express high levels of the high affinity IL-2 receptor CD25 and strongly compete for IL-2 with effector cells. In addition, surface cytotoxic T-lymphocyte-associated 4 (CTLA-4) binds co-stimulatory molecules with very high affinity, thus preventing their interaction with effector cell CD28. CTLA-4 binding initiates the uptake of co-stimulatory molecules and their degradation by Treg cells. IL-35 secreted by Treg cells induces the transcriptional downregulation of CD28 by effector cells, whereas IL-10 fosters an anti-inflammatory environment to promote memory cell development. It is not clear whether Treg cells can directly promote memory T cell function.

1.5 T cell memory

The salient feature of the adaptive immune response is the ability to record the history of previous antigen encounters in the form of memory cells. These cells persist long term in the absence of antigen [200], are able to self-renew through homeostatic proliferation [45], and do not compete with naive cells for tonic TCR signalling as their survival is MHC-independent [201]. Most importantly, they protect the host from recurrent infections. The number of memory antigen-specific CD8+ T cells is 100 - 200x that of naive cells responding in a primary infection [59], and contraction of secondary effector cells is 2 - 4x slower than that of primary effector cells [202]. However, the memory response is not merely quantitatively enhanced, it is qualitatively superior. Memory T cells proliferate very quickly following antigen recognition, and even before the first cell division, they elaborate greater amounts of cytokines and effector proteins than activated naive cells [203]. This swift response is, at least partially, due to the higher abundance of cytokine-encoding mRNAs as well as enhanced protein syn-

thesis capacity in memory cells [60, 204–206]. Additionally, memory T cells are 10 - 50x more sensitive to their cognate antigens compared to naive T cells [207, 208].

1.5.1 TCR functional avidity maturation

In the absence of somatic hypermutation (SHM), optimised TCR signalling is essential to reduce the threshold needed for productive activation. Memory T cells upregulate CD8 expression, thus enhancing cooperative pMHC binding and antigen sensitivity [208–210]. Additionally, antigen-experienced cells upregulate Lck and have a higher proportion of Lck bound to co-receptors, which become strictly localised to the cell membrane [208, 209]. Although the expression of other regulators of proximal TCR signalling is not affected during the course of an immune response, signalling downstream of the TCR complex is more efficient in memory cells [211, 212]. Plasma membranes of memory T cells have more, tightly packed lipid rafts that accumulate higher levels of the adaptor protein LAT [211]. By concentrating signalling intermediates in a confined space, the signal is more swiftly transduced. Furthermore, forced proximity in lipid rafts enhances TCR oligomerisation, and the formation of these higher-order structures increases antigen sensitivity [213, 214]. Therefore, structural re-organisation of the TCR complex and its downstream signalling cascade improves the functional avidity of memory T cells.

1.5.2 Memory T cell subsets

Memory T cells are distributed across different anatomic locations to provide rapid protective responses upon recurrent antigen exposure. Based on their tissue compartmentalisation, memory cells are commonly classified into three subsets; central memory T (TCM) cells, effector memory T (TEM) cells, and tissue-resident memory T (TRM) cells [215] (Fig. 5). Proliferative TCM cells can home to SLOs, while TEM cells cannot. Instead TEM cells, which are rapidly cytotoxic, transiently infiltrate NLTs [216]. In contrast, TRM cells fail to recirculate into the blood and instead establish long term residency in NLTs [217]. TRM cells have been discovered in almost all organs, including surface tissues like lung, gastrointestinal tract, and skin as well as internal organs such as brain and liver [218–220]. Additionally, a subset of lymph node-resident memory T cells was described [221], expanding the scope of TRM cells beyond NLT residency.

The differential expression of chemokine receptors and selectins instructs the migration

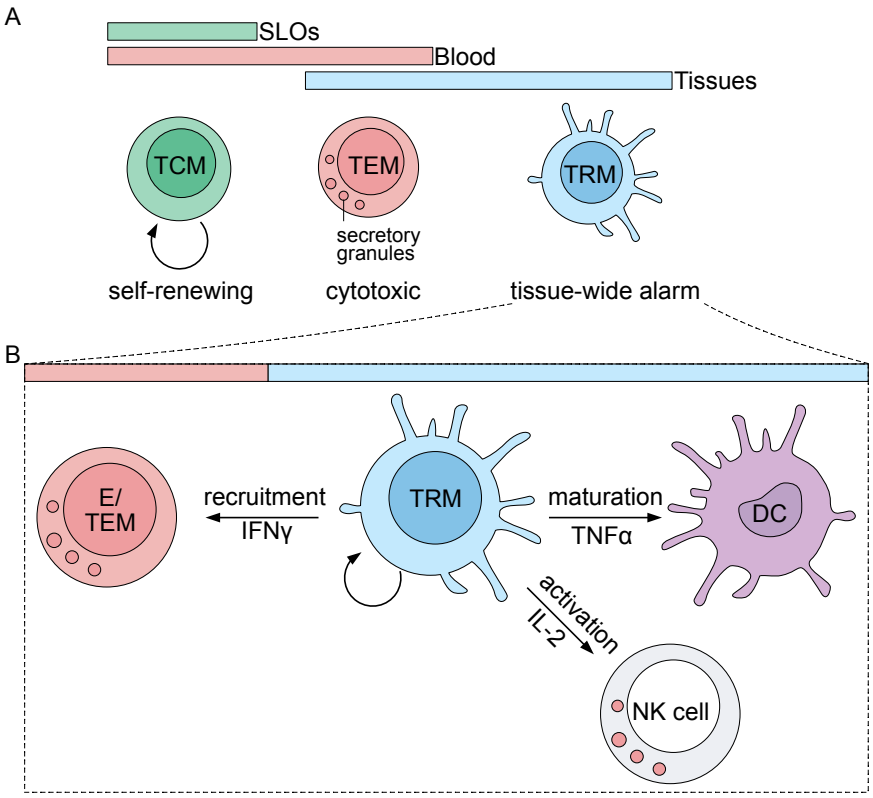

Figure 5: Memory T cell subsets and their functional output

(A) Based on their recirculation potential between secondary lymphoid organs (SLOs), blood, and tissues, memory T cells are grouped into three subsets, which additionally have functional differences. Central memory T (TCM) cells circulate in the blood and can home to SLOs. They undergo homeostatic proliferation and can rapidly expand following antigen recognition. Effector memory T (TEM) cannot home to SLOs but pass transiently through non-lymphoid tissues. Upon activation, TEM cells can quickly release cytotoxic proteins. Tissue-resident memory T (TRM) cells establish durable, sometimes life-long, residency in tissues and thus provide a first-line defence against invading pathogens. (B) Upon activation, TRM cells create a state of tissue-wide alarm. In addition to in situ proliferation, they secrete a group of cytokines that enhance the function of tissue innate immune cells and activate endothelial cells to allow the infiltration of circulating effector and TEM cells. E, effector. DC, dendritic cells. NK, natural killer.

behaviour of memory T cells. TCM cells express CCR7 and CD62L allowing them to home to SLOs [216]. The absence of these two SLO-homing receptors in TEM and TRM cells precludes them from trafficking to lymphoid organs. A subset of TEM cells expresses intermediate levels of the CX3C motif chemokine receptor 1 (CX3CR1) and are able to infiltrate NLTs [222]. The residency of TRM cells is mediated through their insensitivity to the sphingolipid

sphingosine-1-phosphate (S1P), whose concentration is elevated in blood and lymph. S1P receptor-1 ($S1P_1$) and $S1P_5$ are transcriptionally downregulated in TRM cells [223, 224]. Additionally, TRM cells express CD69 [217, 225], which induces the endocytosis of surface $S1P_1$ [226, 227]. Besides CD69, TRM cells in multiple sites express CD103 [217, 225]; an α_E integrin important for the interaction between T cells and E-cadherin-expressing epithelial cells [228]. It should be noted, however, that CD103 expression does not universally identify TRM cells; liver and small intestine (SI) lamina properia TRM cells are CD103-negative [219, 229].

As mentioned, functional distinctions exist between the different subsets. TCM cells are stem cell-like; they are long-lived and undergo antigen-independent homeostatic turnover. Most importantly, they rapidly proliferate upon antigen re-exposure and are able to differentiate into functional effector cells [216, 230, 231]. In contrast, TEM cells are not proliferative, exhibit a faster attrition rate than TCM cells, and express lower levels of the anti-apoptotic protein Bcl-2 [230, 231]. However, adoptive transfer experiments show that TEM cells are more protective against recall infection than TCM cells. This is possibly because TEM cells are immediately cytotoxic and thus are able to deploy faster effector function [231, 232]. Remarkably, secondary and tertiary memory responses are more biassed towards the TEM fate [233–235], which might explain why boosted immune responses are more protective [234]. However, viral infections targeting lymphoid organs are decreasingly controlled with each recurrence [236]. Interestingly, TRM cells combine functional features from both TCM and TEM cells, and are sufficient to control local infections in the absence of input from the circulation [237]. TRM cells in NLTs slowly patrol adjacent cells and form several cell-to-cell contacts. Upon antigen re-exposure, TRM cells are able to proliferate in situ, recruit circulating memory cells, and release cytokines and effector proteins [219, 238–240] (Fig. 5). Importantly, locally activated TRM cells recruit B and T lymphocytes, induce DC maturation, and activate NK cells. This ‘reversed’ direction of T cell-dependent activation of innate immunity is enough to eradicate unrelated infections if they happened to coincide with antigen-specific recall [241–243]. Therefore, the generation of stable TRM cells is an attractive vaccination strategy as they are more adept at controlling escape variants and inducing tissue-wide protective immunity [244–246].

1.5.3 A revised view of memory T cell subsets

Recirculation potential, proliferative capacity, and functional specialisation provide a meaningful framework to group memory T cells with different behaviours and, perhaps, distinct ontogeny. However, advanced single-cell analysis techniques have revealed further intra-group heterogeneity. A subset of CD62L+ TCM cells, for example, is both homeostatically proliferative (as TCM cells should be) and cytotoxic (as TEM cells are reported to be) [247]. Interestingly, during recall responses, it is the quiescent, slowly proliferating, not the cytotoxic, TCM cells that expand and rapidly control the infection. This dichotomy in the TCM pool is thought to protect T cells from replicative senescence; after repeated exposure, the average number of cell divisions in the pool of memory T cells does not significantly increase. Additionally, although stringent parabiosis experiments have repeatedly shown that TRM cells do not leave their tissue-of-choice [233, 248], recent evidence suggests that TRM cells can egress into the lymphatics and establish residency in draining lymph nodes [249, 250]. Repeated infection also induces the migration of TRM cells into the circulation, where they can feed the TCM and TEM compartments, although they maintain a higher tendency to infiltrate their original tissue and re-differentiate into TRM cells [251]. These new findings highlight the great plasticity in CD8+ memory T cells and caution against making assumptions about one memory T cell feature based on another.

1.5.4 CD8+ memory T cell homeostasis

Memory T cell subsets have shared and unique homeostatic requirements. In all cases, tonic TCR signalling is dispensable for memory maintenance [201, 252]. Instead, memory T cells differentially rely on cytokine signalling for survival [253]. Both circulating (TEM and TCM) and TRM cells require IL-15 signalling for homeostatic proliferation and persistence [221, 233, 234, 237, 254, 255]. IL-15 shares two receptor subunits with IL-2, namely IL-2Rβ and γ_c. The third, IL-15-specific subunit, IL-15Rα, is expressed by IL-15-producing cells and is used to present IL-15 to target cells [256, 257]. IL-15 induces PI3K and MAPK signalling as well as the upregulation of Bcl-2 [258], culminating in enhanced survival and proliferation of memory T cells [259–263].

The transcription factors T-bet and Eomesodermin (Eomes) control the expression of IL-2Rβ [264]. Because all memory T cell subsets express one of these two transcription factors

(albeit at low levels in TRM cells), all subsets are IL-15 sensitive [237, 265–268]. Mice with germline deficiency of IL-15 or IL-15Rα quickly lose memory T cells after viral clearance and cannot support the homeostatic proliferation of adoptively transferred circulating memory T cells [262, 263]. Similarly, very few skin or lung TRM cells could be recovered from IL-15 knockout mice following localised infection [225, 269]. TEM cells seem to be especially dependent on IL-15 signalling [145]. However, with recurrent antigen exposure, secondary and tertiary TEM cells become IL-15-independent [233, 234].

TEM and TRM cells express very low levels of IL-7Rα and are very likely IL-7-independent [231, 267, 270]. On the other hand, TCM cells are IL-7Rα-positive, and TCM cells adoptively transferred to IL-7-deficient mice fail to undergo homeostatic proliferation [45, 155, 271, 272]. Notably, along with the expression of CD62L and lack of killer cell lectin-like receptor subfamily G member 1 (KLRG1) expression, IL-7Rα is commonly used to identify early effector cells biassed towards the long-lived memory fate [145, 155, 212, 230, 231, 270, 273]. Specifically, IL-7Rα+KLRG1- cells are referred to as memory precursor effector cells (MPECs), while IL-7Rα-KLRG1+ cells are termed short-lived effector cells (SLECs) [145].

Unlike TCM and TEM cells, TRM cell development and maintenance require transfoming growth factor β (TGFβ) signalling, especially in organs where TRM cells express CD103, like skin, lung, and SI intraepithelial lymphocytes (IELs) [225, 237, 252, 269]. In addition to inducing CD103 expression, TGFβ inhibits $S1P_1$ and $S1P_5$ transcription and thus prevents T cell egress [223, 224, 269]. These effects are mediated through the downregulation of the transcription factors T-bet, Zeb-2, and T cell factor 1 (Tcf-1). Effectively, cytokine signalling imprints the transcriptional signature of memory T cell subsets.

1.6 Metabolic control of T cell function

A single naive CD8+ T cell transferred to a new host can reconstitute the entire immune response with characteristic effector and memory T cell subsets following immunisation with its cognate antigen [274], identifying it as a pluripotent stem cell [275]. Like adult stem cells, naive T cells rely on catabolic metabolism for their energy requirements and long term stability. Glucose-derived pyruvate and fatty acid-derived acetyl coenzyme A (CoA) feed into the tricarboxylic acid (TCA) cycle, where high energy electrons are transferred to electron carriers for mitochondrial electron transport chain, oxidative phosphorylation (OXPHOS), and aden-

osine triphoshpate (ATP) synthesis [276]. This metabolic program is maintained by continuous IL-7 signalling [52, 277], further underscoring its importance for naive T cell homeostasis.

1.6.1 Effector T cell metabolism

T cell activation is energetically expensive; a T cell needs to grow in size, synthesise nucleotides for DNA and RNA polymerisation, amino acids for mRNA translation, and lipids for plasma and endosomal membranes. While an activated T cell substantially increases nutrient uptake, many intermediates are synthesised *de novo* [278–280]. TCR, co-stimulatory, and cytokine signalling collaborate to completely rewire cellular metabolism [281]. The new metabolic program coordinates clonal expansion with epigenetic regulation, transcription, effector function, and migration behaviour [282, 283]. Generally, T cell activation instructs a global anabolic program, integrating aerobic glycolysis, the pentose-phosphate pathway (PPP), one-carbon metabolism, glutaminolysis, and lipogenesis [276, 278, 282, 284–286] (Fig. 6). Understandably, T cells employ several 'metabolic checkpoints' to ensure that the effector differentiation program does not proceed without the appropriate metabolic shift [287].

Like cancer cells, activated T cells rely on aerobic glycolysis (or Warburg metabolism) to rapidly generate energy and biosynthetic intermediates [279, 280, 287–289]. A naive cell is poised for a swift glycolytic switch following activation. Many glycolytic enzymes are already expressed in naive T cells, and they have exceptionally long half-lives; glyceraldehyde 3-phosphate dehydrogenase (GAPDH), for example, has a half-life of 231 hours, exactly 231x the half-life of CD62L [60]. Within minutes of TCR activation, T cells switch to aerobic glycolysis, even before an increase of glucose uptake becomes detectable [290]. This rapid reprogramming is directly downstream of TCR signalling. Lck and ZAP70 phoshorylate and activate pyruvate dehydrogenase kinase 1 (PDHK1), which directly inhibits pyruvate import into the mitochondria. Cytoplasmic pyruvate is then readily fermented to lactate by lactate dehydrogenase (LDH) [290]. Additional co-stimulatory signalling is required for maximal glucose uptake [115]. CD28 acts through the PI3K/Akt/mTOR pathway to induce the upregulation and surface translocation of the glucose transporter Glut-1 [115, 291]. Besides CD28 signalling, autocrine and paracrine IL-2 [292] and insulin receptor signalling [293] activate mTOR and support glycolysis even after the activated T cell has disengaged from the APC. In addition to enhancing glucose uptake, mTOR induces the expression of several glycolytic enzymes, including the rate-limiting enzyme hexokinase 2 (HK2), through modulation of the transcrip-

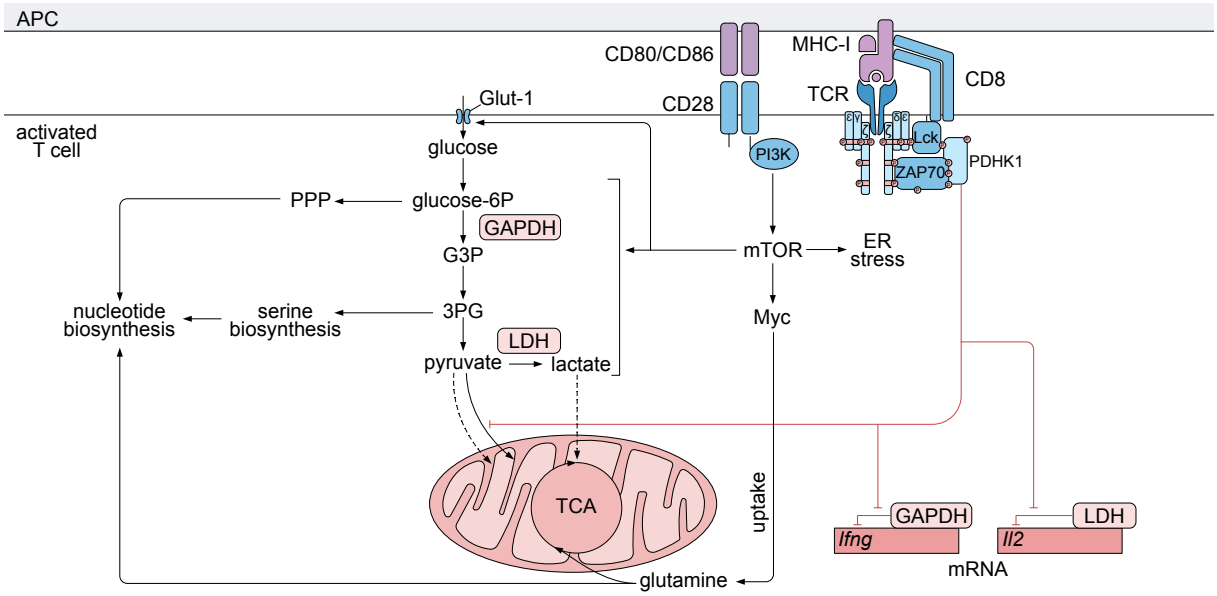

Figure 6: Effector T cell metabolism integrates clonal expansion and effector functions

Immediately following cognate antigen recognition, T cells engage aerobic glycolysis. This early effect results from Lck- and ZAP70-mediated phosphorylation of pyruvate dehydrogenase kinase 1 (PDHK1). Activated PDHK1 inhibits import of pyruvate into the mitochondria, thus promoting its cytoplasmic fermentation to lactate. Sustained aerobic glycolysis is induced downstream of co-stimulatory signalling and the activation of mammalian target of rapamycin (mTOR). mTOR induces the upregulation of glucose transporter 1 (Glut-1), glucose uptake, and glycolysis as well as the activation of protein synthesis (not shown). Myc activation enhances the uptake of glucose and glutamine. Glutamine supports the tricarboxylic acid (TCA) cycle and protein synthesis. Aerobic glycolysis generates intermediates required for the pentose-phosphate pathway (PPP), serine biosynthesis, and nucleotide biosynthesis. The glycolytic enzymes glyceraldehyde-3-phosphate dehydrogenase (GAPDH) and lactate dehydrogenase (LDH) bind AU-rich elements in the 3′-untranslated regions of *Ifng*, *Tnfa*, and *Il2* mRNAs thus preventing their translation. When recruited for aerobic glycolysis, this inhibition is relieved and the cytokines are expressed. mTOR activation is constantly coupled to the cellular metabolic needs and environmental nutrient content. Unchecked mTOR signalling can lead to endoplasmic reticulum (ER) stress and cell death.

Dahsed arrows indicate carbon assimilation revealed by recent *in vivo* tracing experiments. T cells can efficiently use lactate and puruvate as alternative carbon sources to fuel the TCA cycle, particularly at the peak of the immune response. glucose-6P: glucose-6-phosphate. G3P: glyceraldehyde-3-phosphate. 3PG: 3-phosphoglycerate.

tion factors Myc and hypoxia-inducible factor 1-α (HIF-1α) [276, 292].

Aerobic glycolysis couples anabolism to T cell effector function. In naive T cells, several glycolytic enzymes (like GAPDH and LDH) bind to *Il2, Ifng*, and *Tnfa* mRNAs and inhibit their translation [60, 290, 294]. Glycolytic occupancy of these enzymes relieves mRNAs from translational repression. Furthermore, in CD4+ T_H1 cells, lactate-derived acetyl coA is used as a cofactor for histone acetylation at the *Ifng* locus, supporting *de novo Ifng* transcription [295].

The glycolytic switch in activated T cells does not mean that mitochondrial metabolism is completely inhibited. On the contrary, mitochondrial biogenesis and fusion are significantly induced within one day of T cell activation [284]. Newly made mitochondria contribute to one-carbon metabolism and participate in nucleotide salvage pathways. In addition, mitochondrial reactive oxygen species (ROS) production is required for optimal calcium release, NFAT activation, and IL-2 secretion [296]. The glutaminolysis product α-ketoglutarate (α-KG) is more efficiently incorporated into the TCA cycle following activation [276]. Glutamine uptake and glutaminolysis are controlled by the transcription factor Myc, whose levels increase within 2 hours of TCR ligation [276] and is further maintained downstream of mTOR [297]. Glutamine is a proteinogenic amino acid and is required for the hexosamine pathway, polyamine cycle, and nucleotide synthesis, all of which are necessary for cell growth and division [276, 278, 298]. Furthermore, α-KG is a co-factor for epigenetic regulators [299, 300], and induces chromatin accessibility at *Ifng*, and *Hk2* loci, while restraining *Sell* (which encodes CD62L) transcription [301].

mTOR signalling is a central regulatory node in T cell activation [302]. It coordinates several metabolic aspects required for cell growth and proliferation [115, 285, 286, 291, 297, 303]. Additionally, master transcription factors are directly regulated by mTOR, including T-bet induction [304]. However, sustained mTOR activation is counterproductive [305, 306]. T cells sense their internal nutrient status using sphingolipids, which inhibit mTOR signalling. Although loss of sphingolipid synthesis sustains mTOR activity, antigen-induced proliferation is curtailed and T cells quickly succumb to apoptosis [307]. Therefore, mTOR signalling needs to be constantly fine-tuned to intra- and extracellular nutrient levels.

Most of the above referenced reports analysed T cell metabolism *in vitro*, but they do not all faithfully reflect the *in vivo* situation. For example, data from *in vitro* studies suggest that the contribution of glucose and fatty acids to TCA intermediates is reduced in activated T cells [276]. In contrast, *in vivo* metabolic tracing experiments show that following *L. monocytogenes* infection, early effector cells both dramatically increase their glycolytic rate and

substantially channel pyruvate into TCA intermediates [280]. Moreover, at the peak of the immune response, glucose is preferentially used for OXPHOS. Furthermore, lactate was recently shown to fuel the TCA cycle in activated CD8+ T cells *in vitro* and *in vivo* and to be required for T cell expansion and function following infection [308]. These results highlight the plastic ability of T cells to adjust their bioenergetic capacity to the environment and caution against making conclusions about T cell metabolism based on physiologically irrelevant cell culture conditions.

1.6.2 Memory T cell metabolism

The same checkpoints that induce T cell contraction (see section 1.4) allow effector cells to mature into the memory catabolic program. By limiting co-stimulatory signalling, CTLA-4 was shown to inhibit mTOR activation [115, 291] and subsequent glycolysis [309]. Similarly, PD-1 signalling decreases Glut-1 levels, glucose uptake, and glycolysis [309]. Additionally, PD-1 enhances the expression of carnitine palmitoyltransferase 1a (Cpt1a), the rate limiting enzyme in fatty acid (FA) β-oxidation [309]. Fused, densely packed mitochondria with multiple cristae are abundant in memory T cells and are required for OXPHOS and survival [310–312]. Although memory cells do use glucose for OXPHOS, the preferred substrate is FAs [313].

Short-chain FAs, either from diet or as byproducts of normal flora metabolism, signal T cells to disconnect glycolysis from the TCA cycle, and induce long-chain FA uptake [314]. Once inside the cell, hydrophobic FAs bind to chaperones from the FA-binding protein (FABP) family, which are highly expressed in TRM cells from different tissues and are necessary for their survival [315, 316], but are dispensable for circulating memory cells [315]. Instead, TCM cells engage an energetically futile cycle downstream of IL-7Rα signalling [317]. They enhance glycerol uptake and condensation with free FAs to synthesise triacylglycerol (TAG) and store it in lipid droplets [317]. These lipid droplets later fuse with lysosomes and lysosomal acid lipase (LAL) is used to release free FAs that are later imported into the mitochondria for oxidation [312]. It is not clear why such an intermediate TAG step is required, but it is needed to support TCM survival and proliferation [317] (Fig. 7).

In light of the important role mTOR signalling plays in effector T cell metabolism, pharmacologic [318] and genetic [319] inhibition of mTOR were shown to improve memory T cell differentiation and function. TCM, but not TEM, cells release ATP into the extracellular space [320]. This serves two functions; first, it decreases the intracellular ATP/adenosine

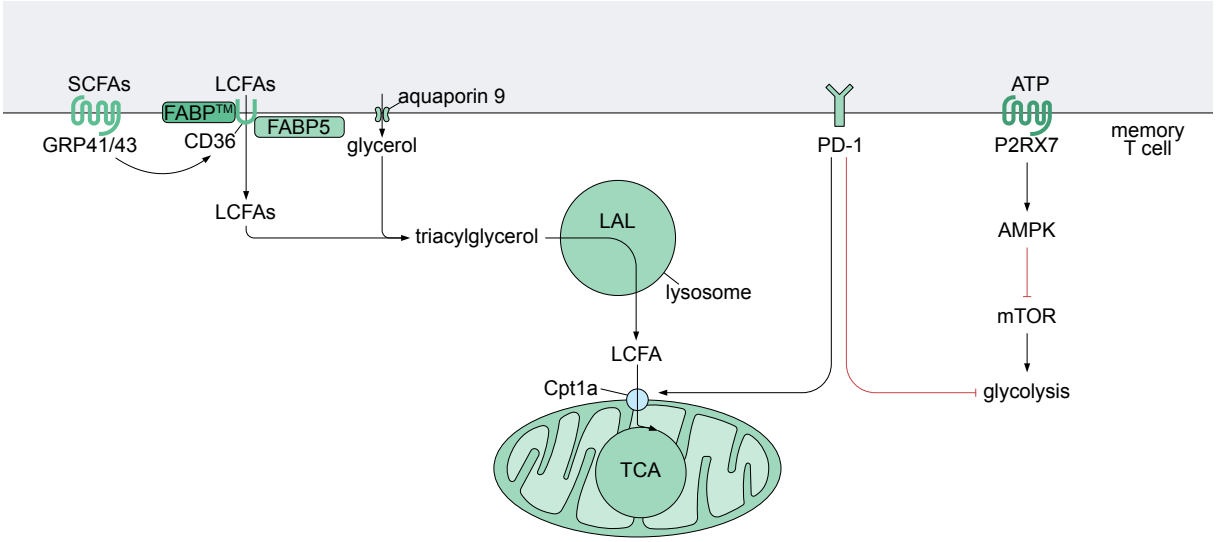

Figure 7: Fatty acid oxidation characterises memory T cell metabolism

A glycolytic-to-oxidative shift accompanies memory T cell development. Dietary or mirobiota-produced short-chain fatty acids (SCFAs) act on the G-protein coupled receptors GRP41 and GRP43 to induce enhanced uptake of long-chain fatty acids (LCFAs). The scavenger receptor CD36 associates with lipid chaperones fatty acid-binding proteins (FABP, shown here is isoform 5 expressed in skin TRM cells) and FABP transmembrane (FABP^{TM}), to facilitate the intracellular transport of hydrophobic LCFAs. IL-7 signalling induces the expression of the glycerol transporter acquaporin 9, and together with LCFAs, glycerol is condensed to triacylglycerol. Lysosomal acid lipase (LAL) liberates LCFAs from triacylglycerol and carnitine-palmitoyl-transferase (Cpt1a) facilitates the mitochondrial uptake of LCFAs for subsequent oxidation. The checkpoint receptor PD-1 induces the transcription of Cpt1a and suppresses glucose uptake and glycolysis. In addition, memory T cells have high levels of the purinergic receptor P2RX7, which enhances the activity of adenosine-mono-phosphate kinase (AMPK) to further suppress glycolysis.

monophosphate (AMP) ratio and activates AMP kinase (AMPK), which inhibits mTOR activity. Second, TCM cells express the purinergic receptor P2RX7, which senses extracellular ATP and enhances AMPK function [320]. This self-regulatory pathway suppresses mTOR activity in TCM and TRM cells, inhibiting both cell death and prolonged T cell activation [320, 321].

TEM cells maintain a higher rate of glycolysis than other memory T cell subsets [322, 323]. Sustained glycolytic metabolism and decreased reliance on FA oxidation are, in fact, required for their effector functions, especially under hypoxic and nutrient-depleted conditions [323, 324]. Although much is known about how glycolytic metabolism controls the epigenetic and transcriptional profile of effector T cells, the molecular link between FA oxidation

and memory T cell function is still unclear.

1.7 T cell exhaustion

Memory T cells are classically defined as long-lived cells that are homeostatically maintained after antigen clearance [215]. However, in some situations, T cells persist in the presence of antigen. This leads to either memory inflation and the accumulation of a functional pool of antigen-specific T cells [325], or to T cell exhaustion [326]. Exhausted T cells are a developmentally distinct T cell lineage that differentiates in the context of continuous antigen exposure [327–329], as in chronic infections with hepatitis C virus (HCV) [330], hepatitis B virus (HBV) [331], and human immunodeficiency virus (HIV) [332], and in cancer [333, 334].

T cell exhaustion was first described as an immune evasion mechanism established by chronic viral infections that leads to the physical deletion of antigen-specific T cells [335]. Currently, the definition is extended to dysfunctional, yet persistent, T cells [326, 336] characterised by hierarchical loss of effector function and proliferative capacity [337–339], sustained co-expression of several inhibitory receptors [338, 340], unique usage of transcription factor networks [341], blunted response to homeostatic cytokines [342], and altered metabolic behaviour [338, 343, 344]. Importantly, exhausted T cells are transcriptionally and epigenetically distinct from effector and memory T cells developing within the course of acutely resolved infections; epigenetic analyses revealed that exhausted T cells are as different from effector and memory T cells as B cells are from monocytes [329, 345, 346]. Once established, the epigenetic identity of exhausted T cells remains stable even after antigen withdrawal [347, 348], largely due to *de novo* global DNA methylation that silences key functional genes, including *Ifng* [349], but spares the *Pdcd1* locus [350]. Notably, despite pronounced dysfunction, loss of exhausted T cells leads to uncontrolled viremia [351–353], while sustained antigen stimulation without concomitant exhaustion leads to severe immunopathology in mouse models of chronic infection [354, 355], suggesting that immune exhaustion is, in fact, a protective coping mechanism.

1.7.1 Induction and metabolic correlates of exhaustion

How an early effector cell decides to commit to exhaustion rather than differentiate into functional effectors is an area of intensive research. Reversible features of exhaustion are

already detectable very early after chronic infection or tumour induction [339, 356]. Multiple factors synergise to establish a state of T cell exhaustion (Fig. 8A), including the magnitude and duration of antigenic stimulation [336, 342, 357] and the lack of CD4+ T cell help [326, 358–362]. Additionally, increased levels of several cytokines, such as IL-10 [363], TGFβ [364], and type I IFNs [365–367], have been implicated in T cell exhaustion. In tumours, the selective depletion of nutrients [368–370] and the accumulation of toxic waste products [371–374] instigate T cell dysfunction while simultaneously promoting the differentiation and/or survival of immunosuppressive cells [375]. Furthermore, exhausted T cells accumulate functionally impaired, depolarised mitochondria that fail to engage oxidative metabolism [351, 376–378]. This phenotype is induced by continuous TCR signalling and possibly PD-1 ligation, hypoxia, and glucose deprivation in the tumour microenvironment [343, 379]. Importantly, pharmacologically inducing mitochondrial dysfunction can itself imprint the transcriptional and epigenetic profile of exhaustion [343, 379, 380], while restoring mitochondrial biogenesis improves T cell function in chronic infections and cancer [376, 377, 379], indicating that metabolic dysregulation drives exhaustion. Mechanistically, loss of mitochondrial function is associated with the accumulation of mitochondrial ROS resulting in the activation of NFAT [379]. In the absence of its AP-1 partners, NFAT induces the transcription of inhibitory receptors like PD-1, lymphocyte-activation gene 3 (Lag-3), and T-cell immunoglobulin and mucin-domain containing-3 (Tim-3) [381, 382]. Although they have different mechanisms of actions, engagement of most inhibitory receptors leads to TCR desensitisation and signal termination [172–174, 383, 384].

NFAT signalling also induces the expression of thymocyte selection-associated high mobility group box protein (Tox), a nuclear transcription factor that induces widespread transcriptional and epigenetic changes associated with exhaustion [385–388]. High Tox expression is detectable as early as 4 days post chronic infection, and it promotes the expression of PD-1, Lag-3, and Tim-3 among other key markers of exhaustion, while suppressing the transcription of cytotoxic proteins and cytokines [387]. Consistent with the stability of the epigenetic signature of exhaustion, loss of Tox expression late in the course of exhaustion fails to rescue T cells [388]. Importantly, Tox induces its own transcription, and this positive feedback mechanism allows it to become independent of NFAT signalling [387]. A similar feed-forward loop has also been described for some inhibitory receptors. For example, PD-1 inhibits mTOR signalling and thus activates the transcription factor Forkhead box protein O1

(FoxO1), which in turn induces further PD-1 transcription and inhibits T-bet expression [351]. Altogether, these mechanisms sustain and stabilise the exhaustion signature.

1.7.2 Maintenance of exhausted T cells

Although exhausted cells develop from memory precursors [389], they fail to acquire cardinal features of memory [342, 347, 348, 389, 390]. Nevertheless, exhausted T cells are a heterogenous pool of cells with different effector, proliferative, and cytotoxic capacities [391–393] (Fig. 8B). Interestingly, a precursor-product relationship has been identified between these exhausted subsets [394]. Progenitor cells express stem-cell markers including Tcf-1, Id-3, and c-Myb, and due to their upregulation of CD62L and CXCR5, they are able to home to specific locations within SLOs, where they can establish residence [355, 356, 393, 395–398]. This population undergoes antigen-induced proliferation [356, 392, 393], and with CD4+ T cell help, a subset of their progeny differentiates into effector cells that are responsible for clearing the infection or killing cancer cells [362, 399–401]. Although this transitory effector population expresses the inhibitory receptors PD-1 and Tim-3, it retains high levels of cytotoxic proteins and is marked by the expression of CX3CR1 [362, 399]. In addition, transitory cells upregulate $S1P_1$, and thus are able to egress lymphoid tissues and presumably target infected cells or infiltrate tumours [399]. However, persistent antigen exposure forces effector cells into terminal exhaustion and induces the upregulation of a second wave of inhibitory receptors, including CD101, CD200R and CD7R, loss of cytotoxicity, as well as the establishment of residency in non-lymphoid tissues [397, 399].

Differential expression of key transcription factors controls subset transitions [394]. Progenitor exhausted cells have high expression of Tcf-1, which induces Eomes and c-Myb expression and maintains the survival of this pool by driving Bcl-2 transcription [355, 399, 402]. Newly divided transitory cells lose Tcf-1 and Eomes, and instead express the transcription factor T-bet, which induces effector gene transcription [394]. Loss of Tox expression in this population further induces cytokine production and cytotoxicity [387, 394]. Persistent antigen exposure re-induces Tox, which transcriptionally silences T-bet as well as many effector genes [387, 388, 394]. Remarkably, the progenitor and the terminal exhaustion programs are co-regulated in chronic infection and in cancer [355, 403]. For example, by limiting persistent TCR signalling, PD-1 preserves the stability of progenitor cells [402, 404]. Additionally, Tox expression is critical for maintenance of this subset, because it directly activates Tcf-1 and

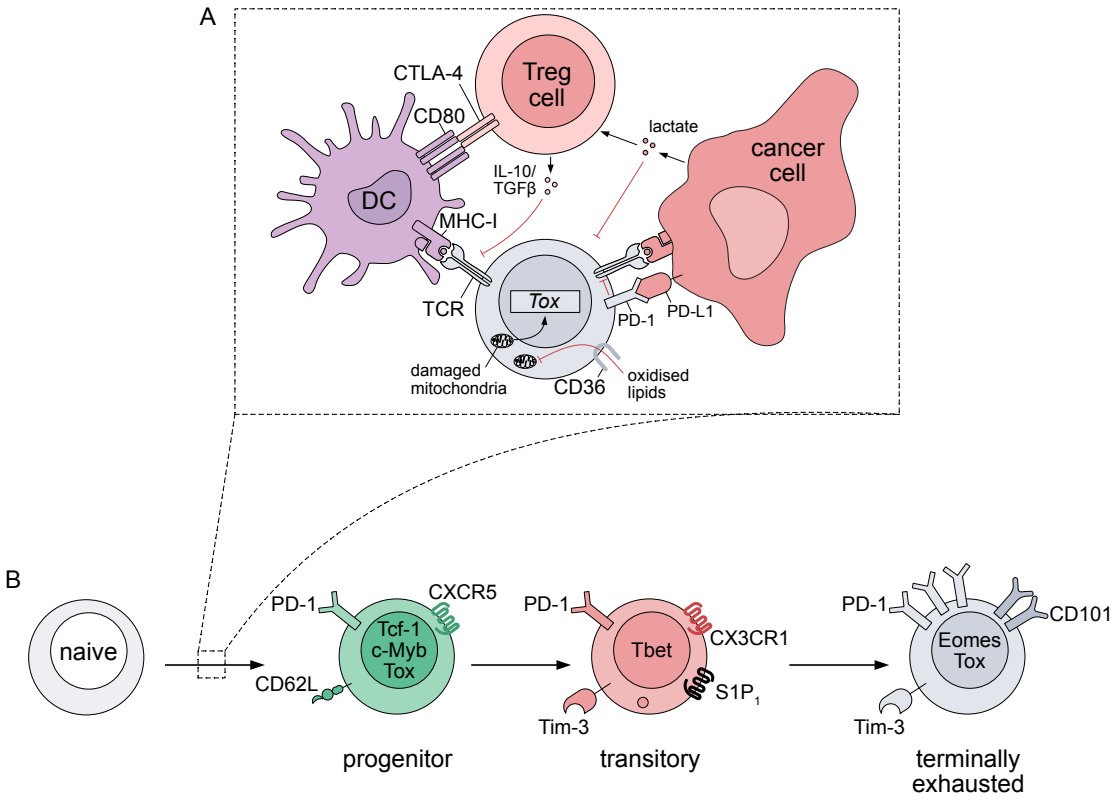

Figure 8: Induction and maintenance of T cell exhaustion

(A) In chronic infections and cancer, T cells gradually acquire an exhausted phenotype. Sustained antigen exposure, especially in the presence of inhibitory cytokines like IL-10 and TGFβ and in the absence of co-stimulatory signalling, leads to the upregulation of the transcription factor Tox, which initiates genome-wide epigentic modifications and upregulates several inhibitory receptors, including PD-1. Cancer cells express high levels of PD-L1 and thus inhibit T cell effector functions. Additionally, cancer cells secrete great quantities of lactate thus limiting IFNγ production in exhausted T cells while promoting regulatory T (Treg) cell expansion and suppressive function. Additionally, tumour infiltrating T cells express high levels of CD36 allowing them to accumulate oxidised lipids and depolarised mitochondria, which by itself precipitates T cell exhaustion.

(B) Exhausted T cells are maintained by a small number of progenitor exhausted cells, which express CXCR5 and CD62L and are resident in lymphoid tissues. Although these cells express Tox, they also express the stem cell transcription factors Tcf-1 and c-Myb and are therefore able to self-renew. A subset of their progeny egresses from lymphoid tissues and differentiates into a transitory cytotoxic population, which expresses a different set of chemokine receptors. Transitory cells downregulate Tox and upregulate the effector cell transcription factor T-bet. As a result, they are largely responsible for the residual function of the exhausted T cell pool. With persistent antigen exposure, however, transitory cells become terminally differentiated, re-upregulate Tox, and further upregulate several inhibitory receptors.

Eomes transcription [385, 387, 388], and loss of Tox induces T cell apoptosis and deletion of antigen-specific cells [386, 387]. In this way, a protracted immune response is maintained without fatal autoimmunity.

1.8 T cell-targeted immunotherapy

The cancer immunosurveillance hypothesis proposed that tumour-associated or neoantigens could be recognised by immune cells to induce a protective immune response [405, 406]. Conclusions made from epidemiological studies and experiments in immunodeficient mouse strains provided support for this hypothesis, which was later integrated in a more comprehensive view of cancer development referred to as cancer immunoediting [407]. In this model, the process of carcinogenesis proceeds in three stages: 1) elimination: immune cells kill transformed and pre-malignant cells, 2) equilibrium: immune cells fail to completely eradicate transformed cells but manage to limit their outgrowth, and 3) escape: cancer cells acquire mutations that allow them to rapidly grow and suppress immune responses [408]. Therefore, a central prediction of the cancer immunoediting hypothesis is that the immune system could be leveraged to treat cancer.

Most immunotherapeutic approaches aim at either re-activating the endogenous T cell response or transplanting effector T cells that were expanded and/or manipulated *ex vivo*. Immune checkpoint blockade (ICB) falls in the first category while adoptive T cell therapy (ACT) and chimeric antigen receptor (CAR) T cells belong to the second group [409].

ICB refers to the use of blocking antibodies against inhibitory receptors expressed by exhausted CD8+ T cells and/or regulatory T cells. Consistent with its role in terminating TCR and dampening costimulatory signalling (see section 1.4 and Fig. 4), antibodies against CTLA-4 have shown great success in preclinical cancer models [410] and in patients with melanoma [411–413], and are currently approved for late-stage, metastatic, unresectable melanoma [414]. The therapeutic effect of the anti-CTLA-4 antibody is dependent on CD8+ T cells [415], but was shown to additionally induce regulatory T cell depletion through antibody-dependent cell-mediated cytotoxicity [416]. However this effect was not observed in humans [417]. The other checkpoint molecule commonly targeted for therapy is PD-1, which is highly expressed by exhausted T cells [418]. Cancer cells express high levels of PD-L1 and can be induced to further upregulate it following IFNγ exposure [419–421]. In addition, im-

munosuppressive cells in the tumour microenvironment express PD-L1 [422, 423]. Treatment with antibodies targeting the PD-1 axis limits tumour growth [420, 424] and achieves better response rates than treatment with anti-CTLA-4 antibodies [425–427]. PD-1/PD-L1 blocking antibodies induce a brief burst of proliferation that is largely due to the expansion of progenitor exhausted cells [362, 393, 399, 428]. However, this population contracts over time with continued therapy [428, 429]. Furthermore, the epigenetic profile of exhausted cells does not change with PD-1 blockade [345, 349], suggesting that responding patients either manage to control tumour growth within the initial proliferation burst or have newly primed T cells [430]. Blocking antibodies against other inhibitory receptors are under clinical investigation [431]. Because an exhausted T cell expresses several immune checkpoints with non-redundant functions, combinatorial blockade of two, or more, inhibitory receptors provides synergistic improvement of T cell function [340].

Instead of attempting to rejuvenate endogenous T cells, ACT relies on the transfer of exogenously activated, cytotoxic T cells [432]. This approach stems from the early observation that allogenic bone marrow transplantation results in a strong graft-versus-leukaemia effect [433]. In one strategy, tumour-infiltrating lymphocytes (TILs) are isolated from resected tumours and are expanded *ex vivo*, where they are relieved from tumour-induced suppression. Large numbers of these TILs are then transferred back to the patient [434–436]. This methodology could be further refined by selecting for T cells that recognise tumour-derived antigens or neoantigens [437], or by transducing cells with TCRs that recognise said targets [438]. Extending this paradigm, CAR T cells are engineered to express chimeric receptors that recognise antigens in an MHC-independent fashion [439]. By linking the variable chains of an antibody to CD3ζ and the cytoplasmic domains of one or more co-stimulatory receptors, CAR T cells maintain reactivity against cancer cells that downregulate MHC expression [440–442].

An important consideration in ACT strategies is the differentiation state of the T cell to be transferred. Durable response correlates with the abundance of less differentiated, stem-cell like cells in the infused TIL product [443]. Similarly, the success of CAR T cell therapy relies on the persistence of transferred T cells [444], and this feature is largely influenced by cell culture conditions [445]. IL-2 is commonly used because it enhances effector cell cytotoxicity [435, 436], but it also induces terminal effector differentiation and activation-induced cell death [132, 133, 446, 447]. In contrast, using memory cell homeostatic cytokines, like IL-15, to skew T cell differentiation towards the stem-cell or central memory phenotype greatly improves T

cell and CAR T cell persistence *in vivo*, but at the cost of their cytotoxic effector functions [448–451]. Furthermore, memory cells rapidly acquire the exhausted phenotype of endogenous T cells [452], underscoring the requirement for balancing T cell stemness and function to achieve durable tumour control.

2 Aim of the work

Despite the impressive success of immunotherapy in cancer, fewer than 50% of patients have durable responses [453]. The reduced persistence of transferred T cells and their rapid exhaustion, which becomes refractory to rejuvenation, are major causes of therapy resistance and tumour relapse. Additionally, fundamental questions regarding memory T cell development and homeostasis remain open.

2.1 Investigating approaches to enhance anti-tumour immunity

Response to ICB and ACT is largely dependent on the stem cell-like progenitor subset that is either infused or targeted by the administered antibodies. This population shares, at least some, features with TCM cells, but is rapidly converted to terminally exhausted cells that have desensitised TCRs. In contrast, TCM cells are self-renewing, long-lived, and have enhanced antigen sensitivity.

The central aim of the current work is to transfer knowledge from TCM cell biology to the realm of cancer immunotherapy. In particular, changes that correspond to functional avidity maturation of TCM cells were investigated to balance T cell persistence and cytotoxic function. Towards this aim, memory cells developing after acute LCMV infection were analysed using flow cytometry, which was complemented with high-throughput sequencing analyses. Using an *in vitro* T cell differentiation approach, the phenotypic, metabolic, and functional features of modified T cells were investigated before testing their anti-tumour potential in a syngeneic melanoma mouse model.

2.2 Identifying the source of IL-15 for memory T cell homeostasis

All memory T cell subsets, and especially TEM cells, rely on IL-15 signalling for long-term survival. Its function was demonstrated using mice with germline loss of IL-15 signalling or mice that were systemically treated with anti-IL-15 antibodies. However, IL-15 is constitutively expressed by many haematopoietic and non-haematopoietic cells, and acts through direct cell-to-cell contact. The second aim of this study was to investigate the relevant cellular source of IL-15 for memory T cell maintenance. For this purpose, different mouse strains with cell type-specific deletion of *Il15* were acutely infected with LCMV and the mature circulating memory

population was analysed using flow cytometry.

2.3 Factors controlling lung TRM cell differentiation

TRM cells in many non-lymphoid tissues establish life-long residence. However, lung TRM cells are notoriously short-lived, which possibly accounts for the waning cellular immunity against respiratory infections. Using a mouse model of influenza infection, factors controlling the differentiation of lung TRM cells were investigated in several genetically modified mouse strains. In addition, findings were extended to TRM cells in the liver, which is a generally immuno-tolerant organ.

Altogether, the current work investigated questions pertaining to the three memory T cell subsets (Fig. 9). The first aim is discussed in the main body of this thesis, while the second and third aims are discussed in Appendix I and II, respectively.

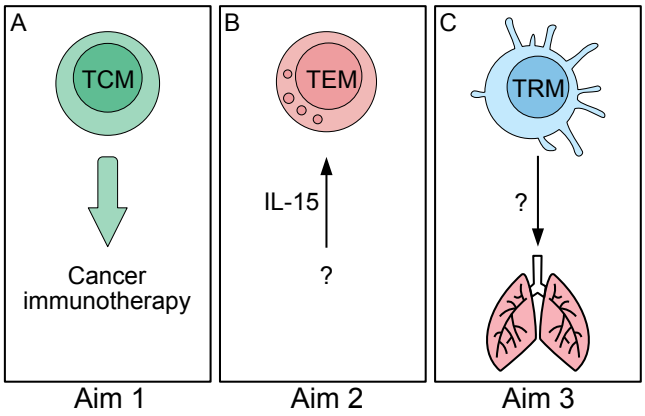

Figure 9: Aim of the work

The current study investigated three questions pertaining to basic memory cell biology and cancer immunotherapy.

(A) The central aim of this work was to induce TCM-like phenotypic changes in T cells expanded *in vitro* to enhance their anti-tumour function in a pre-clinical melanoma mouse model.

(B) The second question was concerned with the identity of cells secreting IL-15 following the resolution of infection. These cells would be largely responsible for homeostatic maintenance of all memory T cell subsets and TEM cells in particular.

(C) The third question investigated factors contributing to the development and maintenance of lung TRM cells. To address this question, several genetically modified mouse strains were infected with recombinant influenza virus and findings were later extended to TRM cells in other tissues.

3 Materials

3.1 Biological material

3.1.1 Mouse strains

Table 1: Mouse strains

Short name	Full name	Provider/Ref	Identifier
B6	C57BL/6N	Janvier	
P14	Tg(TcrLCMV)327Sdz	[454]	MGI:2665105
CD4-Cre	Tg(Cd4-cre)1Cwi/BfluJ	[455]	017336
FoxP3^{Cre}	B6.129(Cg)-Foxp3$^{tm4(YFP/icre)Ayr}$/J	The Jackson Laboratory, [456]	MGI:J:134513
Il15$^{-/-}$	C57BL/6N-Il15$^{1a(EUCOMM)Hmgu}$	MRC Harwell, [260]	MGI:4455931
Il15$^{Fl/Fl}$	C57BL/6N-Il15$^{tm1c(EUCOMM)Hmgu}$	MRC Harwell	EM:10738
Mck^{Cre}	B6.FVB(129S4)-Tg(Ckmm-cre)5Khn/J	The Jackson Laboratory, [457]	MGI:J:51266
Cmv^{Cre}	B6.C-Tg(CMV-cre)1Cgn/J	The Jackson Laboratory, [458]	MGI:J:75204
Stat6 KO	B6.129S2(C)-Stat6^{tm1Gru}/J	The Jackson Laboratory, [459]	MGI:J:31932
Il4$^{Fl/Fl}$ *x* *Il13*$^{Fl/Fl}$	B6.129P2(Cg)-Il4/Il13$^{tm1.1Lky}$/J	The Jackson Laboratory, [460]	MGI:J:157129
LysM^{Cre}	B6.129P2-Lyz2$^{tm1(cre)Ifo}$/J	The Jackson Laboratory, [461]	MGI:J:67924

3.1.2 Viruses

All initial viral stocks were kind gifts from Prof. Dr. Susan Kaech (Salk Institute for Biological Sciences, La Jolla, CA, USA).

Table 2: Viral strains

Virus	Reference
LCMV Armstrong (Arm)	[462]
LCMV clone 13 (cl-13)	[463]
Influenza A/X-31(H3N2)-GP33 (X31-GP33)	[464]
Influenza A/Puerto Rico/8/1934-GP33 (PR-GP33)	[464]

3.1.3 Mammalian cell lines and bacteria

Table 3: Cell lines and bacteria

Cells	Identifier	Provided by
B16.F10.$gp_{33\text{-}41}$ (GP33)		Prof. Dr. Hanspeter Pircher, Max Planck Institut für Immunbiologie und Epigenetik, Freiburg, Germany
BHK		Prof. Dr. Susan Kaech, Salk Institute for Biological Sciences, La Jolla, CA, USA
Vero		
HEK293T		
Subcloning Efficiency™ DH5α Competent Cells	18265017	Thermo Fisher Scientific (Waltham, MA, USA)

3.2 Chemicals and reagents

Anesthetic drugs (ketamine, xylazine, and isofluran) were acquired from the German Cancer Research Centre's narcotics pharmacy.

Table 4: Chemicals and solutions

Chemical/reagent	Company	Identifier
^{13}C-glucose	Sigma-Aldrich/ Merck KGaA (Darmstadt, Germany)	389374
^{13}C-glutamine	Sigma-Aldrich/ Merck KGaA (Darmstadt, Germany)	605166

1-StepTM Turbo TMB-ELISA Substrate Solution	Thermo Fisher Scientific (Waltham, MA, USA)	34022
2-Deoxy-D-glucose (2-DG)	Cayman Chemical (Ann Arbor, MI, USA)	14325-5
2-(N-[7-nitrobenz-2-oxa-1,3-diazol-4-yl]amino)-2-deoxyglu-cose (2-NBDG)	Cayman Chemical (Ann Arbor, MI, USA)	11 046
30% Acrylamide/Bis Solution, 29:1	Serva (Heidelberg, Germany)	10687.01
4,4-difluoro-5,7-dimethyl-4-bora-3a,4a-diaza-s-indacene-3-hexadecanoic acid (Bodipy C16)	Thermo Fisher Scientific (Waltham, MA, USA)	D3821
4x Laemmli Sample Buffer	Bio-Rad Laboratories (Hercules, CA, USA)	1610747
6x Orange DNA Loading Dye	Thermo Fisher Scientific (Waltham, MA, USA)	R0631
Agarose	Sigma-Aldrich/ Merck KGaA (Darmstadt, Germany)	A9539-500G
All-*trans*-retinoic acid (ATRA)	Sigma-Aldrich/ Merck KGaA (Darmstadt, Germany)	R2625-100MG
Ammonium Persulfate (APS)	Bio-Rad Laboratories (Hercules, CA, USA)	161-0700
AMPure XP beads	Beckman Coulter (Brea, CA, USA)	A63880
Antimycin A (AA)	Sigma-Aldrich/ Merck KGaA (Darmstadt, Germany)	A8674
AS1517499	Axon Medchem (Groningen , Netherlands)	1992
AS605240	Echelon Biosciences (Salt Lake City, UT, USA)	B-0301

BioColl® cell separating solution (Density 1.077 g/ml, isotonic)	Bio & SELL GmbH (Feucht, Germany)	L 6115
Bovine Serum Albumin (BSA)	Sigma-Aldrich/ Merck KGaA (Darmstadt, Germany)	A9647
BPTES	Bio-techne/ Tocris (Bristol, UK)	5301
Brefeldin A Solution	Biolegend (San Diego, CA, USA)	420601
Carbonyl cyanide 4-(trifluoromethoxy) phenylhydrazone (FCCP)	Cayman Chemical (Ann Arbor, MI, USA)	15218-50
Clarity™ Western ECL Substrate	Bio-Rad Laboratories (Hercules, CA, USA)	1705060S
Coomassie Brilliant Blue R-250 Destaining Solution	Bio-Rad Laboratories (Hercules, CA, USA)	1610438
Coomassie Brilliant Blue R-250 Staining Solution	Bio-Rad Laboratories (Hercules, CA, USA)	1610436
Crystal Violet	TCS Biosciences (Buckingham, UK)	HD1295-25
Cyclosporin A	Santa Cruz Biotechnology (Santa Cruz, CA, USA)	sc-3503
D-(+)-Glucose solution	Sigma-Aldrich/ Merck KGaA (Darmstadt, Germany)	G8769
Dialyzed Fetal Bovine Serum	Sigma-Aldrich/ Merck KGaA (Darmstadt, Germany)	F0392-100ML
Digitonin	Sigma-Aldrich/ Merck KGaA (Darmstadt, Germany)	D141-500MG
eBioscience™ Foxp3 / transcription factor staining buffer set	Thermo Fisher Scientific (Waltham, MA, USA)	00-5523-00
Fetal bovine serum (FBS)	Sigma-Aldrich/ Merck KGaA (Darmstadt, Germany)	F0804
Fluoromount™ Aqueous Mounting Medium	Sigma-Aldrich/ Merck KGaA (Darmstadt, Germany)	F4680-25ML

Fixation Buffer	BioLegend (San Diego, CA, USA)	420801
G418 sulphate	Karl Roth (Karlsruhe, Germany)	239.3
Gene Ruler 1 kb plus	Thermo Fisher Scientific (Waltham, MA, USA)	SM1333
Gibco® 0,25% Trypsin-EDTA (1X)	Thermo Fisher Scientific (Waltham, MA, USA)	25200-055
Gibco® 2-Mercaptoethanol (1000X)	Thermo Fisher Scientific (Waltham, MA, USA)	21985-023
Gibco® ACK Lysis Buffer	Thermo Fisher Scientific (Waltham, MA, USA)	A10492-01
Gibco® DMEM (1X) (4,5 g/l D-Glucose, L-Glutamine, no pyruvate)	Thermo Fisher Scientific (Waltham, MA, USA)	41965-039
Gibco® DPBS (1X)	Thermo Fisher Scientific (Waltham, MA, USA)	14040-091
Gibco® MEM NEAA (100X)	Thermo Fisher Scientific (Waltham, MA, USA)	11140050
Gibco® Opti-MEM™ I Reduced Serum Medium	Thermo Fisher Scientific (Waltham, MA, USA)	31985062
Gibco® Penicillin-Streptomycin (Pen Strep)	Thermo Fisher Scientific (Waltham, MA, USA)	14140-122
Gibco® RPMI Medium 1640	Thermo Fisher Scientific (Waltham, MA, USA)	21875-034
Guanidinium thiocyanate	Sigma-Aldrich/ Merck KGaA (Darmstadt, Germany)	G9277-100G
Histopaque-1077	Sigma-Aldrich/ Merck KGaA (Darmstadt, Germany)	10771
Invitrogen™ CellTrace™ Violet Cell Proliferation Kit, for flow cytometry	Thermo Fisher Scientific (Waltham, MA, USA)	C34557
Invitrogen™ Permeabilization Buffer 10X	Thermo Fisher Scientific (Waltham, MA, USA)	00-8333-56

Ionomycin	Sigma-Aldrich/ Merck KGaA (Darmstadt, Germany)	10634-1MG
L-Glutamine solution	Sigma-Aldrich/ Merck KGaA (Darmstadt, Germany)	G7513-100ML
Live/dead fixable dead cell stain kit	Thermo Fisher Scientific (Waltham, MA, USA)	L23102
Magnesium Chloride ($MgCl_2$)	Sigma-Aldrich/ Merck KGaA (Darmstadt, Germany)	M8266
N,N-Dimethylformamide	Sigma-Aldrich/ Merck KGaA (Darmstadt, Germany)	227056-1L
NP-40 Surfact-Amps™ Detergent Solution ™	Thermo Fisher Scientific (Waltham, MA, USA)	85124
Oligomycin	Merck Millipore (Burlington, MA, USA)	495455-10mg
PageRuler™ Prestained Protein Ladder	Thermo Fisher Scientific (Waltham, MA, USA)	26616
Paraformaldehyde	Thermo Fisher Scientific (Waltham, MA, USA)	02-003-576
Percoll™	GE Healthcare (Chalfont, UK)	17-0891-01
PMA (Phorbol 12-myristate 13-acetate)	Sigma-Aldrich/ Merck KGaA (Darmstadt, Germany)	P8139-1MG
Poly D-Lysine	Merck Millipore (Burlington, MA, USA)	A-003-E
Protein A/G PLUS-Agarose	Santa Cruz Biotechnology (Santa Cruz, CA, USA)	sc-2003
Rapamycin	Enzo Life Sciences	BML-A275-0005
RIPA Lysis Buffer System	Santa Cruz Biotechnology (Santa Cruz, CA, USA)	sc-24948
Rotenone (Rot)	Cayman Chemical (Ann Arbor, MI, USA)	13995-5
RPMI 1640 (no L-Glutamine, no D-Glucose)	Biological Industries (Beit HaEmek, Israel)	01-101-1A

sch772984	TargetMol Chemicals (Wellesley Hills, MA, USA)	T6066
SeaKem® ME Agarose	Lonza (Basel, Switzerland)	50014
Skimmed milk powder	GERBU Biotechnik (Heidelberg, Germany)	16020500
Sodium Azide (NaN_3)	Sigma-Aldrich/ Merck KGaA (Darmstadt, Germany)	S2002-5G
Sodium Chloride (NaCl)	Sigma-Aldrich/ Merck KGaA (Darmstadt, Germany)	S9888
Sucrose	Sigma-Aldrich/ Merck KGaA (Darmstadt, Germany)	1008925000
SYBER safe DNA stain	Thermo Fisher Scientific (Waltham, MA, USA)	S33102
SYBR ™ Green I nucleic acid	Thermo Fisher Scientific (Waltham, MA, USA)	S7563
T5224	Cayman Chemical (Ann Arbor, MI, USA)	22904
Tetramethylethane-1,2-diamine (TEMED)	Bio-Rad Laboratories (Hercules, CA, USA)	161-0801
Tissue-Tek OCT compound	Science Services (Munich, Germany)	SA62550-01
Triton™ X-100	Sigma-Aldrich/ Merck KGaA (Darmstadt, Germany)	X100-500ML
Trypan Blue solution	Sigma-Aldrich/ Merck KGaA (Darmstadt, Germany)	T81544-100ML
Trypton/Pepton aus Casein	Karl Roth (Karlsruhe, Germany)	8952.2
TWEEN® 20	Sigma-Aldrich/ Merck KGaA (Darmstadt, Germany)	9005-64-5
TWEEN® 80	Sigma-Aldrich/ Merck KGaA (Darmstadt, Germany)	P1754-1L
X-tremeGENE 9 DNA transfection reagent 1.0 ML	Sigma-Aldrich/ Merck KGaA (Darmstadt, Germany)	6365787001

XF Base Medium	Agilent Technologies (Santa Clara, CA, USA)	102353-100
XF Calibrant	Agilent Technologies (Santa Clara, CA, USA)	100840-000
Yeast extract, ultrapure	Gerbu Biotechnik GmbH (Heidelberg, Germany)	1133

3.3 Buffers and solutions

Where needed, de-ionised water was used to prepare or dilute buffers.

Table 5: Composition of home-made buffers and growth media

Buffer/Solution	Composition
1.0 M Tris-HCl buffer	1.0 M Tris base Water pH = 6.8
1.5 M Tris-HCl buffer	1.5 M Tris base Water pH = 8.8
ATAC 2x Transposition buffer	20 mM Tris-HCl pH 7.6 3 mM $MgCl_2$ 20% (v/v) Dimethyl Formamide Water
ATAC Lysis buffer	0.01% Digitonin (w/v) 1% (v/v) NP40 0.1% (v/v) Tween-20 Water
ATAC Resuspension buffer	10 mM Tris-HCl pH 7.4 10 mM NaCl 3 mM $MgCl_2$ Water

Complete DMEM	10% (v/v) FBS 1% (v/v) PenStrep 1% (v/v) NEAA DMEM
Complete RPMI	10% (v/v) FBS 1% (v/v) PenStrep 1% (v/v) NEAA 0.1% (v/v) 2-Mercaptoethanol RPMI 1640
ELISA Blocking buffer	1% (w/v) BSA PBS-T
ELISA Coating buffer	15 mM Na_2CO_3 30 mM $NaCO_3$ Water pH = 9.6
ELISA Stop solution	0.2 M H_2SO_4 Water
ELISA Wash buffer	PBS-T
FACS buffer	2% (v/v) FBS 0.2% (w/v) NaN_3 PBS
Freezing medium	10% (v/v) DMSO FBS
Lysogeny broth (LB) medium	1% (w/v) Tryptone/Peptone 0.5% (w/v) Yeast extract 0.17 M NaCl Water
MACS buffer	0.5% (v/v) FBS PBS
Minimal RPMI	10% (v/v) Dialyzed FBS 0.1% (v/v) 2-Mercaptoethanol RPMI 1640 (no L-Glutamine, no D-Glucose)

PBS-T	0.01% (v/v) Triton X-100 PBS
Plaque assay buffer	1% (w/v) Crystal violet 20% (v/v) Methanol Water
SDS running buffer	25 mM Tris 0.19 M Glycine 1% (w/v) SDS Water
SDS-PAGE Resolving gel (8%)	8% Acrylamide/Bis Solution 375 mM Tris-HCl pH 8.8 0.1% (w/v) SDS 0.1% (w/v) APS 0.04% (w/v) TEMED Water
SDS-PAGE Stacking gel (5%)	5% Acrylamide/Bis Solution 125 mM Tris-HCl pH 6.8 0.1% (w/v) SDS 0.1% (w/v) APS 0.04% (w/v) TEMED Water
TAE buffer	40 mM Tris Acetate 1 mM EDTA Water pH = 7.4
Western blot transfer buffer	25 mM Tris 190 mM Glycine 20% (v/v) Methanol Water

3.4 Kits

Table 6: Commercial kits

Kit name	Company	Identifier
CD4+ T cell Isolation Kit	Miltenyi Biotec (Bergisch Gladbach, Germany)	130-104-454
CD8+ T cell Isolation Kit	Miltenyi Biotec (Bergisch Gladbach, Germany)	130-104-075
Mouse IL-15 DuoSet ELISA	R&D systems (Minneapolis, MN, USA)	DY447
NAb™ Protein G Spin Kit	Thermo Fisher Scientific (Waltham, MA, USA)	89979
Pierce™ F(ab')$_2$ preparation kit	Thermo Fisher Scientific (Waltham, MA, USA)	44988
Pierce™ BCA™ Protein Assay kit	Thermo Fisher Scientific (Waltham, MA, USA)	23225
Q5® Site-Directed Mutagenesis Kit	New England Biolabs (Ipswich, MA, USA)	E0554S
QIAGEN Plasmid Midi kit	Thermo Fisher Scientific (Waltham, MA, USA)	12143
QIAquick Gel extraction kit	Thermo Fisher Scientific (Waltham, MA, USA)	28704
QIAquick PCR purification kit	Thermo Fisher Scientific (Waltham, MA, USA)	28104
Qubit™ dsDNA HS and BR Assay Kits	Thermo Fisher Scientific (Waltham, MA, USA)	Q32851

3.5 Antibodies

Table 7: Fluorescently-labelled antibodies

Antibody	Clone	Dilution	Company	Identifier
AF488 anti-mouse cleaved caspase 3	Asp175	1:200	Cell Signaling Technology (Danvers, MA, USA)	9661S
AF488 anti-mouse TCF1/TCF7	C63D9	1:100	Cell Signaling Technology (Danvers, MA, USA)	6444S
AF488 Donkey anti-rabbit IgG	Poly4064	1:1000	BioLegend (San Diego, CA, USA)	406416
AF647 anti-mouse GzmB	GB11	1:200	BioLegend (San Diego, CA, USA)	515406
AF647 Donkey anti-rabbit IgG	Poly4064	1:1000	BioLegend (San Diego, CA, USA)	406414
APC anti-mouse CD103	2E7	1:400	BioLegend (San Diego, CA, USA)	121414
APC anti-mouse CD25	3C7	1:400	BioLegend (San Diego, CA, USA)	101910
APC anti-mouse CD98	REA861	1:200	Miltenyi Biotec (Bergisch Gladbach, Germany)	130-114-642
APC anti-mouse CXCR3	CXCR3-173	1:400	BioLegend (San Diego, CA, USA)	126512
APC anti-mouse CXCR6	SA051D1	1:400	Biolegend (San Diego, CA, USA)	151105
APC anti-mouse FoxP3	FJK-16s	1:100	Thermo Fisher Scientific (Waltham, MA, USA)	17-5773-82
APC anti-mouse Lag3	C9B7W	1:400	BioLegend (San Diego, CA, USA)	125210
APC anti-mouse Perforin	S16009A	1:400	Miltenyi Biotec (Bergisch Gladbach, Germany)	154303

APC anti-mouse/human CD11b	M1/70	1:400	BioLegend (San Diego, CA, USA)	101212
APC-Cy7 anti-mouse CD38	90	1:400	BioLegend (San Diego, CA, USA)	102728
APC-Cy7 anti-mouse CD4	GK1.5	1:400	Becton Dickinson (Franklin Lakes, NJ, USA)	552051)
APC-Cy7 anti-mouse CD8a	53-6.7	1:400	Becton Dickinson (Franklin Lakes, NJ, USA)	557654
APC-Cy7 anti-mouse CD90.2	30-H12	1:400	BioLegend (San Diego, CA, USA)	105328
APC-Cy7 anti-mouse Ly-6G/Ly-6C (Gr-1)	RB6-8C5	1:400	BioLegend (San Diego, CA, USA)	108424
APC-Cy7 anti-mouse/human CD44	IM7	1:400	BioLegend (San Diego, CA, USA)	103028
APC-Fire750 anti-mouse GzmB	QA16A02	1:400	Biolegend (San Diego, CA, USA)	372210
BV421 anti-human CD45RO	UCHL1	1:400	BioLegend (San Diego, CA, USA)	304216
BV421 anti-mouse CD4	GK1.5	1:400	BioLegend (San Diego, CA, USA)	562891
BV421 anti-mouse CD45.1	A20	1:400	BioLegend (San Diego, CA, USA)	110732
BV421 anti-mouse Tim3	B8.2C12	1:400	BioLegend (San Diego, CA, USA)	134019
BV421 Donkey anti-rabbit IgG	Poly4064	1:1000	BioLegend (San Diego, CA, USA)	406410
BV421 Strep-tavidin		1:1000	BioLegend (San Diego, CA, USA)	B285222

BV650 anti-mouse CD45.2	104	1:400	BioLegend (San Diego, CA, USA)	109836
BV650 anti-mouse CD62L	MEL-14	1:400	BioLegend (San Diego, CA, USA)	104453
BV711 anti-mouse CD45	30-F11	1:1000	BioLegend (San Diego, CA, USA)	103147
BV711 anti-mouse CD45.1	A20	1:400	BioLegend (San Diego, CA, USA)	110739
BV711 anti-mouse CD103	2E7	1:400	BioLegend (San Diego, CA, USA)	121435
eFluor 660 anti-mouse T-bet	eBio4B10	1:200	Thermo Fisher Scientific (Waltham, MA, USA)	50-5825-82
FITC anti-human CD62L	DREG-56	1:400	BioLegend (San Diego, CA, USA)	304838
FITC anti-mouse CD122	TM-β1	1:200	Miltenyi Biotec (Bergisch Gladbach, Germany)	130-102-481
FITC anti-mouse CD4	GK1.5	1:200	BioLegend (San Diego, CA, USA)	100406
FITC anti-mouse CD71	RI7217	1:400	BioLegend (San Diego, CA, USA)	113806
FITC anti-mouse CD8b	YTS156.7.7	1:200	BioLegend (San Diego, CA, USA)	126606
FITC anti-mouse CD69	H1.2F3	1:100	Miltenyi Biotec (Bergisch Gladbach, Germany)	130-103-983
FITC anti-mouse CX3CR1	SA011F11	1:200	BioLegend (San Diego, CA, USA)	149020
FITC anti-mouse KLRG1	2F1/KLRG1	1:200	BioLegend (San Diego, CA, USA)	138410
FITC anti-mouse TCR-vα2	B20.1	1:200	BioLegend (San Diego, CA, USA)	127806
FITC anti-mouse TNF-α	MP6-XT22	1:100	Miltenyi Biotec (Bergisch Gladbach, Germany)	130-102-294

FITC Streptavidin		1:1000	BioLegend (San Diego, CA, USA)	B252409
PE anti-mouse CD127	mIL4R-M1	1:400	Becton Dickinson (Franklin Lakes, NJ, USA)	561695
PE anti-mouse CD39	Duha59	1:400	BioLegend (San Diego, CA, USA)	143804
PE anti-mouse CD8b	YTS156.7.7	1:200 (IV)	BioLegend (San Diego, CA, USA)	126608
PE anti-mouse Eomes	REA116	1:100	Miltenyi Biotec (Bergisch Gladbach, Germany)	130-102-419
PE anti-mouse ID3	S30-778	1:400	BioLegend (San Diego, CA, USA)	564564
PE anti-mouse IL-7Rα	A7R34	1:400	BioLegend (San Diego, CA, USA)	135010
PE anti-mouse TIGIT	1G9	1:400	BioLegend (San Diego, CA, USA)	142104
PE anti-mouse TNF-α	MP6-XT22	1:400	BioLegend (San Diego, CA, USA)	506306
PE anti-mouse/rat/human CD27	LG.3A10	1:400	BioLegend (San Diego, CA, USA)	124209
PE-Cy7 anti-mouse CD62L	MEL-14	1:400	BioLegend (San Diego, CA, USA)	104418
PE-Cy7 anti-mouse CD69	H1.2F3	1:400	BioLegend (San Diego, CA, USA)	104512
PE-Cy7 anti-mouse IFN-γ	XMG1.2	1:400	BioLegend (San Diego, CA, USA)	505826
PE-Cy7 anti-mouse Ki67	REA183	1:200	Miltenyi Biotec (Bergisch Gladbach, Germany)	130-120-419
PE-Cy7 anti-mouse KLRG1	2F1/KLRG1	1:400	BioLegend (San Diego, CA, USA)	138416

PE-Cy7 anti-mouse PD-1	29F.1A12	1:400	BioLegend (San Diego, CA, USA)	135216
PE-Vio770 anti-mouse Bcl2	REA356	1:200	Miltenyi Biotec (Bergisch Gladbach, Germany)	130-105-475
PerCP anti-human CD3	OKT-3	1:200	BioLegend (San Diego, CA, USA)	317306
PerCP anti-human CD8a	HIT8a	1:200	BioLegend (San Diego, CA, USA)	300922
PerCP-Cy5.5 anti-mouse CD8a	53-6.7	1:200	BioLegend (San Diego, CA, USA)	100734
PerCP-Cyanine5.5 anti-mouse CD8b	YTS156.7.7	1:200	BioLegend (San Diego, CA, USA)	126610
PerCP-Vio700 anti-mouse CD45.2	104-2	1:200	Miltenyi Biotec (Bergisch Gladbach, Germany)	130-103-787
VioBright FITC anti-mouse Tim3	REA602	1:100	Miltenyi Biotec (Bergisch Gladbach, Germany)	130-120-823

Table 8: Biotin- and HRP-conjugated antibodies

Antibody	**Clone**	**Dilution**	**Company**	**Identifier**
Biotin-Goat anti-rat IgG Fab Secondary Antibody		1:500	Thermo Fisher Scientific (Waltham, MA, USA)	PA1-29634
HRP Donkey anti-rabbit IgG	Poly4064	1:500	BioLegend (San Diego, CA, USA)	406401
HRP Goat anti-mouse IgG	Poly4053	1:5000	BioLegend (San Diego, CA, USA)	405306

Table 9: Unconjugated antibodies

Antibody	Clone	Dilution	Company	Identifier
Anti-mouse CD8a	53-6.7	10 µg/mL	BioLegend (San Diego, CA, USA)	100763
Anti-mouse STAT6 (phospho Y641)	polyclonal	1:1000	Abcam (Cambridge, UK)	ab28829
*InVivo*MAb anti-mouse PD-L1 (B7-H1)	10F.9G2	200 µg/ mouse	Bio X Cell (NH, USA)	BE0101
*InVivo*MAb rat IgG2b isotype control, anti-keyhole limpet hemocyanin	LTF-2	200 µg/ mouse	Bio X Cell (NH, USA)	BE0090
Purified anti-mouse CD185 (CXCR5)	L138D7	1:500	BioLegend (San Diego, CA, USA)	145502
Rabbit anti-mouse Phospho-Lck (Tyr505)	polyclonal	1:200 (FACS)	Cell Signaling Technology (Danvers, MA, USA)	2751S
Rabbit anti-mouse Phospho-Zap-70 (Tyr319)/Syk (Tyr352)	monoclonal	1:200 (FACS)	Cell Signaling Technology (Danvers, MA, USA)	2717S
Rat anti-mouse CD8a	4SM15	1:200	Thermo Fisher Scientific (Waltham, MA, USA)	14-0808-82
Ultra-LEAF™ Purified anti-mouse CD16/32	93	1:400	BioLegend (San Diego, CA, USA)	101330

Ultra-LEAF™ Purified anti-mouse CD28	E18	0.2 - 0.5 µg/mL	BioLegend (San Diego, CA, USA)	122022
Ultra-LEAF™ Purified anti-mouse CD3	17A2	0.2 - 1 µg/mL	BioLegend (San Diego, CA, USA)	100238
Ultra-LEAF™ Purified anti-mouse CD3ε	145-2C11	0.2 - 1 µg/mL	BioLegend (San Diego, CA, USA)	100340

3.6 Peptides, enzymes, and cytokines

Lyophilised recombinant cytokines were reconstituted in sterile 0.1% BSA (w/v) in de-ionised water and were stored at -20 °C.

Table 10: Peptides, enzymes, and cytokines

Item	Company	Identifier
5x Taq Master Mix	New England Biolabs (Ipswich, MA, USA)	M0285L
AsiSI	New England Biolabs (Ipswich, MA, USA)	R0630L
Collagenase D	Sigma-Aldrich/ Merck KGaA (Darmstadt, Germany)	11088882001
Dnase I	Sigma-Aldrich/ Merck KGaA (Darmstadt, Germany)	D4527
GP_{33-41} (GP33)	GenScript (Piscataway Township, NJ, USA)	RP20091
MluI	New England Biolabs (Ipswich, MA, USA)	R0198L
NEBNext High Fidelity 2x Master Mix	New England Biolabs (Ipswich, MA, USA)	M0541L
Recombinant Human TGF-β2 (Insect derived)	Peprotech (Rocky Hill, NJ, US)	100-35

Recombinant mouse IL-13	Peprotech (Rocky Hill, NJ, US)	210-13
Recombinant Mouse IL-15 (carrier-free)	BioLegend (San Diego, CA, USA)	566304
Recombinant Mouse IL-2 (carrier-free)	BioLegend (San Diego, CA, USA)	575408
Recombinant Mouse IL-4	Peprotech (Rocky Hill, NJ, US)	214-14
Tagment DNA Enzyme 1	Illumina (San Diego, CA, USA)	20034198

3.7 Consumables

Table 11: Disposable consumables

Item	Company	Identifier
Cellstar® White 96 Well Cell Culture Microplate	Greiner Bio-One (Kremsmünster, Austria)	655073
Costar® 50 ml Reagent Reservoir	Coring (Corning, New York, USA)	4870
Falcon™ 15 ml Polypropylene Conical Tube	Thermo Fisher Scientific (Waltham, MA, USA)	352096
Falcon™ 5 ml Polystyrene Round-Bottom Tube	Thermo Fisher Scientific (Waltham, MA, USA)	352054
Falcon™ 50 ml Polypropylene Conical Tube	Thermo Fisher Scientific (Waltham, MA, USA)	352070
Falcon™ Cell Strainer 70 µm Nylon	Thermo Fisher Scientific (Waltham, MA, USA)	352350
LS colums	Miltenyi Biotec (Bergisch Gladbach, Germany)	130-042-401
Micro sample tube Citrate 3.2%, venous blood collection	SARSTEDT (Nümbrecht, Germany)	41.1506
NORM-JECT®-F Luer Solo Syringe	B.Braun (Melsungen, Germany)	NJ-9166017
Nylon Mesh SEFAR NITEX	Sefar (Edling, Germany)	3A03-0150-115-00

Pierce™ Blotting Paper	Thermo Fisher Scientific (Waltham, MA, USA)	LC2010
PVDF membrane	Santa Cruz Biotechnology (Santa Cruz, CA, USA)	sc-358811
Safe Lock Tube 1.5 ml	Eppendorf (Hamburg, Germany)	30120086
Safe Lock Tube 2 ml	Eppendorf (Hamburg, Germany)	30120094
Safe Lock Tube 5 ml	Eppendorf (Hamburg, Germany)	30119487
Seahorse XFe96 FluxPak	Agilent Technologies (Santa Clara, CA, USA)	102416-100
SuperFrost® Plus glass microscopic slides	Thermo Fisher Scientific (Waltham, MA, USA)	630-0950
TipOne 10 µl Graduated Tip	StarLab (Hamburg, Germany)	S1111-3700
TipOne 1000 µl Graduated Tip	StarLab (Hamburg, Germany)	S1111-6701
TipOne 200 µl Yellow Tip	StarLab (Hamburg, Germany)	S1111-0706
Zellkulturflasche 75cm^2	Techno Plastic Products TPP (Trasadingen, Switzerland)	90076
Zellkulturtestplatte 6 Well	Techno Plastic Products TPP (Trasadingen, Switzerland)	92006
Zellkulturtestplatte 96U Well	Techno Plastic Products TPP (Trasadingen, Switzerland)	92697

Table 12: Reusable consumables

Item	**Company**	**Identifier**
Counting chamber BLAUBRAND® Neubauer pattern, w/o clips double ruling	Brand (Wertheim, Germany)	718605
Digital caliber	Tesa technology (Renens, Switzerland)	725202

Mr. Frosty™ Freezing Container	Thermo Fisher Scientific (Waltham, MA, USA)	5100-0001

3.8 Machines and instruments

Table 13: Machines and instruments

Instrument	Company
Block heater SBH130D	Cole-Parmer (Staffordshire, UK)
Cell incubator Heraeus Hera cell 150	Thermo Fisher Scientific (Waltham, MA, USA)
Centrifuge 5415R (for 24 tubes)	Eppendorf (Hamburg, Germany)
Centrifuge 5810R	Eppendorf (Hamburg, Germany)
Centrifuge 5920R	Eppendorf (Hamburg, Germany)
CFX Duet Real-Time PCR system	Bio-rad (Hercules, CA, USA)
Electrophoresis Power supply E864	Consort (Turnhout, Belgium)
FACSAria™ flow cytometer	Becton Dickinson (Franklin Lakes, NJ, USA)
FACSAria™ Fusion flow cytometer	Becton Dickinson (Franklin Lakes, NJ, USA)
FACSCanto™ II flow cytometer	Becton Dickinson (Franklin Lakes, NJ, USA)
Hearaeus Pico17 (for 24 tubes)	Thermo Fisher Scientific (Waltham, MA, USA)
Horizon® 11.14 Gibco BRL Gel Electrophoresis Apparatus	Thermo Fisher Scientific (Waltham, MA, USA)
Leica CM 3050 S	Leica Camera (Wetzlar, Germany)
Leica CM1950	Leica Camera (Wetzlar, Germany)
LSR II flow cytometer	Becton Dickinson (Franklin Lakes, NJ, USA)
LSRFortessa™ flow cytometer	Becton Dickinson (Franklin Lakes, NJ, USA)
Mastercycler	Eppendorf (Hamburg, Germany)

Megafuge3.0RS	Heraeus (Hanau, Germany)
Microscope brightfield Nikon eclipse TS100	Nikon (Minato, Japan)
Microwave R-941STW	Sharp (Osaka, Japan)
Mini-PROTEAN® Tetra cell	Bio-Rad Laboratories (Hercules, CA, USA)
Molecular Imager GelDoc XR+	Bio-Rad Laboratories (Hercules, CA, USA)
Orion L Microplate Luminometer	Berthold Detection Systems (Pforzheim, Germany)
Oxion Inverso Camera	Euromex (Arnhem, The Netherlands)
peQPOWER	VWR (Radnor, DE, USA)
PH meter ProfiLine pH 3210	Consort (Turnhout, Belgium)
PowerPac	Bio-Rad Laboratories (Hercules, CA, USA)
Sartorius Analytic	Sartorius (Göttingen, Germany)
Sartorius Universal	Sartorius (Göttingen, Germany)
Seahorse XFe96 analyzer	Agilent (Santa Clara, CA, USA)
Shaker	Edmund Bühler (Bodelshausen, Germany)
Stirrer D-6010	NeoLab (Heidelberg, Germany)
T100™ Thermal Cycler	Bio-Rad Laboratories (Hercules, CA, USA)
Thermomixer compact	Eppendorf (Hamburg, Germany)
Vortexer Vortex Genie 2	Scientific industries (Bohemia, NY, USA)
VWR Digital Heatblock	VWR (Radnor, DE, USA)
Waterbath WNE 7	Memmert (Schwabach, Germany)
Zeiss Cell Observer	Zeiss Microscopy (Jena, Germany)
Zeiss LSM 710 ConfoCor 3	Zeiss Microscopy (Jena, Germany)

3.9 Software

Table 14: Software and web-based platforms

Software/Platform	**Company/Reference**
Affinity designer 1.9.2	Serif (West Bridgford, UK)
DExSI	[465]

EndNote X.9	Thomson Reuters (Toronto, Canada)
FACS Diva™	Becton Dickinson (Franklin Lakes, NJ, USA)
FlowJo V10.1	Becton Dickinson (Franklin Lakes, NJ, USA)
Graph Pad Prism 9	GraphPad Software (San Diego, CA, USA)
ImageJ 1.52a	NIH (Bethesda, MD, USA)
Jupyter notebook	The Jupyter community on GitHub
Microsoft Office Professional Plus 2013	Microsoft (Redmond, WA, USA)
Rstudio Workbench 1.4.1103	Rstudio (Boston, MA, USA)
SnapGene® Viewer 5.1.4.1	SnapGene (Chicago, IL, USA)
Wave 2.6.0	Agilent (Santa Clara, CA, USA)

3.10 Sequencing datasets

Table 15: ATAC-seq and ChIP-seq datasets

Data	Code	Reference
P14 cells isolated from the spleen or IEL on day 7 after LCMV infection	GSE107373	[466]
FoxP3+ and FoxP3- cells isolated from spleen or CNS of mice with experimental auto-immune encephalitis (EAE)	GSE121764	[467]
P14 and OT1 cells isolated from B16-Ova melanoma tumours	GSE93013	[468]
Mouse lung-resident P14 cells isolated on day 8 after X31-GP33 infection		this work
Mouse naïve splenic circulating P14 cells		this work
Stat6 ChIPseq of mouse peritoneal macrophages treated for 1h with IL-4	GSE134167	[469]

Table 16: Bulk RNA-seq and microarray datasets

Data	Code	Reference
Human CD8+ T cells collected from blood or epidermis	GSE83637	[470]
T cells isolated from the spleen of mice infected with *Listeria monocytogenes*	GSE89307	[452]
T cells isolated from the liver of mice with liver cancer	GSE89307	[452]
Human CD8+ T cells collected from non-small cell lung cancers and surrounding normal tissues	GSE90730	[471]
Human CD8+ T cells collected from spleen or lung	GSE94964	[472]
Antigen-specific CD8+ tissue memory T cells isolated 30 - 60 days post-infection	GSE47045	[225]

Table 17: Single-cell RNA-seq (scRNA) datasets

Data	Code	Reference
Human CD45+ cells isolated from melanoma patients	GSE120575	[473]
Human peripheral blood regulatory T cells	GSE175604	[474]
ILC2 cells isolated from different organs of ILC2 reporter mice	GSE117567	[475]
Mouse lung endothelial cells	GSE128944	[476]
P14 cells isolated from the small intestine at different time points after LCMV infection	GSE131847	[477]
Pancreatic CD8+ T cells isolated from NOD mice of different ages	GSE141784	[478]
P14 cells isolated from spleen or B16-GP33 tumours	GSE147081	[479]

3.11 R and python packages

For analysis of sequencing data, R versions 3.6.2 and 4.0.4 [480] as well as python 3.8.2 [481] were used. R packages are listed in table 18 and python packages are in table 19. Dependencies are not included.

Table 18: R packages

Package	Version	Date	Source	Reference
affy	1.64.0	2019-10-29	Bioconductor	[482]
annotate	1.64.0	2019-10-29	Bioconductor	[483]
AUCell	1.10.0	2020-04-27	Bioconductor	[484]
BiocManager	1.30.10	2019-11-16	CRAN (R 3.6.0)	[485]
biomaRt	2.42.1	2020-03-26	Bioconductor	[486]
cellranger	1.1.0	2016-07-27	CRAN (R 3.6.0)	[487]
dplyr	1.0.2	2020-08-18	CRAN (R 3.6.2)	[488]
edgeR	3.28.1	2020-02-26	Bioconductor	[489]
fgsea	1.12.0	2019-10-29	Bioconductor	[490]
genefilter	1.68.0	2019-10-29	Bioconductor	[491]
GEOquery	2.54.1	2019-11-18	Bioconductor	[492]
ggplot2	3.3.3	2020-12-30	CRAN (R 3.6.2)	[493]
limma	3.42.2	2020-02-03	Bioconductor	[494]
Matrix	1.2-18	2019-11-27	CRAN (R 3.6.3)	[495]
msigdbr	7.1.1	2020-05-14	CRAN (R 3.6.3)	[496]
org.Hs.eg.db	3.10.0	2020-05-06	Bioconductor	[497]
org.Mm.eg.db	3.10.0	2020-04-23	Bioconductor	[498]
pheatmap	1.0.12	2019-01-04	CRAN (R 3.6.0)	[499]
RColorBrewer	1.1-2	2014-12-07	CRAN (R 3.6.0)	[500]
readr	1.4.0	2020-10-05	CRAN (R 3.6.2)	[501]
readxl	1.3.1	2019-03-13	CRAN (R 3.6.0)	[502]
Seurat	4.0.4	2021-08-20	CRAN(R 4.0.2)	[503]
stringr	1.4.0	2019-02-10	CRAN (R 3.6.0)	[504]
tidyr	1.1.2	2020-08-27	CRAN (R 3.6.2)	[505]

Table 19: Python packages

Package	Version	Reference
matplotlib	3.4.2	[506]
numpy	1.18.4	[507]

pandas	1.0.3	[508]
scanpy	1.7.2	[509]

4 Methods

4.1 Mouse work

All animal experiments were approved by the German regional council at the Regierungspräsidium Karlsruhe and were performed following internal DKFZ guidelines.

4.1.1 Maintenance and housing

C57BL/6N and P14 mice were bred and maintained in the German Cancer Research Center (DKFZ) specific pathogen-free animal facility. Live mice were handled under sterile conditions. Male and female, 6 - 10 weeks old mice were used for experiments.

4.1.2 Tumour implantation

B16.F10-$gp_{33\text{-}41}$ (B16-GP33) melanoma cells were reusupended in plain DMEM supplemented with 1% non-essential amino acids (NEAA) at a final density of 3 or 10 million cells/mL. Mice were anesthetised using isofluran (3.5% v/v in oxygen for induction and 2% for maintenance) and were injected subcutaneously with 100 µL of B16-GP33 cell suspension (0.3 or 1 million cells/mouse). The injection was made in the right flank at a flow rate of 10 µL/second using a 27G needle.

4.1.3 Tumour size measurement

Tumour sizes were measured every 2 - 3 days starting on day 8 after tumour implantation. Two perpendicular diameters were measured using a digital caliber and the size was calculated using the formula:

$$size = \frac{length\ x\ width^2}{2}$$

When more than one tumour was palpable, total tumour size was calculated as the sum of individual tumour sizes.

Mice were randomised to different groups so that average tumour size as well as standard deviation were comparable between groups. Mice were sacrificed when tumours were ulcerative and/or necrotic or when the longest diameter (or the sum of the longest diameters) exceeded 15 mm.

4.1.4 Influenza infection

Mice were anesthetised through intraperitoneal (ip) injection of a mixture of ketamine (100 mg/kg) and xylazine (10 mg/kg). Following narcosis, 8 x 10^4 median tissue culture infectious dose (TCID50) of the X31-33 (X31) strain of influenza A virus (subtype H3N2) was injected dropwise intranasally in 30 µL PBS. In some experiments, mice were re-infected with 1500 TCID50 of the PR8-33 (PR8) strain of influenza A virus (subtype H1N1) on day 21 post primary infection.

Mouse weight and general health conditions were monitored daily for the first 7 days after primary infection. Mice were sacrificed when they were visibly lethargic or when weight loss exceeded 20% of the initial body weight.

4.1.5 LCMV infection

Mice were infected with 2 x 10^5 plaque-forming units (pfu) of the Armstrong strain of the lymphocytic choriomeningitis virus (LCMV Arm). Virus was ip injected in 200 µL plain RPMI. In some experiments, mice received an intravenous (IV) injection of 2 x 10^6 pfu of the clone 13 strain of LCMV 60 days after primary infection.

4.1.6 Intravenous injection

Mouse tail was heated using a red light lamp and the tail skin was wiped with 70% ethanol. Injections were made in the left tail vein over a three-second interval.

4.1.7 Adoptive T cell transfer

B16 melanoma-bearing mice received 0.2 or 1 million T cells, prepared as in section 4.5.2 Differentiation of memory-like T cells and resuspended in 100 µL plain RPMI.

C57BL/6N mice were injected with 1 x 10^4 antigen-specific P14 cells on the same day as, or one day after, infection with either LCMV Arm or X31. In some cases, naive mice received a total of 2 x 10^4 P14 cells prepared as a 1:1 mixture of congenically mis-matched P14 cells of different genotypes before X31 infection.

4.1.8 Antibody treatment

Depletion antibodies

Naive, wildtype mice were intravenously injected with the full length αCD8α antibody (100 µg/mouse in 100 µL PBS), or αCD8α Fab′ (25 or 50 µg/mouse in 100 µL PBS, prepared as in section 4.6.1 αCD8α Fab′ generation).

Immune checkpoint blockade combinations

Tumour-bearing mice were randomised into 4 groups on day 10 after tumour implantation. One group received αPD-L1 (200 µg/mouse) and another group received Rat IgG2b, κ as an isotype control. αCD8α Fab′ fragment (20 µg per mouse; prepared as in section 4.6.1 αCD8α Fab′ generation) was injected in combination with either the isotype control or αPD-L1 antibodies to the third and fourth groups, respectively. Mice received 4 ip injections on days 11, 13, 15, and 17 after tumour implantation.

Labelling antibodies

To fluorescently label circulating CD8+ T cells, flu-infected mice were intravenously injected with PE-labelled anti-CD8β antibody (2 µg/mouse in 100 µL PBS) 5 minutes before being sacrificed.

4.1.9 Drug treatment

Starting on day 8 after X31 infection, mice were injected with different doses of the Stat6 inhibitor AS1517499. The drug was dissolved in a mixture of absolute ethanol and Tween 80. Afterwards, normal saline (0.9% sodium chloride in water) was added dropwise so that the final concentration of ethanol was 10% and of Tween 80 was 1%. Mice received a total of three injections on days 8, 11, and 14 post infection.

4.1.10 Mouse euthanasia and blood sampling

Mice were sacrificed using cervical dislocation. In some cases, blood was collected from the submandibular vein prior to euthanasia.

4.2 Mouse organ harvesting and preparation

Unless otherwise indicated, samples were centrifuged for 2 minutes at 2000 rounds per minute (rpm) at room temperature.

4.2.1 Blood

Mouse blood was collected from the submandibular vein in tubes containing 50 µL of 3.2% sodium citrate. Tubes were flipped 3 - 4 times and were kept on ice till further processing. Blood samples (30 - 40µL) were centrifuged. After discarding the supernatant, the pellet was used for two rounds of red blood cell (RBC) lysis using 100 µL ACK lysis buffer. Remaining cells were then resuspended in FACS buffer and used for FACS staining.

4.2.2 Tumour

Murine tumours were collected in 15 mL falcon tubes containing 3 - 4 mL of 1% RPMI and kept on ice. Solid tumours were then smashed through a 70 µm cell strainer using the plunger of a syringe. Strainers were washed with 5 - 10 mL 1% RPMI and cells were centrifuged. Pellets were resuspended in 2 mL ACK lysis buffer and incubated for 1 minute at room temperature before adding 3 - 4 mL 1% RPMI and centrifuging. Finally, the pellet was resuspended in 0.2 - 10 mL complete RPMI (depending on tumour mass), passed through nylon mesh, and 200 µL of the tumour cell suspension were used for FACS staining.

4.2.3 Spleen

Spleens were harvested in 1.5 mL eppendorf tubes containing cold 1% RPMI. They were then passed through 70 µm cell strainers, which were washed with 5 - 10 mL cold 1% RPMI. Cell suspensions were centrifuged and the pellets resuspended in 1 mL ACK lysis buffer and incubated at room temperature for 1 minute before dilution with 3 mL cold 1% RPMI and spinning. White pellets were then resuspended in 1 mL complete RPMI and filtered through nylon mesh. After counting, 2 - 3 million cells were used for FACS staining.

4.2.4 Lymph nodes

Mesenteric and inguinal lymph nodes were harvested in 2 mL eppendorf tubes containing 1 mL cold 1% RPMI. They were forced through 70 µm cell strainers and centrifuged. Cell pellets

were resuspended in 500 µL complete RPMI.

4.2.5 Lung

Lungs were collected in 2 mL eppendorf tubes containing 2 mL DNAse I (200 µg/mL) and collagenase D (200 µg/mL) diluted in 1% RPMI. Lungs were cut into small pieces using scissors, incubated at 37 °C for 45 minutes, and flipped every 15 minutes. Afterwards, digested lungs were further smashed through 70 µm cell strainers and washed with 15 - 20 mL 1% RPMI and centrifuged. After discarding the supernatant, pellets were centrifuged again so that any residual supernatant could be removed. Pellets were resuspended in 40% v/v percoll (prepared in plain RPMI) and were carefully layered over 5 mL 80% v/v percoll (prepared in plain RPMI) in 15 mL falcon tubes. The gradient was centrifuged at 1200 rpm for 15 minutes at 20 °C with no brakes. Lung epithelial cells in the upper most layer were discarded and the middle later (containing leukocytes and RBCs) was collected in new 15 mL falcon tubes and washed with 15 mL 1% RPMI. After ACK lysis, cells were resuspended in 1 mL complete RPMI.

4.2.6 Liver

Liver pieces were collected in 15 mL falcon tubes containing 3 mL 4% paraformaldehyde (PFA) and were incubated for at least 4 hours at room temperature. After fixation, livers were incubated in 6 - 8 mL 30% w/v sucrose (prepared in double-distilled water) over night and then embedded in OCT and frozen over dry ice. Frozen blocks were stored at -20 °C.

Alternatively, livers were harvested in 15 mL falcons containing 3 mL 1% RPMI, smashed over 70 µm cell strainer and washed. Cell pellets were resuspended in 40% v/v percoll and liver-infiltrating lymphocytes were enriched following the same protocol as in section 4.2.5. Cells were counted and used for flow cytometry.

4.2.7 Small intestine (SI)

Portions of the duodenum were dissected and all attached fat tissue was carefully removed. Faecal matter was flushed using 3 mL cold PBS and the clean small intestine was carefully flattened and rolled in a spiral, which was carefully transferred to a plastic mold. OCT was poured on top of the spiral and tissue was frozen over dry ice. Cryopreserved samples were stored at -20 °C or -80 °C.

In experiments where SI intra-epithelial lymphocytes (IEL) were used for FACS, the entire SI was dissected out and cut diagonally. After cleaning, it was cut into 1 - 2 cm pieces that were incubated in a flask containing 20 mL serum-free RPMI (RPMI supplemented with 25 mM HEPES, 1% NEAA, 50 µM 2-mercaptoethanol (2-ME), 5mM EDTA, and 0.145 mg/mL DL-Dithiothreitol (DTT)). Tissue pieces were magnetically stirred for 20 minutes at 37 °C. Afterwards, the contents of the flask were sieved through a 70 µm strainer and remaining tissue pieces were shaken vigorously in 10 mL serum-free RPMI and passed through the same strainer for 2 - 3 more rounds. The flow-through of the several straining steps was pooled, centrifuged, and used for flow cytometry.

4.2.8 Kidney

The left kidney was dissected out removing the attached ureter and adrenal glands and was rinsed with cold PBS. Kidney was embedded in OCT and frozen over dry ice.

4.3 Human samples

All human samples were handled in a biosafety level 2 laboratory.

4.3.1 Human blood

Blood samples were collected from healthy female donors (25, 28, and 41 years old) reporting to the German Red Cross (DRK). Blood was diluted 1:4 with room temperature PBS and 25 mL of the blood-PBS mixture were layered on top of 20 mL Biocoll density gradient centrifugation medium in 50 mL falcon tubes. The gradient was centrifuged at 2000 rpm for 15 minutes at room temperature with the brakes set to a speed of 2. Peripheral blood mononuclear cell (PBMCs) were collected from the plasma-Biocoll interphase and washed once with 20 mL PBS. After two rounds of RBC lysis using ACK lysis buffer, 3 million PBMCs were stained for flow cytometry.

4.3.2 Colon cancer samples

During surgical resection of colon cancer, cancer tissue samples as well as samples of adjacent, normal tissue were collected. Tissues were incubated in plain RPMI containing 200 µg/mL collagenase D for 30 minutes at 37 °C. Digested tissue pieces were then passed through

70 µm cell strainers. Cells were resuspended in 10 mL percoll (40% v/v in plain RPMI) and layered on top of 5 mL percoll (80% v/v in plain RPMI) and centrifuged at 2000 rpm for 20 minutes at room temperature with braking speed at 2. The middle layer (containing T cells) was collected into a new 15 mL falcon tube and washed twice with 1% RPMI before being used for FACS staining.

4.4 Cell biology

4.4.1 Cell culture of immortalised cell lines

B16-GP33 cells were maintained in complete DMEM supplemented with 400 µg/mL Geneticin (G418-sulphate). BHK, Vero, and HEK 293T cells were maintained in complete DMEM. Cells were cultured in T75 flasks and were split when they reached 50% confluency. For splitting, the medium was removed and cells were washed with 5 mL PBS. Then, cells were incubated with 3 mL of 0.25% Trypsin-EDTA for 2 - 10 minutes at 37 °C, washed with 10 mL complete DMEM, and centrifuged. Cells were cultured at 1:20 - 1:100 of their initial density. One day before tumour implantation, 2 million B16-GP33 cells were seeded per flask to achieve 50% confluency on injection day.

For long term storage of cells, 5 million cells were resuspended in 1 mL freezing medium (10% v/v DMSO in FBS) in cryotubes and were frozen at -80 °C in Mr. Frosty™ freezing container half-filled with isopropanol. Frozen cells were rapidly thawed in a 37 °C water bath and washed with 20 mL complete DMEM and seeded in T75 flasks. One day later, the medium was changed to remove floating dead cells, and cells were split (if necessary).

4.4.2 Cell counting

Single cell suspensions were diluted 1:20 or 1:200 in Trypan blue and 10 µL were loaded on a Brand™ Neubauer counting chamber. Colourless cells in two squares were counted per sample and the final cell count (million cells/mL) was calculated using this formula:

$$Number\ of\ cells = \frac{count}{2} x\ dilution\ factor\ x10^4$$

4.4.3 LCMV production

BHK cells were seeded in a 6-well plate at a density of 0.5 million cells/well in 1.5 mL complete DMEM. On the following day, cells were infected with LCMV Arm at a multiplicity of infection (MOI) of 0.001 and were incubated for 90 minutes at 37 °C. Then, 3 mL pre-warmed complete DMEM were added per well and cells were incubated for 4 days at 37 °C. Finally, supernatants containing viral particles were harvested, centrifuged to remove any detached BHK cells, and frozen in 1 mL aliquots at -80 °C.

4.4.4 Plaque assay

Vero cells were seeded in a 6-well plate at a density of 0.5 million cells/well in 1.5 mL complete DMEM. One day later, a 1:10 serial dilution of viral stock was added to the cells (in 100 µL) and cells were incubated for 1.5 hours at 37 °C. Meanwhile, an agarose solution (1% w/v in plain DMEM) was diluted 1:1 with complete DMEM and allowed to cool to 37 °C before using 4 mL of the final solution to overlay each well of infected Vero cells. The plates were incubated for 10 minutes at room temperature followed by 4 days at 37 °C. Solid agar disks were carefully removed from each well and 2 mL plaque assay buffer were added per well. After 10 minutes at room temperature, the plaque assay buffer was removed and plates were rinsed with running tap water. Plates were allowed to dry at room temperature and empty spots (plaques) were counted to calculate the viral titer of the virus stock as plaque-forming unit (pfu) per mL.

4.4.5 Retrovirus production

A mixture of 100 µL Opt-MEM™, 4 µL X-tremeGENE 9 DNA transfection reagent, 1 µg murine stem cell virus (MSCV)-GFP retroviral vector, and 0.5 µg Eco-helper virus was allowed to stand at room temperature for 20 minutes. Afterwards, the mixture was added dropwise to HEK 293T cells, which had been seeded at a density of 0.5 million cells/2 mL/well in a 6-well plate one day earlier. One day after transfection, 1 mL of the supernatant was discarded. On the following day, the supernatant (containing released viral particles) was collected, centrifuged to remove any floating cells, and frozen at -80 °C.

4.5 T cell methods

4.5.1 Negative T cell selection

CD4+ and CD8+ T cells were negatively selected using CD4+ T Cell Isolation Kit or CD8+ T Cell Isolation Kit, respectively, following the manufacturer's protocol with minor changes.
Ten million splenocytes were resuspended in 40 µL cold MACS buffer, mixed with 10 µL Biotin-Antibody cocktail (different for different kits), and incubated at 4 °C for 10 minutes. Cells were then washed with 5 mL cold MACS buffer and centrifuged at 2000 rpm for 2 minutes. Pellets were resuspended in 80 µL cold MACS buffer, mixed with 20 µL anti-Biotin microbeads, and incubated for 10 minutes at 4 °C. Cells were passed through LS columns pre-wetted with 3 mL MACS buffer and fitted to a MACS magnetic separator. Columns were washed twice with cold 3 mL MACS buffer and the flow through (containing CD4+ or CD8+ T cells) was collected, centrifuged and resuspended in complete RPMI. The volume of MACS buffer, antibody cocktail, and beads was scaled up with the number of splenocytes initially used.

4.5.2 Differentiation of memory-like T cells

P14 splenocytes were incubated with 10 ng/mL $gp_{33\text{-}41}$ (GP33) and 10 ng/mL IL-2 in complete RPMI in 24-well plates at a density of 1 million cells/mL/well for 3 days at 37 °C. Cells were then washed twice with cold PBS before being resuspended in 6 mL room temperature PBS. Cells were divided into 3 x 2 mL-fractions, and each was layered carefully on top of 2 mL of room temperature Histopaque-1077 in 5 mL round-bottom tubes. The gradient was centrifuged at 1200 rpm for 15 minutes at room temperature with brake speed set to 2. The middle layer containing living cells was collected into clean 15 mL falcon tubes and washed twice with cold 1% RPMI.

Cells were then differentiated with 10 ng/mL IL-15 in complete RPMI in the presence or absence of 10 µg/mL αCD8α full length antibody, or 6 or 12 µg/mL αCD8α Fab′ (prepared as in section 4.6.1 αCD8α Fab′ generation). Cells were incubated at a density of 1 million cells/mL/well in 24-well plates for 24 hours at 37 °C.

When cells were prepared for intravenous adoptive transfer to tumour-bearing mice (see section 4.1.6) or for Gas chromatography-mass spectrometry (GC-MS), the gradient centrifugation step was done **after**, not before, cell differentiation to ensure that only living cells were used.

In some experiments, live, activated P14 cells were differentiated with IL-15 and αCD8α antibody in the presence of cyclosporin A (NFAT inhibitor, 20 µM), AS605240 (PI3Kγ inhibitor, 2 µM), rapamycin (mTORC inhibitor, 10 nM), Sch772984 (Erk1/2 inhibitor, 100 nM), T5224 (cFos inhibitor, 10 µM), BPTES (GLS inhibitor, 24 µM), 2-deoxyglucose (HK inhibitor, 1 mM), or 1 or 5 µg/mL αIL-2 antibody. Alternatively, cells were differentiated in minimal RPMI containing 10% dialysed FCS and 50 µM 2-ME supplemented with either 2 mM glutamine and/or 6.7 mM glucose.

4.5.3 Differentiation of resident memory-like T cells

P14 splenocytes were activated with 10 ng/mL GP33, 10 ng/mL transforming growth factor β2 (TGF-β2), and 5 µM retenoic acid (RA) in the presence or absence of 100 nM IL-4. Cells were incubated at a density of 1 million cells/mL/well in a 24-well plate for 3 days.

4.5.4 T cell restimulation

P14 cells differentiated under different conditions as in section 4.5.2 were washed twice with PBS. After counting, 0.2 - 0.5 million cells were activated with 10 ng/mL GP33 in the presence of 5 µg/mL Brefeldin A (BFA) in round-bottom, 96-well plates (200 µL per well). Alternatively, splenocytes and TILs were incubated with either 10 ng/mL GP33 or 25 ng/mL Phorbol 12-myristate 13-acetate (PMA) and 1 µM ionomycin, all in the presence of 5 µg/mL BFA. Cells were incubated for 4 - 6 hours at 37 °C and washed before FACS staining.

4.5.5 CellTrace Violet labeling

T cells were washed and incubated in complete RPMI containing 5 µM CellTrace violet (CTV) at a density of 5 million cells/mL. After 15 - 20 minutes at 37 °C, cells were washed twice with PBS and resuspended in complete RPMI.

4.5.6 B16 co-culture

B16.F10 (B16) cells were seeded in round-bottom, 96-well plates (4 x 10^4 cells per well). One day later, cells were incubated at 37 °C for at least 2 hours with 10 ng/mL GP33 in complete RPMI. Afterwards, B16 cells were washed twice with PBS and incubated with CTV-labelled P14 cells differentiated as in section 4.5.2 at a T cell : B16 cell ratio of 5:1. After one day of co-

culture in the presence of BFA, the supernatant (containing T cells) was collected and washed with PBS. T cells were used for FACS staining to assess cytokine production.

For cells co-cultured in the absence of BFA, attached B16 cells were washed twice with PBS and detached from the plates using rough, up-and-down pipetting. In subsequent flow cytometric analyses, B16 cells were defined as CTV-negative cells.

Alternatively, after three days of co-culture, T cells in the supernatant were collected, washed, and stained for flow cytometry to follow cell proliferation (defined as CTV dilution).

4.5.7 Chronic T cell stimulation

P14 splenocytes were incubated with 10 ng/mL GP33 and 10 ng/mL IL-2 in complete RPMI in round-bottom 96-well plates at a density of 0.2 - 0.5 million cells per well. After one day, cells were washed twice with PBS and incubated either with GP33 (for chronic stimulation) or IL-2 alone (for acute stimulation). Two days later (on day 3), cells were split in two (the contents of each well divided into two wells). Acutely stimulated cells were re-incubated with IL-2, while chronically stimulated cells were incubated with GP33 for two more days (till day 5). This process was repeated for one more round (till day 7) and the cells incubated for one extra day. On day 8 after initial activation, cells were stained for flow cytometry. All incubation steps were made at 37 °C under normoxic conditions.

4.5.8 Short term T cell activation

Splenocytes harvested from naive P14 mice or from mice that were infected with LCMV Arm 25 days earlier were seeded at 0.5 million cells/well in round-bottom 96-well plates. Cells were incubated with either 1 µg/mL αCD3ε or with 10 µg/mL αCD8α for 15 minutes at 37 °C. Cells were then washed and were immediately used for Phospho-flow cytometry.

4.5.9 Spin transduction

Freshly isolated P14 splenocytes were seeded at a density of 1 - 3 million cells/mL/well in 24-well plates. Cells were activated with 1 µg/mL αCD3 and 0.5 µg/mL αCD28 antibodies in the presence of 10 ng/mL IL-2 for 24 hours. Afterwards, cells were harvested and the supernatant (activation medium) was kept at 4 °C. Cells were resuspended in 4 mL 30% v/v percoll (prepared in complete RPMI) and were carefully layered on top of 3 mL 60% v/v percoll

(in complete RPMI). The gradient was centrifuged at 800x g for 20 minutes at 20 °C with no brakes. The middle layer, enriched for live, activated CD8+ T cells was harvested into a clean 15 mL falcon and washed twice with PBS. The cell density was adjusted to 1 - 3 million cells/mL using the stored activation medium. Cell suspension was mixed with MSCV-GFP viral particles (prepared as in section 4.4.5) in a 1:1 ratio and plated in 24-well plates. T cells were transduced by spinning at 2000x g for 60 minutes at 30 °C followed by incubation for at least 4 hours at 37 °C. Afterwards, cells were washed twice with PBS and used either for IV injection or further incubated with 10 ng/mL GP33 and 10 ng/mL TGFβ2 for two more days.

4.5.10 Regulatory T cell suppression assay

Lymphocytes (pooled from the spleen and lymph nodes) were used for CD4+ T cell selection (see section 4.5.1). Enriched CD4+ T cells were surface stained and were fluorescently sorted into regulatory (live CD4+CD25+) and conventional (CD4+CD25-) cells. When cells from LCMV Arm-infected mice were used, regulatory cells were defined as CD4+CD25+IL-7 receptor α-. In some experiments, transgenic mice with the *Foxp3*$^{YFP/cre}$ mutation were used. In these mice, FoxP3 expression was detectable as YFP fluorescence and regulatory T cells were sorted as the CD4+YFP+ population.

Conventional T cells were labelled with CTV (as in section 4.5.5) and 2 x 10^4 cells were incubated with a serial dilution of regulatory T cells along with Mouse T-Activator CD3/CD28 Dynabeads™ (2 cells per bead). Cells were cultured for 2 days at 37 °C before FACS staining.

4.5.11 Regulatory T cell activation

Round-bottom, 96-well plates were coated with 10 µg/mL αCD3 and 5 µg/mL αCD28 antibodies. A 4x-antibody mix was prepared in PBS and 50 µL were added per well. Plates were incubated at 37 °C for at least 1 hour before washing twice with PBS.

Sorted regulatory and conventional CD4+ T cells were separately resuspended in 200 µL complete RPMI medium and were added to coated wells. After activation for 3 days at 37 °C, 100 µL of the supernatant were used for Enzyme-linked immunosorbent assay (ELISA), while cells were lysed as in section 4.6.3 Sodium dodecyl sulfate polyacrylamide gel electrophoresis (SDS-PAGE) sample preparation and their protein content was quantified.

4.6 Molecular biology

4.6.1 αCD8α Fab′ generation

The Pierce™ F(ab′)$_2$ kit was used in an attempt to digest the full length αCD8α monoclonal antibody (mAb) into F(ab′)$_2$ fragments. The manufacturer's protocol was followed and the digestion was allowed to proceed for 6 hours. The digest was purified using either the Nab™ Protein G Spin kit or protein A/G PLUS agarose beads. When using the kit, protein G column and buffers were equilibrated to room temperature before washing the column twice with 1 mL PBS. The digested mAb was added to the column, which was end-to-end mixed for 10 minutes at room temperature. The column was then centrifuged for 1 minute at 1000x g and the flow-through was used to wash the column twice to increase the yield. When the protein A/G PLUS agarose beads were used, 200 µL beads were used per 500 µL mAb digest. The mixture was incubated over night on a flat shaker at 4 °C before spinning at 5000x g for 5 minutes and collecting the supernatant.

4.6.2 Measuring protein concentrations

Protein concentrations were measured using the Pierce™ BCA™ protein assay kit. Following the manufacturer's protocol, 2 µL samples were diluted with 8 µL water and used for the analysis. When the purified αCD8α Fab′ fragments were investigated, the full length antibody was used as a control along with the standards supplied by the manufacturer.

4.6.3 Sodium dodecyl sulfate polyacrylamide gel electrophoresis (SDS-PAGE) sample preparation

Cells to be used for western blotting were washed with cold PBS before centrifugation at 13000 rpm for 2 minutes at room temperature. The supernatant was removed and the pellet was resuspended in RIPA lysis buffer supplemented with protease inhibitors, sodium orthovandate, and phenylmethylsulfonyl fluoride (PMSF). 50 µL of the mix were used per million cells. Samples were incubated at -80 °C for 10 minutes before thawing at room temperature. Samples were then centrifuged at 13000 rpm for 2 minutes at room temperature and the supernatant was removed to clean tubes. Protein concentrations were measured as in section 4.6.2 and 10 - 30 µg protein were mixed with the approperiate volume of 4x laemmli buffer containing 2-ME, and boiled for 10 minutes at 95 °C. Samples were allowed to cool for

2 minutes on ice before spinning. The supernatant was then used for SDS-PAGE.

When digested antibodies were used for SDS-PAGE, full length antibody, digested antibody, as well as purified fragments were diluted with the appropriate volume of 4x laemmli buffer without 2-ME supplementation and boiled for 10 minutes at 95 °C. Samples were then cooled for 2 minutes on ice.

4.6.4 SDS-PAGE

SDS-polyacrylamide gels were manually prepared. The resolving gel mixture (8 - 12% acrylamide) was poured between glass slides with 1.5 mm spacer. The surface of the gel was smoothened by adding 200 - 500 µL isopropanol. After polymerisation, isopropanol was removed, the stacking gel mixture was poured, and a 10-well comb was carefully inserted. The glass plates and the comb were throughly washed to remove any traces of reducing agents before use. The gel was stored at 4 °C and used within 1 week.

For running, gels were installed in a Mini-PROTEAN Tetra Cell chamber (also throughly washed) that was filled with fresh SDS running buffer (when Fab′ fragments were being analysed) or running buffer that had been used maximum once. Samples were loaded along with 10 µL pre-stained protein ladder. Empty wells were loaded with 5 µL 4x laemmli buffer. Samples were run at constant voltage (90 V) for 30 minutes then for 60 minutes at 120 V.

Gels were then removed from the glass slides and were used either for Coomassie staining or for blotting proteins to a PVDF membrane. For protein transfer, the resolving gel was removed and a wet-transfer sandwich was prepared as follows: a PVDF membrane was activated with absolute ethanol until colour change was visible before throughly wetting the gel, the membrane, two filter papers, and two foam pads in wet transfer buffer. On the white side of the gel holder cassette, a foam pad was layered followed by a filter paper, the PVDF membrane, the gel, another filter paper, and the second foam pad. Wet transfer was performed at 400 mA (constant current) for 90 minutes at 4 °C. Afterwards, the membrane was blocked by incubation with either 5% skimmed milk (w/v in PBS-T) or 5% BSA (w/v in PBS-T) for 1 hour at room temperature. Primary antibodies (diluted in blocking buffer) were incubated with the membrane over night at 4 °C. Unbound antibodies were removed by washing 3 times each for 10 minutes with PBS-T. HRP-conjugated secondary antibodies of the appropriate specificity were diluted in blocking buffer and incubated with the membrane at room temperature for

1 hour before washing three times. Protein bands were visualised by adding a 1:1 mixture of the two components of the Clarity™ Western ECL substrate to the membrane and detecting using a chemiluminescence imager.

4.6.5 Coomassie staining

When αCD8α mAb and its digestion products were investigated using SDS-PAGE, the gel was washed with double-distilled water for 10 minutes while shaking. Afterwards, it was incubated in 7 - 10 mL Coomassie Brilliant Blue R-250 Staining Solution for 1 hour before destaining with Coomassie Brilliant Blue R-250 Destaining Solution. The destaining solution was changed three times at 45 minute-intervals. Final destaining was achieved by incubating the gel overnight in double-distilled water on a shaker. Gel pictures were taken using Orion L Microplate Luminometer.

4.6.6 Agarose gel electrophoresis

Agarose gels were prepared by mixing 1 g agarose with 100 mL TAE buffer and intermittantly boiling till a clear solution was obtained. The mix was allowed to cool to room temperature before adding 5 µL SYBER safe DNA stain in TBE and pouring into a gel cast and inserting a comb. When the gel solidified, the comb was removed and samples (up to 20 µL mixed with an appropriate volume of 6x Orange DNA Loading Dye) were loaded along with 10 µL DNA plus ladder. The gel was exposed to 120 V for 30 - 40 minutes and was imaged using Molecular Imager GelDoc XR+.

4.6.7 Enzyme-linked immunosorbent assay (ELISA)

To assess the CD8-binding potential of CD8 Fab′, wells of a round-bottom 96-well plate were coated with 50 µL of activated, CD8+ T cell lysates (200 µg/mL diluted in coating buffer). The plate was incubated at 4 °C for 12 hours. Afterwards, wells were washed three times with ELISA washing buffer before blotting the plate dry on clean tissue paper, and adding 200 µL/well of ELISA blocking buffer. The plate was incubated for 1 hour at 37 °C before washing 3 times. Purified Fab′ fragments were diluted 1:2 in blocking buffer and a mixture of 25 µL mAb (final concentration = 10 µg/mL) and 25 µL diluted Fab′ fragment was added per well (a final volume of 50 µL per well). The plate was incubated at 37 °C for 90 minutes and washed three times. Bound mAb was detected using 50 µL/well of αRat-HRP antibody (diluted 1:10,000 in

blocking buffer). The plate was again incubated for 90 minutes at 37 °C. Unbound detection antibody was removed by washing three times. Fifty microlitres of 1-Step™ Ultra TMB-ELISA (adjusted to room temperature) were added to each well and the plate was incubated in the dark for 10 - 30 minutes at room temperature before adding 25 µL/well of ELISA stop solution. Color intensity was read at 450 nm using Orion L Microplate Luminometer.

To measure the concentration of IL-15 in the supernatants of activated regulatory and conventional CD4+ T cells (see section 4.5.11), the mouse IL-15 DuoSet ELISA kit was used following the manufacturer's protocol. The concentration of IL-15 was normalised to the protein content in cell pellets.

4.6.8 Bacterial transformation

Plasmids were amplified by transforming competent *Escherichia coli* (*E. coli*) cells. One microgram plasmid or 2 µL of ligation reaction mix (see section 4.6.9 Cloning) were mixed with 50 µL bacteria and were incubated on ice for 30 minutes. The mixture was then heat-shocked at 42 °C for exactly 20 seconds before removing it to ice for at least 2 minutes. Afterwards, 950 µL of LB medium were added to the cells before incubating at 37 °C for 1 hour. The bacterial cell suspension was centrifuged at 2000 rpm for 1 minute and the supernatant was discarded. The pellet was gently resuspended in the remaining volume of the supernatant and was added dropwise to LB-agar plates containing 50 µg/mL ampicillin or kanamycin (depending on the resistance gene cassette in the plasmid). Sterilised glass beads were used to optimally distribute cells on the plates, which were incubated at 37 °C for 10 - 12 hours.

Colonies were carefully picked up and allowed to grow over night in liquid LB medium (containing 50 µg/mL of either ampicillin or kanamycin). Plasmid DNA was purified using the QIAprep Spin Miniprep Kit or QIAprep Spin Maxiprep Kit, following the manufacturer's protocol.

4.6.9 Cloning

Murine Stat6 (NM_009284) Tagged open reading frame (ORF) plasmid was purchased from Origene. The Stat6 overexpression (OE) plasmid as well as the MSCV-GFP retroviral vector (modified to include the recognition sites of SgfI, AsiSI, RsrII, and MluI in its multiple cloning site and thus it was dubbed SARM-GFP) were digested over night at 37 °C using the restriction

enzymes AsiSI and MluI combining reagents as in table 20.

Table 20: Restriction digestion reaction mix

Reagent	Volume/mass
Plasmid DNA	1 µg
AsiSI	1 µL
MluI	1 µL
10x Cutsmart	2.5 µL
Nuclease-free water	ad 25 µL

The digested Stat6 OE plasmid was used for Agarose gel electrophoresis and the Stat6 band ($\sim$ 2.5 kb) was cut out of the gel and purified using the QIAquick Gel Extraction Kit. The digested SARM-GFP vector was purified using the QIAquick PCR Purification Kit. Purified Stat6 ORF and SARM-GFP vector were ligated over night at 16 °C following the protocol in table 21.

Table 21: Ligation reaction mix

Reagent	Volume/mass
SARM-GFP	100 ng
Stat6 ORF	300 ng
10x T4 DNA ligase buffer	1.5 µL
T4 ligase	1 µL
Nuclease-free water	ad 15 µL

The ligation product was introduced into competent *E. coli* cells and plasmid DNA was purified from individual colonies (see section 4.6.8). Purified plasmids were then screened using a diagnostic digest with the same reaction mixture as in table 20 for 1 hour at 37 °C before analysing the digestion products using agarose gel electrophoresis. Positive clones showed a band at $\sim$ 2.5 kb corresponding to mouse Stat6 ORF.

4.6.10 Site-directed mutagenesis

To generate a constitutively active form of Stat6, two mutations were introduced into the Src homology 2 (SH2) domain. The amino acids valine (V) and threonine (T) at positions

547 and 578, respectively, were substituted with two alanine (A) amino acids, thus making a V547A/T548A mutant (referred to as Stat6-VT). Therefore, the thymidine and adenosine nucleotides at positions 1640 and 1642, respectively, of the Stat6 ORF were changed to cytosine and guanosine. This changed the codons from 5′ GUC ACU 3′ (encoding VT) to 5′ GCC GCU 3′ (encoding AA).

The Stat6-VT plasmid was derived from the Stat6-SARM plasmid using Q5® Site-Directed Mutagenesis Kit starting with a PCR reaction as in tables 22 and 23 using Stat6-VT forward primer (5′ AAG CAA TAT GCC GCT AGC CTT CTC 3′) and Stat6-VT reverse primer (5′ ACT AAT AAA GCC AAT GAT CAG 3′).

Table 22: Reagent volumes used for site-directed mutagenesis PCR

Reagent	Volume (µL)
Q5 Hot Start High-Fidelity 2X Master Mix	12.5
10 µM Stat6-VT forward Primer	1.25
10 µM Stat6-VT reverse Primer	1.25
Stat6-SARM	1 (25 ng)
Nuclease-free water	9

Table 23: Site-directed mutagenesis PCR program

Time	Temperature (°C)	Number of cycles
30 seconds	98	1
10 seconds	98	25
30 seconds	58	
1 minute	72	
2 minutes	72	1

Since primers were designed to be back-to-back, the linear PCR product was phosphorylated and ligated, and the template DNA was digested in one step using the kit-provided kinase-ligase-DpnI (KLD) enzyme mix by setting up a reaction as in table 24 and incubating at room temperature for 5 minutes.

The product of this reaction was used to transform bacteria (see section 4.6.8). Plasmid DNA was purified and positive clones were identified using Sanger sequencing.

Table 24: KLD reaction mix

Reagent	Volume (µL)
PCR product	1
2x KLD reaction buffer	5
10x KLD enzyme mix	1
Nuclease-free water	3

4.6.11 Reverse transcription-quantitative polymerase chain reaction (RT-qPCR)

RNA was extracted using Qiagen RNAeasy mini kit following the manufacturer's. 1.5 µg RNA per sample were used for reverse-transcription (RT) to cDNA using the SuperScript™ IV system, according to manufacturer's instructions. For qPCR, 2 µL cDNA were mixed with 1 µL of 5 µM mix of forward and reverse primers, 2 µL of SYBR green mix, and 5 µL distilled water. The reaction was performed in the CFX Duet Real-Time PCR system according to the cycling conditions in table 25. Mouse-specific primer sequences are provided in table 26.

Table 25: Cycling program for RT-qPCR

Time	Temperature (°C)	Number of cycles
5 minutes	72	1
30 seconds	98	1
10 seconds	98	39
30 seconds	63	
1 minute	72	
1 minute	72	1

4.7 Flow cytometry

In all experiments, samples stained with only one antibody (single stains) served as control for compensation and samples stained with all but one antibody (fluorescence-minus-one, FMO) were used as guides for gating.

Table 26: Sequence of RT-qPCR primers

Reagent	Volume (µL)
Actb forward	TGTGATGGTGGGAATGGGTCAGAA
Actb reverse	TGTGGTGCCAGATCTTCTCCATGT
Aifm2 forward	TGTGATGGTGGGAATGGGTCAGAA
Aifm2 reverse	TAGGCAGGTCCTGAGCAGA
Dgat1 forward	CCCATACCCGGGACAAAGAC
Dgat1 reverse	CCCATACCCGGGACAAAGAC
Gls1 forward	CCGTGGTGAACCTGCTATTT
Gls1 reverse	TGCGGGAATCATAGTCCTTC
Gpx4 forward	GGTGGTGCGGCCGCATGAGCTGGGGCCGTC
Gpx4 reverse	GGTGGTGCGGC CGCATGAGCTGGGGCCGTC
Il15 forward	TGGATGGATGGCAGCTGGA
Il15 reverse	AAAACAGAGGCCAACTGGAT
Il15ra forward	GACACCAAAGGTGACCTCACAG
Il15ra reverse	CTGTCTCTGTGGTCATTGCGGT
Lal forward	GCAAAGGTCCCAGACCAGTT
Lal reverse	TCATCAAAACTGAAGGCCCAGA

4.7.1 Surface staining

Mouse cells were incubated with purified anti-mouse CD16/32 antibody in FACS buffer at a final concentration of 1.25 µg/mL to prevent non-specific binding of antibodies to Fc receptors. Cells were then washed with 150 µL FACS buffer and centrifuged for 2 minutes at 2000 rpm. Mouse and human cells were stained in 50 µL mixture of antibodies and cells were incubated at room temperature for at least 10 minutes in the dark. Cells were then washed with 150 µL FACS buffer, resuspended in 50 - 100 µL FACS buffer, and kept at 4 °C until acquisition.

CXCR5 staining

CXCR5 expression was detected using a 3-step staining protocol. Samples were incubated with unconjugated rat anti-CXCR5 antibody for 1 hour at 4 °C before washing twice with FACS buffer. Afterwards, cells were incubated with biotin-conjugated, goat anti-rat Fab′ for

30 minutes at 4 °C. Then, cells were stained with fluorescently-labelled streptavidin for 30 minutes at 4 °C. After washing, cells were incubated with other antibodies specific for surface antigens.

4.7.2 Cytokine staining

After surface staining, 50 µL fixation buffer/sample was added on top of the surface staining antibody mixture and mixed well. Cells were incubated for at least 10 minutes at room temperature in the dark before centrifugation. Cells were washed twice with 150 µL of 1x Permeabilization Buffer (diluted in double-distilled water). Afterwards, cells were incubated with 50 µL antibody mixture prepared in 1x Permeabilization Buffer for at least 10 minutes in the dark. Cells were washed with 150 µL 1x Permeabilization Buffer, centrifuged, and pellets were resuspended in 50 - 100 µL 1x Permeabilization Buffer.

4.7.3 Staining of transcription factors

Surface-stained cells were incubated in 200 µL FoxP3 fixation buffer (prepared by mixing Foxp3 Fixation/Permeabilization Concentrate with Foxp3 Fixation/Permeabilization Diluent in a 1:3 ratio) for at least 2 hours at 4 °C. Cells were then centrifuged and washed twice with 1x Permeabilization Buffer before incubation with 50 µL antibody mixture diluted in 1x Permeabilization Buffer. Cells were stained for at least 10 minutes in the dark, washed, and resuspended in 50 - 100 µL 1x Permeabilization Buffer.

4.7.4 Phospho-flow cytometry

Cells were re-suspended in 100 µL fixation buffer and incubated at room temperature for 10 minutes before adding 150 µL of ice-cold 70% methanol (v/v in double-distilled water) on top. Cells were incubated at 4 °C for 1 hour before washing twice with FACS buffer. Cells were then incubated with antibodies recognising phosphorylated antigens (pLck and pZap70) for 15 minutes at room temperature before washing and incubation with fluorescently-labelled secondary antibodies in 50 µL FACS buffer for 15 minutes at room temperature.

4.7.5 Fluorescence-activated cell sorting (FACS)

Cells were surface stained and resuspended in 2 mL cold MACS buffer before cell sorting using a 100 µm nozzle.

4.8 Metabolic analyses

4.8.1 Metabolite uptake

IL-15-differentiated cells (as in section 4.5.2) were washed and seeded at a density of 0.5 million cells per well in a 96-well plate. Cells were starved in PBS for 10 minutes at 37 °C before adding either 10 µg/mL 2-NBDG or 1 µM C16-Bodipy in PBS. Cells were allowed to uptake the nutrient analogues for 15 - 20 minutes at 37 °C before washing 3 times with 200 µL FACS. Cells were then stained for flow cytometry and nutrient uptake was detected on the FITC channel.

4.8.2 Seahorse extracellular flux analysis

One day before the assay, the Seahorse sensor cartridge was hydrated using 200 µL autoclaved double-distilled water per well. The Seahorse XF Cell Culture Microplate was coated with poly-D-Lysine (50 µL per well of 50 µg/mL poly-D-Lysine diluted in Seahorse XF Calibrant). Both the cartridge and the cell culture microplate were incubated over night at 37 °C in the absence of CO_2.

On the day of the assay, water was removed from the cartridge, which was re-wetted using 180 µL of pre-warmed Seahorse XF Calibrant for at least 30 minutes at 37 °C in the absence of CO_2. For the Mito stress test, drugs were prepared in Seahorse XF assay medium containing 10 mM glucose and were injected as in table 27.

Table 27: Drug injection protocol for Mito stress test

Drug	Final concentration	Port	Volume	ETC target
Oligomycin	2 µM	A	20 µL	Complex V
FCCP	1.5 µM	B	22 µL	Inner mitochondrial membrane
Rot+AA	1.5 µM each	C	25 µL	Complex I and III, respectively

Alternatively, drugs for the Glycolysis stress test were prepared in Seahorse XF assay medium containing 2 mM glutamine and were injected following the protocol in table 28.

Table 28: Drug injection protocol for Glycolysis stress test

Drug	Final concentration	Port	Volume	Target
Glucose	10 mM	A	20 µL	Glycolysis
Oligomycin	2 µM	B	22 µL	Complex V
2-DG	50 mM	C	25 µL	Glycolysis

The cell culture microplate was washed with PBS and 0.5 million cells per well were added in 180 µL of the appropriately prepared Seahorse XF assay medium. Medium (without cells) was added to the 4 corner wells to serve as background control. The microplate was then briefly centrifuged to allow the cells to settle before incubation for at least 30 minutes at 37 °C in a non-CO_2 incubator. The cartridge and the microplate were placed in the Seahorse XFe96 Analyzer and analysed following the program in table 29.

Table 29: Seahorse instrument protocol

Step	Time (minutes)	Cycles
Calibration and Equilibration	standard	-
Baseline	Mix and measure (3 + 3 minutes)	3
Inject port A	Mix and measure (3 + 3 minutes)	3
Inject port B	Mix and measure (3 + 3 minutes)	3
Inject port C	Mix and measure (3 + 3 minutes)	3
Final measurement	Mix and measure (3 + 3 minutes)	3

Relevant metabolic parameters were extracted from raw data based on the following set of equations:

$$Glycolytic\ Capacity = Maximal\ ECAR\ -\ Basal\ ECAR$$

$$Glycolytic\ Reserve = Maximal\ ECAR\ -\ ECAR\ after\ glucose\ injection$$

$$Spare\ respiratory\ capacity\ (SRC) = Maximal\ OCR\ -\ Basal\ OCR$$

where ECAR is the extracellular acidification rate and OCR is the oxygen consumption rate. The average of the three measurement cycles was used for calculation.

4.8.3 Gas chromatography-mass spectrometry (GC-MS)

Cells were differentiated as in section 4.5.2. Ten million cells were resuspended in 500 µL PBS + 1% FCS containing either 2 mM ^{13}C-glutamine or 10 mM ^{13}C-glucose. Cells were incubated for 30, 60, or 120 minutes at 37 °C before quenching the reaction with 1 mL of ice-cold 0.9% NaCl. Cells were centrifuged at full speed for 1 minute before washing again with ice-cold 0.9% NaCl. A final centrifugation step was performed to remove any residual supernatant and cells were snap-frozen on dry ice and stored at - 80 °C.

GC-MS analysis was done in collaboration with Dr. Michael Buettner at the Metabolomics Core Technology Platform, Centre for Organismal Studies (COS), University of Heidelberg, Heidelberg, Germany. Briefly, frozen pellets were extracted in 100% methanol at 70 °C for 15 minutes before adding chloroform then water and centrifugation. After phase separation, the polar phase was collected and vacuum-dehydrated. Metabolites were then derivatised at 37 °C in a multi-purpose auto-sampler with 20 mg/mL methoxyamine hydrochloride in pyrimidine and 13 µL MTBSTFA (N-tert-butyldimethylsilyl-N-methyltrifluoroacetamide).

Samples were allowed to cool to room temperature before injecting 1 µL of each sample in a splitless mode to a GC column at an injection temperature of 250 °C. Helium was used as a carrier gas at a constant linear velocity. The connected time-of-flight (ToF) system was operated at the same temperature of injection (250 °C). The solvent cut time was set to 9 minutes, the mass-to-charge (m/z) scan range was between 50 and 600, and spectra were acquired at a rate of 17 spectra/second.

To calculate total metabolite abundance, the areas of all detectable peaks (regardless of the number of incorporated heavy carbon atoms) were summed.

4.9 Microscopy

4.9.1 Bright field microscopy

Live cell imaging was performed using an inverted light microscope fitted with a camera.

4.9.2 Cryosectioning and immunofluorescence

Frozen liver and SI samples were adhered to metal mounts using a drop of tap water. Samples were then cut into 4 - 5 µm-thick sections using a cryostat at a temperature set between -16

and -20 °C. Sections were collected using a clean, fine-hair brush and were transferred to poly-L-Lysine-coated slides, which were kept at -20 or -80 °C till staining.

Before staining, slides were air-dryed for 15 minutes then immersed in 4% PFA for 10 minutes at room temperature. Then, tissue sections were washed twice with PBS for a total of 10 minutes and immersed in 0.2% Triton X (v/v in PBS) for 15 minutes to permeabilise. After washing with PBS, sections were blocked using 1% BSA (w/v in PBS) for 1 hour at room temperature and incubated with primary antibodies diluted in 1% BSA (between 20 and 50 µL depending on section area). Sections were stained over night in a humid chamber at 4 °C before washing twice with 0.2% Triton X for a total of 30 minutes followed by washing two times with fresh PBS for 15 minutes each. Secondary antibodies were prepared in 1% BSA and were added to the sections for 1 hour at room temperature. Sections were washed again with 0.2% Triton X and PBS before adding DAPI in PBS for 5 minutes and washing. Finally, a water-based mounting medium was used before sections were topped with glass cover slips. Images were taken using an inverted wide-field microscope within two days of staining.

4.10 ATAC-seq

Lung-resident and spleen circulating P14 cells sorted as in section 4.7.5 were used for Assay for Transposase-Accessible Chromatin using sequencing (ATAC-seq) using home-made buffers with help from Joschka Hey at the Cancer Epigeneomics department, DKFZ, Heidelberg, Germany. At least 5000 cells per replicate were used as input for a modified Omni-ATAC protocol [510]. Cells were washed with PBS and nuclei were isolated using cold ATAC lysis buffer. Nuclei were resuspended in ATAC resuspension buffer before centrifugation at 500x g for 10 minutes. Pelleted nuclei were resuspended in 2x transposition buffer. DNA was tagmented by additing 2.5 µL Tagment DNA Enzyme 1 and rotating the mixture at 37 °C for 30 minutes at 1000 rpm. Transposed chromatin was then purified using a 1:7 mixture of 5 M guanidinium thiocyanate and AMPure XP beads and used for amplification. To avoid PCR-introduced artefacts, library amplification was performed in two steps; in the initial step, the protocols in tables 30 and 31 were followed.

Five microlitres of the PCR product were used for qPCR (after mixing with Sybr Green I nucleic acid) by applying the program in table 32, in order to determine how many extra cycles were required for optimal amplification.

Table 30: Reagent volumes used for the first ATAC library amplification step

Reagent	Volume (µL)
NEBNext High Fidelity 2x Master Mix	25
10 µM custom Nextera PCR Primer 1	0.8
10 µM custom Nextera PCR Barcode	0.8
transposed DNA	25

Table 31: PCR program for the first ATAC library amplification step

Time	Temperature (°C)	Number of cycles
5 minutes	72	1
30 seconds	98	1
10 seconds	98	5
30 seconds	63	
1 minute	72	
1 minute	72	1

Based on this analysis, it was determined that 6 more cycles were required and were applied in a second PCR step to the remaining pre-amplified mixture using the same protocol as in table 31 (but with 6 instead of 5 repeats). Finally, the amplified library was purified with a one-sided size selection applying 1.4x of AMPure XP beads and resuspended in 1X EB buffer. Concentration of the library was measured using the Qubit dsDNA HS Assay Kit and quality control was performed using the Agilent High Sensitivity DNA Kit. Sequencing was performed at the DKFZ Genomics and Proteomics Core Facility using the High Seq 2000 v4 Paired-End 125 bp platform.

ATAC-seq data processing *Performed by J. Hey*

Processing of the ATAC-seq reads were performed using the ENCODE ATAC-seq pipeline https://doi.org/10.5281/zenodo.156534 using default parameters. Briefly, adaptors were trimmed using cutadapt [511] with default adaptor error rate and a minimum read length > 5. Subsequently, reads were aligned to the mm10 reference genome using Bowtie2 (v.2.2.6) using the –X2000, –local, and –mm flags [512]. Alignment and filtering of unmapped, duplic-

Table 32: Quantitative PCR program

Time	Temperature (°C)	Number of cycles
30 seconds	98	1
10 seconds	98	
30 seconds	63	20
1 minute	72	
1 minute	72	1

ated, not-primary aligned reads as well as reads that had failed quality control was achieved using samtools (v.1.2), picard-tools (v. 1.126), and bedtools (v. 2.22) [513, 514]. Finally, peak-calling was performed using MACS2 (v.2.1.0) [515]. At least 20000 non-duplicated, non-mitochondrial reads were mapped per replicate. The irreproducible discovery rate was less than two for each group of replicates and the fraction of reads in called peak regions was above 0.5.

4.11 Analysis of sequencing data

4.11.1 ATAC-seq and ChIP-seq data

Bigwig files generated during the course of this work or downloaded from the Gene Expression Omnibus (GEO) were read and analysed using the trackplot function [516].

4.11.2 Microarray

Microarray data were downloaded from the GEO using the code GSE47045. Data were log2 transformed and highly variable genes were selected using the varFilter function of the genefilter R package. Then, gene annotations were retrieved using the getBM function from the biomaRt package with the filter set to "affy_mogene_1_0_st_v1". Of all features, 75% were uniquely annotated. Differential gene expression analysis was done using the limma package. Using the fgsea package, the enrichment of transcriptional factor targets in the list of differentially expressed genes was tested.

4.11.3 Bulk RNA-seq

T cells infiltrating mouse liver

Normalised RNA-seq counts were downloaded from GEO using the accession code GSE89307. Gene symbols were retrieved from the org.Mm.eg package using the getSYMBOL function from the annotate package. A set of known memory and effector T cell markers were subsetted from the normalised count matrix and heatmaps were drawn using the pheatmap package.

Analysis of raw RNA-seq data

Raw RNA-seq counts were downloaded from GEO. Normalisation and differential gene expression analysis were performed using the edgeR package. To filter out lowly expressed genes, a counts-per-million (cpm) threshold was set to 1. In some cases, the fgsea package was used to analyse differential enrichment of selected gene sets.

4.11.4 Single-cell RNA-seq (scRNA-seq)

Publicly available single-cell RNA-seq (scRNA-seq) data were downloaded from GEO and were analysed using the python implementation of scanpy. Cells expressing fewer than 200 genes as well as genes expressed in fewer than 3 cells were filtered out. Apoptotic cells (with mitochondrial gene reads > 5% of total reads) as well as duplicates (cells with more than 2500 different genes expressed) were excluded. Counts were normalised by total counts and were log-transformed. Finally, highly variable genes were filtered for subsequent analysis.

Human melanoma-infiltrating CD8+ T cells

scRNAseq of sorted CD45+ cells were accessed using the code GSE120575 [473]. The analysis focused on protein-coding genes (using the same list of genes published with the original manuscript). Further, CD8+ T cells were defined based on the expression of both *CD3E* and *CD8A*: log(*CD3E*) > 1.5 and *CD8A* > 1.5 were set as the cut-off.

Gene signature enrichment

To analyse the enrichment of the Stat6 target genes in single cells, the R package AUCell was used. Pre-processed scRNAseq data were downloaded. For each cell, genes were descendingly ordered based on their expression using the AUCell_buildRankings function. The target

gene set "STAT6_01" was retrieved from the molecular signature data base using the msigdbr package. Calculated enrichment scores were then used to generate a t-distributed stochastic neighbour embedding (t-SNE) plot.

5 Results

5.1 CD8 expression is dynamic and is tightly regulated

The first aim of this work was to dissect functional TCR avidity maturation in TCM cells and apply this knowledge to improve immunotherapeutic approaches. Earlier studies have shown that the efficiency of TCR signal transduction is improved in memory cells without changing the expression of downstream signalling components [211]. In contrast, some reports suggested that effector cells have transiently-reduced antigen binding capacity that is recovered in memory cells [210, 517], and that this difference might be due to changes in the levels of the CD8 co-receptor [208]. To follow up on this concept, I started by validating changes in CD8 surface expression during the course of an immune reaction. Unless otherwise specified, I use CD8 to refer to the CD8α subunit. Wildtype (WT) C57BL/6 (B6) mice were infected with LCMV Armstrong (Arm), which causes an acute, systemic infection. Endogenous liver and splenic T cells were examined for their CD8 levels. In both cases, CD8 expression was at its lowest at the peak of the immune response (day 8 after infection, D8), but it was regained by memory T cells (D30) (Fig. 10A, B), confirming that effector cells transiently lose CD8 expression and that memory cells regain it.

I stained equal numbers of spleen cells for flow cytometry and used fluorescent antibodies in excess to compensate for any changes arising from the big difference in CD8 counts at different stages of infection. Nevertheless, to avoid any confounding effects due to differences in size or autofluorescence, I analysed *Cd8a* locus accessibility and transcriptional regulation. I transferred P14 cells to B6 mice infected on the same day with a recombinant flu virus strain (X31) expressing the $GP_{33\text{-}41}$ epitope (X31-GP33) recognised by P14 cells. Donor P14 cells were sorted from the lung 8 days later and were used for Assay for Transposase-Accessible Chromatin with high-throughput sequencing (ATAC-seq) to study the differential accessibility of genomic loci. Both the *Cd8a* and *Cd8b1* loci were less accessible in lung resident P14 cells compared to naive splenic P14 cells (Fig. 10C). In contrast, *Klrg1* was more accessible in lung cells as would be expected for effector cells [145, 270]. To confirm that chromatin accessibility changes were stable on the transcriptomic level, I analysed RNA sequencing (RNA-seq) data of TCR_{TAG} cells adoptively transferred to mice infected with recombinant *L. monocytogenes* expressing the cognate antigen TAG [452]. *Cd8a* clustered with memory cell markers like *Il7r, Tcf7, Bcl2*, and, *Sell* (which encodes CD62L), and showed an expression

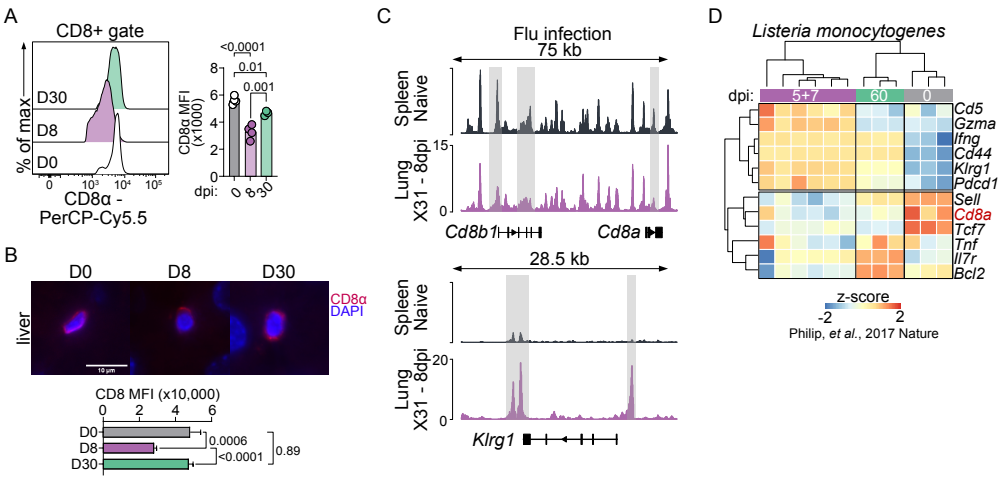

Figure 10: CD8 expression is actively regulated during the course of infection

(A) Expression levels of CD8α in polyclonal splenic CD8+ T cells at the indicated days (D) after infection with LCMV Arm. MFI, mean fluorescence intensity. dpi, days post infection.

(B) Top: Representative fluorescence microscopic images of liver sections from mice infected with LCMV Arm. scale bar = 10 µm. Bottom: Bar plot quantifying CD8α expression.

(C) ATAC-seq analysis of antigen-specific P14 CD8+ T cells sorted from the spleen of naive mice or from the lung 8 days following infection with X31-GP33 flu virus. Differentially accessible regions are highlighted in grey.

(D) A heatmap of normalised RNA-seq counts of antigen-specific TCR_{TAG} cells isolated from the spleen of mice infected with recombinant *Listeria monocytogenes* at different time points after infection [452].

Data (A & B) are representative of 2 - 4 independent experiments (n = 3 - 4 mice per time point per experiment) or are from one trial (C; n = 2 - 3 mice per group). *P*-values were calculated using one-way ANOVA. Error bars represent s.e.m.

pattern distinct from effector cell markers like *Cd44, Ifng*, and, *Klrg1*. Importantly, *Cd8a* levels were highest in naive cells (0dpi) followed by late memory cells (60dpi), and were the lowest in effector cells (5+7dpi) in good agreement with both flow cytometry and ATAC-seq analyses (Fig. 10D). Together, these results show that CD8 expression is dynamic and is actively regulated on the epigenetic, transcriptional, and translational levels. Importantly, this phenomenon is generalisable as it was independent of the infectious agent or the tissue from which CD8+ T cells were isolated.

5.2 Stem cell-like memory T cells upregulate CD8 expression

Peripheral CD8+ T cells are a heterogenous population expressing variable levels of CD62L and CD44. The co-expression pattern of these two markers divides cells into naive (CD62L+ CD44-), effector/TEM (CD62L- CD44+), and TCM (CD62L+ CD44+) cells [215, 216]. These populations are also detectable in naive mice (Fig. 11A) [518]. In naive T cells, CD8 levels are under the control of both tonic TCR and IL-7R signalling [57] (see Fig. 1). I asked whether CD8 expression would be similarly dynamic in different T cell subsets in the absence of inflammation. In naive splenocytes, there was a gradient of CD8 expression that reflected the activation status of the cell; naive T cells exhibited the highest levels of CD8 followed by TCM-like cells, while effector-like TEM cells had the lowest CD8 expression (Fig. 11A). This confirms that while surface CD8 expression is generally downregulated by cells with features of antigen-experience, memory cells regain higher CD8 levels. To directly examine the contribution of tonic TCR signalling to changes in CD8 levels *in vivo*, I measured the expression of IL-7Rα in freshly isolated splenocytes with a focus on different CD8+ subsets. There was a direct correlation between CD8 and IL-7Rα levels (Fig. 11B), confirming that CD8 expression is dynamically regulated *in vivo* in response to the strength of tonic TCR signalling [57]. Together these results suggest that changing surface CD8 levels is a strategy used by T cells in naive mice as well as during the course of an immune response.

Because memory cells themselves are a heterogenous population with distinct cytotoxic and proliferative capacities [216, 230, 519], I examined whether CD8 expression was particularly upregulated by certain memory T cell subsets. KLRG1 expression marks memory cells with residual effector function, while IL-7Rα and CD62L are upregulated by long-lived, stem cell-like cells [145, 231, 270]. On day 30 post LCMV Arm infection, splenic polyclonal ($CD44^{high}$) KLRG1+IL-7Rα- short-lived effector cells (SLECs) expressed significantly lower levels of CD8 compared to KLRG1-IL-7Rα+ memory precursor effector cells (MPECs) (Fig. 11C). This was also true for KLRG1+CD62L- cells (Q1), which downregulated CD8 in comparison to their KLRG1-CD62L+ counterparts (Q3).

In addition to studying the polyclonal memory cell population, I used MHC class I tetramers to specifically analyse antigen-specific T cell clones. Cells specific to the viral nucleoprotein residues 396-404 ($NP_{396\text{-}404}$; NP396) showed the same behaviour as polyclonal cells; SLEC and Q1 cells had lower CD8 expression compared to MPEC and Q3 cells, respectively

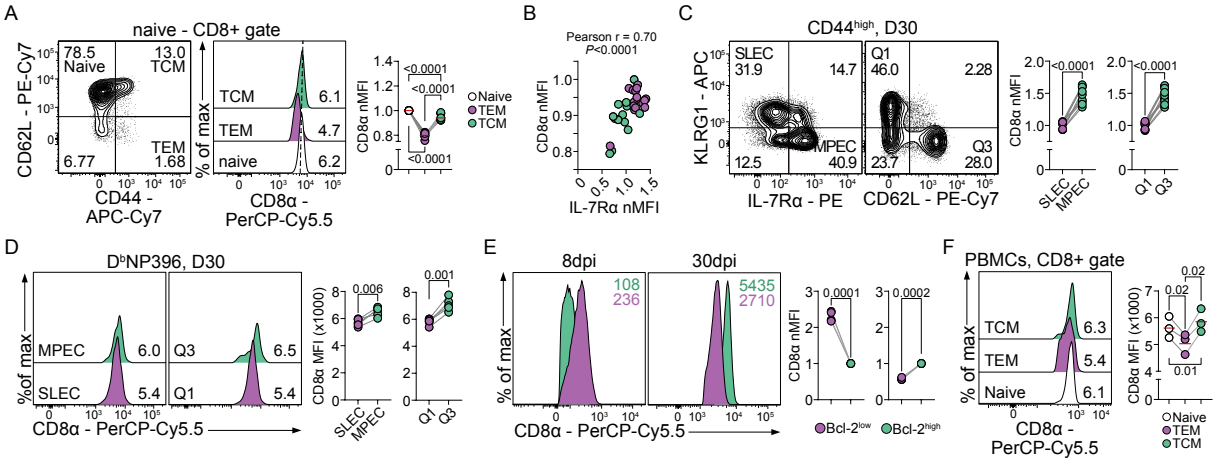

Figure 11: Stem cell-like memory T cells upregulate CD8 expression

(A) Left: Contour plot showing the gating of different CD8+ T cell subsets. Numbers indicate the percentage of gated cells. TCM, central memory T cells. TEM, effector memory T cells. Middle: Histograms showing CD8 expression in different splenic T cell populations. Numbers indicate MFI x 1000. Right: Line graphs comparing CD8α expression among different T cell subsets. MFI values were normalised (nMFI) to CD8α MFI for naive cells in the same mouse.

(B) Correlation between the expression of IL-7Rα and CD8α in splenic CD8+ TEM and TCM cells. MFI values were normalised to naive cells.

(C) Quantification of CD8α expression by the indicated polyclonal memory T cell subsets. SLEC, short-lived effector cells. MPEC, memory precursor effector cells. Q, quadrant.

(D) CD8α protein expression by NP396-specific memory T cells (defined as in C). Numbers on the histograms are CD8α MFI x 1000.

(E) CD8α levels were compared between Bcl-2^{low} and Bcl-2^{high} cells using flow cytometry.

(F) Human peripheral blood mononuclear cells (PBMCs) were isolated from 3 healthy donors and CD8α expression was compared between different populations. Naive cells: CD62L+CD45RO-, TEM cells: CD62L-CD45RO+, TCM cells: CD62L+CD45RO+. Numbers on histograms are CD8α MFI x 1000.

Data are pooled from 2 - 3 independent experiments (A - D; n = 10), are representative of 3 experiments (E, n = 4 - 5 mice per experiment), or are from one trial (F). *P*-values were calculated using paired Student's *t*-test (C - E) or repeated measures (RM) one-way ANOVA (A & F).

(Fig. 11D). These findings highlight the strong association between enhanced survival and proliferative capacity (in MPECs and Q3 cells) and CD8 upregulation.

Memory T cell longevity is dependent on the expression of the anti-apoptotic protein Bcl-2 [520]. To establish a clearer relationship between CD8 regulation and memory cell po-

tential, CD8 levels were longitudinally examined in Bcl-2^{low} and Bcl-2^{high} cells. Interestingly, CD8 expression correlated negatively with Bcl-2 on day 8 post infection, but there was a positive correlation between the two proteins at a memory time point (when most of the cells are Bcl-2^{high}) (Fig. 11E). This shows that after antigen clearance, CD8 expression is differentially regulated in memory T cell subsets with distinct functions.

Finally, these observations were extended to human peripheral blood mononuclear cells (PBMCs). The lower expression of CD8 protein by TEM cells (CD62L-CD45RO+) and its upregulation by TCM cells (CD62L+CD45RO+) was conserved in humans (Fig. 11F). Together, results presented in figures 10 and 11 show that CD8 upregulation is part of the transcriptional signature of memory cells, specifically those with proliferative, stem cell-like potential.

5.3 Non-genetic modulation of CD8 signalling

Having confirmed the upregulation of CD8 levels in memory cells and established its correlation to T cell persistence, I investigated whether it served a functional purpose. CD8 is important for TCR signalling [521–524] and thus is required for positive thymic selection [525, 526]. Therefore, it would be technically challenging to use a genetic loss-of-function model to study the contribution of CD8 signalling to memory T cell development and survival without influencing CD8+ T cell thymic production and primary effector functions. Instead, I used a non-genetic, gain-of-function approach, in which I treated cells with an agonistic anti-CD8α monoclonal antibody (clone 53.6.7; CD8 mAb) [91, 527, 528]. I validated the agonistic effect of this antibody on two levels: 1) TCR antigen binding, and 2) TCR signalling.

P14 T cells express an MHC-I-restricted TCR that could be detected using fluorescently-labelled, $GP_{33\text{-}41}$-loaded MHC-I tetramers (D^bGP33). Therefore, changes in TCR binding affinity could be inferred from the fluorescence intensity of the D^bGP33 signal. I incubated naive P14 splenocytes with D^bGP33 before washing and incubating cells with CD8 mAb. Alternatively, cells were incubated with CD8 mAb alone before staining with D^bGP33. In a third condition, cells were simultaneously stained with both CD8 mAb and D^bGP33 (Fig. 12A). I found that when T cells encounter their antigen in the presence of CD8 mAb, D^bGP33 fluorescence intensity is enhanced, indicating an increase in TCR binding affinity (Fig. 12B). This effect was evident regardless of whether CD8 mAb was already bound to the cells, suggesting that CD8 mAb does not sterically hinder antigen binding.

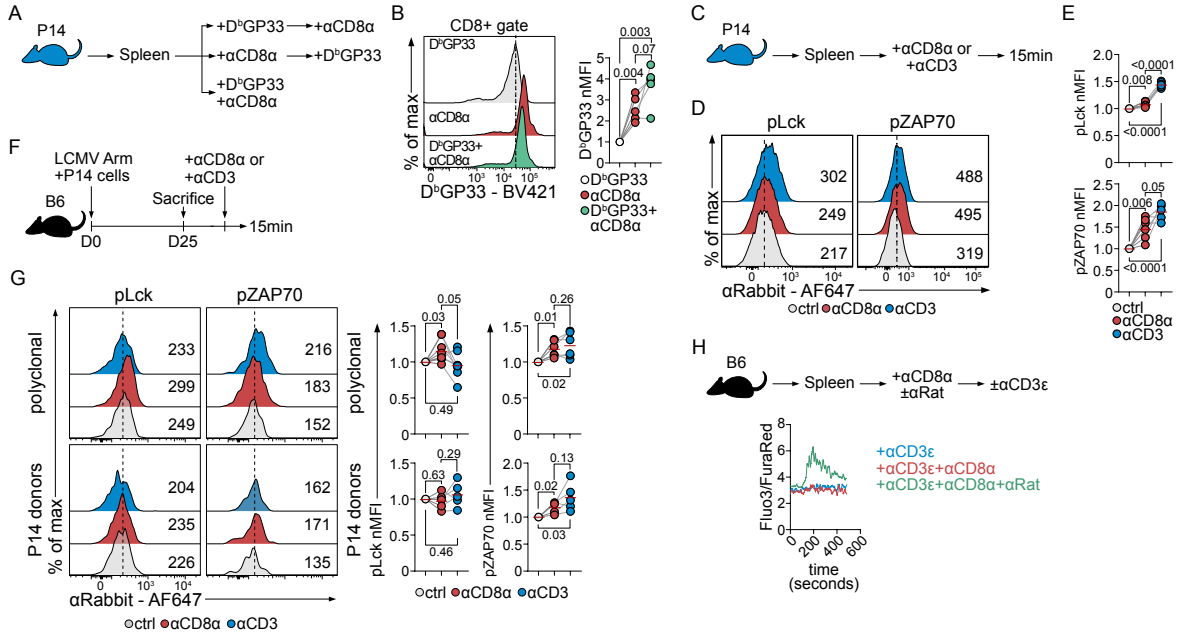

Figure 12: Agonistic anti-CD8α antibody induces proximal TCR signalling

(A) Experimental design for panel B.

(B) Histograms and line graphs showing changes in D^bGP33 fluorescence intensity.

(C) Experimental design for panels D and E.

(Dand E) Histograms and quantifications, respectively, of pLcK and pZAP70 in naive P14 cells treated with either αCD3 or αCD8α antibodies or left untreated (ctrl). Numbers on histograms are MFIs.

(F) Experimental design for panel G.

(G) Expression of pLck and pZAP70 in polyclonal and antigen-specific (P14) memory cells treated as indicated. Numbers on histograms are MFIs.

(H) Experimental design and line graph showing changes in intracellular calcium release following treatment of naive wild type splenocytes with the indicated antibodies.

Data are either from one experiment with 8 mice (G), pooled from 2 independent experiments (B & E; n = 5 - 6), or representative of 5 experiments (H). *P*-values were calculated using RM one-way ANOVA.

Second, I investigated whether CD8 mAb alone, in the absence of antigenic stimulation, could induce TCR signalling (Fig. 12C). Short-term treatment of freshly isolated P14 splenocytes with CD8 mAb caused phosphorylation of the tyrosine kinases Lck and ZAP70 (Fig. 12D, E), both integral components of the TCR proximal signalling machinery [529]. Because memory CD8+ T cells regain higher levels of CD8 expression (Fig. 10), I repeated the experiment using splenocytes harvested from mice 25 days post LCMV Arm infection (Fig. 12F). I again detected higher levels of phospho-Lck (pLck) and pZAP70 in endogenous CD44+ poly-

clonal memory T cells following CD8 ligation with CD8 mAb (Fig. 12G). Moreover, in both P14 donors and host memory CD8+ T cells, CD8 mAb and anti-CD3 antibody-induced ZAP70 phosphorylation were comparable. Lck and ZAP70 phosphorylation show that CD8 mAb treatment can induce proximal TCR signalling even in the absence of cognate antigen recognition.

I additionally tested whether CD8 mAb-induced pLck and pZAP70 were stable enough to be propagated to downstream signalling pathways. Although CD8 mAb (raised in rat), even in combination with anti-CD3 antibody (raised in hamster), was not able to induce significant changes in intracellular calcium ions (Fig. 12H), cross-linking of CD8 mAb using an anti-rat antibody was necessary for calcium release. This confirms that TCR binding/signalling is cooperatively enhanced by CD8 mAb and suggests that CD8 clustering induced by the anti-rat antibody, which potentially aggregates the intracellular Lck-bound domains, is important for signal propagation. Together, these data show that CD8 mAb enhances TCR binding and is able to induce proximal TCR signalling even in absence of cognate antigen recognition.

5.4 CD8 agonism induces a hybrid phenotype

In the next set of experiments, I examined whether using CD8 mAb could enhance the functional potential of IL-15 differentiated cells, which show moderate success when adoptively transferred to pre-clinical tumour models [448–451]. I used a previously published protocol to differentiate memory-like T cells *in vitro* [134]. Following this approach, P14 cells were activated with their cognate antigen (GP33) for 3 days before removing the antigen and incubating cells with IL-15 (Fig. 13A). Co-treatment of cells with IL-15 and CD8 mAb also enhanced Lck and ZAP70 phosphorylation (Fig. 13B).

In line with improved TCR signalling, CD8-ligated T cells gained some effector T cell features like the formation of bigger cell clusters (Fig. 13C). Furthermore, CD8 mAb-treated cells were blasting (had higher forward scatter (FSC-A)), and more granular (as measured by side scatter (SSC-A)) compared to cells treated with IL-15 alone (Fig. 13D). A more comprehensive analysis of CD8-ligated cells revealed that they develop a unique phenotype (Fig. 13E); while CD8 agonism enhanced the expression of some activation markers like CD44, PD-1, T-bet, and the proliferation marker Ki67, the cells were not less stem-cell like. Instead, they also upregulated the stemness and survival proteins Tcf-1 and Bcl-2. Although CD62L MFI was significantly reduced by CD8 mAb treatment, there was no difference in the percentage of stem

cell-like CD62L+CD27+ cells (Fig. 13F). Taken together, these results show that CD8 agonism induces the differentiation of a hybrid state, where cells gain both effector and stemness markers.

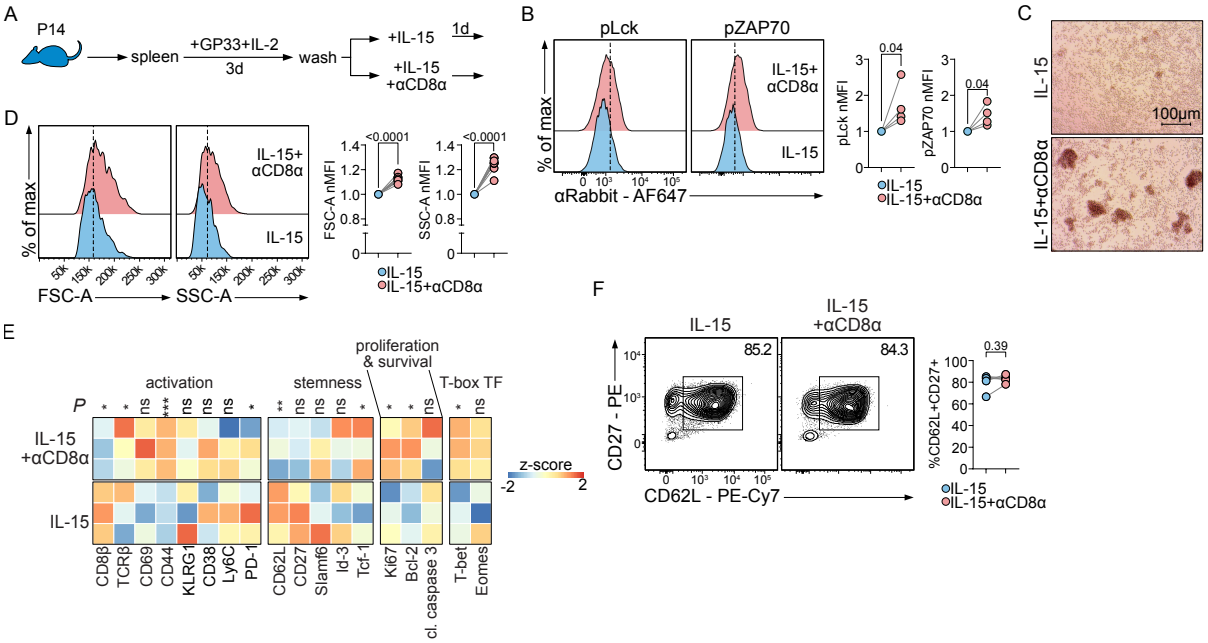

Figure 13: CD8 agonism creates a hybrid differentiation state

(A) Experimental protocol for *in vitro* differentiation of memory-like CD8+ T cells.

(B) Expression of pLck and pZAP70 following treatment with αCD8α antibody.

(C) Bright field microscopic pictures of cells differentiated in the presence or absence of αCD8α antibody. Scale bar = 100 µm.

(D) Cells differentiated as in A were analysed using flow cytometry for their cell size (FSC-A) and granularity (SSC-A).

(E) A heatmap showing scaled flow cytometry MFI values for the indicated markers. Cl., cleaved.

(F) Expression of CD27 and CD62L in *in vitro*-differentiated cells.

Data are representative of 10 experiments (C), pooled from 2 - 4 independent experiments (B & D - F; n = 4 - 8 mice). *P*-values were calculated using paired Student's *t*-test. *: $P < 0.05$, **: $P < 0.01$, ***: $P < 0.001$. ns, not-significant ($P > 0.05$).

5.5 CD8 agonism reprograms memory-like T cell metabolism

Metabolic changes occur within minutes of T cell activation [290], and effector and memory cells have distinct nutrient dependencies [283]. Therefore, I investigated differences in nutrient uptake, accumulation, and utilisation following CD8 ligation.

5.5.1 CD8 agonism enhances metabolite uptake and accumulation

CD8 agonism induced the expression of the neutral amino acid transporter CD98 but decreased the level of transferrin transporter CD71 (Fig. 14A). Consistent with effector T cell features, CD8-ligated cells showed enhanced uptake of the fluorescent glucose analogue 2-[N-(7-nitrobenz-2-oxa-1,3-diazol-4-yl) amino]-2-deoxy-D-glucose (2-NBDG) (Fig. 14A). However, they maintained the same level of long-chain fatty acid uptake as cells treated with IL-15 alone. This is inferred from fluorescence of the long-chain fatty acid analogue Bodipy C16 (Fig. 14A), and suggests that fatty acid metabolism induced by IL-15 [134] was not inhibited by CD8 mAb treatment. TCM and IL-15-differentiated T cells rely on triacylglycerol (TAG) synthesis followed by lipolysis and oxidation of the newly liberated fatty acids [312, 317]. Therefore, I examined the expression of diacylglycerol acyltransferase 1 (Dgat1), the rate limiting enzyme in TAG synthesis, and lysosomal acid lipase (Lal), the enzyme responsible for TAG lipolysis. I found that CD8 agonism induces the transcription of both enzymes (Fig. 14B), indicating that while CD8-ligated cells did not change their capacity for lipid uptake, they were better equipped to synthesise triglycerides and to break them down, probably for subsequent energy generation. Importantly, CD8-ligated cells contained higher transcript levels of glutathione-peroxidase 4 (Gpx4) and apoptosis-inducing factor mitochondria-associated 2 (Aifm2, also known as ferroptosis suppressor protein 1; Fsp1) (Fig. 14C), suggesting that they were not susceptible to ferroptosis induced by increased concentrations of lipid peroxides. Although it requires further testing, the downregulation of CD71 might also contribute to ferroptosis resistance in CD8-ligated cells by limiting the intracellular iron pool.

Next, I used gas chromatography-mass spectrometry (GC-MS) to study the accumulation of different nutrients in CD8-ligated cells. In accord with the enhanced expression of CD98, I found CD8 mAb-treated cells to contain higher levels of proteinogenic amino acids (Fig. 14D). Furthermore, CD8 agonism increased the abundance of nitrogenous bases, which serve as nucleic acid building blocks. These observations are in agreement with the increased size of CD8-ligated cells (Fig. 13D) and suggest that CD8 agonsim induces a significant metabolic shift in memory-like T cells.

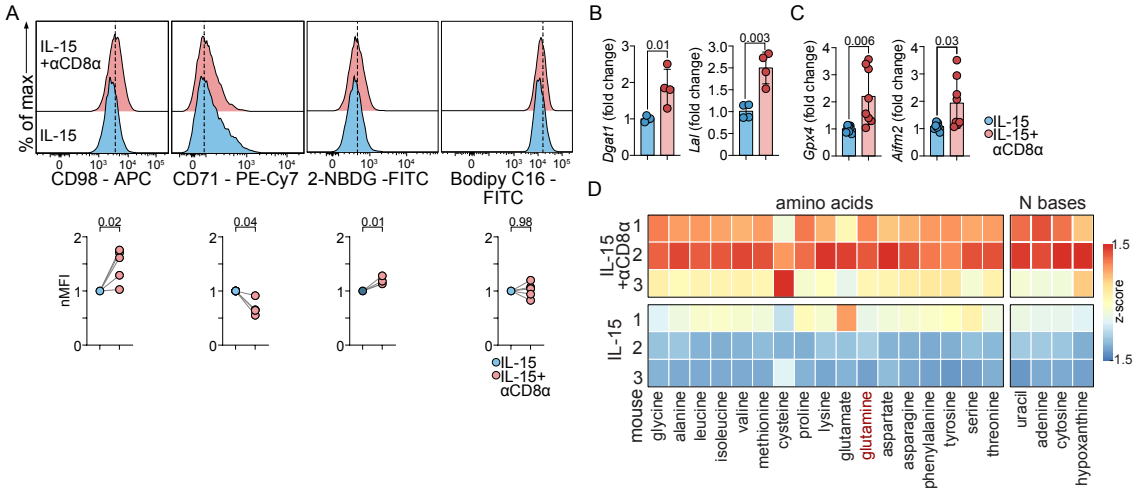

Figure 14: CD8 ligation enhances nutrient accumulation

(A) Cells differentiated as in Fig. 13A were assayed for the expression of CD98 and CD71 and for the uptake of glucose (2-NBDG) and long-chain fatty acids (Bodipy C16).

(B and C) RNA isolated from *in vitro*-differentiated cells was used for qRT-PCR to measure transcript levels of the indicated genes.

(D) A heatmap showing scaled peak areas of the indicated amino acids and nitrogenous (N) bases detected using GC-MS.

Data are from one experiment (D; n = 3), representative of 2 experiments (B & C; n = 4 - 8), or are pooled from 5 independent experiments (A; n = 5). *P*-values were calculated using paired Student's *t*-test.

5.5.2 CD8 agonism limits glucose assimilation in TCA cycle intermediates

Although IL-15-differentiated cells increase glucose uptake, they do not efficiently use it for glycolysis [134]. On the other hand, effector T cells rely on glycolysis for their differentiation and function [290, 294]. I asked whether excess glucose taken up by CD8-ligated cells was rerouted differently. To follow glucose-derived carbon atoms, I pulsed cells differentiated with IL-15 in the presence or absence of CD8 mAb with ^{13}C-glucose for different time intervals. Afterwards, the polar metabolome was extracted and analysed using GC-MS. Precise mass changes were used to understand whether CD8 ligation quantitatively and/or qualitatively influenced ^{13}C-isotope incorporation (Fig. 15A).

At all time intervals analysed, CD8 ligation minimally affected glucose assimilation into the glycolytic intermediates pyruvate and lactate (Fig. 15B). However, glucose carbon incorporation into the TCA cycle intermediates fumarate, malate, and aspartate/oxaloacetete (OAA) was significantly inhibited following treatment with CD8 mAb. Since CD8-ligated cells

contained higher amounts of glutamine compared to cells treated with IL-15 alone (Fig. 14D), I investigated whether glutamine was used to support anaplerotic reactions. I repeated the experiment but pulsed cells with ^{13}C-glutamine (Fig. 15C). I found that glutamine did not compensate for glucose in regenerating TCA cycle metabolites and was even less efficiently converted to aspartate/OAA by CD8-ligated cells (Fig. 15D).

Because cells were pulsed for extended time periods, I was able to detect metabolites that incorporated ^{13}C atoms from different glucose molecules. For example, the first ^{13}C-glucose molecule used by a cell yields an increase in the mass of citrate by 2 (citrate M+2). The two heavy carbon atoms then flow in the TCA cycle generating OAA M+2. When OAA M+2 is condensed with acetyl co-enzyme A (acetyl CoA) derived from the second glucose molecule, it generates citrate M+4. Therefore, by comparing the abundance of citrate M+4 to that of citrate M+2, it was possible to infer the *rate* of carbon flow from glucose into the TCA cycle (Fig. 15E). A similar approach, but with different stoichiometry, could be applied to glutamine metabolism (Fig. 15F). In agreement with decreased abundance of glucose-derived TCA intermediates, I found a slight, yet significant, reduction in the ability of CD8-ligated cells to funnel glucose carbons into citrate. However, glutamine-derived citrate was unaffected by CD8 mAb treatment. Together, these isotope tracing experiments show that CD8-ligated cells do not efficiently use glucose for mitochondrial respiration and that such defect is not compensated for using glutamine.

To examine why increased levels of glutamine did not translate as enhanced glutaminolysis in CD8-ligated cells, I measured transcript levels of glutaminase (*Gls1*), which catalyses the first glutaminolysis step. I found that CD8 agonism did not influence *Gls1* transcription (Fig. 16A). This finding suggests that although CD8-ligated cells have higher levels of glutamine, they do not have a corresponding increase in their capacity to assimilate it into TCA intermediates. Nevertheless, the abundance of total TCA intermediates, regardless of heavy carbon content, was increased in CD8-ligated cells, with the exception of citrate and α-ketoglutarate (α-KG) (Fig. 16B). Combined with the increased levels of succinate, the sharp decrease in α-KG translated into a much higher succinate/α-KG ratio in CD8-ligated cells compared to cells treated with IL-15 alone (Fig. 16C). These results suggest that despite the reduced glucose assimilation in TCA cycle intermediates, anaplerotic reactions other than glutamine fuel the TCA cycle.

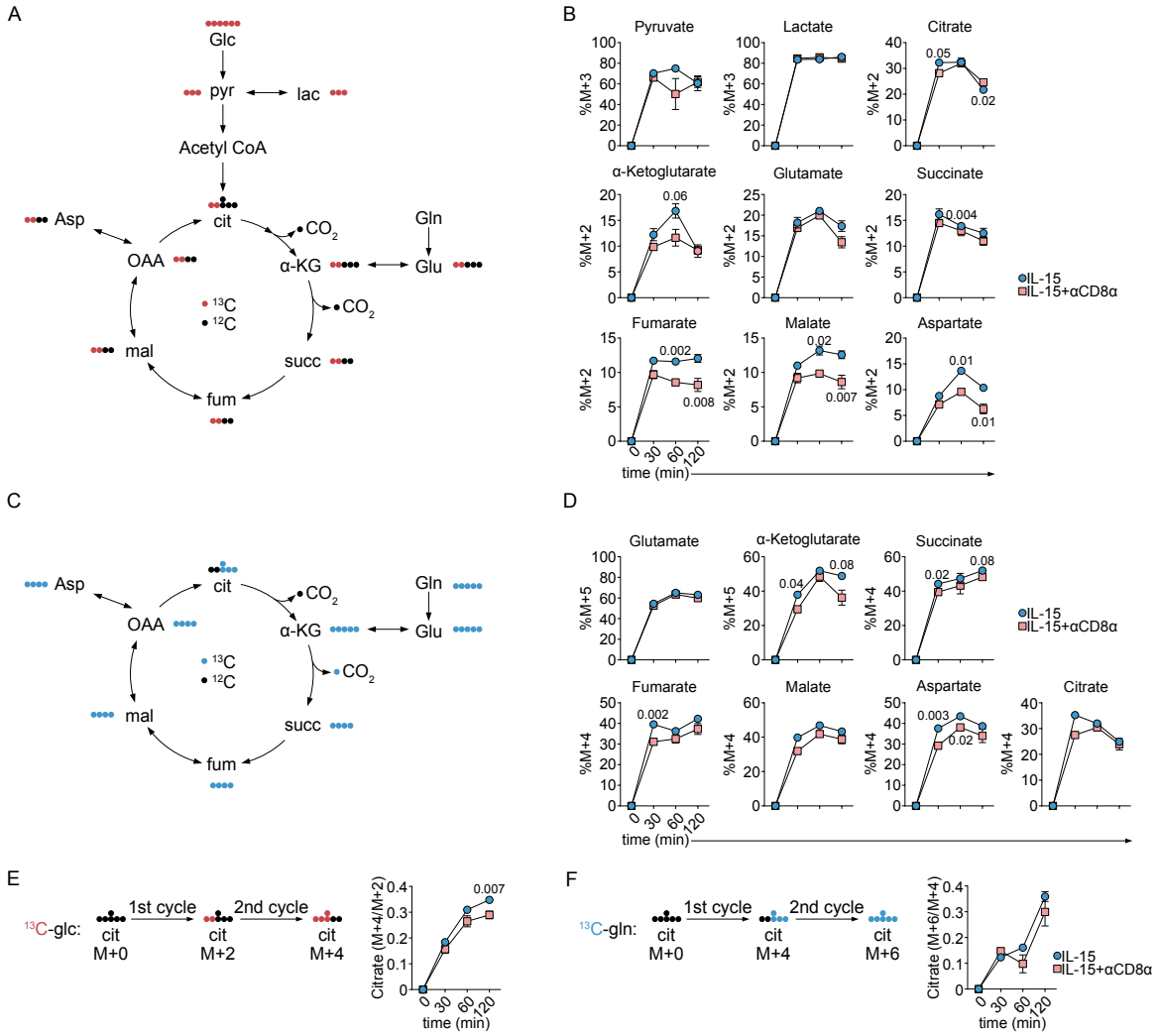

Figure 15: CD8-ligation modestly limits oxidative phosphorylation of glucose

P14 cells were treated as in Fig.13A and pulsed with ^{13}C-glucose or ^{13}C-glutamine for 30, 60, or 120 minutes before being used for GC-MS with help from Dr. Michael Buettner.

(A and C) Flow of glucose-derived (A) and glutamine-derived (C) ^{13}C in glycolysis and Krebs cycle. Circles indicate carbon atoms, which are either ^{12}C (black) or ^{13}C (coloured).

(B and D) Percentage of metabolic intermediates labelled in the first cycle of ^{13}C flow from glucose (B) or glutamine (D). M, mass.

(E and F) Schematics and line graphs following the accumulation of labelled intermediates in the second cycle of ^{13}C-glucose (E) or -glutamine (F) assimilation. glc, glucose. gln, glutamine.

GC-MS experiments were done once with 3 - 4 mice per time point. *P*-values were calculated using paired Student's *t*-test.

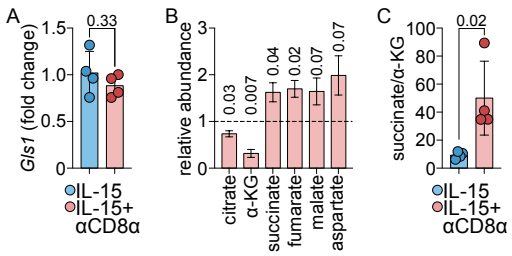

Figure 16: The TCA cycle is not inhibited in CD8-ligated cells

(A) P14 cells were treated as in Fig. 13A. RNA was extracted and used for qRT-PCR analysis of glutaminase (*Gls1*) levels. Representative of two experiments.

(B and C) P14 cells were cultured as in Fig. 15. The sum of peak areas was used to estimate total abundance of individual metabolites.

(B) Metabolite abundance in CD8-ligated cells relative to cells treated with IL-15 alone.

(C) Ratio of succinate abundance to that of α-ketoglutarate (α-KG).

Data represent the mean ± s.d. *P*-values were calculated using paired Student's *t*-test.

5.5.3 CD8 agonism enhances aerobic glycolysis and spare respiratory capacity

Since levels of labelled glycolytic intermediates already reached a plateau after pulsing cells for only 30 minutes (Fig. 15B), I studied aerobic glycolysis in real-time using extracellular metabolic flux (seahorse) experiments. Glucose-starved CD8-ligated cells were able to sustain a higher level of basal glycolysis compared to cells treated with IL-15 alone and were able to maintain their superiority in the presence of glucose (Fig. 17A - B). Importantly, these changes did not decrease the glycolytic reserve (the difference between maximal extracellular acidification rate (ECAR) and glucose-induced ECAR), which suggests that the entire ECAR curve is y-shifted and implies that the glycolytic fitness/machinery is increased rather than reaching earlier saturation. Mitochondrial metabolism, a feature of IL-15-differentiated cells [134], was not compromised by CD8 ligation as shown by similar basal oxygen consumption rate (OCR) (Fig. 17C - D). In addition, CD8-ligated cells were better equipped to respond to increased energy demands since they had a significantly higher spare respiratory capacity (SRC). Collectively, these results show that CD8 mAb treatment enhances nutrient uptake and rewires cellular energetics to support anabolism without sacrificing important features of memory cell metabolism.

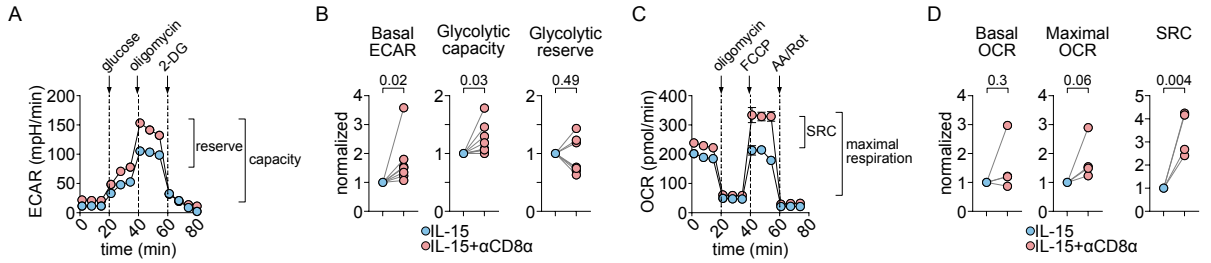

Figure 17: CD8 agonism enhances aerobic glycolysis and oxidative phosphorylation

P14 cells were treated as in Fig. 13A and were used for seahorse extracellular flux analysis.

(A) Representative extracellular acidification rate (ECAR) curve. 2-DG, 2-deoxyglucose.

(B) Basic parameters extracted from ECAR curves as in A.

(C) Oxygen consumption rate (OCR) curve. AA/Rot, antimycin A/rotenone. FCCP, carbonyl cyanide-p-trifluoromethoxyphenylhydrazone. SRC, spare respiratory capacity.

(D) OCR parameters extracted from curves as in C.

Data are either representative of (A & C) or are pooled from (B & D) 2 - 4 experiments (n = 4 - 9 mice). *P*-values were calculated using paired Student's *t*-test.

5.6 CD8 agonism induces effector T cell functions in memory-like T cells

I next asked whether CD8 mAb-induced phenotypic and metabolic changes translated into enhanced functionality. I tested the proliferative and cytotoxic function of CD8-ligated cells using T cell-B16 cell co-cultures. B16 cells were coated with GP33 (B16-GP33) and incubated with T cells for different time intervals (Fig. 18A). As a positive control, I incubated *in vitro*-differentiated T cells with GP33 peptide alone to account for cancer cell-specific factors. T cell proliferation was measured as CellTrace Violet (CTV) dilution and cytotoxicity was estimated as changes in the percentage of dead cancer cells.

Compared to IL-15 differentiated cells, CD8-ligated cells proliferated better in the presence or absence of B16 cells (Fig. 18B) and accumulated more cytokines (like TNFα and IFNγ) and effector proteins (granzyme B (GzmB) and perforin) (Fig. 18C). The combination of enhanced proliferation and cytokine production is likely responsible for improved killing of cancer cells (Fig. 18D). Together, these results show that CD8 agonism activates memory-like CD8+ T cells and supports their *in vitro* anti-tumour effector functions.

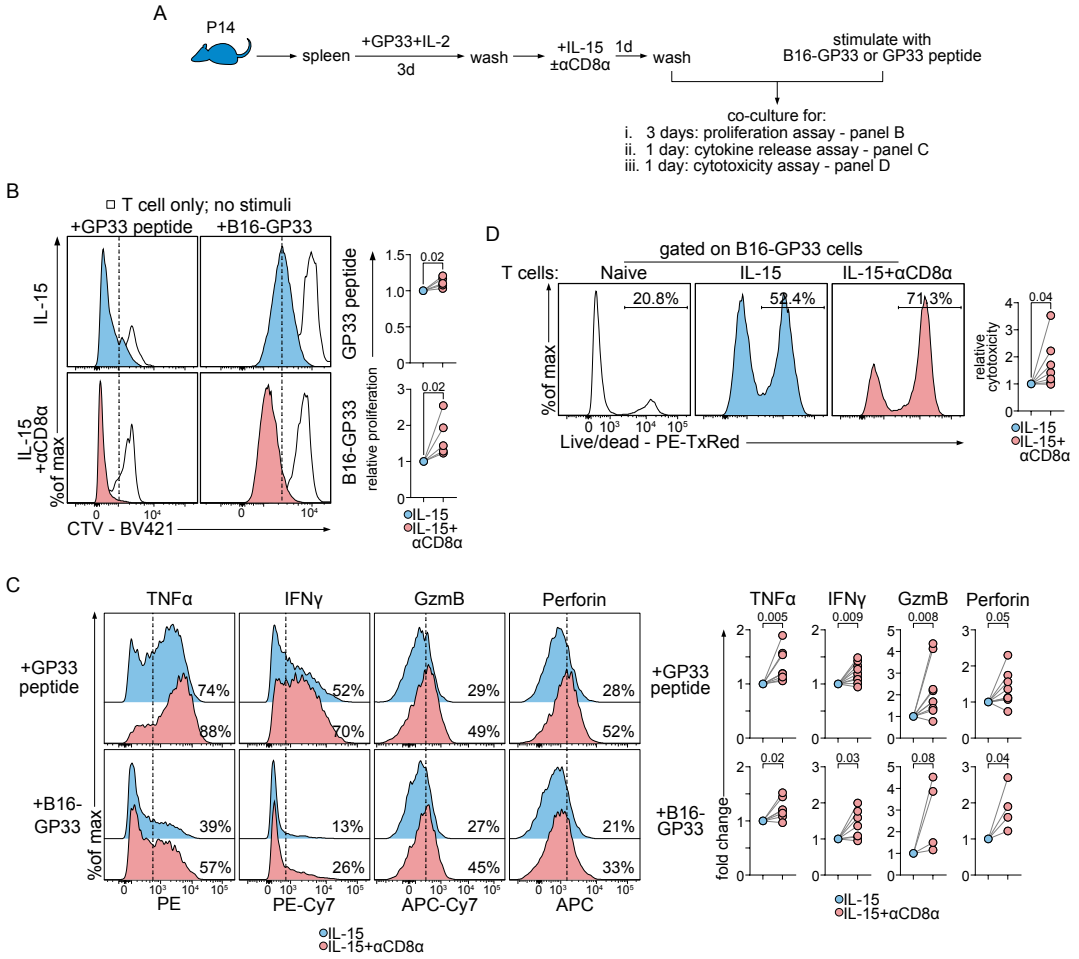

Figure 18: CD8 agonism enhances the effector function of memory-like CD8+ T cells

(A) Schematic of experimental design.

(B) *In vitro*-differentiated P14 cells were labelled with CTV and co-cultured with B16-GP33 cells or GP33 peptide. Shown are histograms and line graphs quantifying cell proliferation (CTV dilution).

(C) Flow cytometric measurements of cytokine production. Fold change was measured as the percentage of CD8-ligated cells positive for each cytokine normalised to the percentage of cytokine-positive IL-15-differentiated cells.

(D) B16-GP33 cell death was measured as positive staining with a fixable live/dead dye.

Data are pooled from 2 - 6 independent experiments (n = 4 - 9 mice). *P*-values were calculated using paired Student's *t*-test.

5.7 Glucose and glutamine control CD8 agonism-induced functional activation

TCR activation induces aerobic glycolysis earlier than measurable changes in glucose uptake, and this process is required for acute cytokine production [290]. Because CD8 agonism in-

duced proximal TCR signalling (Fig. 12) as well as glucose uptake (Fig. 14A), I wanted to understand the contribution of each pathway to the enhanced cytokine production exhibited by CD8-ligated cells. To this end, I differentiated memory-like P14 cells in the presence or absence of inhibitors of different signalling pathways downstream of TCR activation (Fig. 19A, B). Afterwards, I re-stimulated cells in order to assess potential changes in cytokine production.

As would be expected, strong inhibition of TCR signalling using the NFAT inhibitor (NFAT-i) cyclosporin A abrogated cytokine production irrespective of CD8 mAb treatment (Fig. 19C). This confirms that changes induced by CD8 agonism are TCR signalling-mediated. Inhibition of Akt/mTOR or Erk/cFos signalling had minimal influence on cytokine production regardless of CD8 agonism (Fig. 19C), further supporting that these pathways do not control acute cytokine release following TCR activation [290]. CD8 mAb treatment caused the formation of more and bigger cell clusters (Fig. 13C), which have been reported to induce autocrine IL-2 signalling [530]. I tested whether potential IL-2 secretion by CD8-ligated cells was responsible for their enhanced TNFα and IFNγ production, and I found that treatment with increasing doses of an anti-IL-2 antibody showed no effect (Fig. 19C).

I then investigated whether metabolic modulation was responsible for enhanced cytokine production in CD8-ligated cells. I tested this hypothesis in two ways; first, I skewed cells in presence of glutaminase (GLS) and hexokinase inhibitors (BPTES and 2-deoxyglucose (2-DG), respectively), thus inhibiting glutamine and glucose metabolism. Alternatively, I differentiated cells under minimal nutrient conditions in the absence of glutamine or glucose. Inhibition of glutamine metabolism, both pharmacologically and by limiting glutamine availability, enhanced cytokine production in control and CD8-ligated cells (Fig. 19C - D). This is in accord with the notion that glutaminolysis inhibits cytokine production [531]. Importantly, BPTES treatment brings IFNγ levels in IL-15 differentiated cells to those observed in untreated CD8-ligated cells. Combined with the lack of enhanced glutamine metabolism (Fig. 15D) despite higher glutamine abundance (Fig. 14D), these results suggest that latent glutaminolysis inhibition might support cytokine production in CD8-ligated cells.

Similarly, I found that 2-DG, which inhibits the first glycolytic enzyme, enhanced cytokine production regardless of CD8 ligation (Fig. 19C). In IL15-differentiated cells, glucose deprivation similarly induced higher levels of cytokine production. However, in the absence of glucose, but not in presence of 2-DG, IFNγ production in CD8-ligated cells was reduced by al-

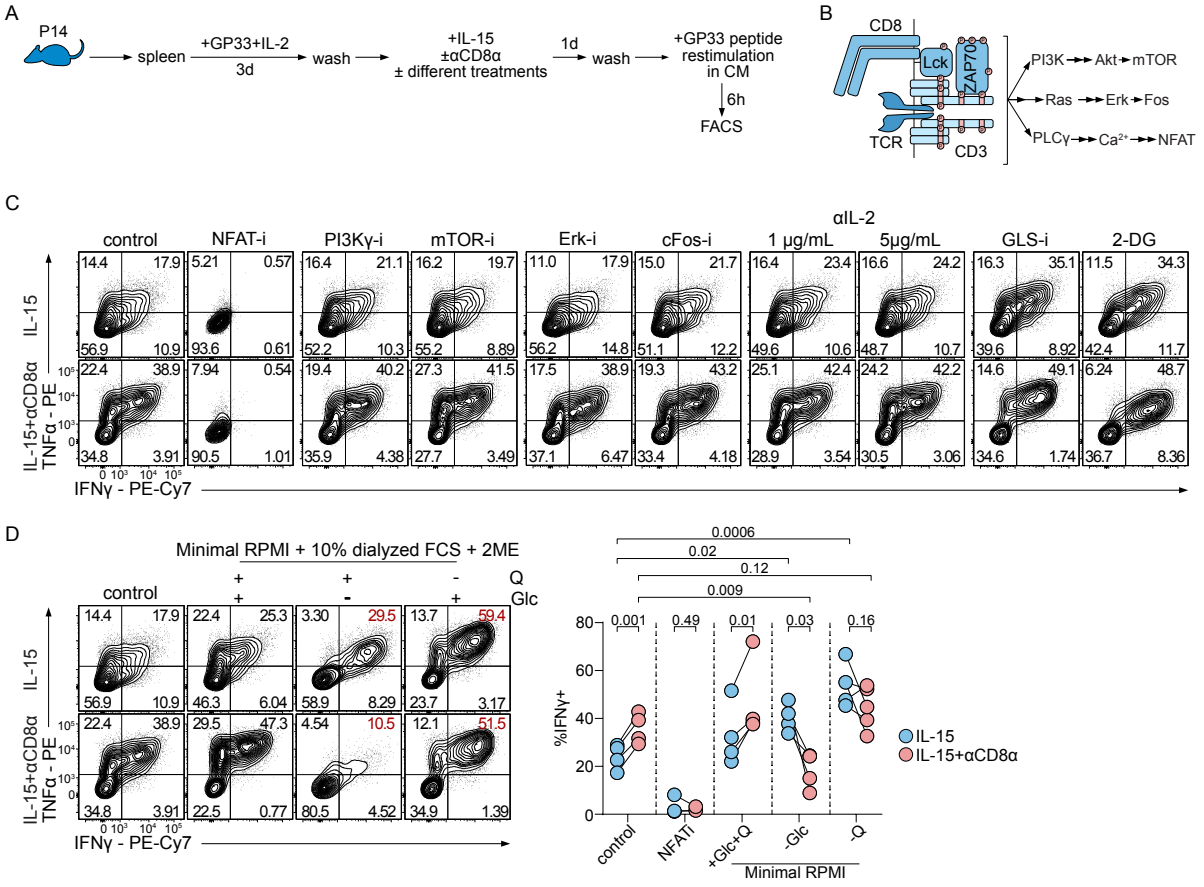

Figure 19: CD8 mAb-induced effector functions are dependent on glucose and glutamine metabolism

(A) Experimental design. Cells were skewed with IL-15, IL-15+αCD8α, or IL-15+αCD8α+different drugs or under different culture conditions. One day later, cells were washed before re-activation with GP33. CM, complete medium.

(B) A schematic showing the signalling cascade downstream of TCR activation.

(C) Representative contour plots showing the accumulation of TNFα and IFNγ in cells differentiated in the presence of the indicated inhibitors or two doses of αIL-2.

(C) TNFα and IFNγ production in cells differentiated in complete medium (control) or minimal RPMI supplemented with glucose (Glc), glutamine (Q), or both.

Data are representative of 2 independent experiments (C) or are pooled from 3 - 4 experiments (D; n = 3 - 5 mice). *P*-values were calculated using paired Student's *t*-test.

most 60% (Fig. 19D). This suggests that although CD8-ligation requires glucose to enhance cytokine production, the contribution of glucose is not entirely through glycolysis. Taken together, these results show that metabolic adaptations induced by CD8 agonism, namely altered glucose and glutamine metabolism, promote effector T cell functions.

5.8 CD8 ligation enhances anti-tumour responses

I originally sat out to identify features in TCM cells that could be translated into immunotherapeutic approaches. CD8-ligated cells have superior anti-tumour effector functions *in vitro* (Fig. 18), which were dependent on metabolic conditioning (Fig. 19). I tested whether CD8 mAb-treated cells would sustain enhanced functions *in vivo*. I labelled *in vitro* differentiated P14 cells with CTV and transferred them to B6 mice that were implanted with B16-GP33 melanoma tumours 11 days prior (Fig. 20A). Because P14 cells were congenically distinct from B6 mice, I was able to detect donor cells infiltrating tumours two days after transfer (Fig. 20B). Significantly fewer CD8-ligated cells were retrieved from tumours and spleens of host mice compared to cells treated with IL-15 alone (Fig. 20C). It is possible that residual full length CD8 mAb decorating the surface of ligated cells caused their depletion through antibody-dependent cell-mediated cytotoxicity (ADCC) [532]. Nevertheless, I was able to detect enough donor cells to support further analysis.

Because cells were CTV-labelled, it was possible to follow their proliferation in situ. In extension of their enhanced antigen-induced proliferation *in vitro* (Fig. 18C), a higher percentage of proliferating CD8 mAb-treated cells was detected both in tumours and spleens of host mice compared to IL-15-treated donor cells (Fig. 20D). Furthermore, I found a significant increase in the frequency of cells that underwent 4 or more cell cycles (Fig. 20D; red lines and numbers). Since TIL proliferation usually generates terminally exhausted T cells [344, 393, 396], I analysed the expression of exhaustion markers by CD8-ligated donors. I did not find a difference in the expression of PD-1, Lag-3, or Tigit between cells treated with IL-15 alone and CD8 mAb-treated cells (Fig. 20E), suggesting that CD8-ligated cells were not susceptible to faster exhaustion.

I then asked whether the descendants of CD8-ligated cells (which did not have surface-bound CD8 mAb) would be more efficient at controlling tumour growth. I repeated the experiment but followed tumour sizes over a prolonged time interval (Fig. 21A). While IL-15-differentiated cells were able to slow tumour progression, they were unable to inhibit it. On the other hand, CD8-ligated cells caused tumour regression in most host mice (Fig. 21B). One way to quantify tumour growth is to calculate the area under the curve (AUC) for each mouse. Compared to IL-15-differentiated cells, CD8 mAb treatment caused $\sim$ 50% reduction in AUC values (Fig. 21C) and $\sim$ 75% reduction in tumour mass (Fig. 21D). This suggests that

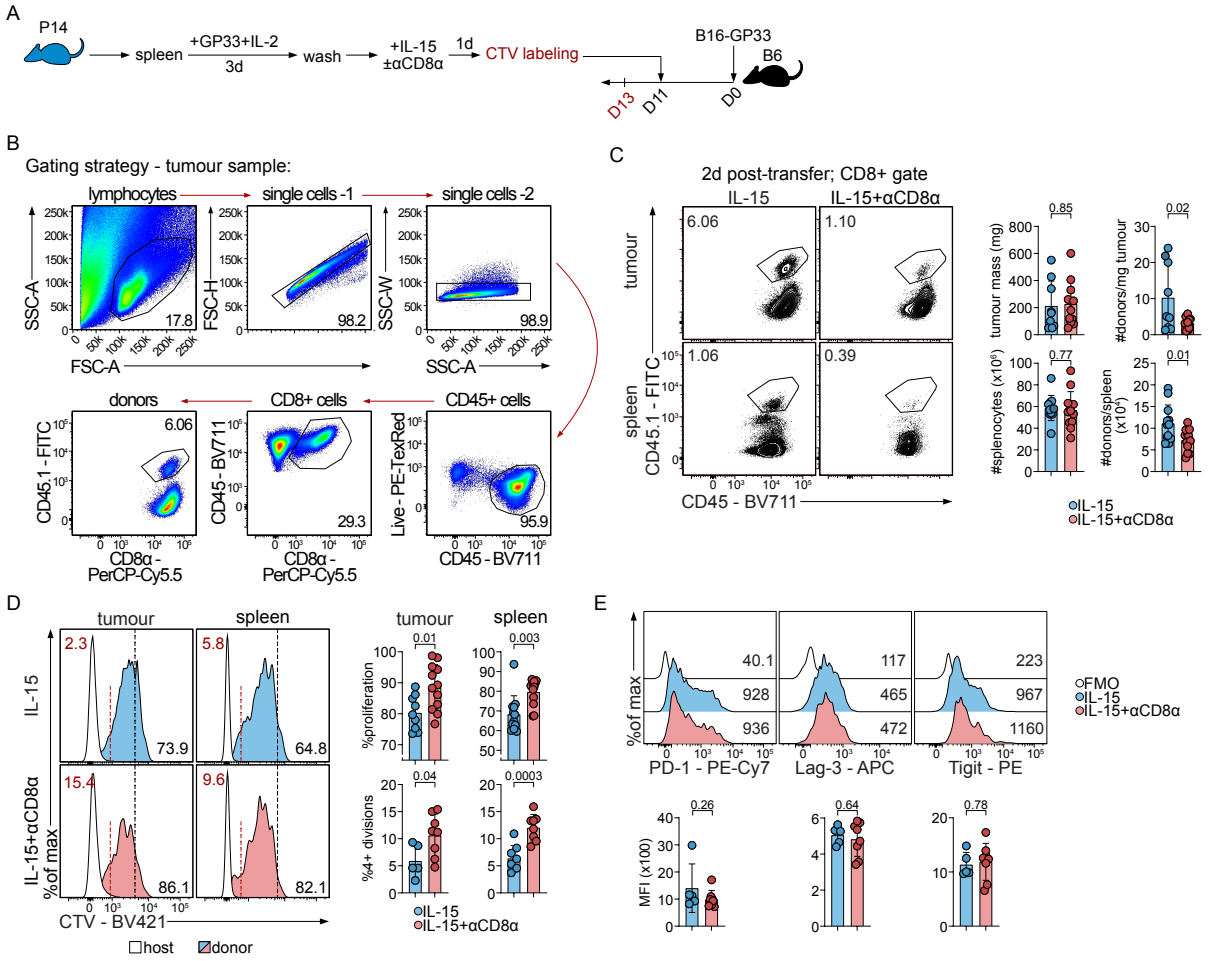

Figure 20: CD8 ligation enhances *in vivo* proliferation of adoptively transferred T cells

(A) Experimental design. Differentiated cells were labelled with CTV before transfer to mice bearing B16-GP33 tumours. Mice were sacrificed two days later.

(B) Gating strategy used to define donor cells.

(C) Frequency of donor cells recovered from tumour and spleen.

(D) Frequency of total proliferating donor cells (black line in histograms) and cells that went through 4 or more cell cycles (red line in histograms). Numbers on histograms indicate the percentage of cells in the similarly coloured gate.

(E) Expression of the indicated exhaustion markers in tumour-infiltrating donor T cells. FMO, fluorescence minus one. Numbers on histograms are MFIs.

Data are pooled from (C & D) or are representative of (E & percentage of 4+ divisions in panel C) 2 experiments (n = 8 - 12 mice). Shown are means ± s.d. *P*-values were calculated using unpaired Student's *t*-test.

despite their earlier disadvantage, CD8-ligated cells and/or their offspring had significantly better anti-tumour functions.

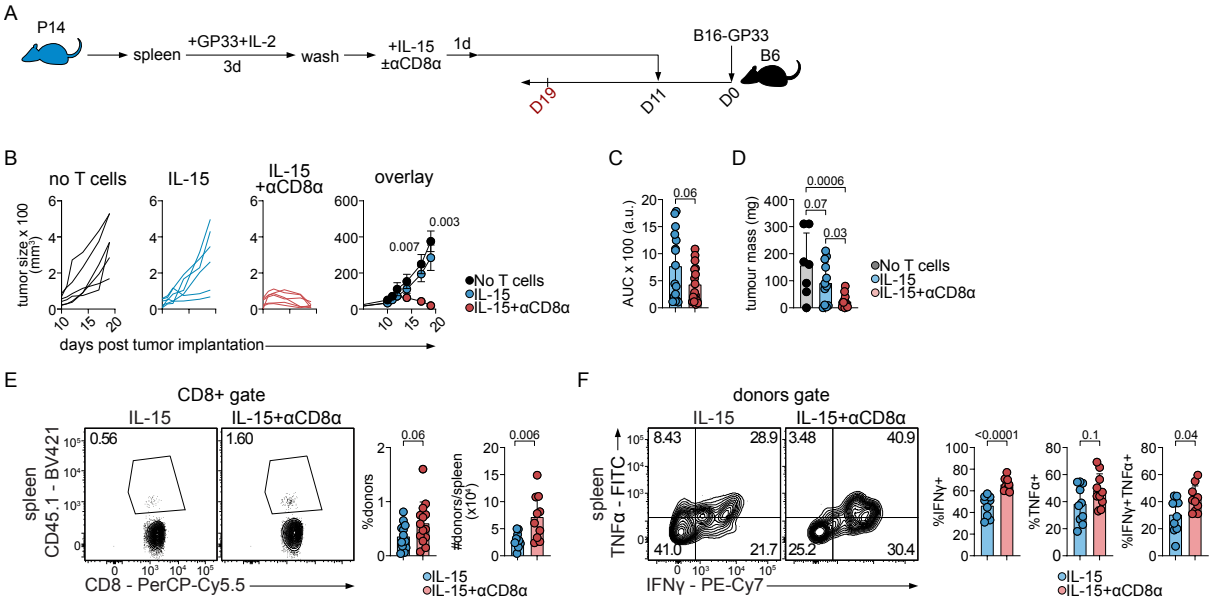

Figure 21: CD8 ligation enhances response to adoptive T cell therapy

(A) Experimental design. Cells were differentiated as in Fig. 13A and were intravenously injected into B16-GP33 melanoma-bearing mice that were sacrificed 8 days after adoptive transfer (or earlier if they reached termination criteria).

(B) Tumour growth in different treatment groups.

(C) Tumour growth rate was quantified as area under the curve (AUC) for every line (corresponding to a single mouse) as in B.

(D) A bar plot comparing tumour masses of differently treated mice.

(E) Frequency and absolute numbers of donor cells recovered from the spleen 8 days after transfer.

(F) Spleen cells were stimulated *ex vivo* with GP33 for 4 - 6 hours and cytokine production was analysed by flow cytometry.

Data are representative (B) or are pooled from 2 - 3 independent experiments (C - F; n = 10 - 14 mice per group). Error bars refer to s.d. *P*-values were calculated using unpaired Student's *t*-test (C, E, and F) or one-way ANOVA (D).

Because of tumour regression in almost all mice treated with CD8-ligated cells, it was not possible to perform a comparative in-depth analysis on TILs. Instead, I focused on circulating cells in the spleen. CD8 agonism increased the number of splenic donor cells (Fig. 21E), suggesting that it enhanced antigen-independent survival. Additionally, *ex vivo* stimulation of splenocytes with GP33 revealed the enhanced capacity of CD8 mAb-treated cells for cytokine production (Fig. 21F). Taken together, these data show that the hybrid differentiation state induced by CD8 agonism supports T cell anti-tumour function *in vivo* without compromising

long-term survival. Hand-in-hand, these two features efficiently control tumour growth.

5.9 Exhausted CD8+ T cells upregulate CD8 expression

Motivated by the superior tumour control achieved by adoptively transferred CD8-ligated cells, I wanted to investigate the utility of this approach for revitalising endogenous T cells. Specifically, I asked whether injecting tumour-bearing mice with an agonistic anti-CD8 antibody would control tumour growth. I examined surface CD8 expression levels in TILs in order to infer which cell populations would be targeted by this therapy. For this purpose, I analysed publicly available ATAC-seq and RNA-seq data. Mognol and colleagues implanted B16 cells expressing ovalbumin (Ova) in B6 mice and transferred pre-activated antigen-specific OT1 cells (recognising Ova) as well as T cells with an irrelevant TCR (P14 cells) [468]. Both OT1 and P14 cells were later sorted from the tumour and used for ATAC-seq to find changes caused by specific antigen recognition. The *Cd8a* locus and enhancer elements separating it and the *Cd8b1* locus, but not the *Cd8b1* locus itself, were more accessible in OT1 cells, which are antigen-specific, compared to P14 cells (Fig. 22A). OT1 cells were additionally more exhausted as evidenced by enhanced accessibility of the exhaustion marker Tim-3 (encoded by *Havcr2*).

Next, I analysed single-cell RNA-seq (scRNA-seq) data of 2,124 P14 cells isolated from B16-GP33 tumours (and thus were more exhausted) and 6,306 P14 cells harvested from the spleen [479]. Compared to splenic P14 cells, TILs significantly upregulate *Cd8a* expression (Fig. 22B, C). Since T cell exhaustion happens gradually [339], I longitudinally followed changes in CD8 expression by TCR_{TAG} cells infiltrating hepatocellular carcinoma in AST-Cre-ER^{T2} mice [452]. In these mice, liver cancer is autochthonous and tamoxifen-inducible, with cancer cells expressing the TAG antigen [339]. RNA-seq analysis showed that during the early dysfunctional state (days 5 to 7 post tumour initiation [452]), TCR_{TAG} cells downregulated *Cd8a*, which coincided with the upregulation of effector T cell markers like *Cd44, Klrg1*, and *Ifng* (Fig. 22D). However, as cells became terminally exhausted (starting on day 14), *Cd8a* levels increased.

I additionally performed a cross-sectional analysis of CD8 protein expression in endogenous B16-infiltrating T cells. By day 19 after tumour implantation, three distinct populations could be identified (Fig. 22E); PD-1-Tim-3- cells are the least exhausted and PD-1+Tim-3+ cells are terminally differentiated (and thus have the least functional TCR signalling pathway).

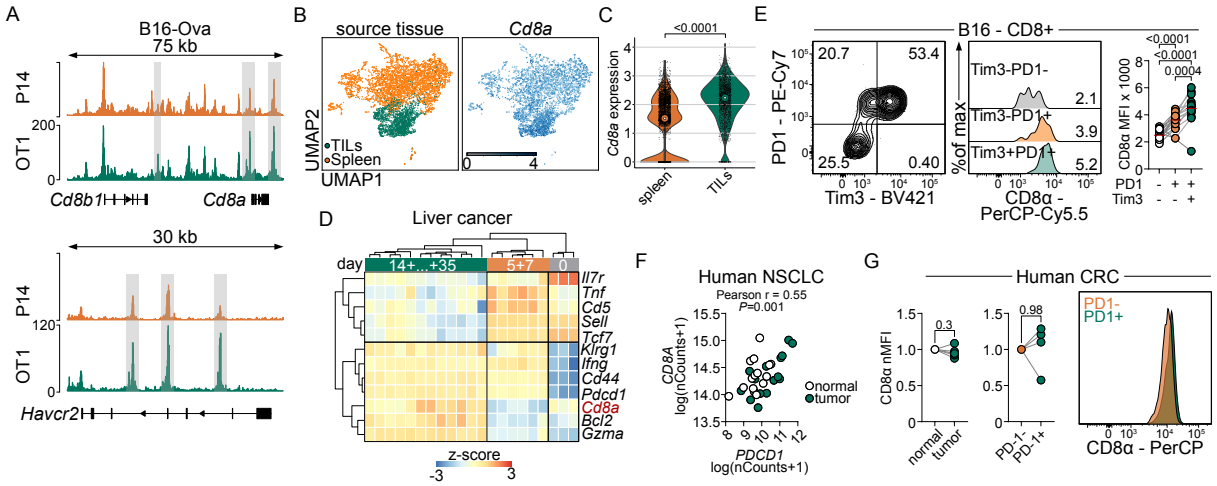

Figure 22: Terminally exhausted, tumour-infiltrating T cells upregulate CD8 expression

(A) B16-Ova-bearing mice received OT1 and P14 T cells. ATAC-seq was performed on donor cells sorted from the tumour 8 days after adoptive transfer [468]. Differentially accessible regions are highlighted in grey.

(B) Seven days following P14 T cell transfer to B16-GP33 tumour-bearing mice, P14 cells were sorted from spleen and tumour and used for scRNA-seq [479]. Shown is a Uniform Manifold Approximation and Projection (UMAP) representation of P14 cells coloured by tissue-of-origin or by normalised expression of *Cd8a*.

(C) Expression of *Cd8a* in P14 cells sorted as in B.

(D) A heatmap showing normalised counts of the indicated genes in antigen-specific TCR_{TAG} cells isolated from the tumour of liver cancer-bearing mice on different days following tumour initiation [452].

(E) Mice were implanted with B16-GP33 cells. After 19 days, tumour-infiltrating CD8+ T cells were analysed for CD8 expression levels. Numbers on histograms are CD8α MFI x 1000.

(F) Correlation between the expression of *PDCD1* and *CD8A* in CD8+ T cells isolated from the tumour and adjacent normal tissue of 16 patients with non-small cell lung cancer (NSCLC) [471].

(G) Normal and tumour tissues were sampled from 4 patients with colorectal carcinoma (CRC). CD8α protein expression was compared between the indicated groups.

Data are representative of 5 independent experiments (E; n = 15). *P*-values were calculated using Mann-Whitney *t*-test (C), RM one-way ANOVA (E), or Student's paired *t*-test (G).

PD-1+Tim-3- cells, however, are polyfunctional, proliferative, and responsive to immune-checkpoint blockade (ICB) [344, 392, 393]. This gradient of T cell exhaustion was matched by a gradient of CD8 protein expression (PD-1+Tim-3+ > PD-1+Tim-3- > PD-1-Tim-3-). Together, these results further support that CD8 levels are tightly regulated and emphasise the dependence of CD8 expression on functional TCR signalling.

Finally, I transferred these observations to human TILs. CD8+ T cells were sorted from tumour and adjacent normal tissue sampled from patients with non-small cell lung cancer (NSCLC) [471]. RNA-seq analysis of these cells showed a direct correlation between the degree of exhaustion (the expression of *PDCD1*, which encodes PD-1) and *CD8A* mRNA levels (Fig. 22F). CD8 protein expression by CD8+ T cells isolated from colorectal carcinoma (CRC) samples was comparable to cells sorted from adjacent normal tissue. However, in 3 out of 4 patients, PD-1+ TILs expressed higher levels of CD8 protein relative to less exhausted PD-1- TILs isolated from the same patient (Fig. 22G). These data show that in humans and mice, exhausted TILs isolated from different tumours upregulate CD8 expression on the transcriptional and protein levels. Because exhausted T cells have dysfunctional TCR signalling [533], these results are in line with my earlier observation that memory cells, which survive in the absence of TCR activation, have higher CD8 levels. Besides, these findings suggest that exhausted T cells are potential targets for anti-CD8 antibodies.

5.9.1 TCR desensitisation causes CD8 upregulation in TILs

To confirm that CD8 downregulation in TILs was due to TCR desensitisation and not other tumour-related factors, I cultured T cells *in vitro* under exhaustion-inducing conditions [379]. P14 cells were repeatedly pulsed with their cognate antigen in a normoxic, nutrient-replete environment (Fig. 23A). Alternatively, after initial antigen recognition, *acutely* activated P14 cells were maintained in the presence of IL-2 only. Chronic antigen exposure led to the upregulation of Tim-3 and PD-1 (Fig. 23B) confirming T cell exhaustion. Chronically activated P14 cells had a higher level of CD8 (Fig. 23C). Additionally, PD-1+Tim-3- cells had an intermediate level of CD8 expression compared to the other cell subsets, similar to what was observed for TILs (Fig. 22E). Response to ICB therapy is highly dependent on this intermediate population, which proliferates to give rise to terminally exhausted PD-1+Tim-3+ cells (with higher CD8 levels) [344, 393, 396]. Indeed, when I analysed scRNA-seq of human TILs isolated from patients with melanoma [473], I found that responders (R) to ICB upregulate T cell stemness

factors like *IL7R, CCR7,* and *TCF7* in addition to *CD8A* (Fig. 23D). In fact, the ability to upregulate *CD8A* following ICB treatment was unique to responders. For non-responders (NR), *CD8A* expression was comparable between CD8+ T cells sorted pre- and post-therapy (Fig. 23E).

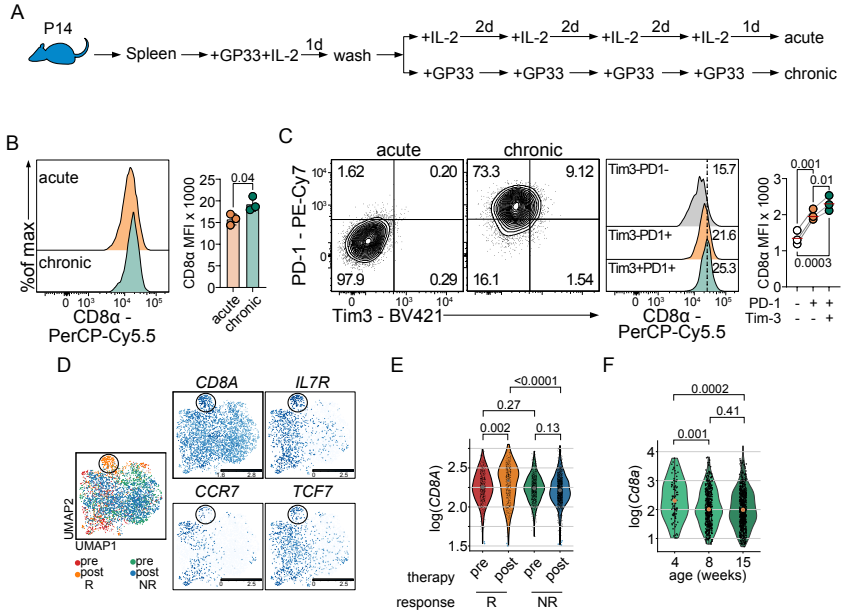

Figure 23: Chronic antigen exposure upregulates CD8 expression in dysfunctional T cells

(A) Schematic of experimental design to generate exhausted T cells *in vitro*.

(B) CD8α expression in P14 cells treated as in A.

(C) Chronically activated P14 cells (as in A) were assayed for the expression of the exhaustion markers Tim-3 and PD-1, and CD8α levels by the indicated populations was measured.

(D and E) Tumour infiltrating CD45+ cells were sorted from patients with melanoma before and after treatment with immune checkpoint blockers and used for scRNA-seq [473]. CD8+ T cells were selected based on the co-expression of *CD3E* and *CD8A*.

(D) A UMAP representation of 3,850 CD8+ T cells colour-coded based on treatment response and time of collection or normalised expression of the indicated genes. Encircled are cells belonging to responders after therapy. Pre, pre-therapy. Post, post-therapy. R, responders. NR, non-responders.

(E) A violin plot of *CD8A* expression in the different groups.

(F) Expression of *Cd8a* in pancreatic islet-infiltrating CD8+ T cells in non-obese diabetic (NOD) mice of the indicated ages [478].

Data are representative of 2 experiments (B & C; n = 3 - 4 mice per experiment). *P*-values were calculated using unpaired Student's *t*-test (B), RM one-way ANOVA (C), or one-way ANOVA with Tukey's correction (E & F).

Finally, I asked whether chronic antigen exposure *per se* or the resulting TCR desensitisation were responsible for CD8 upregulation in cancer. An insight into this question could be derived from analysing auto-reactive CD8+ T cells in non-obese diabetic (NOD) mice [534]. In this model, T cells are continuously exposed to their cognate antigen, but they remain functional and gradually (with age) destroy pancreatic islets [535]. Analysis of scRNA-seq data of pancreatic CD8+ T cells sorted from NOD mice [478] revealed that T cells have significantly lower *Cd8a* expression by 8 weeks of age, which coincides with the onset of major structural and cellular changes in the pancreas [536]. Despite chronic antigen exposure, *Cd8a* levels remain low in 15-weeks old mice (Fig. 23F). Collectively, these data show that active TCR signalling is tightly linked to CD8 downregulation. Antigenic clearance or chronic antigen exposure lead to increased CD8 levels in stem cell-like memory cells and exhausted T cells, respectively. Importantly, these experiments suggest that both progenitor and terminally exhausted cells are potential targets of injected anti-CD8 antibodies because they express the highest levels of surface CD8.

5.10 CD8 antigen-binding fragment recapitulates CD8 mAb effects

ADCC-mediated depletion of CD8 mAb-bound cells (Fig. 20) precludes therapeutic injection of this antibody. Therefore, I investigated whether using only the antigen-binding fragment, which does not induce ADCC, would be enough to induce effects similar to those observed with the full-length antibody. Pepsin digestion of immunoglobulins generates a bivalent antigen-binding fragment, F(ab′)2, and fragment crystallisable (Fc) domain (Fig. 24A) [537, 538]. I tried two different approaches to purify the F(ab′)2 fragment, which was successfully generated following digestion (Fig. 24B, C; see band at 110 kDa). The CD8 mAb I used is a rat antibody of the IgG2a isotype whose Fc fragment binds protein G. I used protein G columns and protein G beads from two different vendors, but I was only able to purify a 55 kDa fragment which likely corresponds to Fab′ (Fig. 24B, C). It is possible that the F(ab′)2 fragment was reduced into Fab′ at one point during purification (Fig. 24D).

To verify that the purified fragment (referred to as Fab′) was able to bind CD8 antigen, I performed a competitive enzyme-linked immunosorbent assay (ELISA) (Fig. 24E). Activated P14 splenocytes (>98% CD8+ cells) were lysed and the protein lysate was incubated with 10 µg/mL CD8 mAb and a serial dilution of Fab′. CD8 mAb was detected using a secondary HRP-conjugated anti-rat antibody. The ability of Fab′ to bind CD8 antigen was detected as a de-

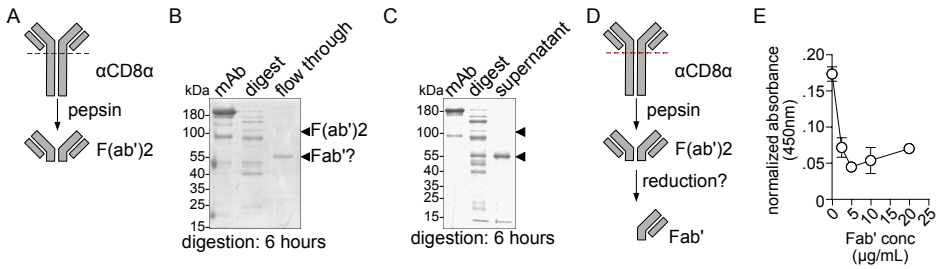

Figure 24: CD8α Fab′ recovery after pepsin digestion of full length antibody

(A) Diagram showing the schematic structure of F(ab′)2 following pepsin digestion.

(B and C) Full length αCD8α antibody was pepsin-digested and digestion products were purified using either protein G columns (B) or protein A/G PLUS agarose beads (C). Samples were used for SDS-PAGE and Coomassie blue staining. Arrow heads indicate the expected size of the F(ab′)2 and Fab′ fragments.

(D) Schematic of a possible reaction sequence, where the F(ab′)2 fragment gets reduced to Fab′.

(E) The ability of the recovered Fab′ fragment to bind CD8 was tested using competitive ELISA. Protein lysate of activated P14 CD8+ T cells was used as antigen. Shown are means ± s.d.

Data are representative of 2 (E) or 5 (B & C) experiments.

crease in bound secondary antibody, which indicated that the CD8 mAb was out-competed. The Fab′ fragment was indeed able to bind CD8 evidenced by the almost 75% decrease in CD8 mAb binding in the presence of 5 µg/mL of Fab′. Significantly, this strongly supports that the purified fragment was indeed Fab′, as 10 µg of the full-length antibody (bivalent, 180 kDa) should be able to bind the same amount of antigen as 6.1 µg of the Fab′ fragment (monovalent, 55 kDa).

In the next set of experiments, I tested whether CD8 Fab′ was able to induce the same effector T cell features as CD8 mAb. I differentiated memory-like P14 cells in the presence of 10 µg/mL CD8 mAb or 6 µg/mL CD8 Fab′. I observed the formation of CD8 blasts induced by CD8 Fab′, although they were much fewer compared to clusters formed by cells treated with the full-length antibody (Fig. 25A). Furthermore, GP33-induced cytokine production was promoted by CD8 Fab′ treatment compared to treatment with IL-15 alone (Fig. 25B). Again, the full-length antibody was more efficient at stimulating cytokine production. These results suggest that at least some of the effector features promoted by CD8 ligation were dependent on the bivalency of the antibody.

The main purpose of generating this Fab′ fragment was to overcome CD8 depletion in-

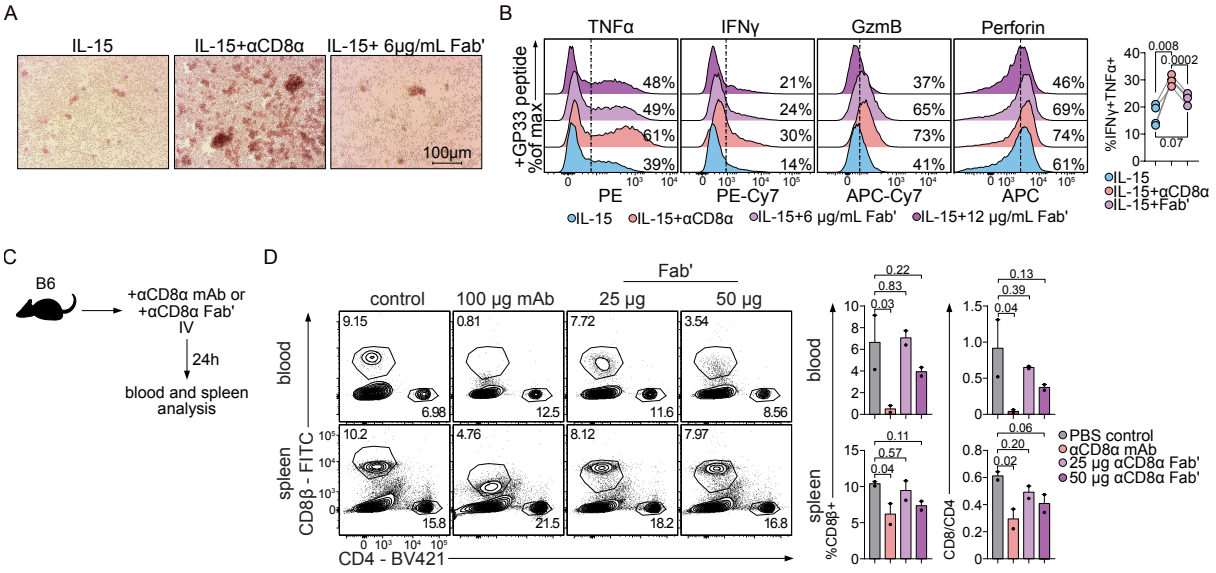

Figure 25: Functional validation of CD8α Fab′ fragment

(A and B) P14 cells were differentiated as in Fig. 13A in the presence or absence of different concentrations of Fab′ fragment.

(A) Bright field microscopic images of clusters formed after incubation with either 10 µg/mL of full length αCD8α antibody or with 6 µg/mL αCD8α Fab′. Scale bar = 100 µm.

(B) Differentiated cells were re-stimulated using GP33 peptide for 4 - 6 hours and cytokine production was measured using flow cytometry. Numbers on histograms represent the percentage of cytokine positive cells.

(C) Experimental set up. Wildtype mice received one intravenous (IV) injection of αCD8α antibody or αCD8α Fab′ in PBS. Mice were sacrificed one day later.

(D) Blood and spleen cells were analysed for the abundance of CD8+ T cells using flow cytometry.

Data are representative of 2 experiments (B; n = 2 - 3 mice/experiment) or are from one trial (D; n = 2 mice per group). Error bars refer to s.d. *P*-values were calculated using RM one-way ANOVA (B) or one-way ANOVA (D).

duced by the full-length antibody. To confirm that CD8 Fab′ did not cause CD8+ T cell depletion, I injected wildtype B6 mice intravenously with either CD8 mAb or Fab′ and evaluated changes in the percentage of blood and spleen CD8+ T cells 24 hours later (Fig. 25C). For flow cytometry, I used an antibody against a different CD8 subunit (CD8β) to avoid competition between antibodies binding the same CD8α epitope. As would be expected, the full-length antibody almost completely depleted blood CD8+ T cells and significantly reduced their abundance in the spleen (Fig. 25D). However, 25 µg CD8 Fab′ did not significantly alter the percentage of CD8+ T cells. A higher dose of CD8 Fab′ caused a slight, but insignificant,

decrease in CD8+ T cell frequency. Together, these results show that the isolated fragment was able to bind the CD8 antigen and induce T cell effector functions without causing T cell depletion.

5.11 CD8 Fab′ reduces tumour growth but does not synergise with ICB

To test the efficacy of CD8 Fab′ as an immunotherapeutic approach, I treated B16 melanoma-bearing mice with CD8 Fab′ and compared the response to mice injected with either anti-PD-L1 antibody (αPD-L1) or with both CD8 Fab′ and αPD-L1 (co-therapy) (Fig. 26A). Treatment with CD8 Fab′ alone caused 60% reduction in tumour size and was comparable in effect to treatment with αPD-L1 (Fig. 26B). However, co-therapy, at best, did not enhance the anti-tumour response (Fig. 26C) and in one experiment, mice receiving co-therapy had even bigger tumours compared to mice treated with either arm alone. This finding supports the functional utility of using CD8 Fab′ for immunotherapy, at least in this one pre-clinical model.

To examine immunophenotypic changes induced by Fab′ treatment, I collected blood, spleen, and tumour samples from mice on day 20 after tumour implantation. The percentage of CD8β+ (CD8+) cells in mice treated with CD8 Fab′ was comparable to isotype-treated mice (Fig. 27A). Similarly, in blood and spleen, there was no difference in the frequency of CD8+ cells between mice treated with αPD-L1 and those receiving co-therapy. I observed a tendency towards higher CD8+ T cell density and lower CD8 MFI in tumour and blood, respect-

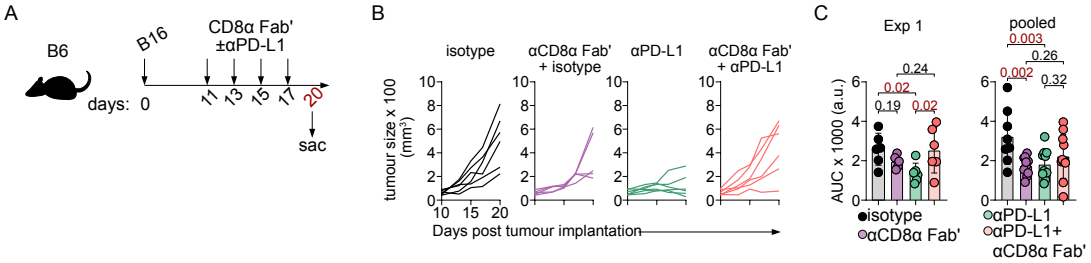

Figure 26: CD8α Fab′ treatment reduces tumour growth but does not enhance response to immune checkpoint blockade

(A) B16 melanoma-bearing mice were treated with 200 µg/mouse of αPD-L1 antibody, IgG isotype control, a combination of 20 µg/mouse CD8α Fab′ and IgG, or a combination of Fab′ and αPD-L1.

(B) Spider plots following tumour growth in differently treated mice.

(C) Bar plots of AUCs of one experiment or pooled from two independent experiments (n = 9 - 10 mice per group). *P*-values were calculated using one-way ANOVA (C).

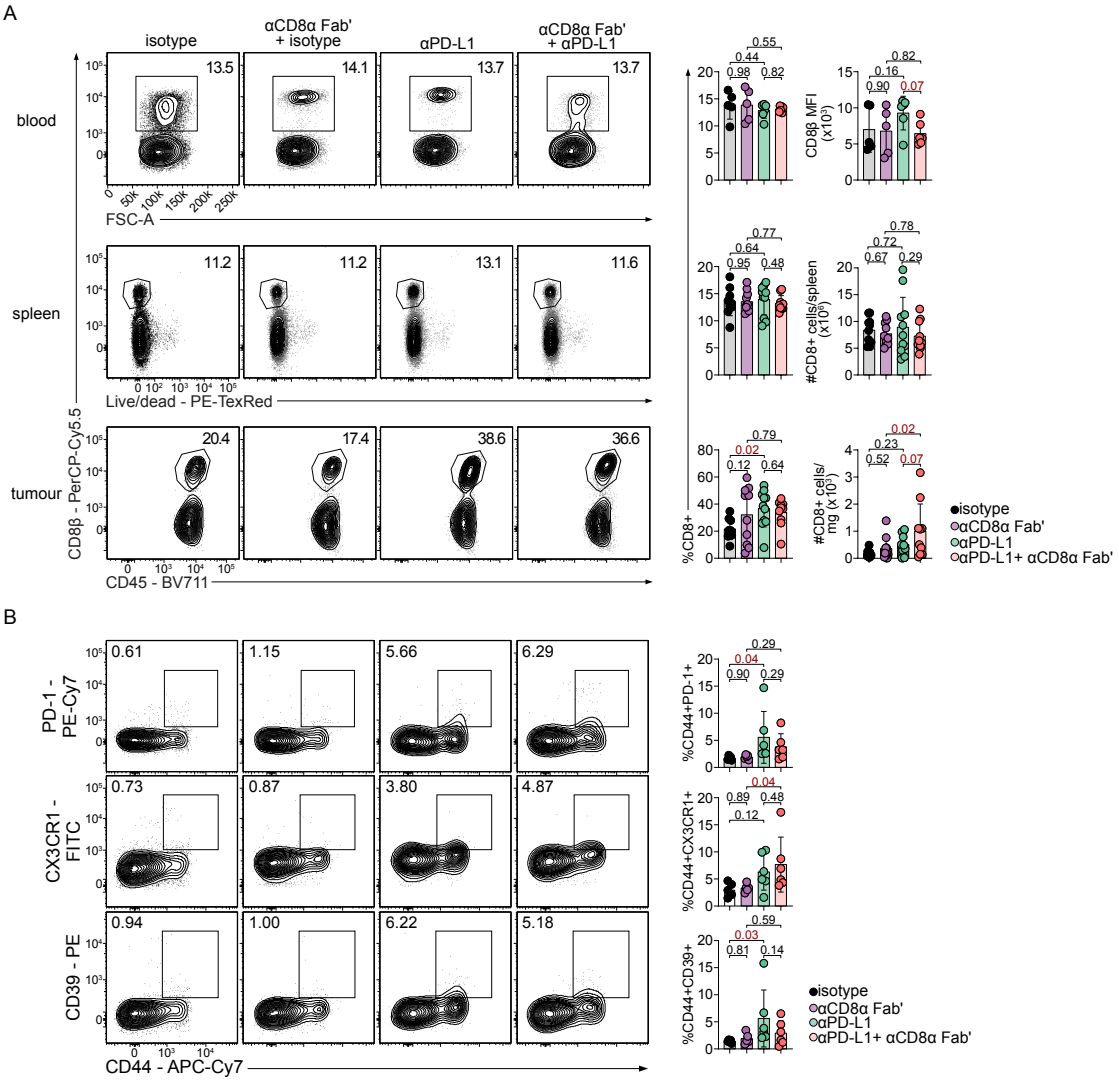

Figure 27: CD8α Fab′ treatment does not change the frequency of circulating anti-tumour CD8+ T cells

Mice were treated as in Fig. 26A, and blood, spleen, and tumour samples were harvested.

(A) Frequency of CD8+ T cells in mice that received different treatments.

(B) PD-1, CX3CR1, and CD39 were used to identify blood tumour-reactive CD8+ T cells.

Data are representative of two independent experiments (n = 9 - 10 mice per group). Shown are means ± s.d. *P*-values were calculated using one-way ANOVA.

ively, of the co-therapy group compared to mice treated with αPD-L1 alone. These data show that repetitive injection of CD8 Fab′ did not cause CD8 depletion, and suggest that qualitative, rather than quantitative, changes might be responsible for the favourable anti-tumour response in Fab′ treated mice.

CD8 is, by definition, expressed by all CD8+ T cells. I tested whether CD8 Fab′ activated

cells that were not specific to tumour antigens and thus might not reflect treatment response. Circulating tumour-specific CD8+ T cells express CX3CR1, CD39, and PD-1 [539]. Compared to isotype-treated mice, αPD-L1 induced an increase in the abundance of PD-1+ and CD39+ cells, which was not observed when mice were treated with CD8 Fab′ (Fig. 27B). Similarly, CD8 Fab′ had no influence on αPD-L1-induced expansion of circulating tumour-specific cells. However, when combined with αPD-L1, CD8 Fab′ caused a significant reduction in the percentage of tumour-reactive, CD44+ T cells among CD8+ TILs (Fig. 28A), indicating that CD8 Fab′ treatment might have recruited by-stander T cells to the tumour.

5.11.1 CD8 Fab′ partially rescues T cell exhaustion

A more in-depth analysis of tumour-specific CD44+ TILs revealed that mono-therapy with CD8 Fab′ decreased the expression of the exhaustion markers CD38 and Tigit, whereas the exhaustion markers Tim-3, Lag-3, and PD-1 were unaffected by CD8 ligation (Fig. 28B). In line with previous reports, αPD-L1 treatment did not change the levels of any of these inhibitory receptors [339]. Interestingly, when compared to treatment with CD8 Fab′ alone, co-therapy caused an increase in CD38 expression and a tendency towards higher levels of Tigit. This observation indicates that while CD8 Fab′ relieves exhaustion to some extent, CD8 agonism in combination with ICB poises TILs towards a more exhausted phenotype.

5.11.2 CD8 Fab′ treatment does not influence cytokine production in TILs

An important feature of T cell exhaustion is loss of effector functions, which is detectable as decreased expression of surface markers, like CX3CR1, and the inability to secrete cytokines [418]. CD8 agonism, either alone or in combination with αPD-L1, did not change the expression of CX3CR1 (Fig. 29A). Unlike CD8 Fab′, αPD-L1 caused a tendency towards increased IFNγ and TNFα production (Fig. 29B). However, none of the treatments examined influenced the expression of perforin and GzmB (Fig. 29C). These results suggest that, on a per-cell basis, CD8 agonism did not change the cytokine-production capacity in TILs.

5.11.3 CD8 agonism induces TIL proliferation

Response to immunotherapy is mediated by a population of CXCR5+ stem cell-like progenitors that proliferate to generate new effectors [393, 396, 399]. Because CD8 agonism induced T cell proliferation *in vitro* and *in vivo*, I asked whether CD8 Fab′ therapy had an effect on TIL

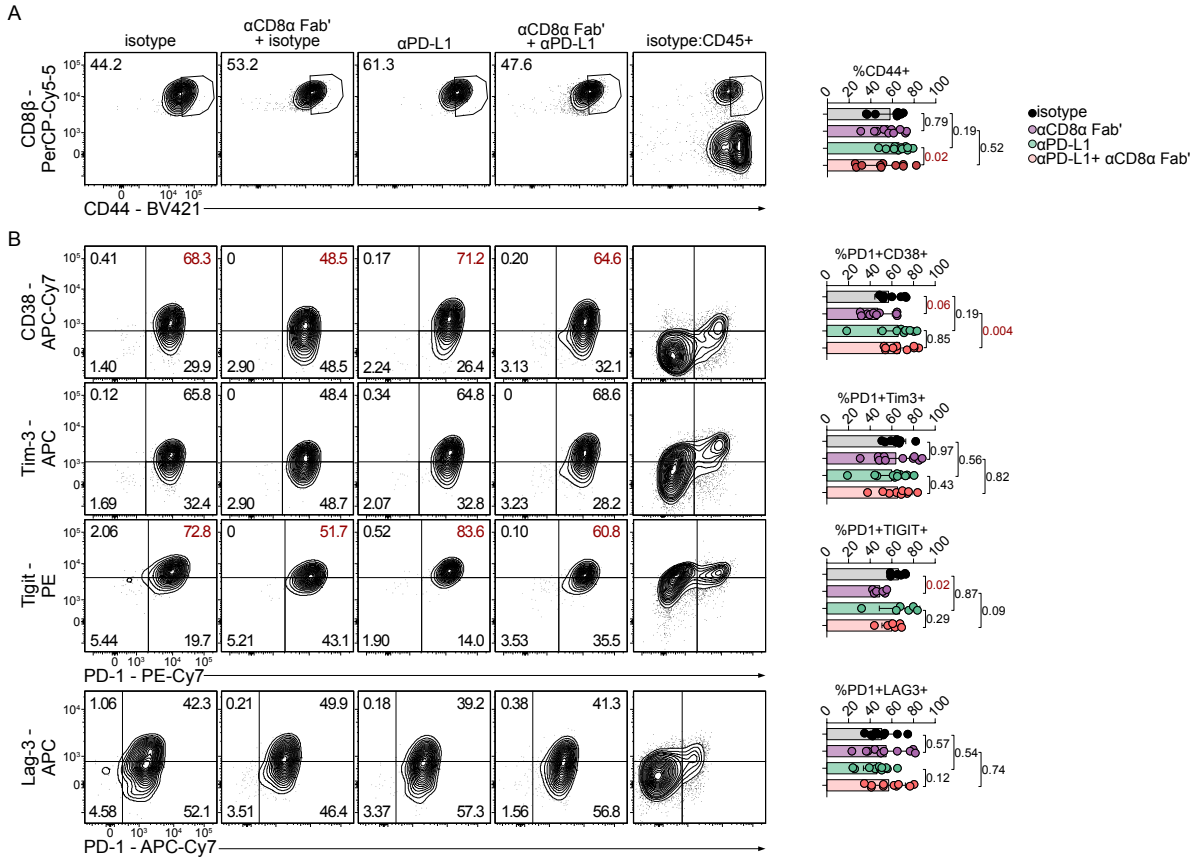

Figure 28: CD8 Fab′ partially relieves TIL exhaustion

Mice were treated as in Fig. 26A and tumour-infiltrating CD8+ T cells were analysed by flow cytometry.

(A) Frequency of CD44+ T cells among CD8+ TILs.

(B) CD44+ cells gated as in (A) were further analysed for the expression of the indicated exhaustion markers.

Live CD45+ cells were used (in addition to FMO) to guide gating. Data are pooled from two independent experiments (n = 9 - 10 mice per group). Shown are means ± s.d. *P*-values were calculated using one-way ANOVA.

proliferation. I found that CD8 Fab′ enhanced T cell expansion, indicated by an increase in the abundance of Ki67+ cells (Fig. 30). This proliferation marker is upregulated in progenitor exhausted cells and their immediate daughters [394]. However, CD8 Fab′-treated mice had a similar frequency of Ki67+ cells among the CXCR5+ progenitors as mice treated with the isotype control (Fig. 30). Importantly, the overall abundance of progenitor exhausted cells (defined as CXCR5+Tim-3-) was not reduced by CD8 Fab′ treatment, indicating that this approach successfully induced proliferation while maintaining the integrity of the progenitor pool. In contrast, αPD-L1 therapy increased the frequency of Ki67+CXCR5+ cells indicating

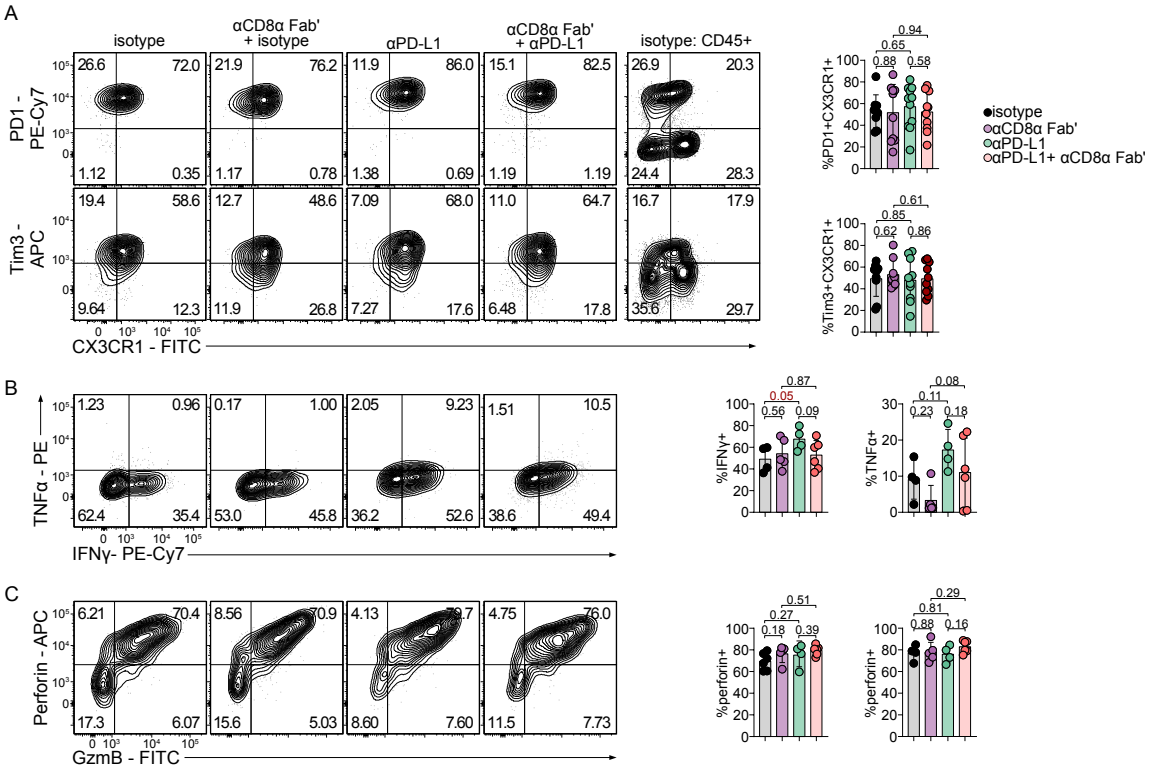

Figure 29: CD8α Fab' treatment does not influence TIL effector function

(A) Expression of the effector T cell marker CX3CR1 in CD8+CD44+ TILs.

(B and C) TILs were activated *ex vivo* with a combination of Phorbol-12-myristate-13-acetate (PMA) and ionomycin, and cytokine production was detected using flow cytometry.

Data are pooled from (A) or are representative of (B & C) two independent experiments (n = 9 - 10 mice per group). Shown are means ± s.d. *P*-values were calculated using one-way ANOVA.

enhanced progenitor cell expansion (Fig. 30). Paradoxically, relative to mice treated with αPD-L1 alone, co-therapy caused a significant reduction in progenitor cell proliferation, and a tendency towards reduced abundance.

Taken together, these experiments suggest that CD8 agonism induces the proliferation of progenitor cells and partially relieves exhaustion, which significantly reduces tumour growth. However, compared to αPD-L1, co-therapy caused a partial depletion of progenitor cells and limited their proliferative potential. This might explain the seemingly antagonistic effect of αPD-L1 and CD8 Fab′. Overall, these results support the therapeutic benefit of CD8 agonism in cancer and imply that this approach might impinge on similar signalling pathways as PD-1 blockade.

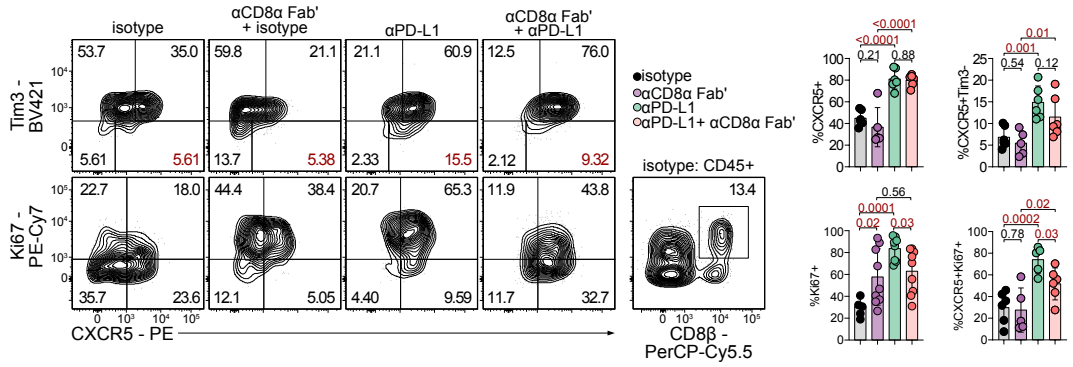

Figure 30: CD8α Fab' treatment induces TIL proliferation *in situ*

Percentage of stem cell-like (Tim3-CXCR5+) and proliferating (Ki67+) cells in CD8+CD44+ TILs isolated from mice treated as in Fig.26A. Total CD45+ cells were used as a gating guide.

Data are representative (CXCR5 staining) or are pooled from two independent experiments (Ki67 staining, n = 9 - 10 mice per group). Shown are means ± s.d. *P*-values were calculated using one-way ANOVA.

6 Discussion

During an immune response, T cells increase their antigen sensitivity by more than 50-fold without changing a single amino acid in the sequence of their TCRs [208]. This upgrade is durable and relies on the optimisation of the TCR machinery as well as downstream signalling pathways [208, 209, 211, 540, 541]. The results presented here suggest that regulation of CD8 expression is one way to improve the functional avidity of memory T cells. I followed changes in CD8 levels in the context of infection, tumour, and auto-immunity, and found that in the absence of productive antigenic stimulation, CD8 expression is upregulated. Using an agonistic anti-CD8 antibody, I was able to harness this feature to improve T cell metabolic profile and effector functions and to enhance the response to adoptive T cell therapy. In addition, the antigen-binding fragment of this same antibody was as efficient as αPD-L1 in controlling tumour growth in a pre-clinical melanoma model. Besides their translational potential, these data extend the classical view of CD8 as a TCR co-receptor.

6.1 Tonic and antigen-specific TCR signalling control CD8 levels

Changes in CD8 protein expression during the course of infection have been previously reported [208–210]. CD8 is downregulated in effector cells before it rebounds in memory cells. By analysing epigenetic and transcriptional data, I provide further support to this notion and exclude that this effect is secondary to differences in cell size, metabolic status, or total protein content between effector and memory cells. Furthermore, analysis of T cell activation in different pathological conditions strongly suggests that CD8 levels are regulated in response to *productive* antigen recognition. This was complemented by *in vitro* experiments using continuous antigen exposure. In this regard, antigenic stimulation is not unique in controlling CD8 expression. In fact, dynamic regulation of CD8 levels is a recurrent theme that seems to guide T cell fate decisions. CD8 downregulation by CD4CD8 double-positive thymocytes plays an integral role in the development of, paradoxically, cytotoxic CD8+ T cells [542, 543]. Further, tonic TCR signalling in response to self-peptides was shown to suppress *Cd8a* transcription in naive T cells [57]. This 'co-receptor tuning' was proposed as a mechanism to maintain T cell survival in the periphery without overt auto-reactivity. I observed selective downregulation of CD8 in TEM cells, which suggests that they use tonic TCR signalling to sustain their cytokine production capacity at the expense of stemness. Indeed, interruption of

the TCR signalling pathway after the resolution of acute LCMV infection severely limits the persistence of TEM, but not TCM, cells [544].

Why would memory cells need to upregulate CD8? CD8 expression dictates the threshold required for TCR activation; low avidity ligands can only activate T cells with high levels of surface CD8 [545], where CD8 can enhance TCR sensitivity by more than 1 million folds in some estimates [546, 547]. Therefore, CD8 upregulation in memory T cells might decrease the stringency of antigen recognition. Indeed, cross reactivity is a direct function of the strength of CD8 interaction with MHC-I [548], which can be protective against heterologous infections. Pre-existing, memory CD8+ T cells have been shown to cross-react to severe acute respiratory syndrome coronavirus 2 (SARS-CoV2) and to protect against the development of severe coronavirus disease 2019 (COVID-19) symptoms [549–551]. Besides its function in regulating TCR signalling, CD8α interacts with paired immunoglobulin-like receptor a (PILRα) expressed by myeloid cells in order to maintain naive and memory CD8+ T cell quiescence and longevity [552]. Combined with findings reported here, this hilights the function of CD8 as a checkpoint regulator of T cell activation and quiescence, even in the absence of cognate antigen recognition.

The correlation between CD8 levels and the functional state of the cell is, however, contextual. First, I observed a negative correlation between CD8 and the anti-apoptotic protein Bcl-2 at an effector time point, but a positive correlation in memory cells. This suggests that memory cells had low surface CD8 levels at the effector phase of the immune response. In support of this scenario, a recent report showed that early after LCMV infection, a subset of cells with restrained proliferation upregulates memory T cell markers like CD62L, Tcf-1, and IL-7Rα, and preferentially differentiates into long-term memory T cells [273]. These cells exhibit strong TCR signalling on 8dpi and are expected to have lower surface CD8 levels, in agreement with my results. Second, high CD8 levels mark cells without active TCR signalling. These include both memory cells that develop with antigen clearance and exhausted T cells with persistent antigen exposure. In fact, the exhaustion ‘gradient’ in T cells isolated from murine B16 melanoma directly matched a gradient of CD8 levels. Exhausted T cells have desensitised TCRs [533] and upregulate PD-1, which inhibits TCR signal transduction [167, 168, 170]. Therefore, this counter-intuitive positive correlation between CD8 expression and T cell exhaustion further supports that *functional* TCR signalling suppresses CD8 expression.

6.2 Therapeutic targeting of CD8

In light of the essential role CD8 plays in TCR signalling regulation [39, 91, 545–548], several therapeutic interventions that target CD8 have been proposed. Non-depleting antagonistic anti-CD8 antibodies were tested in pre-clinical models as a therapeutic option for type 1 diabetes mellitus [553]. By blocking TCR signalling, the antibody severely limits the ability of T cells to persist in pancreatic islets and was even shown to reverse the disease course when administered to young NOD mice [554]. Importantly, long-term tolerance to pancreatic β-cells was maintained even after treatment withdrawal. This is reminiscent of observations made using anti-CD4 antibodies to induce transplantation tolerance [555–557] and highlights the role of co-receptors in determining the choice between anergy and immunological memory. For tumour immunotherapy, strategies to upregulate [558, 559] or downregulate [560] CD8 expression have been described. On one hand, transgenic expression of CD8 heterodimer strongly enhances the effect of tumour antigen-targeting CAR T cells in a leukaemia xenograft mouse model [561]. This effect correlates with enhanced stem cell features and upregulation of TCM cell markers including *TCF7, IL7R*, and *CCR7*. On the other hand, CRISPR-Cas9-mediated deletion of *Cd8a* in antigen-specific T cells synergises with ICB following adoptive transfer to B16 melanoma-bearing mice [560]. The motivation for this experiment was that TCR signal strength correlates both with proliferation and rapid dysfunction, and that hampering antigen recognition by deleting *Cd8a* could protect cells against exhaustion. Therefore, the therapeutic effect of CD8 targeting appears to be context-dependent.

6.3 CD8 agonism rewires metabolism and creates a hybrid phenotype

To investigate the functional consequences of CD8 targeting, I used an agonistic anti-CD8 antibody [91, 527, 528]. Early studies focusing on the function of co-receptors found that anti-CD8 antibodies could induce or suppress antigen recognition, Lck phosphorylation, and cytokine release depending on the antibody clone used and, possibly, subsequent conformational changes induced in the CD8 heterodimer [91, 527, 528, 562, 563]. I validated that the CD8 mAb I used was able to induce proximal TCR signalling in naive, memory, and IL-15-differentiated cells. T cells expanded in the presence of IL-15 display a memory-like phenotype both in terms of function and metabolism [134, 312]. Compared to IL-2-differentiated cells, IL-15-skewed cells are quiescent; they downregulate glycolysis and rely instead on fatty

acid metabolism, and they do not efficiently secrete cytokines. However, IL-15-skewed cells survive longer in host mice after adoptive transfer and are better equipped to control tumour growth [450, 451].

By inducing TCR stimulation under homeostatic (CD8 mAb + IL-15) rather than growth (antigen + IL-2) conditions, I was able to recapitulate effector as well as memory T cell features. CD8-ligated cells upregulate CD44, T-bet, and PD-1 (like effector cells). They were more proliferative and cytotoxic *in vitro* and *in vivo*. At the same time, mAb-treated cells upregulated stemness markers Tcf-1 and Bcl-2 and were more persistent *in vivo*. Together, this dramatically improves tumour control in a mouse model of adoptive T cell therapy. A conceptually similar approach was recently reported, where suboptimal activation of T cells in the presence of an IL-2 partial agonist (also a partial antagonist) reduces cytokine release in favour of enhanced Tcf-1 and CD62L expression and higher SRC [564]. Adoptive transfer of cells expanded with this partial agonist to mice bearing solid or leukaemic malignancies significantly reduced tumour burden, enhanced survival, and tumour 'memory'; cured mice were protected against re-challenge. Therefore, a hybrid effector-memory differentiation state is the optimal T cell for immunotherapy.

6.3.1 CD8 agonism fosters a hybrid effector/memory metabolic state

The intermediate position of CD8-ligated cells on the effector-memory continuum could also be observed on the metabolic level. In fact, I found that the effector function of CD8-ligated cells depended on metabolic reprogramming. In general, an activated T cell is about to embark on an energetically demanding journey, where it will upregulate RNA and protein synthesis, rapidly proliferate, and elaborate cytokines. Therefore, T cell activation requires a concerted series of metabolic changes that are intrinsically linked to effector T cell function. The T cell will upregulate glucose and amino acid transporters [115, 446], it will dramatically enhance its glycolytic rate, and will use glutamine to fuel anaplerotic TCA reactions [276, 298, 565]. These metabolic changes are essential for the expression of master transcription regulators, egress from secondary lymphoid organs, and cytokine production and release [290, 294, 304, 351, 566, 567]. Memory T cell quiescence and longevity, on the other hand, are characterised by, and dependent on, oxidative metabolism particularly of fatty acids [312–314, 317, 324].

CD8 ligated cells acquired features of effector cell metabolism including increased size,

enhanced nutrient uptake, and glycolysis. At the same time, they maintain fatty acid uptake, are predicted to have higher rates of fatty acid β-oxidation (due to *Lal* upregulation), exhibit higher SRC, and downregulate CD71. This second set of features is usually correlated to the memory phenotype. It should be noted that to measure glucose uptake, I used a fluorescent glucose analogue (2-NBDG) [568], whose sensitivity was recently brought into question [569, 570]. Nevertheless, seahorse experiments show that ligated cells are more glycolytic even in the absence of glucose (basal levels). Heavy carbon tracing revealed that CD8-ligated cells do not efficiently use glucose for the TCA cycle. In fact, I observed a significant reduction in the rate of glucose assimilation into fumarate, malate, and aspartate/OAA. This suggests a selective inhibition of succinate dehydrogenase (complex II of the electron transport chain) and results in an increase in the succinate/α-KG ratio. α-KG was depleted in CD8-ligated cells even when the entire pool (labelled and unlabelled) was considered. The succinate/α-KG ratio was recently shown to correlate positively with inflammation and IFNγ production in activated CD4+ T cells [571]. The effects of α-KG itself on IFNγ production were mostly studied in CD4+ and are rather controversial [571–573]. Still, α-KG is an important cofactor in histone and DNA demthylation reactions [299, 300, 574–576], which suggests that its deficiency might alter the epigenetic profile in CD8-ligated cells.

It should be emphasised that the reduction in glucose-derived TCA cycle intermediates after CD8 mAb treatment does not reflect a general inhibition of the TCA cycle. On the contrary, with the exception of α-KG and a slight reduction in citrate, all measured intermediates were more abundant in CD8-ligated cells. It is plausible that mitochondrial metabolism is supported by fatty acids instead of glucose. Although cells were incubated in a fatty acid-free medium for seahorse analyses, CD8-ligated cells could be reasonably expected to contain more lipid stores and to be able to mobilise them due to the higher expression of *Dgat1* and *Lal*, respectively. High *Lal* levels in particular were linked to enhanced SRC [312], which is a measure of how close a cell is to its bioenergetic limit.

Interestingly, despite the pronounced increase in glutamine concentrations in CD8 mAb-treated cells, there was no difference in its assimilation into TCA cycle intermediates. In line with Michaelis-Menten kinetics [577], which would suggest that the enzyme concentration/activity is limiting, my qRT-PCR data show that *Gls1* is not upregulated in CD8 mAb-treated cells, despite the higher intracellular glutamine concentrations. Enhanced glycolytic as well as oxidative T cell metabolism as a result of glutaminase inhibition was previously re-

ported and was linked to improved cytokine release and T cell antitumour function [531]. A latent level of glutaminolysis inhibition provides an explanation for the insensitivity of CD8-ligated cells to glutaminase inhibitors and glutamine deprivation. These treatments upregulate cytokine production in IL-15-treated cells to the same level observed in their untreated, CD8-ligated counterparts, suggesting that inhibition of glutamine metabolism plays a role in enhancing the effector function in CD8 mAb-treated cells. Unexpectedly, and in contrast to several reports demonstrating the importance of glycolysis for effector T cell functions [294, 565, 578], I found that inhibition of glycolysis, either pharmacologically or through glucose deprivation, strongly enhanced cytokine release in control cells differentiated with IL-15 alone. This discrepancy is very likely a product of the experimental design. I deprive T cells of glucose for one day before they are re-introduced to their cognate antigen in nutrient-replete conditions for 6 hours. It was recently shown that transient glucose starvation enhances glucose uptake when cells are re-exposed to glucose, which supports glycolytic, anabolic, and effector functions [579]. To strictly examine the impact of glucose metabolism on cytokine release, antigenic stimulation should ensue in the absence of glucose.

My treatment protocol, however, revealed an unexpected finding that would have very likely been missed otherwise. While inhibition of glycolysis and glucose starvation have similar effects in IL-15-differentiated cells, CD8-ligated cells behave differently in these two conditions. My data suggest that CD8-ligated cells are very sensitive to glycolysis-independent pathways of glucose metabolism. One possibility is that glucose is preferentially used for protein glycosylation in CD8-ligated T cells. TCR signalling was previously shown to induce the synthesis of uridine diphosphate N-acetylglucosamine (UDP-GlcNAc), a high energy donor of GlcNAc for glycosylation reactions [580]. Genetic loss of O-GlcNAc transferase (OGT), the enzyme that catalyses the addition of O-GlcNAc to serine/ threonine residues on several proteins [581], severely impairs CD8+ T cell expansion. However, effector functions were not explored in this report. Conjugated UDP is not detectable using GC-MS. To test this hypothesis, OGT and other glycosyl-transferases could be assayed on the transcript and protein level. Alternatively, liquid chromatography-MS could be used to perform an unbiased analysis of modified proteins. An important glycosylation target is the glucose transporter Glut-1 [582, 583]. Glycosylated Glut1 is more readily translocated to the cell surface in activated T cells, and deglycosylation limits glucose uptake [291]. This would explain the limited ability of CD8-ligated cells to rebound when they re-exposed to glucose.

In line with their rapid proliferation, nutrient import (detected as increased uptake, higher intracellular levels, or upregulation of transporters) was generally enhanced in CD8-ligated cells with the exception of CD71. Also known as transferrin receptor 1, CD71 is important for the uptake of iron from the circulation [584, 585]. Ferrous/Ferric ions are important co-factors for many biochemical reactions including DNA synthesis and repair and mitochondrial electron transport [586–588]. Consistently, CD71 is upregulated by rapidly proliferating cells including cancer cells and activated T cells [447, 589–592]. In fact, there is usually a positive correlation between the expression levels of CD71 and the neutral amino acid transporter CD98 [446, 447, 567], since a growing cell needs both amino acids and iron. I observed an increase in CD98 expression and function following CD8 mAb treatment. CD71, on the other hand, was downregulated. Failure to upregulate CD71 is a feature of anergic T cells that do not receive co-stimulatory signals [593]. However, CD8-ligated cells were not anergic. They were proliferative, cytotoxic, metabolically active, and long-lived. Perhaps another way to explain this conundrum is to consider that CD71 is a ferroptosis marker [594]. Ferroptosis is an iron-dependent form of cell death that can result from the accumulation of reactive oxygen species (ROS) and lipid peroxides [595, 596]. CD8-ligated cells have higher levels of TCR signalling, which is known to induce ROS generation [597–599]. In combination with the likely higher intracellular concentrations of free fatty acids, products of LAL-catalysed lipolysis, CD8 mAb-treated cells can possibly accumulate lipid peroxides [600]. In fact, the upregulation of the ferroptosis inhibitors Gpx4 and Fsp1 in CD8-ligated cells supports this hypothesis. Therefore, it is plausible that CD8 mAb-treated cells actively downregulate CD71 to limit their iron content in order to maintain their viability, although the exact mechanism is unclear. In any case, residual intracellular iron levels must be enough to support the wide array of metabolic processes taking place in a CD8-ligated cell, which are in many cases happening at a higher rate compared to cells treated with IL-15 alone. My data suggest that CD8 agonism achieves a delicate balance between cell growth and viability, which translates into enhanced effector function.

6.4 CD8 agonism as a potential immunotherapeutic strategy

6.4.1 CD8 ligation improves ACT response

Effector T cell function *in vitro* does not necessarily predict *in vivo* control of tumour growth [132, 133, 564]. Indeed, response to ACT correlates with the expression of memory markers and the abundance of T cells that show a stem-cell like phenotype [443, 450]. For T cells to efficiently and durably control tumours, they must meet at least three criteria; T cells must be able to 1) recognise and be activated by the tumour antigen in situ, 2) expand in the tumour microenvironment to give rise to numerous effector cells, and 3) persist at least long enough to eradicate all tumour cells [445, 450, 601]. Functionally and metabolically, CD8-ligated cells achieve a hybrid effector/memory state that allows them to meet all three requirements. These cells were able to recognise the tumour antigen (in this case GP33) with high affinity, were able to expand *in vitro* and *in vivo*, and were more readily detectable in the circulation of host mice even, in many instances, after tumour eradication.

Enhanced SRC is very likely the reason for prolonged persistence of CD8-ligated cells *in vivo*. This phenotype was observed in T cells expanded using IL-15, but also IL-7 and IL-21 [448, 449, 602–605]. The role glycolysis plays in supporting the therapeutic effect of CD8 mAb-treated cells is, however, less clear. Suppression of glucose metabolism was observed in almost all of the studies using IL-7/15/21 to differentiate T cells. Furthermore, pharmacological inhibition of glycolytic enzymes during *in vitro* priming of T cells improves their tumour cell killing capacity [304, 606], which might seem at odds with the repeatedly documented importance of glycolysis for cytokine release and effector immune responses [294, 565, 578]. A recent study provides a possible explanation for this discrepancy. While transient inhibition of glycolysis *in vitro* skews T cell differentiation towards a memory phenotype and augments their antitumour effect following adoptive transfer, genetic deletion of glycolytic enzymes severely hampers antitumour responses [605]. This suggests that intratumoural T cells should be able to engage glycolysis for optimal function. Thus, the higher rate of basal glycolysis and glycolytic capacity I observed in CD8-ligated cells could be reasonably expected to support their antitumour activity.

While CD8 mAb-treated cells successfully controlled tumour growth, they suffered an initial setback. Two days after adoptive transfer, significantly fewer CD8-ligated cells could be recovered from the tumour and circulation of host mice. This was probably due to ADCC me-

diated through the Fc region of the CD8 mAb still bound on the cell surface. The antibody I used is of the clone IgG2a, which binds all activating class I Fc gamma receptors (FcγR-I, III, IV) and induces phagocytosis [532, 607]. A measure of the ability of an antibody to induce cytotoxicity *in vivo* is the ratio of its binding affinity to activating and inhibitory Fcγ receptors; the A/I ratio. For IgG2a, the A/I ratio is 69, which is rather high compared to other antibody classes (0.1 for IgG1 and 7 for IgG2b) [608]. The CD8 mAb I used is, in fact, the same one commonly employed in CD8+ T cell depletion experiments [517, 609]. However, the high proliferative capacity of CD8-ligated cells yields daughters without surface-bound CD8 mAb and thus will not suffer phagocytic death. While ADCC has been shown to contribute to the therapeutic mechanism of many blocking antibodies [416, 610], it was counter-productive in this case and precludes the therapeutic administration of the agonistic CD8 mAb I used.

6.4.2 CD8 Fab′ induces TIL proliferation

CD8α is oligo- or even monomorphic in the human population [611], suggesting that targeting CD8 might be a promising immunotherapeutic approach that is independent of the patient's TCR repertoire. There are two possible strategies to circumvent ADCC induced by CD8 mAb. First, a recombinant antibody that does not bind Fcγ receptors could be expressed, for example, in *Escherichia coli* [612]. This requires prior knowledge of the sequence of the Fab region of this commercial antibody. Second, pepsin digestion, which is Fab sequence-agnostic, cleaves the Fc domain leaving behind the F(ab′)2 fragment. Although IgG2 antibodies have four, instead of the regular two, disulfide bridges between their heavy chains, these bridges are the least stable among IgG isotypes and are easily reduced [613, 614]. Nevertheless, experiments with CD8 Fab′ revealed that, at least some of, the effects of CD8 mAb treatment depend on clustering induced by the bivalent full-length antibody.

CD8 Fab′ treatment induces TIL proliferation and efficiently inhibits tumour outgrowth. This effect might be secondary to enhanced TCR signalling and metabolic rewiring. Another possibility is that CD8 Fab′ blocks the interaction between CD8α and PILRα thus increasing cell cycle entry [552]. Because PILRα is not expressed by T cells [615], this effect would not be observed in *in vitro*-differentiated, CD8-ligated cells. One way to test the influence of CD8 mAb on CD8α-PILRα interaction is to transfect HEK293 T cells with *Cd8a* and compare the binding of fluorescently labelled anti-PILRα antibody to transfected cells in the presence or absence of CD8 mAb. CD8+ T cells in *Pilra*$^{-/-}$ mice do not break their quiescence [552], suggest-

ing that anti-CD8 and anti-PILRα antibodies in combination might prove to be a safe treatment modality.

Interestingly, treatment of melanoma-bearing mice with CD8 Fab′ reduced TIL expression of Tigit and CD38, but not Tim-3 or Lag-3. Because the list of inhibitory receptors I measured is far from exhaustive, it is possible that other inhibitory receptors are also affected by CD8 ligation. The selective reduction of inhibitory receptors might be a function of CD8 Fab′ dosage. Alternatively, it might reflect important mechanistic features of CD8 Fab′ action. Tigit has a T cell-intrinsic and -extrinsic inhibitory functions. It induces a tolerogenic phenotype in DCs (by binding to CD155 and inducing the secretion of IL-10 and reducing IL-12 expression [616]), and, because it has an ITIM domain [616], it can limit TCR signalling in a T cell-intrinsic manner [617]. Importantly, Tigit inhibits T cell glucose uptake and glycolysis [618] and is itself inhibited by OXPHOS [619]. Similarly, CD38 is an ecto-enzyme that catabolises nicotinamide dinucleotide (NAD+) and reduces its intracellular levels [620, 621], and was reported to limit T cell mitochondrial biogenesis [622] and OXPHOS [623]. Therefore, it is tempting to speculate that CD8 Fab′-induced metabolic rewiring is responsible for the downregulation of Tigit and CD38. However, this hypothesis requires further testing.

CD8 Fab′ provides no additive advantage over treatment with αPD-L1 alone. In one experiment, Fab′ even decreased response to αPD-L1, possibly by limiting the abundance of progenitor exhausted cells. One potential explanation for this counter-intuitive response is that both treatment strategies target the same pathway, namely TCR signalling. ICB, in particular blocking PD1/PD-L1 interactions, maintains the functionality of the TCR complex [167, 168, 170] and was shown to directly restore TCR signalling in exhausted T cells following chronic viral infection [533]. Because strong TCR signalling is detrimental to T cell longevity [624–626], it is possible that the co-therapy synergised to increase TCR signalling past survival thresholds. Since progenitor cells express higher levels of CD8 (see Fig. 23) and are the main population responding to anti-PD1 blockade [393], it is understandable that this is the population most affected in co-treated mice. This view is supported by reduced tumour sizes in each mono-therapy. While progenitor cells themselves are not cytotoxic, a subset of their progeny differentiates into effector cells that can elaborate cytokines and kill virally-infected and tumour cells [394, 396, 399, 428]. I did not detect differences, on a per-cell basis, in cytokine release following co-therapy. However, fewer activated CD44+ cells infiltrated the tumour and as a result, the total *number* of cytokine-positive cells was decreased, possibly

due to the relative loss of their stem cell-like precursors.

How do changes in TCR signalling affect the maintenance and stability of progenitor exhausted cells? In mouse models of lung cancer, progenitors are abundant in tumour-draining lymph nodes, where continuous antigen presentation could be expected [398]. Furthermore, in chronically infected mice, progenitor cells interact with antigen-presenting DCs [393]. In human cancer patients, progenitors occupy a special micro-anatomical location in the tumour tissue, where they are in direct contact with APCs [627]. Therefore, the dependency of this population on TCR signalling could be plausibly inferred. Indeed, as this thesis was being written, a report revealed that in chronically infected mice, progenitors display a more active TCR signalling pathway (measured as increased levels of the immediate-early TCR activation marker Nur77) compared to exhausted T cells [355].

When my results are considered in this light, two possible explanations emerge for the selective loss of progenitor exhausted cells in co-treated mice; 1) their differentiation rate exceeded their self-maintenance rate, or 2) they simply died in response to strong TCR signalling. The first would manifest as an increase in the percentage of effectors and/or exhausted cells and a transient dip in tumour sizes, which I did not observe. A more likely explanation is activation-induced cell death. This idea would be in line with another report showing that promoting TCR signal strength limits the stemness of CAR T cells. In essense, reducing the number of the ITAM motifs in the CD3ε molecule decreased the strength of the TCR signal and balanced T cell effector and stemness features, eventually leading to complete tumour eradication in a mouse model of lymphoblastic leukaemia [626]. Therefore, strong TCR stimulation in co-treated mice is likely responsible for the contraction of progenitor exhausted cells.

It is not clear whether the newly recruited, $CD44^{low}$ cells could compensate for loss of progenitors in co-treated mice. Longitudinal analysis of TCR clonotypes infiltrating basal or squamous cell carcinomas shows that anti-PD1 therapy induces the recruitment of extratumoural T cells that expand rapidly and eventually become exhausted [430].

It is important to note that experiments with CD8-ligated cells and CD8 Fab′ are not directly comparable. CD8 mAb was incubated with cells under memory-skewing conditions *in vitro*. On the other hand, systematic administration of CD8 Fab′ presumably targets all CD8+ cells, which are likely at different functional differentiation stages in a tumour-bearing

mouse. The target population is very important in determining the outcome. For example, while IL-2 promotes proliferation and survival after antigen clearance (in the contraction and memory phase of the immune response), it actively induces T cell apoptosis when administered during the expansion phase [157]. Regardless, both treatment strategies proved successful in limiting tumour development, underscoring the validity of CD8 as a therapeutic target.

7 Conclusion

The current work followed, and validated, the dynamic regulation of CD8 expression during the course of a resolving immune response as well as aberrant T cell activation in cancer and autoimmunity. The central finding presented here is that CD8 agonism can induce metabolic and functional features of effector T cells without compromising survival and longevity. *In vitro*, CD8-ligated cells were more glycolytic, potentially more lipolytic, and suppressed glutaminolysis. They were also more proliferative and cytotoxic. Consequently, CD8-ligated cells displayed stronger antitumour effects when transferred to melanoma-bearing mice and showed enhanced persistence *in vivo* (Fig. 31). Although it did not synergise with, and sometimes negatively impacted, αPD-L1 therapy, a non-depleting CD8 Fab′ used as a single agent reduced T cell exhaustion and tumour load. These results highlight the utility of CD8 as an immunotherapeutic target that does not require prior knowledge of tumour neo-antigens or TCR clones.

Several questions remain open and would benefit from further investigation. First, unbiased epigenetic and transcriptional analyses of CD8-ligated cells may reveal distinct regulatory networks engaged by antigen-dependent and antigen-independent TCR signalling. Second, it would be interesting to functionally test the durability/memory phenotype of CD8-ligated cells *in vivo*. Mice in which tumours completely regressed after transfer of CD8-ligated cells could be: 1) re-challenged with a second tumour implantation on the opposite flank, or 2) infected with LCMV (whose epitopes could be recognised by P14 cells). Tumour size and effector T cell features would need to be examined, respectively. Third, to clinically translate this strategy, a screen of agonistic anti-human CD8 antibodies should be performed, preferably selecting for non-depleting antibody isotypes. Fourth, the CD8 Fab′ I used here provides an optimal opportunity to test the reliance of different TIL subsets on TCR signalling *in vivo*. Treating TCR signalling-reporter mice, like Nur77-GFP [628], with different doses of CD8 Fab′ might reveal the threshold at which TCR activation becomes counter-productive. Finally, the safety profile of CD8 Fab′ should be analysed in pre-clinical models. In particular, the effect of enhanced basal TCR signalling on the long term survival of naive T cells as well as potential cross-reactivity need to be investigated.

CD8-ligated, IL-15-differentiated cells have a hybrid phenotype. A growing consensus in cancer immunotherapy is that T cell persistence is more important than cytokine release or

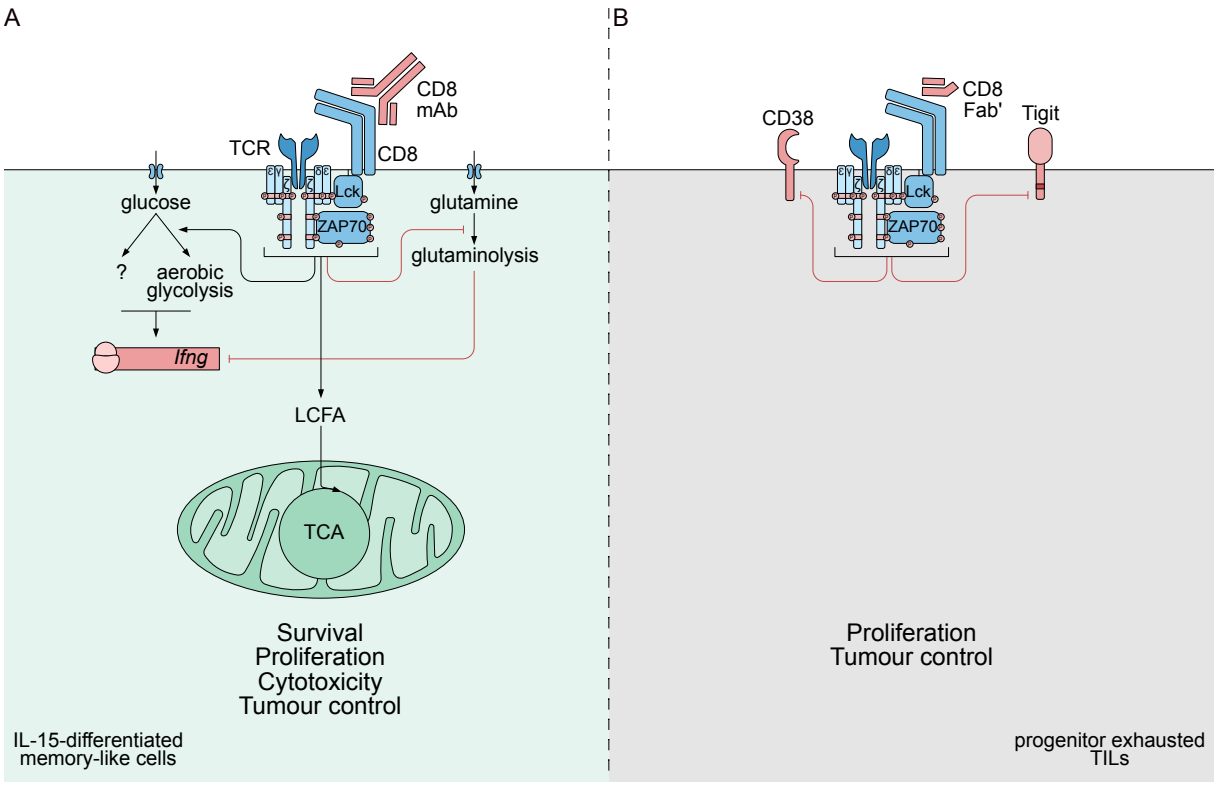

Figure 31: CD8 agonism enhances T cell-mediated antitumour immunity

The current study investigated the effects of *in vitro* and *in vivo* CD8 ligation on tumour control.
(A) An agonistic CD8 antibody rewires the metabolism of *in vitro*-differentiated memory-like cells to enhance effector functions and maintain stemness. Glycolysis-dependent and independent pathways enhance cytokine production. In addition, CD8-ligated cells exhibit a state of latent glutaminolysis inhibition that supports effector function. By possibly enhancing fatty acid oxidation, CD8 agonism improves mitochondrial respiration and T cell longevity. When adoptively transferred to tumour-bearing mice, CD8-ligated cells were better able to control tumour growth.
(B) When administered as a mono-therapy, the antigen-binding fragment of the agonistic anti-CD8 antibody was able to enhance tumour-infiltrating CD8+ T cell expansion and partially reduce exhaustion, resulting in tumour control.

cytotoxicity. An initial burst of effector function that wanes rapidly cannot control the tumour, unlike a prolonged, albeit moderate, response. To maintain T cell functionality, the TCR needs to be only moderately activated. Strong activation leads to desensitisation and exhaustion while weak activation cannot produce an effective immune response. Furthermore, a T cell needs to synchronise its metabolism to its environmental cues and functional requirements. A glucose-addicted T cell might be at a disadvantage in the tumour microenvironment. Even if it were not, it is notoriously short-lived. Fatty acid metabolism, on the

other hand, supports stemness and longevity and was shown to be vital for T cell function in the tumour microenvironment, but it can suppress IFNγ expression. In short, the key word is moderation. We need an average T cell that is neither too strongly nor too weakly activated, neither too glycolytic nor too oxidative, neither too effector-like, nor too memory-like. An ideal T cell is a *hybrid* T cell. Barring that, perhaps an important lesson to learn from the many subsets of memory T cells is that a diverse immune response is a successful immune response.

Appendix I Regulatory T cell-derived IL-15 diversifies CD8+ T cell memory

I.1 Introduction

A central tenet of the adaptive immune response is the persistence of self-renewing, rapidly responding memory cells [629]. The homeostatic cytokine interleukin (IL-) 15 is required for long-term maintenance of all memory T cell subsets: central, effector, and tissue-resident memory T cells (TCM, TEM, and TRM cells, respectively) [221, 233, 234, 237, 255]. In addition, it controls different aspects of memory T cell biology; it is required for homeostatic turnover as well as cell cycle entry upon inflammation, supports the oxidative metabolic lifestyle of memory T cells, induces the rapid elaboration of cytotoxic proteins in an antigen-independent manner, and controls T cell trafficking to inflammed tissues [134, 262, 263, 312, 630–633]. These pleiotropic functions are mediated through a three-subunit receptor complex; IL-2 receptor β (IL-2Rβ, CD122), γ_c, and the IL-15-specific subunit IL-15Rα [256, 634]. Binding of IL-2 or IL-15 to IL-2Rβ and γ_c induces similar morphological changes, and initiates a remarkably similar downstream cascade [635]. However, the non-redundant physiological functions of these cytokines suggest that the context in which a T cell encounters either cytokine is likely the defining factor [636, 637].

IL-15 is presented in *trans* while bound to IL-15Rα [256], suggesting that a direct cell-to-cell contact is required for IL-15 signalling. Both *Il15* and *Il15ra* are widely expressed [630, 634, 638], indicating that the source of the IL-15 signal for TRM cells is very likely the adjacent tissue parenchyma [254]. In contrast, the relevant IL-15 source for circulating memory T cells remains poorly defined. Previous studies used mice with germline deletion of either *Il15* or *Il15ra*, or mice that systemically received anti-IL-15 antibodies [263, 633]. Here, I used different mouse strains with cell type-specific deletion of *Il15*. In order to assess the relative contribution of different cell types to homeostatic IL-15 signalling, the abundance of circulating memory T cells was examined following the resolution of acute infection with the Armstrong strain of lymphocytic choriomeningitis virus (LCMV Arm). My results reveal that IL-15 released by regulatory T (Treg) cells, but not skeletal muscles or myeloid cells, was required for the maintenance of CD62L-IL-7Rα-KLRG1+ terminal effector memory T cells (tTEM). These findings suggest that, in addition to promoting memory T cell differentiation [192], Treg cells

play an important role in diversifying the immune response post pathogen clearance.

I.2 Results & discussion

I.2.1 Treg cells express and can *trans*-present IL-15

IL-15 and its *trans*-presentation receptor IL-15Rα are expressed in a variety of cell types including skeletal muscles, monocytes, and macrophages [639–641]. To assess whether they are also expressed in Treg cells, I analysed the chromatin accessibility of *Il15* and *Il15ra* loci in Treg cells isolated from mice with experimental autoimmune encephalomyelitis (EAE) [467]. Both loci were more accessible in Treg cells sorted from spleen or central nervous system (CNS) compared to FoxP3- conventional T (Tconv) cells (Fig. I.1A), indicating that they were more actively transcribed in Treg cells. In addition, I examined the chromatin accessibility of the myeloid and dendritic cell markers *Marco, Tlr3*, and *Trem1* [642]. None of these loci contained open chromatin regions, excluding that the isolated T cell populations were contaminated with dendritic or myeloid cells. To confirm that IL-15 expression in Treg cells was evolutionarily conserved, I analysed single-cell RNA-sequencing (scRNA-seq) data of human peripheral blood Treg cells [474]. Although *IL15*-expressing cells were fewer than *IL15RA*-positive cells, they were more than *IL10*-expressing cells (Fig. I.1B). Additionally, this analysis revealed that very few, if any, Treg cells express both *IL10* and *IL15*.

To experimentally validate the expression of *Il15* and *Il15ra* in Treg cells, I sorted Tconv and Treg cells from wildtype (WT) mice, mice with germline loss of IL-15 ($Il15^{-/-}$ [260]), and mice with Treg cell-specific deletion of IL-15 ($FoxP3^{Cre}xIl15^{Fl/Fl}$ [639, 643]). Compared to Tconv cells, Treg cells isolated from all strains tended to have a higher level of *Il15ra* transcript (Fig. I.1C). In contrast, *Il15* transcripts in both cell populations were undetectable in $Il15^{-/-}$ mice (Fig. I.1C). Interestingly, relative to Tconv cells, *Il15* mRNA was significantly higher in Treg cells isolated from WT mice 7 days post infection with LCMV Arm (Fig. I.1C). However, this advantage was lost in $FoxP3^{Cre}xIl15^{Fl/Fl}$ mice, validating the efficiency and the specificity of the Treg cell-specific loss of IL-15 in this mouse strain.

Finally, because IL-15 expression is regulated post-transcriptionally [644, 645], I confirmed that Treg cells are able to secrete IL-15. Sorted Treg cells were activated *ex vivo* for 3 days and levels of IL-15 in the supernatant were measured using enzyme-linked immunosorbent assay (ELISA) and were normalised to the protein content in cell pellets. Treg cells sorted from WT,

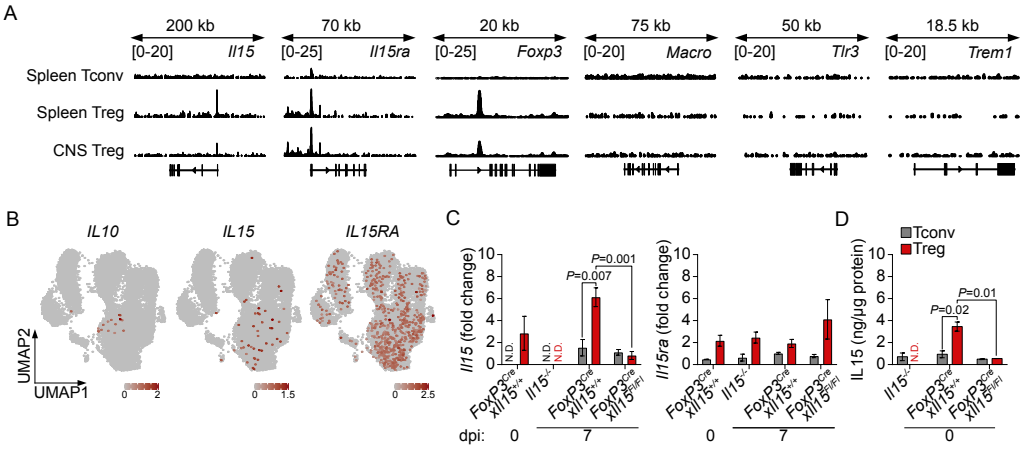

Figure I.1: IL-15 is expressed and secreted by Treg cells

(A) ATAC-seq analysis of conventional (Tconv) and FoxP3+ regulatory T (Treg) cells isolated from the spleen or the central nervous system (CNS) of mice with experimental autoimmune encephalomyelitis (EAE) [467].

(B) Uniform Manifold Approximation and Projection (UMAP) representation of Treg cells isolated from peripheral blood of healthy human donors [474], coloured by normalized gene expression of *IL10, IL15,* and *IL15RA*. Note that the number of *Il15*-expressing cells is higher than the number of *Il10*-expressing cells.

(C) Tconv and Treg cells were sorted from the indicated mouse strains before or 7 days post infection (dpi) with LCMV Arm, and the levels of *Il15* and *Il15ra* transcripts were examined. N.D, not detected.

(D) Tconv and Treg cells sorted from naive mice were activated *ex vivo* for 3 days and the concentration of secreted IL-15 in the supernatant was measured using ELISA.

Data are from 2 independent experiments with 3 – 4 mice per group (C & D). Error bars indicate SEM. *P* values were calculated using two-tailed unpaired Student's *t*-test.

but not *FoxP3*^{Cre}*xIl15*$^{Fl/Fl}$ mice were able to secrete higher amounts of IL-15 compared to Tconv cells (Fig. I.1D). Together these results show that Treg cells are able to express, translate, and *trans*-present IL-15 and suggest that this population might play a role in homeostatic maintenance of memory T cells.

I.2.2 Treg cell-specific loss of IL-15 does not affect the immune phenotype of naive mice

I examined the influence of Treg cell-derived IL-15 on naive T cell development and peripheral maintenance. There was no difference in the total number of thymocytes or lymphocytes isolated from the spleen, mesenteric lymph nodes (mLN), or inguinal lymph nodes

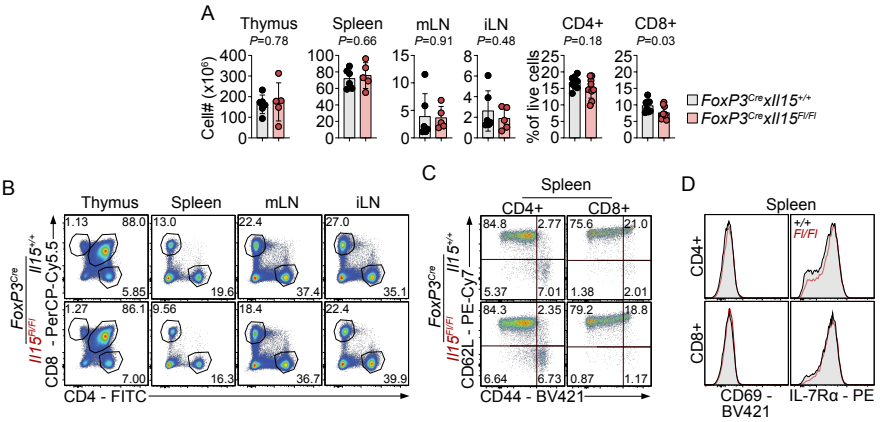

Figure I.2: Normal immune phenotype in *FoxP3^{Cre}xIl15$^{Fl/Fl}$* mice

The indicated organs were harvested from naive *FoxP3^{Cre}xIl15$^{Fl/Fl}$* and their WT littermates and cells recovered were enumerated and analysed using flow cytometry.

(A) Total cell numbers and T cell frequency in the indicated organs. mLN, mesenteric lymph node. iLN, inguinal lymph node.

(B and C) Representative dot plots showing the frequency of CD4+ and CD8+ T cells (B) and their subsets (C) in the indicated organs.

(D) Representative histograms showing the expression of CD69 and IL-7Rα in splenic T cells.

Data are pooled from (A) or are representative (B - D) of 2 - 3 experiments. Error bars indicate s.d. *P* values were calculated using two-tailed unpaired Student's *t*-test.

(iLN) between *FoxP3^{Cre}xIl15$^{Fl/Fl}$* mice and their WT littermates (Fig. I.2A). Furthermore, splenic CD4+ T cells were independent of Treg cell-produced IL-15. There was a slight, but significant, reduction in the abundance of CD8+ T cells in the spleen of *FoxP3^{Cre}xIl15$^{Fl/Fl}$* mice relative to control littermates. This slight difference was consistent in secondary lymphoid organs, but not the thymus (Fig. I.2B), suggesting that Treg cells might use IL-15 to support the survival of naive T cells in the periphery. Because IL-15 was previously shown to maintain memory-phenotype cells in naive mice [260, 261], I examined the frequency of CD62L+ and CD44+ cells in the spleen of *FoxP3^{Cre}xIl15$^{Fl/Fl}$* mice. In both the CD4+ and CD8+ T cell compartments, the frequency of memory-phenotype cells was comparable to WT mice (Fig. I.2C), and the activation status of the cells was not significantly affected as shown by the comparable expression of CD69 and IL-7Rα (Fig. I.2D). Together, these results show that IL-15 secreted by Treg cells has a minimal effect on the differentiation and maintenance of T cells.

IL-15 signalling was previously reported to induce the expression of FoxP3 and the differentiation of Treg cells [646] and to dampen their function [647]. I found no significant differ-

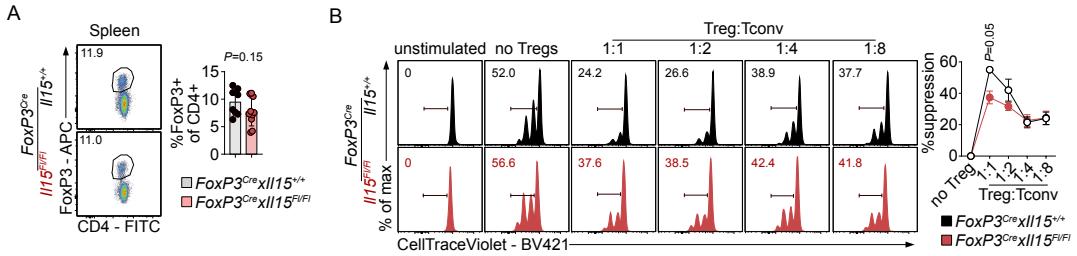

Figure I.3: Autocrine IL-15 signalling does not affect Treg cell identity or function

(A) Frequency of FoxP3+ Treg cells in the spleen of *FoxP3^{Cre}xIl15$^{Fl/Fl}$* mice and WT (*Il15$^{+/+}$*) littermates. (B) Left: Histograms showing proliferation (measured as dilution of CellTrace Violet) of Tconv cells co-cultured with WT or IL-15-deficient Treg cells. Right: Line graph quantifying Treg suppression as the percentage of reduction in Tconv proliferation.

Data are pooled from (A) or are representative of (B) 2 - 3 experiments. *P* values were calculated using two-tailed unpaired Student's *t*-test.

ence in the abundance of peripheral FoxP3+ T cells in naive WT and *FoxP3^{Cre}xIl15$^{Fl/Fl}$* mice (Fig. I.3A). I also compared the suppressive function of IL-15-sufficient and -deficient Treg cells *in vitro*. Treg cells from *FoxP3^{Cre}xIl15$^{Fl/Fl}$* mice were as efficient as WT Treg cells at suppressing the proliferation of FoxP3- Tconv cells (Fig. I.3B), suggesting that autocrine IL-15 signalling does not affect Treg cell identity or function.

I.2.3 Treg cell-derived IL-15 maintains tTEM cells

Having established that Treg cells are a potential IL-15 source for maintaining memory T cells, I investigated the relative contribution of different IL-15-producing cell types to the CD8+ memory T cell homeostasis. I crossed *Il15$^{Fl/Fl}$* mice [639] to *Mck^{Cre}* [648] and *LysM^{Cre}* [649], in addition to *FoxP3^{Cre}* [643] mice to achieve targeted deletion of *Il15* in skeletal muscle, myeloid, and Treg cells, respectively. In addition, I also used *Il15$^{-/-}$* mice as a positive control for global IL-15 deficiency. Skeletal muscle- and myeloid cell-derived IL-15 was previously shown to have no influence on naive T cell development and survival [639, 641]. Sixty days post infection with LCMV Arm, the phenotype of mature circulating memory cells was examined in the individually bred mouse strains and was compared to their respective littermates. Only *Il15$^{-/-}$* mice had a two-fold reduction in the abundance of total memory CD8+ T cells compared to WT mice (Fig. I.4A). In contrast, loss of the IL-15 signal from myeloid, skeletal muscle, or Treg cells had no effect on the size of the memory cell pool. I further examined the frequency

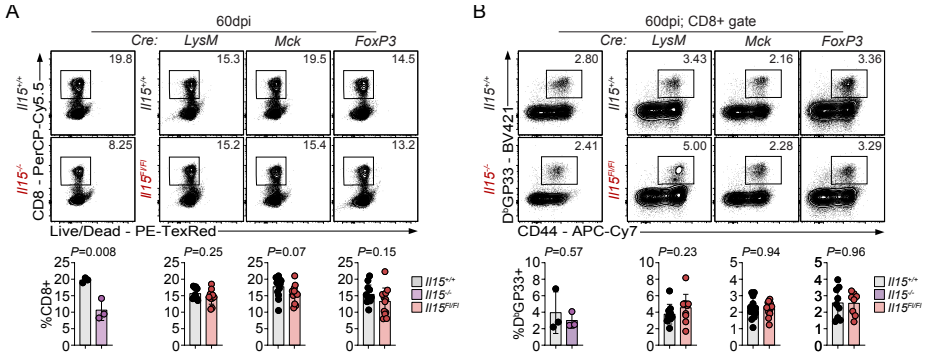

Figure I.4: Normal size of the memory cell pool in mice with cell type-specific IL-15 deletion

(A and B) Abundance of total (A) or antigen-specific (B) CD8+ T cells in the indicated mouse strains 60 days after LCMV Arm infection.

Data are pooled from 2 - 4 independent experiments, except for data concerning *Il15*$^{-/-}$ mice, which are representative of 2 trials. Error bars indicate s.d. *P* values were calculated using two-tailed unpaired Student's *t*-test.

of T cells specific to the GP_{33-41} (GP33) viral epitope, which was comparable to WT mice in all strains (Fig. I.4B).

I then asked whether the distribution of memory T cells between the different subsets was dependent on IL-15 from a particular cell source. KLRG1+IL-7Rα- T cells were previously shown to be especially sensitive to IL-15 signalling [145]. Indeed, this population, referred to as long-lived effector cells (LLEC) [232], was almost absent in *Il15*$^{-/-}$ mice (Fig. I.5A). While myeloid cell- and skeletal muscle cell-derived IL-15 was dispensable for LLECs, loss of IL-15 production by Treg cells caused a two-fold reduction in the frequency of polyclonal (CD44+) and GP33-specific LLECs (Fig. I.5A, B), indicating that at least half of the IL-15 signal received by LLECs is derived from Treg cells.

LLECs are a heterogenous population comprised of cells with different proliferative and cytotoxic capacities [231]. Therefore, I used a published gating scheme to further resolve the main target of Treg cell-derived IL-15 (Fig. I.5C) [231]. This approach defines circulating memory cells as CD62L+IL-7Rα+ TCM cells, CD62L-IL-7Rα+ TEM cells, and CD62L-IL-7Rα- tTEM cells. IL-15 signalling was mostly required for TCM and tTEM cells as indicated by the significant contraction of both subsets in *Il15*$^{-/-}$ mice (Fig. I.5D). The relative abundance of all three subsets was comparable in the presence and absence of skeletal muscle- or myeloid cell-produced IL-15 (Fig. I.5D). In contrast, tTEM, but not TCM, cells were significantly

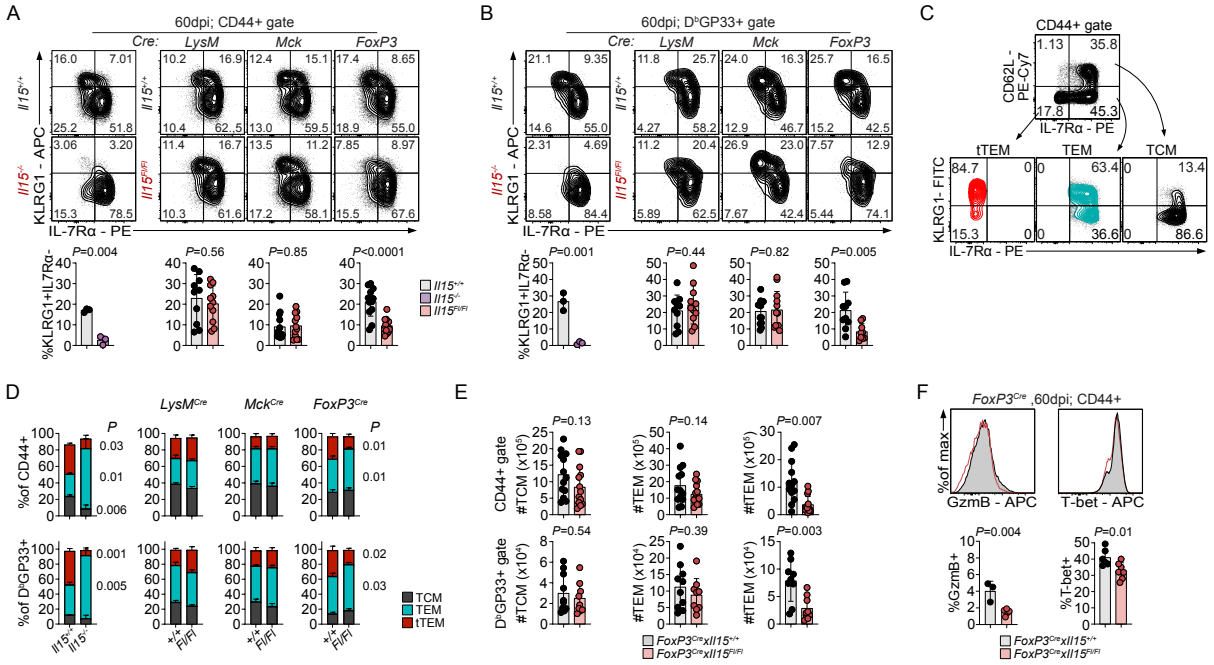

Figure I.5: Treg cell-derived IL-15 maintains tTEM cells

(A and B) Expression of KLRG1 and IL-7Rα among polyclonal (A) or GP33-specific (B) CD8+ T cells in the indicated mouse strains 60 days after LCMV Arm infection.

(C) Gating strategy used to define TCM, TEM, and tTEM cells.

(D) Relative frequency of TCM, TEM, tTEM cells (gated as in C) among polyclonal (top) or GP33-specific (bottom) CD8+ T cells isolated from the indicated mouse strains 60 days after LCMV infection. Numbers on the right of each graph refer to *P* values. Unless indicated, *P* values were greater than 0.05.

(E) Absolute counts of polyclonal (top) and GP33-specific (bottom) memory T cell subsets.

(F) Granzyme B (GzmB) and T-bet expression in polyclonal CD8+ T cells 60 days after infection.

Data are pooled from 2 - 4 independent experiments, except for data concerning *Il15*$^{-/-}$ mice, which are representative of 2 trials. Error bars indicate s.d. *P* values were calculated using two-tailed unpaired Student's *t*-test.

depleted in *FoxP3*^{Cre}*xIl15*$^{Fl/Fl}$ mice (Fig. I.5D). Analysis of the absolute counts of polyclonal and GP33-specific subsets showed that tTEM cells were approximately 3 times less abundant in the absence of Treg cell-derived IL-15 (Fig. I.5E). However, the counts of TCM and TEM cells were comparable between *FoxP3*^{Cre}*xIl15*$^{Fl/Fl}$ mice and their WT littermates, suggesting that the apparent expansion of TEM cells in *FoxP3*^{Cre}*xIl15*$^{Fl/Fl}$ mice (Fig. I.5D) was only relative and caused by the depletion of tTEM cells. Consistent with tTEM cells being more cytotoxic and relying on the transcription factor T-bet for development [231], partial loss of tTEM cells in *FoxP3*^{Cre}*xIl15*$^{Fl/Fl}$ mice caused a slight reduction in the percentage of granzyme

B (GzmB)-producing and T-bet expressing polyclonal cells (Fig. I.5F). Together, these results suggest that different memory T cell subsets receive homeostatic IL-15 signalling from different sources and highlight the strong contribution of Treg cells to maintaining the tTEM subset.

I.2.4 Treg cell-derived IL-15 is dispensable for primary and secondary responses

To understand whether Treg cell-derived IL-15 was responsible for the maintenance or the differentiation of LLEC cells, I analysed the frequency of KLRG1+IL-7Rα- cells at the peak of the primary immune response. Eight days after LCMV Arm infection, *FoxP3*^{Cre}*xIl15*$^{Fl/Fl}$ mice had slightly more GP33-specific CD8+ T cells (Fig. I.6A), but the size of the polyclonal and GP33-specific KLRG1+IL-7Rα- cell pool was comparable to WT mice, indicating that IL-15 production by Treg cells does not contribute to the initial development of this KLRG1+IL-7Rα- cells. This finding is consistent with the dispensability of IL-15 signalling for the primary CD8+ T cell response [145, 263, 636].

I then asked whether the strong reduction of tTEM cells in *FoxP3*^{Cre}*xIl15*$^{Fl/Fl}$ mice would compromise protective immunity. Sixty days after LCMV Arm infection, mice were challenged with a different LCMV strain, LCMV clone 13, and viral titers and immune cell phenotype were analysed 7 days after secondary infection. I found no significant difference in the frequency of total, GP33-specific, or KLRG1+IL-7Rα- cells between *FoxP3*^{Cre}*xIl15*$^{Fl/Fl}$ mice and their control littermates (Fig. I.6B, and data not shown), which were equally able to clear the secondary infection (Fig. I.6C). However, consistent with the contraction of tTEM cells, which are not self-renewing, CD44+ T cells harvested from *FoxP3*^{Cre}*xIl15*$^{Fl/Fl}$ mice were slightly more proliferative as inferred from the higher expression of Ki67 (Fig. I.6D). Furthermore, in line with the normal Treg cell development and function in the absence of autocrine IL-15 signalling, there was no difference in Treg cell frequencies between *FoxP3*^{Cre}*xIl15*$^{Fl/Fl}$ mice and their WT littermates across all time points examined (Fig. I.6E). Together these data show that IL-15 expression by Treg cells does not affect T cell expansion after primary and secondary infection. These results are also consistent with the normal recall response observed in mice with germline IL-15 deletion [263, 636] and are in agreement with secondary memory cell responses being largely independent of IL-15 signalling [233, 234].

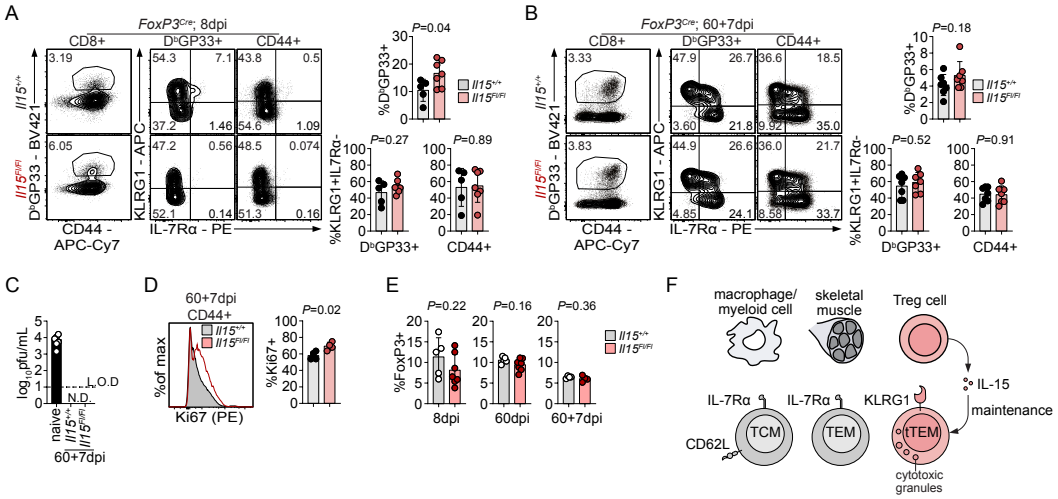

Figure I.6: IL-15 production by Treg cells is not required for primary or recall responses

(A and B) Frequency of GP33-specific cells and expression of KLRG1 and IL-7Rα among polyclonal or GP33-specific CD8+ T cells 8 days after LCMV Arm infection (A) or 7 days after secondary LCMV clone 13 infection (B).

(C) Viral titers of LCMV clone 13 were measured in the serum of naive WT or LCMV Arm-immune mice.

(D)Expression of Ki67 in CD44+ CD8+ T cells isolated from the spleen after secondary infection.

(E) Frequency of Treg cells at the indicated time points after primary or secondary (60+7dpi) infection.

(F) A diagram summarising the main findings in this work.

Data are pooled from 2 independent experiments. Error bars indicate s.d. *P* values were calculated using two-tailed unpaired Student's *t*-test.

I.3 Conclusion

Data presented here show that Treg cells are responsible for at least half of the IL-15 signal maintaining tTEM cells and suggest that different memory subsets rely on non-redundant sources for homeostatic IL-15 signalling (Fig. I.6F). Previous work reported that TCM cells depend on dendritic cell-produced IL-15 for long term survival [640]. This differential preference might result from the different migratory behaviour of TCM and TEM cells [216]. Treg cells secrete IL-10, which induces immune contraction and subsequent development of KLRG1-IL-7Rα+ memory cells [192]. My results indicate that another long-lived memory T cell subset, KLRG1+IL-7Rα-, is also induced by Treg cells but using a different cytokine. Therefore, Treg cells actively induce a diverse immune response, which is required for optimal pathogen control [215, 650].

Whether Treg cell expression of IL-10 and IL-15 is sequential, mutually exclusive, or lim-

ited to cells at different tissue sites is an intriguing question and could benefit from the use of IL-10 and IL-15 reporter mice [651, 652]. It would also be interesting to analyse the contribution of Treg cell-derived IL-15 to the maintenance of TRM cells. Furthermore, the influence of IL-15 produced by Treg cells on protective immunity might be assessed using secondary infections with viruses or bacteria that are, unlike LCMV clone 13, mainly controlled by TEM-type memory cells, such as vaccinia virus or *Listeria monocytogenes* [232, 236].

In summary, the results presented here reveal an essential function for Treg cells beyond immune suppression. By producing IL-15, Treg cells directly contribute to CD8+ T cell memory homeostasis and diversify the immune response.

Appendix II Stat6 regulates tissue resident memory T cell development

II.1 Introduction

The T cell memory response is distributed across several body compartments to provide rapid protection against recurrent infections [215, 653]. As a pool, memory CD8+ T cells are heterogenous, with subsets exhibiting differential epigenetic, transcriptional, and functional profiles [225, 230, 654]. Based on their migration behaviour, memory CD8+ T cells are classified into lymphoid-homing central memory T (TCM) cells, blood-biassed effector memory T (TEM) cells, and non-lymphoid tissue (NLT)-restricted tissue resident memory (TRM) cells [215–217]. TRM cells isolated from different organs have shared and tissue-specific transcription signatures [225, 655]. They commonly upregulate tissue retention markers including CD69 and CD103 and downregulate the egress chemokine receptor sphingosine-1-phosphate receptor 1 ($S1P_1$) [223, 225, 252], and thus largely fail to recirculate into blood or lymph. Positioned at pathogen entry ports, TRM cells provide regionalised and, in many cases, life-long immune surveillance and act as a first-line of defence against repeated infections [239, 240, 656], making them an attractive vaccination target [219, 244, 657]. Additionally, TRM cells at internal body organs, like the liver, provide protective immunity against organ-tropic infections [219], although survival of TRM cells in the liver is poor compared to other organs [658]. In some contexts, however, TRM cells could contribute to tissue pathology [218]. For example, long-lived skin TRM cells play a role in fixed drug eruption [659], psoriasis [660], and contact dermatitis [661]. In the liver, metabolic imbalance induces the differentiation of 'auto-aggressive' TRM cells that cause severe liver damage [662] and precipitate hepatocellular carcinoma [663].

Lung TRM cells formed following influenza (flu) virus infection are often specific to conserved viral epitopes and thus provide rapid protection against heterosubtypic infections [664–666]. However, in mouse models of flu infection, the abundance of virus-specific CD8+ T cells in the lung decreases by more than 100-folds within one month [250, 667], and protective immunity is almost completely lost within two months after initial infection [664]. During the same time interval, the number of skin TRM cells remains largely stable [667, 668]. The reduced persistence of lung TRM cells is shared with other lung-resident immune cells, in-

cluding macrophages [669], suggesting that gradual immune cell attrition is an instructive program in the lung, possibly because the accumulation of immune cells and subsequent inflammation are not compatible with rapid alveolar gas exchange [250]. The fast decay of lung TRM cells was reported to be due to egress into the draining mediastinal lymph node [250], increased apoptosis relative to TRM cells at other tissue sites, and decreased recruitment of TRM-replenishing TEM cells from the circulation [667]. The latter being largely regulated by cytokines [667, 670].

Here, I analysed publicly available gene expression datasets with the aim of identifying cytokine signals directing TRM differentiation and maintenance. This analysis, and subsequent *in vivo* functional validation, showed that interleukin (IL-) 4-mediated signal transducer and activation of transcription (Stat) 6 signalling regulated T cell infiltration and TRM development in various tissues. Through potentially regulating the expression of C-X-C Motif Chemokine Receptor 6 (CXCR6), CD8+ T cell-intrinsic Stat6 signalling induced the migration of circulating memory cells into the lung and liver following flu and lymphocytic choriomeningitis virus (LCMV) infection, respectively. These findings show that the IL-4/Stat6 axis regulates a shared TRM development program regardless of the tissue site and suggest that the short lifespan of lung TRM cells might be due to tissue-intrinsic rather than systemic factors.

II.2 Results & discussion

II.2.1 IL-4Rα signalling is putatively activated in TRM cells

All memory subsets rely on homeostatic IL-15 signalling for maintenance [221, 233, 234, 237, 255]. I asked whether other cytokines provided TRM-specific survival cues. Analysis of gene expression profiles of TEM, TCM, and TRM cells as well as naive CD8+ T cells [225] revealed that 9 cytokine receptor genes were differentially expressed across all groups (Fig. II.1A). As expected, *Il2rb*, which encodes for one of the IL-15 receptor subunits, was highly expressed in all memory T cells. However, only two receptors, namely *Il4ra* and *Il21r*, were specifically upregulated in TRM cells isolated from lung, small intestine (SI), and skin, but not in naive or circulating memory cells. Both IL-4Rα and IL-21 belong to class I cytokine receptors and can dimerise with the common γ chain (γ_c) to induce the phosphorylation and dimerisation of Stat6 and Stat3, respectively, which then translocate to the nucleus where they regulate gene transcription [671–673]. To assess whether these two receptors were involved in active

signalling, I analysed the transcriptional enrichment of Stat6 and Stat3 target genes in TRM cells relative to TCM cells. Because TEM cells were previously shown to convert to TRM cells [667], comparing TRM and TCM cells avoids information loss due to accidentally including trans-differentiating TEM cells. Gene set expression analysis showed that Stat6, but not Stat3, targets were enriched in TRM cells (Fig. II.1A). IL-21 signalling also activates Stat1 [674], and like Stat3 targets, Stat1-regulated genes were not significantly enriched in TRM cells (data not shown). Together, these data suggest that IL-4Rα-induced Stat6 signalling is specifically activated in TRM cells regardless of the tissue of origin.

In order to specify the time window at which IL-4Rα signalling becomes relevant to the TRM fate, I analysed single-cell RNA sequencing (scRNA-seq) data of antigen-specific P14 cells isolated from the SI on different days post acute systemic infection with the Armstrong strain of LCMV (LCMV Arm) [479]. Intraepithelial lymphocytes (IEL) sorted at different phases of the immune response were transcriptionally distinct (Fig. II.1B). As early as 7 days post infection (7dpi), IELs adopted a TRM-like phenotype by upregulating *Itgae*, which codes for CD103, and downregulating the transcription factor *Klf2*, which controls $S1P_1$ expression [223]. The anti-apoptotic factor *Bcl2*, on the other hand, was upregulated following immune contraction, in line with its role in memory T cell longevity [520] (Fig. II.1B). *Il4ra* was briefly induced early after infection (4dpi) but was quickly downregulated before being selectively transcribed in TRM cells 32dpi. Importantly, this expression pattern was partially reflected in the upregulation of the Stat6 gene signature, which was more stable during the contraction phase of the response. Because this analysis was consistent with the TRM fate being imprinted early after CD8+ T cell activation [466], I next analysed Stat6 signalling in lung-resident CD8+ T cells 8 days after flu infection. To facilitate the detection of virus-specific cells, I adoptively transferred naive P14 cells to mice that were later infected with a recombinant strain of HK-X31 influenza A virus expressing the cognate antigen of P14 cells, namely the $GP_{33\text{-}41}$ (GP33) viral epitope (X31-GP33) [675]. To identify resident T cells in the highly vascularised lung, I used an intravital labelling approach [676], where mice received an intravenous (IV) injection of fluorescently-labelled anti-CD8 antibody 5 minutes before they were sacrificed. Tissue-resident T cells are protected from IV labelling and are thus defined as IV negative (IV-) (see Fig. II.2D). Assay for Transposase-Accessible Chromatin with sequencing (ATAC-seq) analysis showed that both *Il4ra* and *Itgae* were more accessible in flu-specific lung-resident CD8+ T cells compared to naive cells (Fig. II.1D). In line with IL-4Rα being upregulated in SI TRM cells

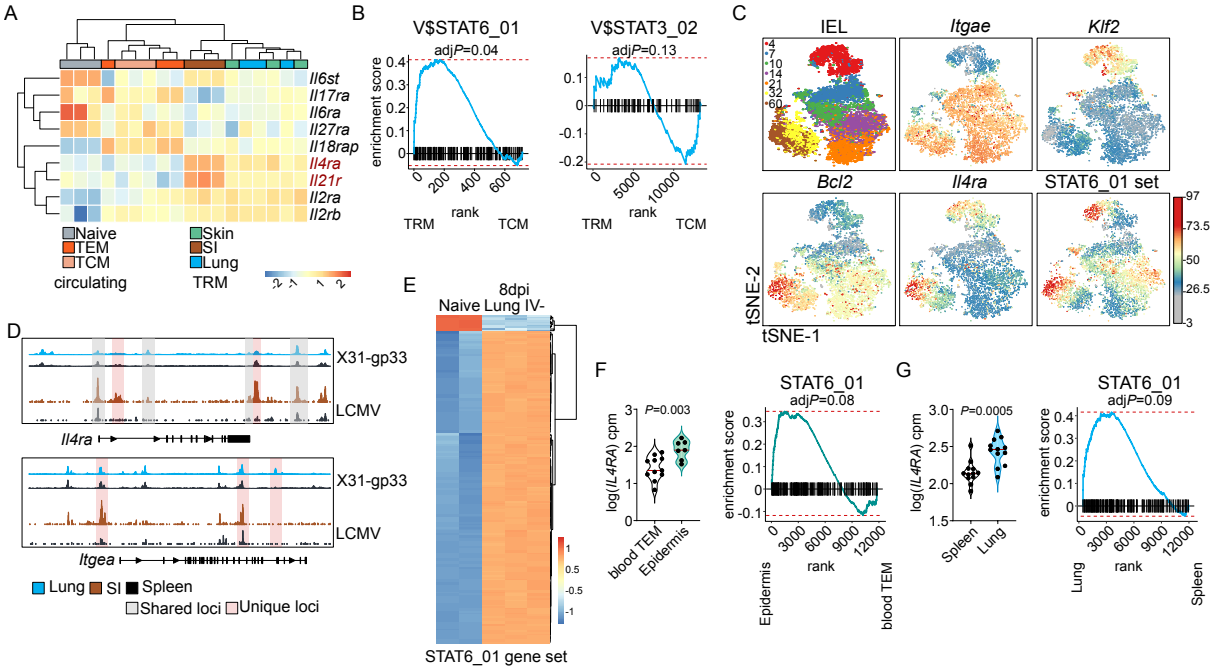

Figure II.1: IL-4Rα and Stat6 signalling are part of the core TRM transcriptional signature

(A) Antigen-specific CD8+ T cells were isolated from the skin, small intestine (SI), or lung 30 - 60 days after infection with herpes simplex virus, LCMV Arm, or influenza virus, respectively. Cells were then used for microarray analysis along with splenic naive, TEM, and TCM cells [225]. Shown is a heatmap depicting normalised expression of the indicated genes.

(B) Data in (A) were used for gene set enrichment analysis to trace the enrichment of Stat6 or Stat3 targets in TRM cells (pooled from skin, SI, and lung) relative to TCM cells. adj*P*, adjusted *P* values.

(C) A Uniform Manifold Approximation and Projection (UMAP) representation of P14 intraepithelial lymphocytes (IEL) isolated from the SI after LCMV Arm infection [479]. Cells are coloured by the day of isolation (numbers in the first UMAP plot), normalised expression of the indicated genes, or enrichment of Stat6 targets.

(D) ATAC-seq analysis of lung-resident P14 cells isolated 8 days after infection with X31-GP33 or from the spleen of naive mice. Preliminary analysis was performed by Dr. Joschka Hey. For comparison, tracks of P14 cells isolated from SI or spleen 7 days after LCMV Arm are included [466].

(E) A heatmap comparing chromatin accessibility of Stat6 target genes between lung resident and naive P14 cells analysed as in (D). dpi, days post infection. IV, intravenous.

(F and G) Human CD8+ TRM cells were collected from epidermis (F) [470] or lung (G) [472] and used for RNA-seq analysis along with the indicated circulating memory cells. Shown are normalised *IL4RA* counts and enrichment analysis of STAT6 targets. cpm, counts per million.

Data in (D) are from one experiment with 2 - 3 mice per group. *P* values were calculated using two-tailed unpaired Student's *t*-test and where indicated, they were corrected using Benjamini-Hochberg adjustment.

(Fig. II.1A, C), I found its locus to contain more open chromatin regions in IELs sorted 7dpi with LCMV Arm relative to circulating effector cells [466]. Furthermore, at this very early time point, almost all Stat6 target genes were more accessible in lung IV- cells compared to circulating cells (Fig. II.1E).

Finally, I confirmed that IL-4Rα signalling is similarly activated in human TRM cells. CD8+ T cells isolated from the skin and lung of organ donors [470, 472] had higher levels of both *IL4RA* and STAT6 target genes relative to circulating memory cells (Fig. II.1F, G). Taken together, these results suggest that Stat6-mediated IL-4Rα signalling is part of the conserved TRM signature in different tissues, and that this pathway is temporally controlled in the same manner as canonical TRM markers.

II.2.2 TRM cells express high levels of IL-4Rα

To experimentally validate these bioinformatic analyses, I measured IL-4Rα expression on the protein level. Activation of CD8+ T cells in the presence of transforming growth factor β (TGFβ) and all-*trans*-retinoic acid (ATRA) leads to the expression of the TRM markers CD69 and CD103 (Fig. II.2A) [252]. These *in vitro*-differentiated TRM-like cells had higher levels of both IL-4Rα and phosphorylated Stat6 (pStat6) (Fig. II.2B, C).

To confirm these findings *in vivo*, I examined IL-4Rα levels in TRM cells isolated from different tissues. Following X31 infection, lung TRM cells (identified using intravital labelling; Fig. II.2D) had higher levels of surface IL-4Rα compared to circulating cells isolated from the same animal, as evident by the ratio of its fluorescence intensity in resident (IV-) to circulating (IV+) cells being greater than one after 30 days of infection (Fig. II.2E). In spite of ATAC-seq data suggesting that the *Il4ra* locus is already accessible 8dpi, I found that the IV-:IV+ ratio of IL-4Rα remained smaller than one until day 15 post infection. This discrepancy might reflect differences in the analysed populations (P14 cells for ATAC-seq vs endogenous polyclonal cells) or the temporal delay between chromatin changes and protein translation. Consistent with scRNA-seq and ATAC-seq analyses (Fig. II.1C, D), IL-4Rα was upregulated by P14 IELs in the SI as early as 8dpi with LCMV Arm, positively correlated with CD103 expression, and remained stable for at least 30 days after infection (Fig. II.2E). LCMV Arm establishes TRM cells in the liver [316, 655], which upregulated IL-4Rα early after infection. However, its levels were relatively downregulated at later time points (Fig. II.2G). Interestingly, IL-4Rα expression by liver CD8+ T cells was mutually exclusive with the liver TRM markers CD69 and CXCR6 [219].

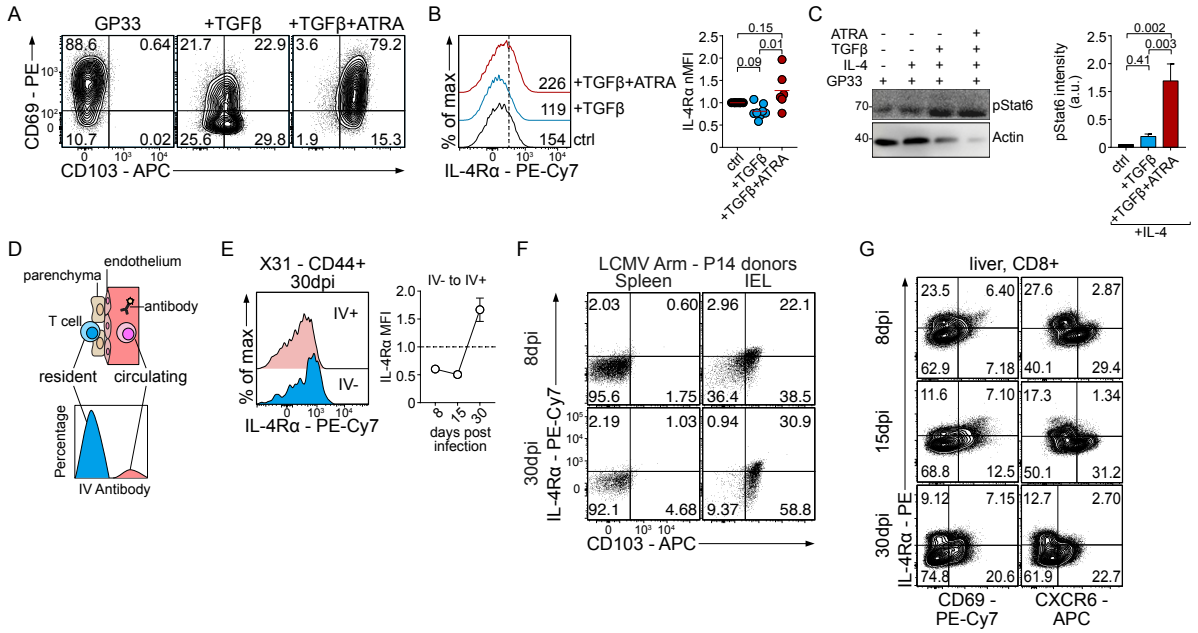

Figure II.2: TRM cells express IL-4Rα *in vitro* and *in vivo*

(A - C) P14 cells were activated with GP33 for three days in the presence or absence of TGFβ, all-*trans*-retinoic acid (ATRA), or IL-4. Cells were either used for flow cytometry (A & B) or protein lysates were used for western blot (C). nMFI, normalised mean fluorescence intensity. a.u., arbitrary units.

(D) A diagram summarising the intravital labelling strategy. IV, intravenous.

(E) IL-4Rα expression in lung-resident (IV-) polyclonal CD8+ T cells was normalised to that in circulating (IV+) cells isolated from the same mouse.

(F) Representative dotplots showing the co-expression pattern of IL-4Rα and CD103 by IELs isolated from the small intestine after LCMV Arm infection.

(E) Representative contour plots showing IL-4Rα expression relative to the liver TRM markers CD69 and CXCR6. Note that in this case, animals were sacrificed on different days leading to slightly different gates at different time points.

Data are either representative of (F & G) or pooled from (A - C & E) 2 - 7 experiments. Error bars indicate s.d. *P*-values (B & C) were calculated using repeated measures (RM) one-way ANOVA.

This finding contrasts with the importance of IL-4Rα for the durability of liver CD8+ T cells following malaria vaccination [677] and with the recently reported transcriptional upregulation of *Il4ra* by liver-resident memory P14 cells following LCMV infection [655]. Notably, at all time points, the 'background' expression of IL-4Rα by CD69+ and CXCR6+ cells was higher than that by IL-4Rα-CD69- and IL-4Rα-CXCR6- cells, respectively (Fig. II.2G), suggesting that low levels of IL-4Rα might be sufficient for mediating its function in liver TRM cells. This supposition would be in line with Stat6 being constitutively phosphorylated in hepatocytes even

in the absence of exogenous IL-4 treatment [678], which indicates that IL-4 levels might be high in the liver microenvironment. Measurement of IL-4 concentration in the liver relative to plasma at different time points following infection is a possible strategy to test this hypothesis. In addition, analysis of pStat6 levels or its target genes in the individually sorted populations might provide information regarding signalling activity of the pathway.

Together, data presented in Figures II.1 and II.2 show that the IL-4Rα/Stat6 axis is activated in TRM cells isolated from different organs, and indicate that this pathway might be part of the residency establishment program of CD8+ T cells in different tissues.

II.2.3 Germline Stat6 deficiency increases TRM cell numbers

To understand whether Stat6 signalling functionally contributed to TRM cell differentiation and/or maintenance, I infected *Stat6*$^{-/-}$ (Stat6 KO [679]) mice and their wildtype (WT) littermates with X31-GP33 and monitored lung TRM formation 30 days later (Fig. II.3A). Germline loss of Stat6 expression resulted in an accumulation of total and GP33-specific TRM cells in the lung (Fig. II.3B). However, the per-cell expression of TRM phenotypic markers was unchanged; in Stat6 KO mice, lung TRM cells expressed comparable levels of CD69 and CD103 as in WT mice (Fig. II.3C). High levels of T-bet expression block optimal TRM positioning in the lung [267], but TRM cells from WT and Stat6 KO mice similarly downregulated T-bet levels (Fig. II.3D). Furthermore, I found no difference in the cytokine-production capacity after *ex vivo* activation (Fig. II.3E).

My next question was whether loss of Stat6 signalling affected the initial differentiation of TRM cells, which takes place around 7 - 8dpi (Fig. II.1C, D), or their subsequent replenishment by circulating memory cells. Therefore, I infected WT C57BL/6N (B6) mice with X31-GP33 and, using a selective Stat6 inhibitor (Stat6i), blocked Stat6 activation 8 days after infection (Fig. II.3F). Stat6i caused a dose-dependent accumulation of resident polyclonal (CD44+) and donor P14 cells in the lung (Fig. II.3G), phenocopying mice with genetic Stat6 deficiency. Furthermore, I found no major difference in CD69, CD103, or T-bet expression in TRM cells between mice treated with Stat6i or the vehicle control. Together, these results suggest that tissue-wide loss of Stat6 activity induces the late accumulation of TRM cells in the lung without significantly affecting their phenotype.

Because Bioinformatic analyses predicted the involvement of IL-4Rα signalling in TRM

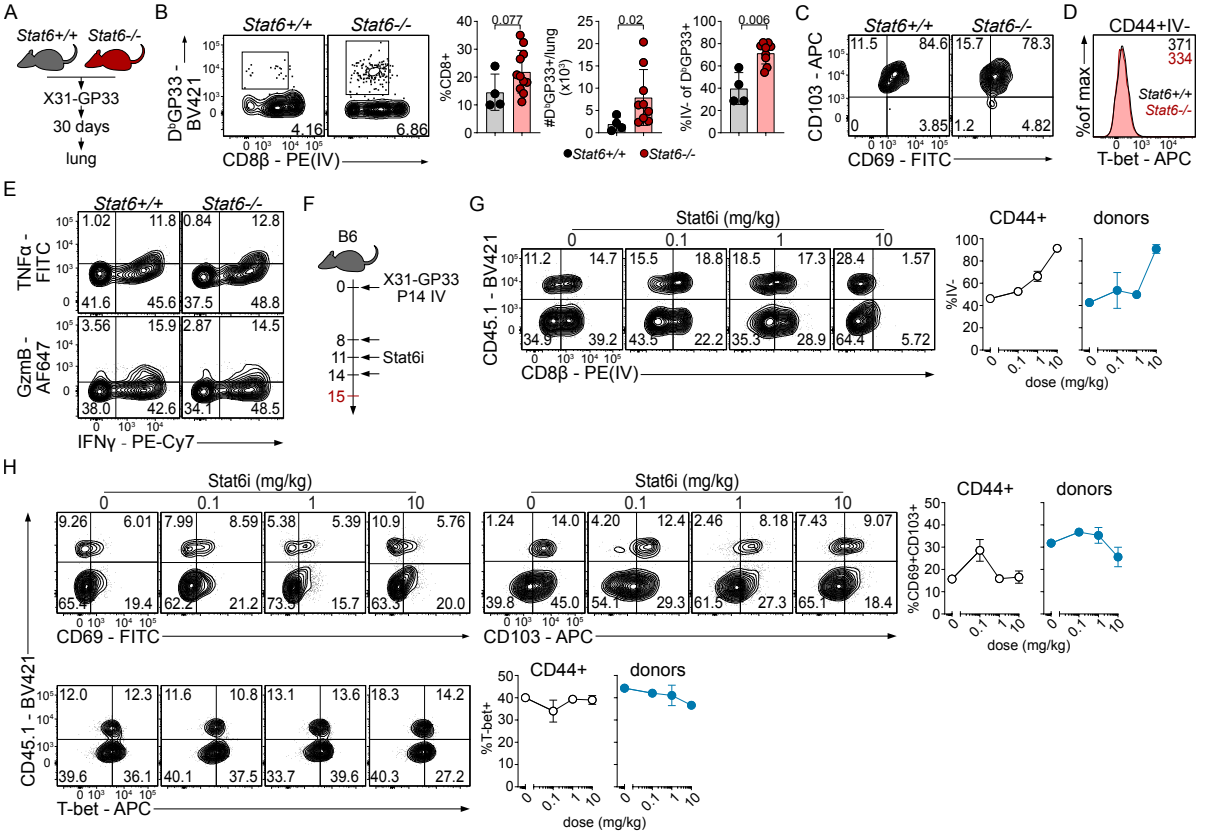

Figure II.3: Tissue-wide loss of Stat6 signalling favours lung TRM formation

(A) Experimental design for panels B - E.

(B) Frequency of total and resident antigen-specific CD8+ T cells, detected using GP33-MHC-I tetramers (D^bGP33) in the lung 30 days after infection.

(C) CD69 and CD103 expression in CD44+ lung-resident cells cells.

(D) T-bet expression in polyclonal (CD44+) lung-resident IV- cells. Numbers on histograms indicate T-bet MFI.

(E) Cytokine production by lung-resident polyclonal TRM cells 6 hours after *ex vivo* stimulation with a combination of Phorbol-12-myristate-13-acetate (PMA) and ionomycin.

(F) Experimental design for panels G & H. Naive P14 T cells were adoptively transferred to WT mice infected with X31-GP33. Eight days later, mice were treated with Stat6 inhibitor (Stat6i) or vehicle.

(G and H) Expression of TRM markers in endogenous and P14 donor (CD45.1+) cells in the CD44+ (G) or the CD44+IV- (H) gates.

Data are either representative of (C - E) or pooled from (B) 3 experiments (n = 4 - 8 mice per group). Data in G & H are from one experiment with 3 mice per Stat6i dose. Error bars indicate s.d. *P* values (B) were calculated using two-tailed unpaired Student's *t*-test.

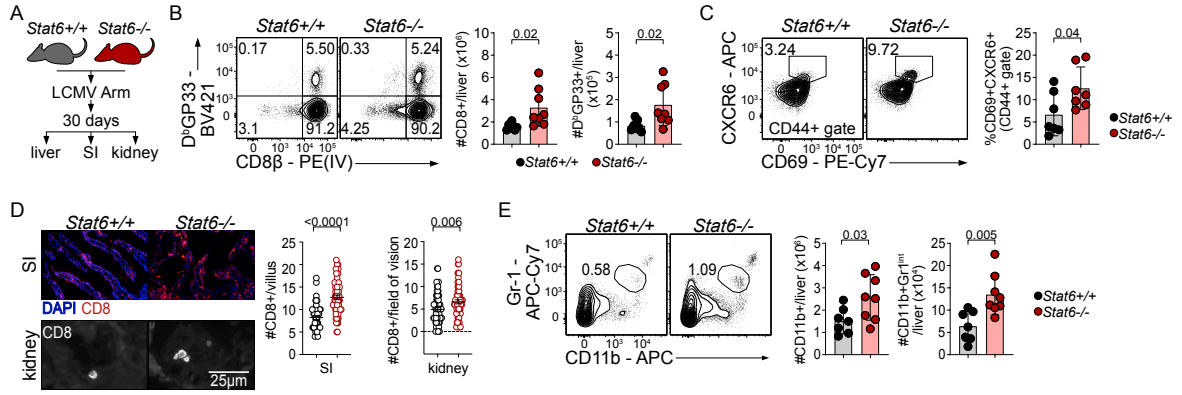

Figure II.4: Tissue-wide loss of Stat6 induces TRM formation at multiple sites

(A) Experimental design.

(B and C) CD8+ T cells were isolated from the liver and their total abundance (B) and expression of liver TRM markers (C) were quantified.

(D) Representative fluorescent photomicrographs of SI and kidney tissue sections stained with 4′,6-diamidino-2-phenylindole (DAPI; blue) and or anti-CD8 antibody (red or white) and quantifications of CD8+ T cell counts. Scale bar = 25 μm.

(E) Frequency of total myeloid (CD11b+) and inflammatory monocytic (Gr-1^{intermediate}, Gr-1^{int}) cells isolated from the liver.

Data are pooled from 2 experiments (n = 6 - 8 mice per group). Error bars indicate SEM (D) or s.d. *P* values were calculated using two-tailed unpaired Student's *t*-test.

cells at multiple sites, I next examined whether the accumulation of TRM cells in Stat6 KO mice was a generalised or a lung-specific phenotype. To this end, I infected WT and Stat6 KO mice with LCMV Arm and analysed the number of TRM cells in different tissues (Fig. II.4A). Using intravital labelling, I found that liver CD8+ T cells in both WT and Stat6 KO mice were predominantly IV+ (Fig. II.4B), consistent with their location in liver sinusoids and their exposure to blood [219]. Therefore, I defined liver TRM cells as CD69+CXCR6+ cells (Fig. II.4C). Similar to flu-infected mice, I found that Stat6 KO mice had higher numbers of TRM cells in the liver (Fig. II.4B, C), SI, and kidney (Fig. II.4D) compared to WT littermates following LCMV Arm infection. Moreover, endogenous GP33-specific cells were not specifically recruited to the liver in Stat6 KO mice as shown by their comparable frequency in WT and KO mice (Fig. II.4B). Rather, the absolute counts of total CD8+ T cells, and therefore GP33-specific T cells, were increased in the liver of Stat6 KO mice.

Results from flu and LCMV Arm infection experiments confirm the importance of Stat6 signalling for TRM cells in multiple tissue sites and are in line with the massive CD8+ and

CD4+ T cell infiltration in lungs of IL-4 deficient mice following flu infection [680]. However, while bioinformatic analyses and increased IL-4Rα levels in WT TRM cells suggest that Stat6 signalling supports TRM cell differentiation, experiments using Stat6 KO mice show the opposite. This discrepancy is potentially caused by the genetic deletion of Stat6 in CD8+ T cells as well other immune and non-immune cells. For example, in the absence of Stat6 signalling, M2-polarised macrophages lose their inhibitory effect on T cell proliferation [681]. Besides, Stat6 activation induces the differentiation and accumulation of regulatory T cells in specific tissue niches [682]. Additionally, IL-4 was previously shown to induce the release of surfactant proteins in the lung and liver, which act to induce M2 macrophage differentiation and support tissue repair [683]. On the other hand, I observed the accumulation of inflammatory monocytes in the liver of Stat6 KO mice (Fig. II.4E). Since the accumulation of T cells in the lung after flu infection associates with age and lung tissue fibrosis [684], it is possible that global IL-4/Stat6 signalling acts to decrease TRM accumulation as a wound healing mechanism that protects tissue integrity.

II.2.4 CD8+ T cell-intrinsic Stat6 signalling regulates infiltration into NLTs

To understand whether increased TRM cell numbers in Stat6 KO mice was due to CD8+ T cell-intrinsic or -extrinsic effects, I performed two complementary experiments. First, I transferred WT P14 cells to Stat6 WT or Stat6 KO littermates that were later infected with GP33-X31 (Fig. II.5A). Because Stat6 signalling was intact in the transferred WT cells, subsequent differences in donor cells in different hosts would be due to CD8+ T cell-extrinsic functions of Stat6. In agreement with my previous observations, I found that the number of endogenous (CD45.1-) IV- cells was higher in Stat6 KO hosts compared to WT littermates (Fig. II.5B). Additionally, the total number of WT donors (CD45.1+) and their bias towards lung residency were increased in Stat6-deficient animals (Fig. II.5B), strongly suggesting that this effect was CD8+ T-cell extrinsic.

In the second experiment, I asked whether CD8+ T cell-intrinsic Stat6 function affected TRM cell differentiation. I crossed Stat6 KO mice to P14 mice and transferred WT or Stat6 KO P14 cells to WT B6 mice that were later infected with X31-GP33. Because host mice had normal Stat6 signalling, differences between groups would be due to CD8+ T cell-intrinsic functions of Stat6. To avoid potentially confounding environmental factors, I transferred equal numbers of congenically mismatched WT and Stat6 KO cells to the same mouse (Fig. II.6A).

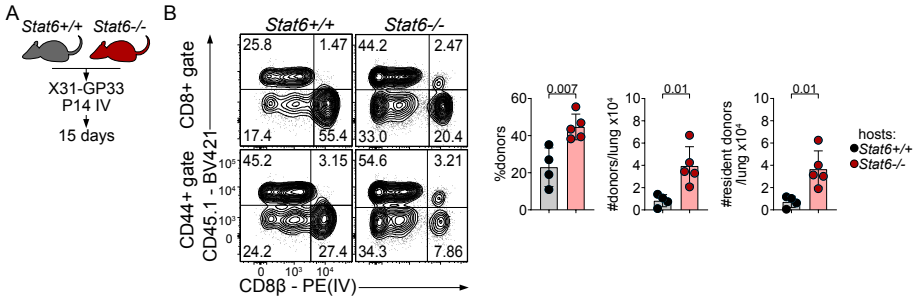

Figure II.5: CD8+ T cell-extrinsic Stat6 signalling limits TRM cell accumulation

(A) Experimental design.

(B) Abundance of donor CD45.1+ cells among total CD8+ or polyclonal CD44+CD8+ T cells isolated from the lung.

Data are from 1 experiment (n = 4 - 5 mice per group). Error bars indicate s.d. *P* values were calculated using two-tailed unpaired Student's *t*-test.

Eight days after infection, I found no difference in the frequency of WT and Stat6 KO donor cells (Fig. II.6B), suggesting that Stat6 signalling is not required for the initial differentiation of TRM cells. However, only one week later, the frequency of Stat6 KO donor cells in the lung was half that of WT donors, suggesting that CD8+ T cell-intrinsic Stat6 signalling is required either for survival of TRM cells or for the continuous recruitment of circulating cells into the lung. To differentiate these two possibilities, I examined the frequency of circulating IV+ donor cells in the lung, which are presumably being recruited into the lung parenchyma. This analysis shows that as early as 8dpi, the abundance of WT donors infiltrating the lung is approximately twice that of Stat6 KO cells (Fig. II.6C), and that this difference remained stable at later time points. Consistent with the phenotype of Stat6 KO mice, T cell-specific deletion of Stat6 had no influence on their phenotype as evident by the comparable expression of CD69 and CD103 between WT and Stat6 KO donor cells (Fig. II.6D). These results indicate that Stat6 signalling controls the continuous recruitment of circulating CD8+ T cells into the lung rather than their differentiation into TRM cells in situ.

I next asked whether *in vivo* re-stimulation of lung TRM cells might rescue the recruitment and/or expansion of Stat6 KO donors. Twenty one days after P14 cell adoptive transfer and initial infection with GP33-X31, I re-challenged mice with a different influenza A virus strain (PR8) that carries the same GP33 epitope (PR8-GP33). Four days later, I analysed the abundance of total and circulating donor cells in the lung. Stat6 KO donor cells, which were already fewer than WT cells before secondary infection, became even less abundant (Fig. II.6E). Ad-

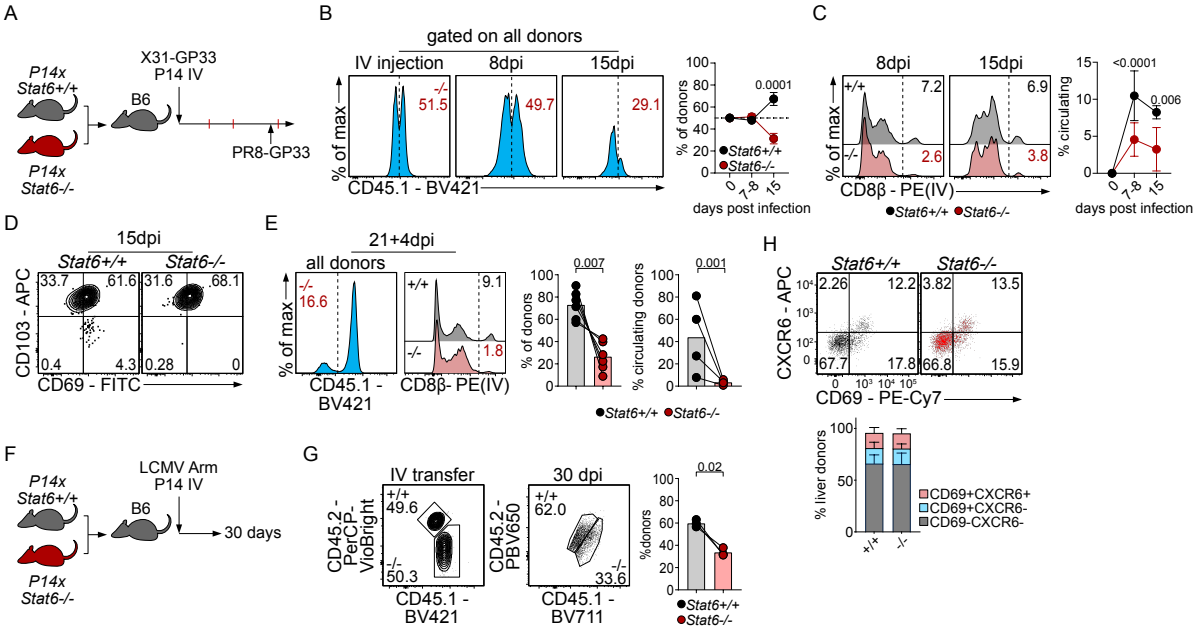

Figure II.6: CD8+ T cell-intrinsic Stat6 signalling directs T cell migration into NLTs

(A) Experimental design for panels B - E.

(B) Congenically marked Stat6 KO donors (CD45.1+) were recovered from the lung and quantified. Numbers on histograms refer to the frequency of Stat6 KO among total donors.

(C) Frequency of circulating IV+ donor cells in lungs of flu-infected mice at different time points. Numbers on histograms indicate the frequency of IV+ cells.

(D) Representative contour plots depicting the expression of CD69 and CD103 in donor cells.

(E) Twenty one days after X31-GP33 infection, mice were challenged with PR8-GP33 and were sacrificed 4 days later (21+4dpi). Shown are histograms and bar graphs quantifying the abundance of total and circulating donor cells. Numbers on histograms indicate the frequency of Stat6 KO donors or of IV+ cells.

(F) Experimental design for panels G & H.

(G) Frequency of donor cells transferred to naive mice or harvested from the liver of LCMV Arm immune mice 30 days after infection.

(H) Expression of liver TRM cell markers in donor cells recovered from the liver.

Data are from 1 experiment (G & H, n = 3 mice) or are pooled from 2 independent experiments (B - E, n = 4 - 6 mice per time point). Where shown, error bars indicate s.d. *P* values were calculated using two-tailed paired Student's *t*-test.

ditionally, while secondary infection increased the abundance of circulating WT donors infiltrating the lung by a factor of 5, the frequency of lung-infiltrating Stat6 KO donors was not affected and remained significantly lower than that of WT cells. These data indicate that Stat6

signalling redirects the migration of circulating cells into the lung both after primary and secondary infections.

Finally, to confirm that the role of T cell-intrinsic Stat6 was conserved in TRM cells at other sites, I transferred a mixture of WT and Stat6 KO donor cells to mice that were infected with LCMV Arm and the abundance of donor cells in the liver was examined 30 days later (Fig. II.6F). I found that Stat6 KO donors were significantly less abundant in liver than WT donors (Fig. II.6G). However, akin to lung TRM cells, there was no difference in the expression of liver TRM markers between WT and Stat6 KO donor cells. Together, these data confirm the requirement for Stat6 signalling for TRM cell development at different tissue sites.

II.2.5 Stat6 potentially regulates CXCR6 expression

Stat6 had minimal influence on the phenotype of lung and liver TRM cells, but seemed to control the recruitment and infiltration of circulating cells into NLTs. This suggests that Stat6 might act by regulating the expression of chemokine receptors that directed T cell migration into several tissues. I found that 3 chemokine receptors, namely *Ccr5, Cxcr3*, and *Cxcr6*, were selectively transcribed in TRM cells regardless of the tissue of origin [225] (Fig. II.7A). Interestingly, all three receptors were previously reported to induce the trans-migration of T cells into non-inflamed lung parenchyma (CCR5) or airways (CXCR3 and CXCR6) [670, 685, 686]. However, only CXCR6-deficient, but not CCR5- or CXCR3-KO, T cells displayed compromised migration into the lung following flu infection [687], in line with its ligand, CXCL16, being constitutively expressed by lung epithelial cells, endothelial cells, and several immune cells in the lung including dendritic cells and macrophages [686, 688].

To understand whether any of these three receptors was directly regulated by IL-4Rα signalling, I analysed published chromatin immunoprecipitation (ChIP) with sequencing (ChIP-seq) data that examined Stat6 DNA binding activity in bone marrow-derived macrophages (BMDMs) pre-treated with IL-4 for 1 hour [469]. Consistent with *Il4ra* being a direct Stat6 target [689], I found that Stat6 binding in the *Il4ra* locus was increased in IL-4 treated cells (Fig. II.7B). Although Stat6 was able to bind at or near the *Cxcr6* and *Ccr5* loci, no binding was detectable around the *Cxcr3*-encoding sequence. This suggests that either *Cxcr3* is not a direct Stat6 target or that simply this genomic locus is not accessible in BMDMs. To demonstrate direct Stat6 regulation of these loci, Stat6 ChIP-quantitative polymerase chain reaction (qPCR) could be performed using TRM-like or activated T cells. I next examined the expression of

these 3 chemokine receptors in IV+ cells infiltrating the lung following flu infection. Although the levels of all 3 receptors were low 8dpi, only CXCR6 was upregulated by 15dpi (Fig. II.7C).

Because the selective upregulation of CXCR6 temporally coincided with the migration defect of Stat6 cells into the lung (Fig. II.6B and Fig. II.7C), and because ChIP-seq analysis

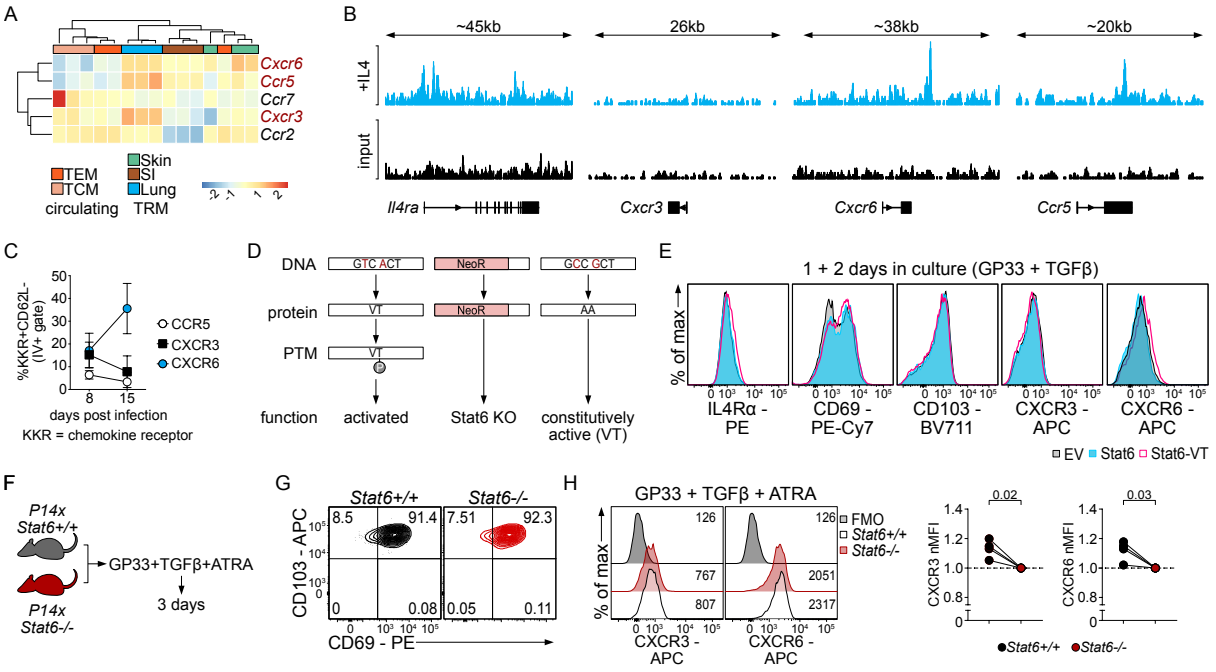

Figure II.7: CXCR6 is a potential Stat6 target

(A) A heatmap showing normalised expression of differentially transcribed chemokine receptor genes across TRM and circulating memory cells analysed as in Fig. II.1A [225].

(B) Stat6 ChIP-seq analysis of IL-4 treated BMDMs [469].

(C) Expression of different chemokine receptors (KKR) by lung-infiltrating polyclonal CD8+ T cells at different time points following X31 infection.

(D) A diagram comparing genetic modifications in Stat KO cells and Stat6-VT vector. NeoR, neomycin-resistance. PTM, post-translational modification. V, valine. T, threonine.

(E) Naive P14 cells were activated for one day, transduced with retroviruses carrying an empty vector (EV), wildtype Stat6, or Stat6-VT, and were further activated for 2 more days in the presence of TGFβ.

(F) Experimental design for panels G & H.

(G) Expression of CD69 and CD103 in WT and Stat6 KO TRM-like cells.

(H) Expression of CXCR3 and CXCR6 by *in vitro*-differentiated TRM-like cells.

Data are from 1 experiment (C & E, n = 3 - 4 mice), are representative of 3 experiments (G), or are pooled from 3 independent experiments (H). Where shown, error bars indicate s.d. *P* values were calculated using two-tailed paired Student's *t*-test.

suggested that it is a potential Stat6 target, I next asked whether Stat6 signalling modulated CXCR6 expression in gain- and loss-of-function models. First, I cloned murine Stat6 and introduced two point mutations that were previously reported to induce Stat6 dimerisation and constitutive activation even in the absence of IL-4 signalling [690] (Fig. II.7D). *In vitro*-differentiated TRM-like cells expressing this mutant protein (termed Stat6-VT) slightly, but significantly, upregulated IL-4Rα as well as CXCR6 (Fig. II.7E) but not CXCR3, CD69, or CD103. In a complementary approach, I examined CXCR6 expression by *in vitro*-differentiated Stat6 KO TRM-like cells. In order to avoid potential differences due to defective antigen presentation by Stat6 KO splenocytes, I mixed congenically mismatched WT and Stat6 KO splenocytes in a 1:1 ratio and cultured the cells under TRM-skewing conditions (Fig. II.7F). In agreement with *in vivo* experiments (Fig. II.6D), there was no difference in the expression of CD69 or CD103 between WT and Stat6 KO TRM-like cells (Fig. II.7G). However, loss of Stat6 activity caused a significant decrease in CXCR6 and CXCR3 expression (Fig. II.7H). Together, these data suggest that Stat6 might license the infiltration of circulating cells into tissue parenchyma through modulating CXCR6, and possibly, CXCR3 expression.

II.2.6 Constitutive Stat6 activity increases liver TRM cell numbers

CXCR6 is a definition marker for liver TRM cells [219], which themselves were less abundant in the absence of T cell-intrinsic Stat6 signalling. Therefore, I next examined whether constitutive Stat6 activity would increase the percentage of CXCR6+ liver TRM cells. I infected WT B6 mice with LCMV Arm and one day later, transferred cells overexpressing Stat6-VT (Fig. II.8A). Three weeks afterwards, I found that constitutively active Stat6 enhanced CXCR6 expression (Fig. II.8B). Furthermore, I found no difference between splenic Stat6-VT-expressing and control donors in terms of CD62L expression (Fig. II.8C), suggesting that Stat6 activity did not influence the balance between TCM and TEM cells in the circulation. On the other hand, liver Stat6-VT-expressing cells had significantly lower CD62L levels than control cells (Fig. II.8C), indicating that Stat6 signalling favours the infiltration of TEM cells into NLTs.

II.2.7 Identifying the source of the Stat6-activating signal

IL4Rα dimerises with either γ_c or IL-13Rα to form type I and type II receptors, respectively [691–693]. While IL-4 is able to bind to and signal through both receptor complexes, IL-13 binds only to type II receptors [694]. Both cytokines are reportedly secreted during the course

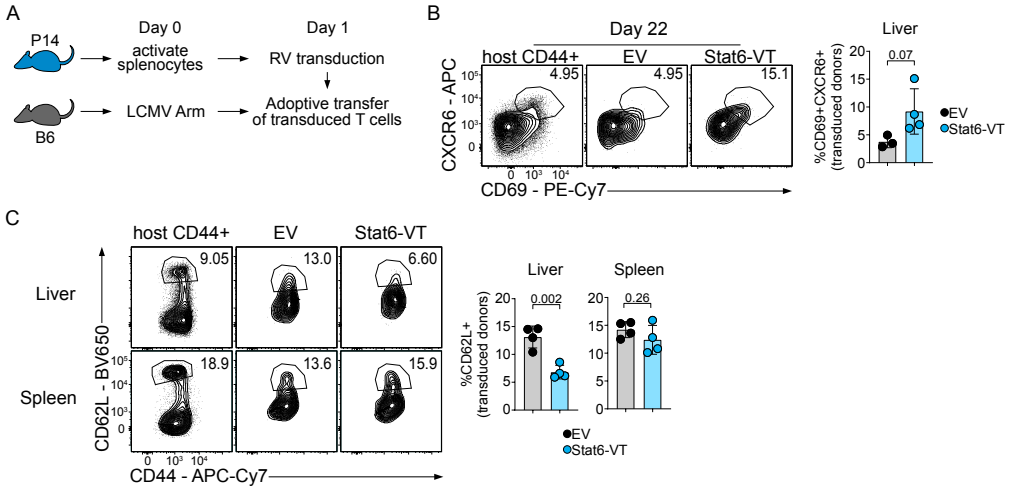

Figure II.8: Stat6-VT induces the accumulation of liver TRM cells

(A) Experimental design. RV, retrovirus.

(B and C) Abundance of TRM cells (B) and TCM cells (C) among trasnduced P14 donors in the liver. Data are from 1 experiment (n = 3 - 4 mice per group) Error bars indicate s.d. *P* values were calculated using two-tailed unpaired Student's *t*-test.

of flu infection [680, 695, 696], and in mice, both of their genes are found on chromosome 11, where they are influenced by common regulatory elements [697]. To study the nature, and source, of the initial signal that induces Stat6 activation in TRM cells, I infected mice that lack both *Il4* and *Il13* expression in all body cells ($Cmv^{Cre}xIl4^{Fl/Fl}xIl13^{Fl/Fl}$ [458, 460]) with X31 (Fig. II.9A). These mice largely phenocopied Stat6 KO mice; they had more total and resident CD8+ T cells in the lung 30 days after flu infection compared to WT littermates (Fig. II.9B).

In models of parasitic lung infections, CD4+ T cells are the major source of IL-4 [698], and they secrete equivalent amounts of both IL-4 and IL-13 into the airways of flu infected mice [696]. Therefore, I tested whether CD4+ T cell-secreted cytokines were responsible for the recruitment of circulating T cells into the lung. Crossing $Il4^{Fl/Fl}xIl13^{Fl/Fl}$ and $Cd4^{Cre}$ [455] mice generates mice lacking *Il4* and *Il13* expression in both CD4+ and CD8+ T cells. Although these mice tended to accumulate more CD8+ T cells in their lungs following flu infection, these cells did not show an enhanced residency potential, as evident by the equivalent abundance of resident polyclonal (IV-CD44+) cells between conditional KO mice and their WT littermates (Fig. II.9C, D), suggesting that T cell-derived IL-4/IL-13 do not control the migration of circulating CD8+ T cells into the lung.

Other candidates for IL-4/IL-13 secretion include type 2 innate lymphoid cells (ILC2) [695,

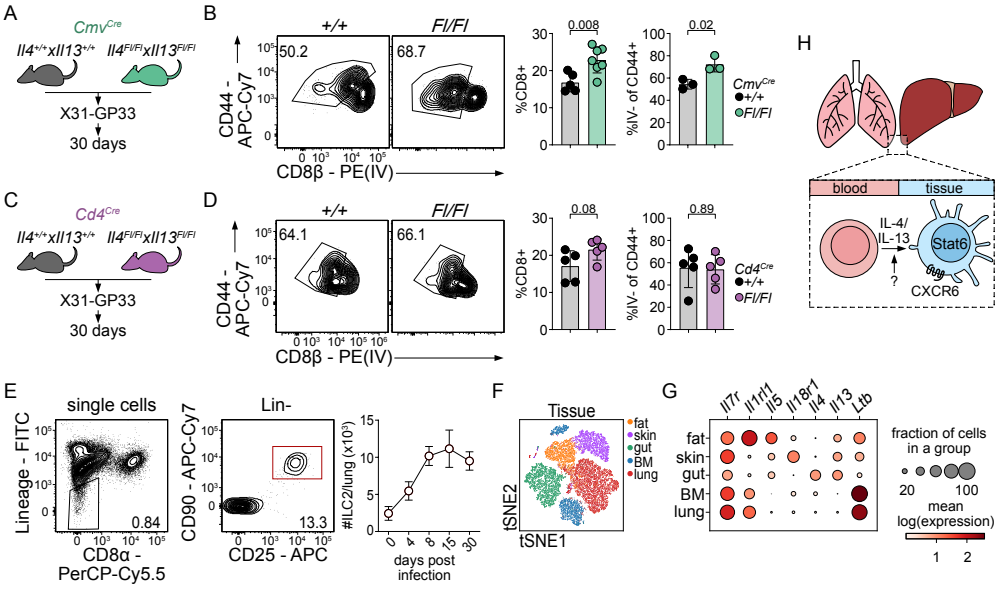

Figure II.9: T cell-derived IL-4/IL-13 do not control the T cell residency program

(A - D) Mice with tissue-wide (A and B) or T cell-specific (C and D) deletion of *Il4* and *Il13* were infected with X31-GP33 and the abundance of total and resident polyclonal cells was quantified 30 days later.

(E) The frequency of ILC2 cells was measured in the lung at different time points following flu infection. Lineage: TCRb, TCRgd, NK1.1, B220, CD19, CD11b, CD11c, Ly6c, Ter119.

(F) A t-distributed stochastic neighbour embedding (tSNE) plot of ILC2 cells isolated from different tissues [678].

(G) Normalised expression level (colour scale) and expression percentage (dot size) of the indicated genes in ILC2 cells sorted from different tissues as in F.

(H) A diagram summarising the main findings of this work.

Data (A - D) are representative of or are pooled from 2 experiments (n = 3 - 7 mice per group). Error bars indicate s.d. *P* values were calculated using two-tailed unpaired Student's *t*-test.

696], which successively accumulate in the lung following flu infection (Fig. II.9E), as previously reported [695]. However, scRNA-seq analysis of 33,074 ILC2 cells isolated from different organs [475] shows that lung ILC2 cells express very low levels of either cytokine (Fig. II.9F, G). Nevertheless, selective depletion of ILC2 cells using, for example, $Il7r^{Cre}xRora^{Fl/+}$ mice [699] is required to provide conclusive evidence regarding the role of ILC2 cells in T cell recruitment to NLTs.

II.3 Conclusion

Results presented here show that Stat6 activation regulates the infiltration of circulating CD8+ T cells into lung and liver potentially through a CXCR6-dependent mechanism (Fig. II.9H), and that subsequent tissue-specific signals play a more important role in instructing TRM differentiation. These findings underscore similarities in the differentiation program of TRM cells from different organs [225, 252, 655]. Importantly, while a detailed understanding of T cell-intrinsic consequences of different signalling pathways is essential, it does not provide a complete picture. Once in NLTs, TRM cells are indoctrinated to become part of the new organ and need to respond to local cues for optimal function. For example, lung CD8+ TRM cells depend on CD4+ T cell help for optimal positioning [267]. My data show that Stat6 regulates immune, and possibly other, cell populations in NLTs that might concertedly act to suppress TRM formation. This supersedes the CD8+ T cell-specific function of Stat6 in supporting the replenishment of TRM cells. It is possible that these seemingly paradoxical roles of Stat6 are a built-in checkpoint that protects against immunopathology precipitated by TRM cells [218, 662, 700]. Differential sensitivity to IL-4Rα ligands might be a mechanism to fine-tune this response. IL-4 and IL-13 levels increase in the lung during flu virus infection [696] and their germline deficiency phenocopies Stat6 loss. However, the cellular source of these two cytokines remains to be explored.

Future experiments might focus on validating the effect of Stat6 on CXCR6 expression. As mentioned, Stat6 ChIP-qPCR is one strategy to show that Stat6 directly induces the transcription of *Cxcr6*. Additionally, luciferase reporter assays might prove useful in this regard. Furthermore, the role of IL-4Rα signalling in inducing the infiltration of pre-TRM cells into NLTs needs to be explored further. For example, IL-4Rα+ and IL-4Rα- cells could be sort-purified from the spleen and transferred to congenically-distinct infection-matched mice. Afterwards, the abundance of liver TRM cells could be assessed. Finally, it would be intriguing to investigate whether auto-aggressive liver TRM cells have abnormal Stat6 activation.

In summary, this work reveals that development of TRM cells occurs in two steps, directed migration of circulating cells towards NLTs, which is regulated by Stat6, and subsequent Stat6-independent tissue imprinting of the TRM fate. My results suggest that Stat6 signalling is involved in nested regulatory circuits that have opposing effects on different cell types, which might act to balance protective immunity with tissue damage.

8 List of publications

Madi A, Wu J, Ma S, Weisshaar N, Mieg A, Hering M, Ming Y, Zettl F, Mohr K, Ten Bosch N, Schlimbach T, Hertel F, Cui G. Regulatory T cell-derived interleukin-15 promotes the diversity of immunological memory. Eur J Immunol. 2022 Oct 20. doi: 10.1002/eji.202149400. Epub ahead of print. PMID: 36263815.

Madi A, Weisshaar N, Buettner M, Poschet G, Ma S, Wu J, Mieg A, Hering M, Ming Y, Mohr K, Ten Bosch N, Cui G. CD8 agonism functionally activates memory T cells and enhances antitumor immunity. Int J Cancer. 2022 Sep 1;151(5):797-808. doi: 10.1002/ijc.34059. Epub 2022 May 21. PMID: 35499751.

Madi A, Cui G. Regulation of immune cell metabolism by cancer cell oncogenic mutations. Int J Cancer. 2020 Jul 15;147(2):307-316. doi: 10.1002/ijc.32888. Epub 2020 Feb 25. PMID: 31994718.

Wu J, **Madi A**, Mieg A, Hotz-Wagenblatt A, Weisshaar N, Ma S, Mohr K, Schlimbach T, Hering M, Borgers H, Cui G. T Cell Factor 1 Suppresses CD103+ Lung Tissue-Resident Memory T Cell Development. Cell Rep. 2020 Apr 7;31(1):107484. doi: 10.1016/j.celrep.2020.03.048. PMID: 32268106.

Weisshaar N*, **Madi A***, Cui G. Early TCR Signaling Sweetens Effector Function through PDHK1. Trends Endocrinol Metab. 2018 Sep;29(9):595-597. doi: 10.1016/j.tem.2018.03.016. Epub 2018 Mar 31. PMID: 29615303. *Equal contribution.

9 List of abbreviations (A-Z)

α-KG	α-ketoglutarate
2-DG	2-Deoxy-D-glucose
2-ME	2-mercaptoethanol
2-NBDG	2-[N-(7-nitrobenz-2-oxa-1,3-diazol-4-yl) amino]-2-deoxy-D-glucose
AA	Antimycin A
ACK	Ammonium-Chloride-Potassium
ACT	Adoptive T cell therapy
ADCC	Antibody-dependent cellular cytotoxicity
AMP	Adenosine monophosphate
AMPK	AMP kinase
AP-1	Activator protein 1
Arm	Armstrong
ATAC-seq	Assay for Transposase-Accessible Chromatin with sequencing
ATP	Adenosine triphosphate
ATRA	All-*trans*-retinoic acid
AUC	Area under the curve
Bcl-2	B-cell lymphoma 2
BFA	Brefeldin A
BHK	Baby Hamster Kidney
BMDM	Bone marrow-derived macrophages
BSA	Bovine serum albumin
CAR	Chimeric antigen receptor
CCR7	C-C chemokine receptor type 7
ChIP-seq	Chromatin immunoprecipitation with sequencing
CLP	Common lymphoid progenitor
CNS	Central nervous system
CoA	coenzyme A
COVID-19	Coronavirus disease 2019
cpm	Counts per million
CRC	Colorectal carcinoma

cTECs	Cortical thymic epithelial cells
CTLA-4	Cytotoxic T-lymphocyte-associated protein 4
CTV	CellTrace violet
CX3CR1	CX3C motif chemokine receptor 1
CXCR6	C-X-C Motif Chemokine Receptor 6
DAG	Diacylglycerol
DAPI	4′,6-diamidino-2-phenylindole
DCs	Dendritic cells
DMEM	Dulbecco's Modified Eagle Medium
DMSO	Dimethyl sulfoxide
DN	Double negative
DP	Double positive
DTT	Dithiothreitol
EAE	Experimental autoimmune encephalomyelitis
ECAR	Extracellular acidification rate
EDTA	Ethylenediaminetetraacetic acid
ENCODE	Encyclopedia of DNA Elements
Eomes	Eomesodermin
ER	Endoplasmic reticulum
Erk	Extracellular signal–regulated protein kinase
FA	Fatty acid
Fab	Fragment antigen-binding
FABP	Fatty-acid-binding protein
FACS	Fluorescence-activated cell sorting
FBS	Foetal bovine serum
FCCP	Carbonyl cyanide-p-trifluoromethoxyphenylhydrazone
FMO	Fluorescence-minus-one
FSP1	Ferroptosis suppressor protein 1
GAPDH	Glyceraldehyde-3-phosphate dehydrogenase
GEF	GTP-exchange factor
GEO	Gene Expression Omnibus
GLS	Glutaminase

GPX4	Glutathione-peroxidase 4
GzmB	Granzyme B
HBV	Hepatitis B virus
HCV	Hepatitis C virus
HEK	Human embryonic kidney
HEPES	4-(2-hydroxyethyl)-1-piperazineethanesulfonic acid
HIF-1α	Hypoxia-inducible factor 1-α
HIV	Human immunodeficiency virus
HK	hexokinase
HK-X31	Hong Kong strain X31
HRP	Horseradish peroxidase
ICB	Immune checkpoint blockade
IELs	Intraepithelial lymphocytes
IFNγ	Interferon gamma
IL-7R	Interluekin 7 receptor
ILC2	Type 2 innate lymphoid cells
iLN	Inguinal lymph node
ip	Intraperitoneal
IP3	Inositol 1,4,5-trisphosphate
ITAMs	Immunoreceptor tyrosine-based activation motif
ITIMs	Immunoreceptor tyrosine-based inhibitory motif
ITSMs	Immunoreceptor tyrosine-based switch motif
IV	Intravenous
Jnk	c-Jun N-terminal kinase
KLRG1	Killer cell lectin-like receptor subfamily G member 1
KO	Knockout
Lag-3	Lymphocyte activation gene 3
LAL	Lysosomal acid lipase
LAT	Linker for activation of T cells
Lck	Lymphocyte-specific protein tyrosine kinase
LCMV	Lymphocytic choriomeningitis virus
LLEC	Long-lived effector cells

mAb	monoclonal antibody
MAPK	Mitogen-activated protein kinase
Mcl-1	Myeloid cell leukaemia 1
MFI	Mean fluorescence intensity
MHC	Major histocompatibility complex
mLN	Mesenteric lymph node
MOI	Multiplicity of infection
MPEC	Memory-precursor effector cells
mTOR	Mammalian target of rapamycin
mTORC	mTOR complex
NEAA	Non-essential amino acids
NF-κB	Nuclear factor-κB
NFAT	Nuclear factor of activated T cells
NK	Natural killer
NLT	Non-lymphoid tissue
NOD	Non-obese diabetic
NSCLC	Non-small cell lung cancer
OAA	Oxaloacetate
OCR	Oxygen consumption rate
ORF	Open reading frame
OXPHOS	Oxidative phosphorylation
PAMPs	Pathogen-associated molecular patterns
PBMCs	Peripheral blood mononuclear cells
PBS	Phosphate-buffered saline
PCR	Polymerase chain reaction
PD-1	Programmed cell death protein 1
PD-L1	Programmed death-ligand 1
PDK1	Phosphoinositide-dependent kinase 1
PFA	Paraformaldehyde
pfu	Plaque-forming unit
PH	Pleckstrin-homology
PI3K	Phosphatidylinositol-3-OH kinase

PILRα	Paired immunoglobulin-like receptor a
PIP2	Phosphatidylinositol 4,5-bisphosphate
PIP3	Phosphatidylinositol 3,4,5-triphosphate
PKB	Protein kinase B
PKCθ	protein kinase C θ
PLCγ	Phospholipase Cγ
PMA	12-O-Tetradecanoylphorbol-13-acetate
pMHC	peptide-major histocompatibility complex
PPP	Pentose-phosphate pathway
PR8	Puerto Rico strain 8
pStat6	Phosphorylated Stat6
PTM	Post-translational modification
qPCR	Quantitative polymerase chain reaction
RBCs	Red blood cells
RM	Repeated measures
RNA-seq	RNA sequencing
ROS	Reactive oxygen species
Rot	Rotenone
rpm	Rounds per minute
RPMI	Roswell Park Memorial Institute
RV	Retrovirus
s.d.	Standard deviation
S1P	Sphingosine-1-phosphate
SARS-CoV2	Severe acute respiratory syndrome coronavirus 2
sc	Subcutaneous
scRNA-seq	Single-cell RNA sequencing
SEM	Standard error of the mean
SH	Src homology domain
SHM	Somatic hypermutation
SHP-1	SH2-containing phosphatase-1
SI	Small intestine
SLEC	Short-lived effector cells

SLO	Secondary lymphoid organs
SP	Single positive
SRC	Spare respiratory capacity
STAT	Signal transducer and activator of transcription
T-bet	T box expressed in T-cells
t-SNE	t-distributed stochastic neighbor embedding
TAG	Triacylglycerol
TCA	Tricarboxylic acid cycle
Tcf-1	T cell factor 1
TCID50	Median Tissue Culture Infectious Dose
TCM	Central memory T cells
Tconv	Conventional T cells
TCR	T cell receptor
TEM	Effector memory T cells
TEMED	Tetramethylethane-1,2-diamine
TGFβ	Transforming growth factor β
Tigit	T cell immunoreceptor with immunoglobulin and ITIM domain
TIL	Tumour-infiltrating lymphocyte
Tim-3	T cell immunoglobulin and mucin domain- containing molecule-3
TNF	Tumour necrosis factor
Tox	Thymocyte selection-associated high mobility group box protein
Treg cell	Regulatory T cell
TRM	Resident memory T cells
tSNE	t-distributed stochastic neighbour embedding
tTEM	terminal effector memory T cells
UDP-GlcNAc	Uridine diphosphate N-acetylglucosamine
UMAP	Uniform Manifold Approximation and Projection
WT	Wildtype
ZAP70	ζ-chain-associated protein kinase 70

10 References

1. Miller, J. F. Vestigial no more. *Nature immunology* **7,** 3–5 (2006).
2. Miller, J. The early work on the discovery of the function of the thymus, an interview with Jacques Miller. *Cell Death & Differentiation* **27,** 396–401 (2020).
3. JF, M. Role of the thymus in murine leukaemia. *Nature* **183,** 1069–1069 (1959).
4. Miller, J. Fate of subcutaneous thymus grafts in thymectomized mice inoculated with leukaemic filtrate. *Nature* **184,** 1809–1810 (1959).
5. Miller, J. Recovery of leukaemogenic agent from non-leukaemic tissues of thymectomized mice. *Nature* **187,** 703–703 (1960).
6. Miller, J. Analysis of the thymus influence in leukaemogenesis. *Nature* **191,** 248–249 (1961).
7. Miller, J. F. Immunological function of the thymus. *The Lancet* **278,** 748–749 (1961).
8. Cooper, M. D., Peterson, R. D. & Good, R. A. Delineation of the thymic and bursal lymphoid systems in the chicken. *Nature* **205,** 143–146 (1965).
9. Miller, J. P. & Mitchell, G. Cell to cell interaction in the immune response: I. Hemolysin-forming cells in neonatally thymectomized mice reconstituted with thymus or thoracic duct lymphocytes. *The Journal of experimental medicine* **128,** 801–820 (1968).
10. Mitchell, G. & Miller, J. Cell to cell interaction in the immune response: II. The source of hemolysin-forming cells in irradiated mice given bone marrow and thymus or thoracic duct lymphocytes. *The Journal of experimental medicine* **128,** 821–837 (1968).
11. Van Epps, H. L. Discovering lymphocyte subsets. *The Journal of experimental medicine* **201,** 5–5 (2005).
12. Murphy, K. & Weaver, C. *Janeway's immunobiology* (Garland science, 2016).
13. Kondo, M., Weissman, I. L. & Akashi, K. Identification of clonogenic common lymphoid progenitors in mouse bone marrow. *Cell* **91,** 661–672 (1997).
14. Pui, J. C. *et al.* Notch1 expression in early lymphopoiesis influences B versus T lineage determination. *Immunity* **11,** 299–308 (1999).
15. Radtke, F. *et al.* Deficient T cell fate specification in mice with an induced inactivation of Notch1. *Immunity* **10,** 547–558 (1999).
16. Takahama, Y. Journey through the thymus: stromal guides for T-cell development and selection. *Nature Reviews Immunology* **6,** 127–135 (2006).
17. Philpott, K. L. *et al.* Lymphoid development in mice congenitally lacking T cell receptor $\alpha\beta$-expressing cells. *Science* **256,** 1448–1452 (1992).
18. Dudley, E. C., Petrie, H. T., Shah, L. M., Owen, M. J. & Hayday, A. C. T cell receptor β chain gene rearrangement and selection during thymocyte development in adult mice. *Immunity* **1,** 83–93 (1994).
19. Shinkai, Y. *et al.* RAG-2-deficient mice lack mature lymphocytes owing to inability to initiate V (D) J rearrangement. *Cell* **68,** 855–867 (1992).
20. Goldrath, A. W. & Bevan, M. J. Selecting and maintaining a diverse T-cell repertoire. *Nature* **402,** 255–262 (1999).
21. Kisielow, P., Teh, H. S., Blüthmann, H. & von Boehmer, H. Positive selection of antigen-specific T cells in thymus by restricting MHC molecules. *Nature* **335,** 730–733 (1988).
22. Hogquist, K. A. *et al.* Identification of a naturally occurring ligand for thymic positive selection. *Immunity* **6,** 389–399 (1997).
23. Murata, S. *et al.* Regulation of CD8+ T cell development by thymus-specific proteasomes. *Science* **316,** 1349–1353 (2007).
24. Alberola-Ila, J., Hogquist, K. A., Swan, K. A., Bevan, M. J. & Perlmutter, R. M. Positive and negative selection invoke distinct signaling pathways. *The Journal of experimental medicine* **184,** 9–18 (1996).
25. Kishimoto, H. & Sprent, J. Negative selection in the thymus includes semimature T cells. *The Journal of experimental medicine* **185,** 263–272 (1997).

26. Anderson, M. S. *et al.* Projection of an immunological self shadow within the thymus by the aire protein. *Science* **298,** 1395–1401 (2002).
27. Maddon, P. J. *et al.* The isolation and nucleotide sequence of a cDNA encoding the T cell surface protein T4: a new member of the immunoglobulin gene family. *Cell* **42,** 93–104 (1985).
28. Clark, S. J., Jefferies, W. A., Barclay, A. N., Gagnon, J. & Williams, A. F. Peptide and nucleotide sequences of rat CD4 (W3/25) antigen: evidence for derivation from a structure with four immunoglobulin-related domains. *Proceedings of the National Academy of Sciences* **84,** 1649–1653 (1987).
29. Snow, P. M. & Terhorst, C. The T8 antigen is a multimeric complex of two distinct subunits on human thymocytes but consists of homomultimeric forms on peripheral blood T lymphocytes. *Journal of Biological Chemistry* **258,** 14675–14681 (1983).
30. Littman, D. R., Thomas, Y., Maddon, P. J., Chess, L. & Axel, R. The isolation and sequence of the gene encoding T8: a molecule defining functional classes of T lymphocytes. *Cell* **40,** 237–246 (1985).
31. Vremec, D. *et al.* The surface phenotype of dendritic cells purified from mouse thymus and spleen: investigation of the CD8 expression by a subpopulation of dendritic cells. *The Journal of experimental medicine* **176,** 47–58 (1992).
32. Jonges, L. *et al.* The phenotypic heterogeneity of human natural killer cells: presence of at least 48 different subsets in the peripheral blood. *Scandinavian journal of immunology* **53,** 103–110 (2001).
33. Gangadharan, D. *et al.* Identification of pre-and postselection TCR$\alpha\beta$+ intraepithelial lymphocyte precursors in the thymus. *Immunity* **25,** 631–641 (2006).
34. Denning, T. L. *et al.* Mouse TCR$\alpha\beta$+ CD8$\alpha\alpha$ intraepithelial lymphocytes express genes that down-regulate their antigen reactivity and suppress immune responses. *The Journal of Immunology* **178,** 4230–4239 (2007).
35. McNicol, A.-M. *et al.* CD8α/α homodimers fail to function as co-receptor for a CD8-dependent TCR. *European journal of immunology* **37,** 1634–1641 (2007).
36. Veillette, A., Bookman, M. A., Horak, E. M. & Bolen, J. B. The CD4 and CD8 T cell surface antigens are associated with the internal membrane tyrosine-protein kinase p56lck. *Cell* **55,** 301–308 (1988).
37. Kim, P. W., Sun, Z.-Y. J., Blacklow, S. C., Wagner, G. & Eck, M. J. A zinc clasp structure tethers Lck to T cell coreceptors CD4 and CD8. *Science* **301,** 1725–1728 (2003).
38. Yin, Y., Wang, X. X. & Mariuzza, R. A. Crystal structure of a complete ternary complex of T-cell receptor, peptide–MHC, and CD4. *Proceedings of the National Academy of Sciences* **109,** 5405–5410 (2012).
39. Salter, R. D. *et al.* A binding site for the T-cell co-receptor CD8 on the α3 domain of HLA-A2. *Nature* **345,** 41–46 (1990).
40. Gao, G. F. *et al.* Crystal structure of the complex between human CD8$\alpha\alpha$ and HLA-A2. *Nature* **387,** 630–634 (1997).
41. Molina, T. *et al.* Profound block in thymocyte development in mice lacking p56lck. *Nature* **357,** 161–164 (1992).
42. Levin, S. D., Anderson, S. J., Forbush, K. A. & Perlmutter, R. M. A dominant-negative transgene defines a role for p56lck in thymopoiesis. *The EMBO journal* **12,** 1671–1680 (1993).
43. Palacios, E. H. & Weiss, A. Function of the Src-family kinases, Lck and Fyn, in T-cell development and activation. *Oncogene* **23,** 7990–8000 (2004).
44. Den Braber, I. *et al.* Maintenance of peripheral naive T cells is sustained by thymus output in mice but not humans. *Immunity* **36,** 288–297 (2012).
45. Schluns, K. S., Kieper, W. C., Jameson, S. C. & Lefrançois, L. Interleukin-7 mediates the homeostasis of naive and memory CD8 T cells in vivo. *Nature immunology* **1,** 426–432 (2000).
46. Tanchot, C., Lemonnier, F. A., Pérarnau, B., Freitas, A. A. & Rocha, B. Differential requirements for survival and proliferation of CD8 naive or memory T cells. *Science* **276,** 2057–2062 (1997).

47. Kimura, M. Y. *et al.* IL-7 signaling must be intermittent, not continuous, during CD8+ T cell homeostasis to promote cell survival instead of cell death. *Nature immunology* **14,** 143–151 (2013).
48. Tan, J. T. *et al.* IL-7 is critical for homeostatic proliferation and survival of naive T cells. *Proceedings of the National Academy of Sciences* **98,** 8732–8737 (2001).
49. Myers, D. R., Zikherman, J. & Roose, J. P. Tonic signals: why do lymphocytes bother? *Trends in immunology* **38,** 844–857 (2017).
50. Takeda, S., Rodewald, H.-R., Arakawa, H., Bluethmann, H. & Shimizu, T. MHC class II molecules are not required for survival of newly generated CD4+ T cells, but affect their long-term life span. *Immunity* **5,** 217–228 (1996).
51. Von Freeden-Jeffry, U. *et al.* Lymphopenia in interleukin (IL)-7 gene-deleted mice identifies IL-7 as a nonredundant cytokine. *The Journal of experimental medicine* **181,** 1519–1526 (1995).
52. Rathmell, J. C., Farkash, E. A., Gao, W. & Thompson, C. B. IL-7 enhances the survival and maintains the size of naive T cells. *The Journal of Immunology* **167,** 6869–6876 (2001).
53. Geiselhart, L. A. *et al.* IL-7 administration alters the CD4: CD8 ratio, increases T cell numbers, and increases T cell function in the absence of activation. *The Journal of Immunology* **166,** 3019–3027 (2001).
54. Sportès, C. *et al.* Administration of rhIL-7 in humans increases in vivo TCR repertoire diversity by preferential expansion of naive T cell subsets. *The Journal of experimental medicine* **205,** 1701–1714 (2008).
55. Stockinger, B., Barthlott, T. & Kassiotis, G. The concept of space and competition in immune regulation. *Immunology* **111,** 241 (2004).
56. Park, J.-H. *et al.* Suppression of IL7Rα transcription by IL-7 and other prosurvival cytokines: a novel mechanism for maximizing IL-7-dependent T cell survival. *Immunity* **21,** 289–302 (2004).
57. Park, J.-H. *et al.* 'Coreceptor tuning': cytokine signals transcriptionally tailor CD8 coreceptor expression to the self-specificity of the TCR. *Nature immunology* **8,** 1049–1059 (2007).
58. Takada, K. & Jameson, S. C. Self–class I MHC molecules support survival of naive CD8 T cells, but depress their functional sensitivity through regulation of CD8 expression levels. *Journal of Experimental Medicine* **206,** 2253–2269 (2009).
59. Murali-Krishna, K. *et al.* Counting antigen-specific CD8 T cells: a reevaluation of bystander activation during viral infection. *Immunity* **8,** 177–187 (1998).
60. Wolf, T. *et al.* Dynamics in protein translation sustaining T cell preparedness. *Nature immunology* **21,** 927–937 (2020).
61. Smith-Garvin, J. E., Koretzky, G. A. & Jordan, M. S. T cell activation. *Annual review of immunology* **27,** 591 (2009).
62. Sallusto, F., Cella, M., Danieli, C. & Lanzavecchia, A. Dendritic cells use macropinocytosis and the mannose receptor to concentrate macromolecules in the major histocompatibility complex class II compartment: downregulation by cytokines and bacterial products. *The Journal of experimental medicine* **182,** 389–400 (1995).
63. Théry, C. & Amigorena, S. The cell biology of antigen presentation in dendritic cells. *Current opinion in immunology* **13,** 45–51 (2001).
64. Guermonprez, P., Valladeau, J., Zitvogel, L., Théry, C. & Amigorena, S. Antigen presentation and T cell stimulation by dendritic cells. *Annual review of immunology* **20,** 621–667 (2002).
65. Dalod, M., Chelbi, R., Malissen, B. & Lawrence, T. Dendritic cell maturation: functional specialization through signaling specificity and transcriptional programming. *The EMBO journal* **33,** 1104–1116 (2014).
66. Förster, R. *et al.* CCR7 coordinates the primary immune response by establishing functional microenvironments in secondary lymphoid organs. *Cell* **99,** 23–33 (1999).
67. Von Andrian, U. H. & Mempel, T. R. Homing and cellular traffic in lymph nodes. *Nature Reviews Immunology* **3,** 867–878 (2003).

68. Katou, F. *et al.* Differential expression of CCL19 by DC-Lamp+ mature dendritic cells in human lymph node versus chronically inflamed skin. *The Journal of Pathology: A Journal of the Pathological Society of Great Britain and Ireland* **199,** 98–106 (2003).
69. Sušac, L. *et al.* Structure of a fully assembled tumor-specific T cell receptor ligated by pMHC. *Cell* **185,** 3201–3213 (2022).
70. Reinherz, E. L. *et al.* Antigen recognition by human T lymphocytes is linked to surface expression of the T3 molecular complex. *Cell* **30,** 735–743 (1982).
71. Meuer, S. C. *et al.* Evidence for the T3-associated 90K heterodimer as the T-cell antigen receptor. *Nature* **303,** 808–810 (1983).
72. Dong, D. *et al.* Structural basis of assembly of the human T cell receptor–CD3 complex. *Nature* **573,** 546–552 (2019).
73. Davis, M. M. & Bjorkman, P. J. T-cell antigen receptor genes and T-cell recognition. *Nature* **334,** 395–402 (1988).
74. Weiss, A. & Littman, D. R. Signal transduction by lymphocyte antigen receptors. *Cell* **76,** 263–274 (1994).
75. Gaud, G., Lesourne, R. & Love, P. E. Regulatory mechanisms in T cell receptor signalling. *Nature Reviews Immunology* **18,** 485–497 (2018).
76. Chapman, N. M. & Chi, H. Hallmarks of T-cell Exit from Quiescence. *Cancer Immunology Research* **6,** 502–508 (2018).
77. Romeo, C., Amiot, M. & Seed, B. Sequence requirements for induction of cytolysis by the T cell antigenFc receptor ζ chain. *Cell* **68,** 889–897 (1992).
78. Samelson, L. & Klausner, R. Tyrosine kinases and tyrosine-based activation motifs: current research on activation via the T cell antigen receptor. *The Journal of biological chemistry (Print)* **267,** 24913–24916 (1992).
79. Straus, D. B. & Weiss, A. Genetic evidence for the involvement of the lck tyrosine kinase in signal transduction through the T cell antigen receptor. *Cell* **70,** 585–593 (1992).
80. Iwashima, M., Irving, B. A., Van Oers, N. S., Chan, A. C. & Weiss, A. Sequential interactions of the TCR with two distinct cytoplasmic tyrosine kinases. *Science* **263,** 1136–1139 (1994).
81. Chan, A. C., Irving, B. A., Fraser, J. D. & Weiss, A. The zeta chain is associated with a tyrosine kinase and upon T-cell antigen receptor stimulation associates with ZAP-70, a 70-kDa tyrosine phosphoprotein. *Proceedings of the National Academy of Sciences* **88,** 9166–9170 (1991).
82. Wange, R., Malek, S., Desiderio, S. & Samelson, L. E. Tandem SH2 domains of ZAP-70 bind to T cell antigen receptor zeta and CD3 epsilon from activated Jurkat T cells. *Journal of Biological Chemistry* **268,** 19797–19801 (1993).
83. Straus, D. & Weiss, A. The CD3 chains of the T cell antigen receptor associate with the ZAP-70 tyrosine kinase and are tyrosine phosphorylated after receptor stimulation. *The Journal of experimental medicine* **178,** 1523–1530 (1993).
84. Zhang, W., Sloan-Lancaster, J., Kitchen, J., Trible, R. P. & Samelson, L. E. LAT: the ZAP-70 tyrosine kinase substrate that links T cell receptor to cellular activation. *Cell* **92,** 83–92 (1998).
85. Wu, J., Motto, D. G., Koretzky, G. A. & Weiss, A. Vav and SLP-76 interact and functionally cooperate in IL-2 gene activation. *immunity* **4,** 593–602 (1996).
86. Mørch, A. M., Bálint, Š., Santos, A. M., Davis, S. J. & Dustin, M. L. Coreceptors and TCR signaling–the strong and the weak of it. *Frontiers in cell and developmental biology* **8,** 597627 (2020).
87. Wu, L. C., Tuot, D. S., Lyons, D. S., Garcia, K. C. & Davis, M. M. Two-step binding mechanism for T-cell receptor recognition of peptide–MHC. *Nature* **418,** 552–556 (2002).
88. Xu, H. & Littman, D. R. A kinase-independent function of Lck in potentiating antigen-specific T cell activation. *Cell* **74,** 633–643 (1993).
89. Hartl, F. A. *et al.* Noncanonical binding of Lck to CD3ε promotes TCR signaling and CAR function. *Nature immunology* **21,** 902–913 (2020).
90. Casas, J. *et al.* Ligand-engaged TCR is triggered by Lck not associated with CD8 coreceptor. *Nature communications* **5,** 1–11 (2014).

91. Jiang, N. *et al.* Two-stage cooperative T cell receptor-peptide major histocompatibility complex-CD8 trimolecular interactions amplify antigen discrimination. *Immunity* **34,** 13–23 (2011).
92. Zareie, P. *et al.* Canonical T cell receptor docking on peptide–MHC is essential for T cell signaling. *Science* **372,** eabe9124 (2021).
93. Malissen, B., Gregoire, C., Malissen, M. & Roncagalli, R. Integrative biology of T cell activation. *Nature immunology* **15,** 790–797 (2014).
94. Voisinne, G. *et al.* Quantitative interactomics in primary T cells unveils TCR signal diversification extent and dynamics. *Nature immunology* **20,** 1530–1541 (2019).
95. Lowenstein, E. *et al.* The SH2 and SH3 domain-containing protein GRB2 links receptor tyrosine kinases to ras signaling. *Cell* **70,** 431–442 (1992).
96. Rodriguez-Viciana, P. *et al.* Phosphatidylinositol-3-OH kinase direct target of Ras. *Nature* **370,** 527–532 (1994).
97. Stephens, L., Jackson, T. & Hawkins, P. Agonist-stimulated synthesis of phosphatidylinositol (3, 4, 5)-trisphosphate: a new intracellular signalling system? *Biochimica et Biophysica Acta (BBA)-Molecular Cell Research* **1179,** 27–75 (1993).
98. Lemmon, M. A. Membrane recognition by phospholipid-binding domains. *Nature reviews Molecular cell biology* **9,** 99–111 (2008).
99. Yang, Y. R. *et al.* Diverse cellular and physiological roles of phospholipase C-γ1 (2012).
100. Hogan, P. G., Chen, L., Nardone, J. & Rao, A. Transcriptional regulation by calcium, calcineurin, and NFAT. *Genes & development* **17,** 2205–2232 (2003).
101. Downward, J., Graves, J. D., Warne, P. H., Rayter, S. & Cantrell, D. A. Stimulation of p21ras upon T-cell activation. *Nature* **346,** 719–723 (1990).
102. Monks, C. R., Kupfer, H., Tamir, I., Barlow, A. & Kupfer, A. Selective modulation of protein kinase C-θ during T-cell activation. *Nature* **385,** 83–86 (1997).
103. Dower, N. A. *et al.* RasGRP is essential for mouse thymocyte differentiation and TCR signaling. *Nature immunology* **1,** 317–321 (2000).
104. Sun, Z. *et al.* PKC-θ is required for TCR-induced NF-κB activation in mature but not immature T lymphocytes. *Nature* **404,** 402–407 (2000).
105. Blonska, M. *et al.* The CARMA1-Bcl10 signaling complex selectively regulates JNK2 kinase in the T cell receptor-signaling pathway. *Immunity* **26,** 55–66 (2007).
106. Chang, L. & Karin, M. Mammalian MAP kinase signalling cascades. *Nature* **410,** 37–40 (2001).
107. Halazonetis, T. D., Georgopoulos, K., Greenberg, M. E. & Leder, P. c-Jun dimerizes with itself and with c-Fos, forming complexes of different DNA binding affinities. *Cell* **55,** 917–924 (1988).
108. Jain, J., Valge-Archer, V. & Rao, A. Analysis of the AP-1 sites in the IL-2 promoter. *The Journal of Immunology* **148,** 1240–1250 (1992).
109. Rincón, M. MAP-kinase signaling pathways in T cells. *Current opinion in immunology* **13,** 339–345 (2001).
110. Tybulewicz, V. L. & Henderson, R. B. Rho family GTPases and their regulators in lymphocytes. *Nature Reviews Immunology* **9,** 630–644 (2009).
111. Ragueneau, M. *et al.* Binding of phosphatidyl-inositol-3-OH kinase to CD28 is required for T-cell signalling. *Nature* **369,** 327–329 (1994).
112. Stokoe, D. *et al.* Dual role of phosphatidylinositol-3, 4, 5-trisphosphate in the activation of protein kinase B. *Science* **277,** 567–570 (1997).
113. Vanhaesebroeck, B., Stephens, L. & Hawkins, P. PI3K signalling: the path to discovery and understanding. *Nature reviews Molecular cell biology* **13,** 195–203 (2012).
114. Chen, L. & Flies, D. B. Molecular mechanisms of T cell co-stimulation and co-inhibition. *Nature reviews immunology* **13,** 227–242 (2013).
115. Frauwirth, K. A. *et al.* The CD28 signaling pathway regulates glucose metabolism. *Immunity* **16,** 769–777 (2002).

116. Jenkins, M. K., Chen, C., Jung, G., Mueller, D. L. & Schwartz, R. H. Inhibition of antigen-specific proliferation of type 1 murine T cell clones after stimulation with immobilized anti-CD3 monoclonal antibody. *The Journal of Immunology* **144,** 16–22 (1990).
117. Sharpe, A. H. Mechanisms of costimulation. *Immunological reviews* **229,** 5 (2009).
118. Kurts, C., Kosaka, H., Carbone, F. R., Miller, J. F. & Heath, W. R. Class I-restricted cross-presentation of exogenous self-antigens leads to deletion of autoreactive CD8+ T cells. *The Journal of experimental medicine* **186,** 239–245 (1997).
119. Albert, M. L., Sauter, B. & Bhardwaj, N. Dendritic cells acquire antigen from apoptotic cells and induce class I-restricted CTLs. *Nature* **392,** 86–89 (1998).
120. Mueller, D. L., Jenkins, M. K. & Schwartz, R. H. Clonal expansion versus clonal inactivation: A costimulatory pathway determines the outcome of T cell antigen receptor occupancy. *Annu Rev Immunol* **7,** 445–480 (1989).
121. Hawiger, D. *et al.* Dendritic cells induce peripheral T cell unresponsiveness under steady state conditions in vivo. *The Journal of experimental medicine* **194,** 769–780 (2001).
122. Green, J. M. *et al.* Absence of B7-dependent responses in CD28-deficient mice. *Immunity* **1,** 501–508 (1994).
123. Hutchcroft, J. E. & Bierer, B. E. Activation-dependent phosphorylation of the T-lymphocyte surface receptor CD28 and associated proteins. *Proceedings of the National Academy of Sciences* **91,** 3260–3264 (1994).
124. Holdorf, A. D., Lee, K.-H., Burack, W. R., Allen, P. M. & Shaw, A. S. Regulation of Lck activity by CD4 and CD28 in the immunological synapse. *Nature immunology* **3,** 259–264 (2002).
125. Huang, J. *et al.* CD28 plays a critical role in the segregation of PKCθ within the immunologic synapse. *Proceedings of the National Academy of Sciences* **99,** 9369–9373 (2002).
126. Kane, L. P., Lin, J. & Weiss, A. It's all Rel-ative: NF-κB and CD28 costimulation of T-cell activation. *Trends in immunology* **23,** 413–420 (2002).
127. Diehn, M. *et al.* Genomic expression programs and the integration of the CD28 costimulatory signal in T cell activation. *Proceedings of the National Academy of Sciences* **99,** 11796–11801 (2002).
128. Rincon, M. & Flavell, R. A. AP-1 transcriptional activity requires both T-cell receptor-mediated and co-stimulatory signals in primary T lymphocytes. *The EMBO journal* **13,** 4370–4381 (1994).
129. Shahinian, A. *et al.* Differential T cell costimulatory requirements in CD28-deficient mice. *Science* **261,** 609–612 (1993).
130. Bonnevier, J. L. & Mueller, D. L. Cutting edge: B7/CD28 interactions regulate cell cycle progression independent of the strength of TCR signaling. *The Journal of Immunology* **169,** 6659–6663 (2002).
131. Acuto, O. & Michel, F. CD28-mediated co-stimulation: a quantitative support for TCR signalling. *Nature Reviews Immunology* **3,** 939–951 (2003).
132. Dudley, M. E. *et al.* Adoptive transfer of cloned melanoma-reactive T lymphocytes for the treatment of patients with metastatic melanoma. *Journal of immunotherapy* **24,** 363–373 (2001).
133. Dudley, M. E. *et al.* A phase I study of nonmyeloablative chemotherapy and adoptive transfer of autologous tumor antigen-specific T lymphocytes in patients with metastatic melanoma. *Journal of immunotherapy (Hagerstown, Md.: 1997)* **25,** 243 (2002).
134. Van der Windt, G. J. *et al.* Mitochondrial respiratory capacity is a critical regulator of CD8+ T cell memory development. *Immunity* **36,** 68–78 (2012).
135. Lantz, O., Grandjean, I., Matzinger, P. & Di Santo, J. P. γ chain required for naive CD4+ T cell survival but not for antigen proliferation. *Nature immunology* **1,** 54–58 (2000).
136. Kündig, T. M. *et al.* Immune responses in interleukin-2-deficient mice. *Science* **262,** 1059–1061 (1993).
137. D'Souza, W. N., Schluns, K. S., Masopust, D. & Lefrançois, L. Essential role for IL-2 in the regulation of antiviral extralymphoid CD8 T cell responses. *The Journal of Immunology* **168,** 5566–5572 (2002).

138. D'Souza, W. N. & Lefrançois, L. IL-2 is not required for the initiation of CD8 T cell cycling but sustains expansion. *The Journal of Immunology* **171,** 5727–5735 (2003).
139. Kalia, V. *et al.* Prolonged interleukin-2Rα expression on virus-specific CD8+ T cells favors terminal-effector differentiation in vivo. *Immunity* **32,** 91–103 (2010).
140. Pipkin, M. E. *et al.* Interleukin-2 and inflammation induce distinct transcriptional programs that promote the differentiation of effector cytolytic T cells. *Immunity* **32,** 79–90 (2010).
141. Curtsinger, J. M. & Mescher, M. F. Inflammatory cytokines as a third signal for T cell activation. *Current opinion in immunology* **22,** 333–340 (2010).
142. Xiao, Z., Casey, K. A., Jameson, S. C., Curtsinger, J. M. & Mescher, M. F. Programming for CD8 T cell memory development requires IL-12 or type I IFN. *The Journal of Immunology* **182,** 2786–2794 (2009).
143. Aichele, P. *et al.* Cutting edge: CD8 T cells specific for lymphocytic choriomeningitis virus require type I IFN receptor for clonal expansion. *The Journal of Immunology* **176,** 4525–4529 (2006).
144. Kolumam, G. A., Thomas, S., Thompson, L. J., Sprent, J. & Murali-Krishna, K. Type I interferons act directly on CD8 T cells to allow clonal expansion and memory formation in response to viral infection. *The Journal of experimental medicine* **202,** 637–650 (2005).
145. Joshi, N. S. *et al.* Inflammation directs memory precursor and short-lived effector CD8+ T cell fates via the graded expression of T-bet transcription factor. *Immunity* **27,** 281–295 (2007).
146. Keppler, S. J., Theil, K., Vucikuja, S. & Aichele, P. Effector T-cell differentiation during viral and bacterial infections: Role of direct IL-12 signals for cell fate decision of CD8+ T cells. *European journal of immunology* **39,** 1774–1783 (2009).
147. Badovinac, V. P., Messingham, K. A., Jabbari, A., Haring, J. S. & Harty, J. T. Accelerated CD8+ T-cell memory and prime-boost response after dendritic-cell vaccination. *Nature medicine* **11,** 748–756 (2005).
148. Whitmire, J. K., Tan, J. T. & Whitton, J. L. Interferon-γ acts directly on CD8+ T cells to increase their abundance during virus infection. *The Journal of experimental medicine* **201,** 1053–1059 (2005).
149. Whitmire, J. K., Eam, B., Benning, N. & Whitton, J. L. Direct interferon-γ signaling dramatically enhances CD4+ and CD8+ T cell memory. *The Journal of Immunology* **179,** 1190–1197 (2007).
150. Murphy, K. M. & Reiner, S. L. The lineage decisions of helper T cells. *Nature Reviews Immunology* **2,** 933–944 (2002).
151. O'Shea, J. J. & Paul, W. E. Mechanisms underlying lineage commitment and plasticity of helper CD4+ T cells. *Science* **327,** 1098–1102 (2010).
152. Tuzlak, S. *et al.* Repositioning TH cell polarization from single cytokines to complex help. *Nature Immunology* **22,** 1210–1217 (2021).
153. Becattini, S. *et al.* Functional heterogeneity of human memory CD4+ T cell clones primed by pathogens or vaccines. *Science* **347,** 400–406 (2015).
154. Tortola, L. *et al.* High-dimensional T helper cell profiling reveals a broad diversity of stably committed effector states and uncovers interlineage relationships. *Immunity* **53,** 597–613 (2020).
155. Kaech, S. M. *et al.* Selective expression of the interleukin 7 receptor identifies effector CD8 T cells that give rise to long-lived memory cells. *Nature immunology* **4,** 1191–1198 (2003).
156. Bouillet, P. *et al.* Proapoptotic Bcl-2 relative Bim required for certain apoptotic responses, leukocyte homeostasis, and to preclude autoimmunity. *Science* **286,** 1735–1738 (1999).
157. Blattman, J. N. *et al.* Therapeutic use of IL-2 to enhance antiviral T-cell responses in vivo. *Nature medicine* **9,** 540–547 (2003).
158. Hildeman, D. A., Zhu, Y., Mitchell, T. C., Kappler, J. & Marrack, P. Molecular mechanisms of activated T cell death in vivo. *Current opinion in immunology* **14,** 354–359 (2002).
159. Weant, A. E. *et al.* Apoptosis regulators Bim and Fas function concurrently to control autoimmunity and CD8+ T cell contraction. *Immunity* **28,** 218–230 (2008).
160. Badovinac, V. P., Tvinnereim, A. R. & Harty, J. T. Regulation of antigen-specific CD8+ T cell homeostasis by perforin and interferon-γ. *Science* **290,** 1354–1357 (2000).

161. Refaeli, Y., Van Parijs, L., Alexander, S. I. & Abbas, A. K. Interferon γ is required for activation-induced death of T lymphocytes. *The Journal of experimental medicine* **196,** 999–1005 (2002).
162. Badovinac, V. P., Porter, B. B. & Harty, J. T. CD8+ T cell contraction is controlled by early inflammation. *Nature immunology* **5,** 809–817 (2004).
163. Ishida, Y., Agata, Y., Shibahara, K. & Honjo, T. Induced expression of PD-1, a novel member of the immunoglobulin gene superfamily, upon programmed cell death. *The EMBO journal* **11,** 3887–3895 (1992).
164. Kalia, V. *et al.* Metabolic regulation by PD-1 signaling promotes long-lived quiescent CD8 T cell memory in mice. *Science translational medicine* **13,** eaba6006 (2021).
165. Freeman, G. J. *et al.* Engagement of the PD-1 immunoinhibitory receptor by a novel B7 family member leads to negative regulation of lymphocyte activation. *The Journal of experimental medicine* **192,** 1027–1034 (2000).
166. Latchman, Y. *et al.* PD-L2 is a second ligand for PD-1 and inhibits T cell activation. *Nature immunology* **2,** 261–268 (2001).
167. Li, K. *et al.* PD-1 suppresses TCR-CD8 cooperativity during T-cell antigen recognition. *Nature communications* **12,** 1–13 (2021).
168. Sheppard, K.-A. *et al.* PD-1 inhibits T-cell receptor induced phosphorylation of the ZAP70/CD3ζ signalosome and downstream signaling to PKCθ. *FEBS letters* **574,** 37–41 (2004).
169. Chemnitz, J. M., Parry, R. V., Nichols, K. E., June, C. H. & Riley, J. L. SHP-1 and SHP-2 associate with immunoreceptor tyrosine-based switch motif of programmed death 1 upon primary human T cell stimulation, but only receptor ligation prevents T cell activation. *The Journal of Immunology* **173,** 945–954 (2004).
170. Okazaki, T., Maeda, A., Nishimura, H., Kurosaki, T. & Honjo, T. PD-1 immunoreceptor inhibits B cell receptor-mediated signaling by recruiting src homology 2-domain-containing tyrosine phosphatase 2 to phosphotyrosine. *Proceedings of the National Academy of Sciences* **98,** 13866–13871 (2001).
171. Parry, R. V. *et al.* CTLA-4 and PD-1 receptors inhibit T-cell activation by distinct mechanisms. *Molecular and cellular biology* **25,** 9543–9553 (2005).
172. Yokosuka, T. *et al.* Programmed cell death 1 forms negative costimulatory microclusters that directly inhibit T cell receptor signaling by recruiting phosphatase SHP2. *Journal of Experimental Medicine* **209,** 1201–1217 (2012).
173. Kamphorst, A. O. *et al.* Rescue of exhausted CD8 T cells by PD-1–targeted therapies is CD28-dependent. *Science* **355,** 1423–1427 (2017).
174. Hui, E. *et al.* T cell costimulatory receptor CD28 is a primary target for PD-1–mediated inhibition. *Science* **355,** 1428–1433 (2017).
175. Brunet, J.-F. *et al.* A new member of the immunoglobulin superfamily—CTLA-4. *Nature* **328,** 267–270 (1987).
176. Chuang, E. *et al.* Regulation of cytotoxic T lymphocyte-associated molecule-4 by Src kinases. *The Journal of Immunology* **162,** 1270–1277 (1999).
177. Linsley, P. S. *et al.* CTLA-4 is a second receptor for the B cell activation antigen B7. *The Journal of experimental medicine* **174,** 561–569 (1991).
178. Krummel, M. F. & Allison, J. P. CD28 and CTLA-4 have opposing effects on the response of T cells to stimulation. *The Journal of experimental medicine* **182,** 459–465 (1995).
179. Krummel, M. F. & Allison, J. P. CTLA-4 engagement inhibits IL-2 accumulation and cell cycle progression upon activation of resting T cells. *The Journal of experimental medicine* **183,** 2533–2540 (1996).
180. Stamper, C. C. *et al.* Crystal structure of the B7-1/CTLA-4 complex that inhibits human immune responses. *Nature* **410,** 608–611 (2001).
181. Qureshi, O. S. *et al.* Trans-endocytosis of CD80 and CD86: a molecular basis for the cell-extrinsic function of CTLA-4. *Science* **332,** 600–603 (2011).

182. Waterhouse, P. *et al.* Lymphoproliferative disorders with early lethality in mice deficient in Ctla-4. *Science* **270,** 985–988 (1995).
183. Vignali, D. A., Collison, L. W. & Workman, C. J. How regulatory T cells work. *Nature reviews immunology* **8,** 523–532 (2008).
184. Dolina, J. S. *et al.* Developmentally distinct CD4+ Treg lineages shape the CD8+ T cell response to acute Listeria infection. *Proceedings of the National Academy of Sciences* **119,** e2113329119 (2022).
185. Hori, S., Nomura, T. & Sakaguchi, S. Control of regulatory T cell development by the transcription factor Foxp3. *Science* **299,** 1057–1061 (2003).
186. Takahashi, T. *et al.* Immunologic self-tolerance maintained by CD25+ CD4+ naturally anergic and suppressive T cells: induction of autoimmune disease by breaking their anergic/suppressive state. *International immunology* **10,** 1969–1980 (1998).
187. Thornton, A. M. & Shevach, E. M. CD4+ CD25+ immunoregulatory T cells suppress polyclonal T cell activation in vitro by inhibiting interleukin 2 production. *The Journal of experimental medicine* **188,** 287–296 (1998).
188. Kastenmuller, W. *et al.* Regulatory T cells selectively control CD8+ T cell effector pool size via IL-2 restriction. *The Journal of Immunology* **187,** 3186–3197 (2011).
189. Wu, Y. *et al.* FOXP3 controls regulatory T cell function through cooperation with NFAT. *Cell* **126,** 375–387 (2006).
190. Wing, K. *et al.* CTLA-4 control over Foxp3+ regulatory T cell function. *Science* **322,** 271–275 (2008).
191. Steinbrink, K., Wölfl, M., Jonuleit, H., Knop, J. & Enk, A. H. Induction of tolerance by IL-10-treated dendritic cells. *The Journal of Immunology* **159,** 4772–4780 (1997).
192. Laidlaw, B. J. *et al.* Production of IL-10 by CD4+ regulatory T cells during the resolution of infection promotes the maturation of memory CD8+ T cells. *Nature immunology* **16,** 871–879 (2015).
193. Kehrl, J. H. *et al.* Production of transforming growth factor beta by human T lymphocytes and its potential role in the regulation of T cell growth. *The Journal of experimental medicine* **163,** 1037–1050 (1986).
194. Collison, L. W. *et al.* The inhibitory cytokine IL-35 contributes to regulatory T-cell function. *Nature* **450,** 566–569 (2007).
195. Jiang, H., Zhang, T., Yan, M.-X. & Wu, W. IL-35 inhibits CD8+ T cells activity by suppressing expression of costimulatory molecule CD28 and Th1 cytokine production. *Translational Cancer Research* **8,** 1319 (2019).
196. Sawant, D. V. *et al.* Adaptive plasticity of IL-10+ and IL-35+ Treg cells cooperatively promotes tumor T cell exhaustion. *Nature immunology* **20,** 724–735 (2019).
197. Deaglio, S. *et al.* Adenosine generation catalyzed by CD39 and CD73 expressed on regulatory T cells mediates immune suppression. *The Journal of experimental medicine* **204,** 1257–1265 (2007).
198. Bopp, T. *et al.* Cyclic adenosine monophosphate is a key component of regulatory T cell–mediated suppression. *The Journal of experimental medicine* **204,** 1303–1310 (2007).
199. Grossman, W. J. *et al.* Human T regulatory cells can use the perforin pathway to cause autologous target cell death. *Immunity* **21,** 589–601 (2004).
200. Lau, L., Jamieson, B. D., Somasundaram, T., Ahmed, R. *et al.* Cytotoxic T-cell memory without antigen. *Nature* **369,** 648–652 (1994).
201. Murali-Krishna, K. *et al.* Persistence of memory CD8 T cells in MHC class I-deficient mice. *Science* **286,** 1377–1381 (1999).
202. Grayson, J. M., Harrington, L. E., Lanier, J. G., Wherry, E. J. & Ahmed, R. Differential sensitivity of naive and memory CD8+ T cells to apoptosis in vivo. *The Journal of Immunology* **169,** 3760–3770 (2002).
203. Veiga-Fernandes, H., Walter, U., Bourgeois, C., McLean, A. & Rocha, B. Response of naive and memory CD8+ T cells to antigen stimulation in vivo. *Nature immunology* **1,** 47–53 (2000).

204. Swanson, B. J., Murakami, M., Mitchell, T. C., Kappler, J. & Marrack, P. RANTES production by memory phenotype T cells is controlled by a posttranscriptional, TCR-dependent process. *Immunity* **17,** 605–615 (2002).
205. Salerno, F., Paolini, N. A., Stark, R., von Lindern, M. & Wolkers, M. C. Distinct PKC-mediated posttranscriptional events set cytokine production kinetics in CD8+ T cells. *Proceedings of the National Academy of Sciences* **114,** 9677–9682 (2017).
206. Salerno, F. *et al.* Translational repression of pre-formed cytokine-encoding mRNA prevents chronic activation of memory T cells. *Nature immunology* **19,** 828–837 (2018).
207. Pihlgren, M., Dubois, P. M., Tomkowiak, M., Sjögren, T. & Marvel, J. Resting memory CD8+ T cells are hyperreactive to antigenic challenge in vitro. *The Journal of experimental medicine* **184,** 2141–2152 (1996).
208. Slifka, M. K. & Whitton, J. L. Functional avidity maturation of CD8+ T cells without selection of higher affinity TCR. *Nature immunology* **2,** 711–717 (2001).
209. Bachmann, M. F. *et al.* Developmental regulation of Lck targeting to the CD8 coreceptor controls signaling in naive and memory T cells. *The Journal of experimental medicine* **189,** 1521–1530 (1999).
210. Xiao, Z., Mescher, M. F. & Jameson, S. C. Detuning CD8 T cells: down-regulation of CD8 expression, tetramer binding, and response during CTL activation. *The Journal of experimental medicine* **204,** 2667–2677 (2007).
211. Kersh, E. N. *et al.* TCR signal transduction in antigen-specific memory CD8 T cells. *The Journal of Immunology* **170,** 5455–5463 (2003).
212. Kaech, S. M., Hemby, S., Kersh, E. & Ahmed, R. Molecular and functional profiling of memory CD8 T cell differentiation. *Cell* **111,** 837–851 (2002).
213. Schamel, W. W. *et al.* Coexistence of multivalent and monovalent TCRs explains high sensitivity and wide range of response. *The Journal of experimental medicine* **202,** 493–503 (2005).
214. Kumar, R. *et al.* Increased sensitivity of antigen-experienced T cells through the enrichment of oligomeric T cell receptor complexes. *Immunity* **35,** 375–387 (2011).
215. Jameson, S. C. & Masopust, D. Understanding subset diversity in T cell memory. *Immunity* **48,** 214–226 (2018).
216. Sallusto, F., Lenig, D., Förster, R., Lipp, M. & Lanzavecchia, A. Two subsets of memory T lymphocytes with distinct homing potentials and effector functions. *Nature* **401,** 708–712 (1999).
217. Gebhardt, T. *et al.* Memory T cells in nonlymphoid tissue that provide enhanced local immunity during infection with herpes simplex virus. *Nature immunology* **10,** 524–530 (2009).
218. Park, C. O. & Kupper, T. S. The emerging role of resident memory T cells in protective immunity and inflammatory disease. *Nature medicine* **21,** 688–697 (2015).
219. Fernandez-Ruiz, D. *et al.* Liver-resident memory CD8+ T cells form a front-line defense against malaria liver-stage infection. *Immunity* **45,** 889–902 (2016).
220. Steinbach, K. *et al.* Brain-resident memory T cells represent an autonomous cytotoxic barrier to viral infection. *Journal of Experimental Medicine* **213,** 1571–1587 (2016).
221. Schenkel, J. M., Fraser, K. A. & Masopust, D. Cutting edge: resident memory CD8 T cells occupy frontline niches in secondary lymphoid organs. *The Journal of Immunology* **192,** 2961–2964 (2014).
222. Gerlach, C. *et al.* The chemokine receptor CX3CR1 defines three antigen-experienced CD8 T cell subsets with distinct roles in immune surveillance and homeostasis. *Immunity* **45,** 1270–1284 (2016).
223. Skon, C. N. *et al.* Transcriptional downregulation of S1pr1 is required for the establishment of resident memory CD8+ T cells. *Nature immunology* **14,** 1285–1293 (2013).
224. Evrard, M. *et al.* Sphingosine 1-phosphate receptor 5 (S1PR5) regulates the peripheral retention of tissue-resident lymphocytes. *Journal of Experimental Medicine* **219** (2022).
225. Mackay, L. K. *et al.* The developmental pathway for CD103+ CD8+ tissue-resident memory T cells of skin. *Nature immunology* **14,** 1294–1301 (2013).

226. Shiow, L. R. *et al.* CD69 acts downstream of interferon-α/β to inhibit S1P1 and lymphocyte egress from lymphoid organs. *Nature* **440,** 540–544 (2006).
227. Bankovich, A. J., Shiow, L. R. & Cyster, J. G. CD69 suppresses sphingosine 1-phosophate receptor-1 (S1P1) function through interaction with membrane helix 4. *Journal of Biological Chemistry* **285,** 22328–22337 (2010).
228. Cepek, K. L. *et al.* Adhesion between epithelial cells and T lymphocytes mediated by E-cadherin and the αEβ7 integrin. *Nature* **372,** 190–193 (1994).
229. Bergsbaken, T. & Bevan, M. J. Proinflammatory microenvironments within the intestine regulate the differentiation of tissue-resident CD8+ T cells responding to infection. *Nature immunology* **16,** 406–414 (2015).
230. Wherry, E. J. *et al.* Lineage relationship and protective immunity of memory CD8 T cell subsets. *Nature immunology* **4,** 225–234 (2003).
231. Milner, J. J. *et al.* Delineation of a molecularly distinct terminally differentiated memory CD8 T cell population. *Proceedings of the National Academy of Sciences* **117,** 25667–25678 (2020).
232. Olson, J. A., McDonald-Hyman, C., Jameson, S. C. & Hamilton, S. E. Effector-like CD8+ T cells in the memory population mediate potent protective immunity. *Immunity* **38,** 1250–1260 (2013).
233. Schenkel, J. M. *et al.* IL-15–independent maintenance of tissue-resident and boosted effector memory CD8 T cells. *The Journal of Immunology* **196,** 3920–3926 (2016).
234. Jabbari, A. & Harty, J. T. Secondary memory CD8+ T cells are more protective but slower to acquire a central–memory phenotype. *The Journal of experimental medicine* **203,** 919–932 (2006).
235. Vezys, V. *et al.* Memory CD8 T-cell compartment grows in size with immunological experience. *Nature* **457,** 196–199 (2009).
236. Nolz, J. C. & Harty, J. T. Protective capacity of memory CD8+ T cells is dictated by antigen exposure history and nature of the infection. *Immunity* **34,** 781–793 (2011).
237. Mackay, L. K. *et al.* T-box transcription factors combine with the cytokines TGF-β and IL-15 to control tissue-resident memory T cell fate. *Immunity* **43,** 1101–1111 (2015).
238. Ariotti, S. *et al.* Tissue-resident memory CD8+ T cells continuously patrol skin epithelia to quickly recognize local antigen. *Proceedings of the National Academy of Sciences* **109,** 19739–19744 (2012).
239. Beura, L. K. *et al.* Intravital mucosal imaging of CD8+ resident memory T cells shows tissue-autonomous recall responses that amplify secondary memory. *Nature immunology* **19,** 173–182 (2018).
240. Park, S. L. *et al.* Local proliferation maintains a stable pool of tissue-resident memory T cells after antiviral recall responses. *Nature immunology* **19,** 183–191 (2018).
241. Schenkel, J. M., Fraser, K. A., Vezys, V. & Masopust, D. Sensing and alarm function of resident memory CD8+ T cells. *Nature immunology* **14,** 509–513 (2013).
242. Ariotti, S. *et al.* Skin-resident memory CD8+ T cells trigger a state of tissue-wide pathogen alert. *Science* **346,** 101–105 (2014).
243. Schenkel, J. M. *et al.* Resident memory CD8 T cells trigger protective innate and adaptive immune responses. *Science* **346,** 98–101 (2014).
244. Shin, H. & Iwasaki, A. A vaccine strategy that protects against genital herpes by establishing local memory T cells. *Nature* **491,** 463–467 (2012).
245. Jiang, X. *et al.* Skin infection generates non-migratory memory CD8+ TRM cells providing global skin immunity. *Nature* **483,** 227–231 (2012).
246. Kadoki, M. *et al.* Organism-level analysis of vaccination reveals networks of protection across tissues. *Cell* **171,** 398–413 (2017).
247. Bresser, K. *et al.* Replicative history marks transcriptional and functional disparity in the CD8+ T cell memory pool. *Nature immunology* **23,** 791–801 (2022).
248. Steinert, E. M. *et al.* Quantifying memory CD8 T cells reveals regionalization of immunosurveillance. *Cell* **161,** 737–749 (2015).

249. Beura, L. K. *et al.* T cells in nonlymphoid tissues give rise to lymph-node-resident memory T cells. *Immunity* **48,** 327–338 (2018).
250. Stolley, J. M. *et al.* Retrograde migration supplies resident memory T cells to lung-draining LN after influenza infection. *Journal of Experimental Medicine* **217** (2020).
251. Fonseca, R. *et al.* Developmental plasticity allows outside-in immune responses by resident memory T cells. *Nature immunology* **21,** 412–421 (2020).
252. Casey, K. A. *et al.* Antigen-independent differentiation and maintenance of effector-like resident memory T cells in tissues. *The Journal of Immunology* **188,** 4866–4875 (2012).
253. Surh, C. D. & Sprent, J. Homeostasis of naive and memory T cells. *Immunity* **29,** 848–862 (2008).
254. Adachi, T. *et al.* Hair follicle–derived IL-7 and IL-15 mediate skin-resident memory T cell homeostasis and lymphoma. *Nature medicine* **21,** 1272–1279 (2015).
255. Verbist, K. C., Field, M. B. & Klonowski, K. D. Cutting edge: IL-15–independent maintenance of mucosally generated memory CD8 T cells. *The Journal of Immunology* **186,** 6667–6671 (2011).
256. Dubois, S., Mariner, J., Waldmann, T. A. & Tagaya, Y. IL-15Rα recycles and presents IL-15 in trans to neighboring cells. *Immunity* **17,** 537–547 (2002).
257. Burkett, P. R. *et al.* Coordinate expression and trans presentation of interleukin (IL)-15Rα and IL-15 supports natural killer cell and memory CD8+ T cell homeostasis. *The Journal of experimental medicine* **200,** 825–834 (2004).
258. Mishra, A., Sullivan, L. & Caligiuri, M. A. Molecular pathways: interleukin-15 signaling in health and in cancer. *Clinical Cancer Research* **20,** 2044–2050 (2014).
259. Zhang, X., Sun, S., Hwang, I., Tough, D. F. & Sprent, J. Potent and selective stimulation of memory-phenotype CD8+ T cells in vivo by IL-15. *Immunity* **8,** 591–599 (1998).
260. Kennedy, M. K. *et al.* Reversible defects in natural killer and memory CD8 T cell lineages in interleukin 15–deficient mice. *The Journal of experimental medicine* **191,** 771–780 (2000).
261. Lodolce, J. P. *et al.* IL-15 receptor maintains lymphoid homeostasis by supporting lymphocyte homing and proliferation. *Immunity* **9,** 669–676 (1998).
262. Judge, A. D., Zhang, X., Fujii, H., Surh, C. D. & Sprent, J. Interleukin 15 controls both proliferation and survival of a subset of memory-phenotype CD8+ T cells. *The Journal of experimental medicine* **196,** 935–946 (2002).
263. Becker, T. C. *et al.* Interleukin 15 is required for proliferative renewal of virus-specific memory CD8 T cells. *The Journal of experimental medicine* **195,** 1541–1548 (2002).
264. Intlekofer, A. M. *et al.* Effector and memory CD8+ T cell fate coupled by T-bet and eomesodermin. *Nature immunology* **6,** 1236–1244 (2005).
265. Joshi, N. S. *et al.* Increased numbers of preexisting memory CD8 T cells and decreased T-bet expression can restrain terminal differentiation of secondary effector and memory CD8 T cells. *The Journal of Immunology* **187,** 4068–4076 (2011).
266. Dominguez, C. X. *et al.* The transcription factors ZEB2 and T-bet cooperate to program cytotoxic T cell terminal differentiation in response to LCMV viral infection. *Journal of Experimental Medicine* **212,** 2041–2056 (2015).
267. Laidlaw, B. J. *et al.* CD4+ T cell help guides formation of CD103+ lung-resident memory CD8+ T cells during influenza viral infection. *Immunity* **41,** 633–645 (2014).
268. Banerjee, A. *et al.* Cutting edge: The transcription factor eomesodermin enables CD8+ T cells to compete for the memory cell niche. *The Journal of Immunology* **185,** 4988–4992 (2010).
269. Wu, J. *et al.* T cell factor 1 suppresses CD103+ lung tissue-resident memory T cell development. *Cell reports* **31,** 107484 (2020).
270. Sarkar, S. *et al.* Functional and genomic profiling of effector CD8 T cell subsets with distinct memory fates. *The Journal of experimental medicine* **205,** 625–640 (2008).
271. Tan, J. T. *et al.* Interleukin (IL)-15 and IL-7 jointly regulate homeostatic proliferation of memory phenotype CD8+ cells but are not required for memory phenotype CD4+ cells. *The Journal of experimental medicine* **195,** 1523–1532 (2002).

272. Goldrath, A. W. *et al.* Cytokine requirements for acute and Basal homeostatic proliferation of naive and memory CD8+ T cells. *The Journal of experimental medicine* **195,** 1515–1522 (2002).
273. Johnnidis, J. B. *et al.* Inhibitory signaling sustains a distinct early memory CD8+ T cell precursor that is resistant to DNA damage. *Science immunology* **6,** eabe3702 (2021).
274. Stemberger, C. *et al.* A single naive CD8+ T cell precursor can develop into diverse effector and memory subsets. *Immunity* **27,** 985–997 (2007).
275. Goronzy, J. J., Fang, F., Cavanagh, M. M., Qi, Q. & Weyand, C. M. Naive T cell maintenance and function in human aging. *The Journal of Immunology* **194,** 4073–4080 (2015).
276. Wang, R. *et al.* The transcription factor Myc controls metabolic reprogramming upon T lymphocyte activation. *Immunity* **35,** 871–882 (2011).
277. Macintyre, A. N. *et al.* The glucose transporter Glut1 is selectively essential for CD4 T cell activation and effector function. *Cell metabolism* **20,** 61–72 (2014).
278. Carr, E. L. *et al.* Glutamine uptake and metabolism are coordinately regulated by ERK/MAPK during T lymphocyte activation. *The Journal of Immunology* **185,** 1037–1044 (2010).
279. Ma, E. H. *et al.* Serine is an essential metabolite for effector T cell expansion. *Cell metabolism* **25,** 345–357 (2017).
280. Ma, E. H. *et al.* Metabolic profiling using stable isotope tracing reveals distinct patterns of glucose utilization by physiologically activated CD8+ T cells. *Immunity* **51,** 856–870 (2019).
281. Buck, M. D., O'sullivan, D. & Pearce, E. L. T cell metabolism drives immunity. *Journal of Experimental Medicine* **212,** 1345–1360 (2015).
282. Finlay, D. & Cantrell, D. A. Metabolism, migration and memory in cytotoxic T cells. *Nature Reviews Immunology* **11,** 109–117 (2011).
283. Reina-Campos, M., Scharping, N. E. & Goldrath, A. W. CD8+ T cell metabolism in infection and cancer. *Nature Reviews Immunology* **21,** 718–738 (2021).
284. Ron-Harel, N. *et al.* Mitochondrial biogenesis and proteome remodeling promote one-carbon metabolism for T cell activation. *Cell metabolism* **24,** 104–117 (2016).
285. Porstmann, T. *et al.* SREBP activity is regulated by mTORC1 and contributes to Akt-dependent cell growth. *Cell metabolism* **8,** 224–236 (2008).
286. Kidani, Y. *et al.* Sterol regulatory element–binding proteins are essential for the metabolic programming of effector T cells and adaptive immunity. *Nature immunology* **14,** 489–499 (2013).
287. Wang, R. & Green, D. R. Metabolic checkpoints in activated T cells. *Nature immunology* **13,** 907–915 (2012).
288. Warburg, O. On the origin of cancer cells. *Science* **123,** 309–314 (1956).
289. Liberti, M. V. & Locasale, J. W. The Warburg effect: how does it benefit cancer cells? *Trends in biochemical sciences* **41,** 211–218 (2016).
290. Menk, A. V. *et al.* Early TCR signaling induces rapid aerobic glycolysis enabling distinct acute T cell effector functions. *Cell reports* **22,** 1509–1521 (2018).
291. Jacobs, S. R. *et al.* Glucose uptake is limiting in T cell activation and requires CD28-mediated Akt-dependent and independent pathways. *The Journal of Immunology* **180,** 4476–4486 (2008).
292. Finlay, D. K. *et al.* PDK1 regulation of mTOR and hypoxia-inducible factor 1 integrate metabolism and migration of CD8+ T cells. *Journal of Experimental Medicine* **209,** 2441–2453 (2012).
293. Tsai, S. *et al.* Insulin receptor-mediated stimulation boosts T cell immunity during inflammation and infection. *Cell metabolism* **28,** 922–934 (2018).
294. Chang, C.-H. *et al.* Posttranscriptional control of T cell effector function by aerobic glycolysis. *Cell* **153,** 1239–1251 (2013).
295. Peng, M. *et al.* Aerobic glycolysis promotes T helper 1 cell differentiation through an epigenetic mechanism. *Science* **354,** 481–484 (2016).
296. Sena, L. A. *et al.* Mitochondria are required for antigen-specific T cell activation through reactive oxygen species signaling. *Immunity* **38,** 225–236 (2013).
297. Yang, K. *et al.* T cell exit from quiescence and differentiation into Th2 cells depend on Raptor-mTORC1-mediated metabolic reprogramming. *Immunity* **39,** 1043–1056 (2013).

298. Johnson, M. O. *et al.* Distinct regulation of Th17 and Th1 cell differentiation by glutaminase-dependent metabolism. *Cell* **175,** 1780–1795 (2018).
299. Tahiliani, M. *et al.* Conversion of 5-methylcytosine to 5-hydroxymethylcytosine in mammalian DNA by MLL partner TET1. *Science* **324,** 930–935 (2009).
300. Ito, S. *et al.* Role of Tet proteins in 5mC to 5hmC conversion, ES-cell self-renewal and inner cell mass specification. *Nature* **466,** 1129–1133 (2010).
301. Chisolm, D. A. *et al.* CCCTC-binding factor translates interleukin 2-and α-ketoglutarate-sensitive metabolic changes in T cells into context-dependent gene programs. *Immunity* **47,** 251–267 (2017).
302. Chi, H. Regulation and function of mTOR signalling in T cell fate decisions. *Nature reviews immunology* **12,** 325–338 (2012).
303. So, L. *et al.* The 4E-BP–eIF4E axis promotes rapamycin-sensitive growth and proliferation in lymphocytes. *Science signaling* **9,** ra57–ra57 (2016).
304. Rao, R. R., Li, Q., Odunsi, K. & Shrikant, P. A. The mTOR kinase determines effector versus memory CD8+ T cell fate by regulating the expression of transcription factors T-bet and Eomesodermin. *Immunity* **32,** 67–78 (2010).
305. O'Brien, T. F. *et al.* Regulation of T-cell survival and mitochondrial homeostasis by TSC1. *European journal of immunology* **41,** 3361–3370 (2011).
306. Yang, K., Neale, G., Green, D. R., He, W. & Chi, H. The tumor suppressor Tsc1 enforces quiescence of naive T cells to promote immune homeostasis and function. *Nature immunology* **12,** 888–897 (2011).
307. Wu, J. *et al.* Loss of neurological disease HSAN-I-associated gene SPTLC2 impairs CD8+ T cell responses to infection by inhibiting T cell metabolic fitness. *Immunity* **50,** 1218–1231 (2019).
308. Kaymak, I. *et al.* Carbon source availability drives nutrient utilization in CD8+ T cells. *Cell Metabolism* (2022).
309. Patsoukis, N. *et al.* PD-1 alters T-cell metabolic reprogramming by inhibiting glycolysis and promoting lipolysis and fatty acid oxidation. *Nature communications* **6,** 1–13 (2015).
310. Buck, M. D. *et al.* Mitochondrial dynamics controls T cell fate through metabolic programming. *Cell* **166,** 63–76 (2016).
311. Geltink, R. I. K. *et al.* Mitochondrial priming by CD28. *Cell* **171,** 385–397 (2017).
312. O'Sullivan, D. *et al.* Memory CD8+ T cells use cell-intrinsic lipolysis to support the metabolic programming necessary for development. *Immunity* **41,** 75–88 (2014).
313. Pearce, E. L. *et al.* Enhancing CD8 T-cell memory by modulating fatty acid metabolism. *Nature* **460,** 103–107 (2009).
314. Bachem, A. *et al.* Microbiota-derived short-chain fatty acids promote the memory potential of antigen-activated CD8+ T cells. *Immunity* **51,** 285–297 (2019).
315. Pan, Y. *et al.* Survival of tissue-resident memory T cells requires exogenous lipid uptake and metabolism. *Nature* **543,** 252–256 (2017).
316. Frizzell, H. *et al.* Organ-specific isoform selection of fatty acid–binding proteins in tissue-resident lymphocytes. *Science immunology* **5,** eaay9283 (2020).
317. Cui, G. *et al.* IL-7-induced glycerol transport and TAG synthesis promotes memory CD8+ T cell longevity. *Cell* **161,** 750–761 (2015).
318. Araki, K. *et al.* mTOR regulates memory CD8 T-cell differentiation. *Nature* **460,** 108–112 (2009).
319. Shrestha, S. *et al.* Tsc1 promotes the differentiation of memory CD8+ T cells via orchestrating the transcriptional and metabolic programs. *Proceedings of the National Academy of Sciences* **111,** 14858–14863 (2014).
320. Borges da Silva, H. *et al.* The purinergic receptor P2RX7 directs metabolic fitness of long-lived memory CD8+ T cells. *Nature* **559,** 264–268 (2018).
321. Da Silva, H. B. *et al.* Sensing of ATP via the purinergic receptor P2RX7 promotes CD8+ Trm cell generation by enhancing their sensitivity to the cytokine TGF-β. *Immunity* **53,** 158–171 (2020).

322. Phan, A. T. *et al.* Constitutive glycolytic metabolism supports CD8+ T cell effector memory differentiation during viral infection. *Immunity* **45,** 1024–1037 (2016).
323. Xu, Y. *et al.* Glycolysis determines dichotomous regulation of T cell subsets in hypoxia. *The Journal of clinical investigation* **126,** 2678–2688 (2016).
324. Ecker, C. *et al.* Differential reliance on lipid metabolism as a salvage pathway underlies functional differences of T cell subsets in poor nutrient environments. *Cell reports* **23,** 741–755 (2018).
325. Karrer, U. *et al.* Memory inflation: continuous accumulation of antiviral CD8+ T cells over time. *The Journal of Immunology* **170,** 2022–2029 (2003).
326. Zajac, A. J. *et al.* Viral immune evasion due to persistence of activated T cells without effector function. *The Journal of experimental medicine* **188,** 2205–2213 (1998).
327. Virgin, H. W., Wherry, E. J. & Ahmed, R. Redefining chronic viral infection. *Cell* **138,** 30–50 (2009).
328. Wherry, E. J. T cell exhaustion. *Nature immunology* **12,** 492–499 (2011).
329. McLane, L. M., Abdel-Hakeem, M. S., Wherry, E. J. *et al.* CD8 T cell exhaustion during chronic viral infection and cancer. *Annu Rev Immunol* **37,** 457–495 (2019).
330. Lechner, F. *et al.* Analysis of successful immune responses in persons infected with hepatitis C virus. *The Journal of experimental medicine* **191,** 1499–1512 (2000).
331. Ye, B. *et al.* T-cell exhaustion in chronic hepatitis B infection: current knowledge and clinical significance. *Cell death & disease* **6,** e1694–e1694 (2015).
332. Day, C. L. *et al.* PD-1 expression on HIV-specific T cells is associated with T-cell exhaustion and disease progression. *Nature* **443,** 350–354 (2006).
333. Ahmadzadeh, M. *et al.* Tumor antigen–specific CD8 T cells infiltrating the tumor express high levels of PD-1 and are functionally impaired. *Blood, The Journal of the American Society of Hematology* **114,** 1537–1544 (2009).
334. Kim, P. S. & Ahmed, R. Features of responding T cells in cancer and chronic infection. *Current opinion in immunology* **22,** 223–230 (2010).
335. Moskophidis, D., Lechner, F., Pircher, H. & Zinkernagel, R. M. Virus persistence in acutely infected immunocompetent mice by exhaustion of antiviral cytotoxic effector T cells. *Nature* **362,** 758–761 (1993).
336. Gallimore, A. *et al.* Induction and exhaustion of lymphocytic choriomeningitis virus–specific cytotoxic T lymphocytes visualized using soluble tetrameric major histocompatibility complex class I–peptide complexes. *The Journal of experimental medicine* **187,** 1383–1393 (1998).
337. Wherry, E. J., Blattman, J. N., Murali-Krishna, K., Van Der Most, R. & Ahmed, R. Viral persistence alters CD8 T-cell immunodominance and tissue distribution and results in distinct stages of functional impairment. *Journal of virology* **77,** 4911–4927 (2003).
338. Wherry, E. J. *et al.* Molecular signature of CD8+ T cell exhaustion during chronic viral infection. *Immunity* **27,** 670–684 (2007).
339. Schietinger, A. *et al.* Tumor-specific T cell dysfunction is a dynamic antigen-driven differentiation program initiated early during tumorigenesis. *Immunity* **45,** 389–401 (2016).
340. Blackburn, S. D. *et al.* Coregulation of CD8+ T cell exhaustion by multiple inhibitory receptors during chronic viral infection. *Nature immunology* **10,** 29–37 (2009).
341. Doering, T. A. *et al.* Network analysis reveals centrally connected genes and pathways involved in CD8+ T cell exhaustion versus memory. *Immunity* **37,** 1130–1144 (2012).
342. Shin, H., Blackburn, S. D., Blattman, J. N. & Wherry, E. J. Viral antigen and extensive division maintain virus-specific CD8 T cells during chronic infection. *The Journal of experimental medicine* **204,** 941–949 (2007).
343. Yu, Y.-R. *et al.* Disturbed mitochondrial dynamics in CD8+ TILs reinforce T cell exhaustion. *Nature immunology* **21,** 1540–1551 (2020).
344. Guo, Y. *et al.* Metabolic reprogramming of terminally exhausted CD8+ T cells by IL-10 enhances anti-tumor immunity. *Nature immunology* **22,** 746–756 (2021).

345. Pauken, K. E. *et al.* Epigenetic stability of exhausted T cells limits durability of reinvigoration by PD-1 blockade. *Science* **354,** 1160–1165 (2016).
346. Sen, D. R. *et al.* The epigenetic landscape of T cell exhaustion. *Science* **354,** 1165–1169 (2016).
347. Utzschneider, D. T. *et al.* T cells maintain an exhausted phenotype after antigen withdrawal and population reexpansion. *Nature immunology* **14,** 603–610 (2013).
348. Abdel-Hakeem, M. S. *et al.* Epigenetic scarring of exhausted T cells hinders memory differentiation upon eliminating chronic antigenic stimulation. *Nature Immunology* **22,** 1008–1019 (2021).
349. Ghoneim, H. E. *et al.* De novo epigenetic programs inhibit PD-1 blockade-mediated T cell rejuvenation. *Cell* **170,** 142–157 (2017).
350. Youngblood, B. *et al.* Chronic virus infection enforces demethylation of the locus that encodes PD-1 in antigen-specific CD8+ T cells. *Immunity* **35,** 400–412 (2011).
351. Staron, M. M. *et al.* The transcription factor FoxO1 sustains expression of the inhibitory receptor PD-1 and survival of antiviral CD8+ T cells during chronic infection. *Immunity* **41,** 802–814 (2014).
352. Utzschneider, D. T. *et al.* T cell factor 1-expressing memory-like CD8+ T cells sustain the immune response to chronic viral infections. *Immunity* **45,** 415–427 (2016).
353. Wu, T. *et al.* The TCF1-Bcl6 axis counteracts type I interferon to repress exhaustion and maintain T cell stemness. *Science immunology* **1,** eaai8593 (2016).
354. Barber, D. L. *et al.* Restoring function in exhausted CD8 T cells during chronic viral infection. *Nature* **439,** 682–687 (2006).
355. Tsui, C. *et al.* MYB orchestrates T cell exhaustion and response to checkpoint inhibition. *Nature,* 1–7 (2022).
356. Utzschneider, D. T. *et al.* Early precursor T cells establish and propagate T cell exhaustion in chronic infection. *Nature immunology* **21,** 1256–1266 (2020).
357. Mueller, S. N. & Ahmed, R. High antigen levels are the cause of T cell exhaustion during chronic viral infection. *Proceedings of the National Academy of Sciences* **106,** 8623–8628 (2009).
358. Matloubian, M., Concepcion, R. J. & Ahmed, R. CD4+ T cells are required to sustain CD8+ cytotoxic T-cell responses during chronic viral infection. *Journal of virology* **68,** 8056–8063 (1994).
359. Fröhlich, A. *et al.* IL-21R on T cells is critical for sustained functionality and control of chronic viral infection. *Science* **324,** 1576–1580 (2009).
360. Elsaesser, H., Sauer, K. & Brooks, D. G. IL-21 is required to control chronic viral infection. *Science* **324,** 1569–1572 (2009).
361. Yi, J. S., Du, M. & Zajac, A. J. A vital role for interleukin-21 in the control of a chronic viral infection. *Science* **324,** 1572–1576 (2009).
362. Zander, R. *et al.* CD4+ T cell help is required for the formation of a cytolytic CD8+ T cell subset that protects against chronic infection and cancer. *Immunity* **51,** 1028–1042 (2019).
363. Brooks, D. G. *et al.* Interleukin-10 determines viral clearance or persistence in vivo. *Nature medicine* **12,** 1301–1309 (2006).
364. Tinoco, R., Alcalde, V., Yang, Y., Sauer, K. & Zuniga, E. I. Cell-intrinsic transforming growth factor-β signaling mediates virus-specific CD8+ T cell deletion and viral persistence in vivo. *Immunity* **31,** 145–157 (2009).
365. Wilson, E. B. *et al.* Blockade of chronic type I interferon signaling to control persistent LCMV infection. *Science* **340,** 202–207 (2013).
366. Teijaro, J. R. *et al.* Persistent LCMV infection is controlled by blockade of type I interferon signaling. *Science* **340,** 207–211 (2013).
367. Stelekati, E. *et al.* Bystander chronic infection negatively impacts development of CD8+ T cell memory. *Immunity* **40,** 801–813 (2014).
368. Chang, C.-H. *et al.* Metabolic competition in the tumor microenvironment is a driver of cancer progression. *Cell* **162,** 1229–1241 (2015).
369. Geiger, R. *et al.* L-arginine modulates T cell metabolism and enhances survival and anti-tumor activity. *Cell* **167,** 829–842 (2016).

370. Bian, Y. *et al.* Cancer SLC43A2 alters T cell methionine metabolism and histone methylation. *Nature* **585,** 277–282 (2020).
371. Quinn III, W. J. *et al.* Lactate limits T cell proliferation via the NAD (H) redox state. *Cell reports* **33,** 108500 (2020).
372. Frumento, G. *et al.* Tryptophan-derived catabolites are responsible for inhibition of T and natural killer cell proliferation induced by indoleamine 2, 3-dioxygenase. *The Journal of experimental medicine* **196,** 459–468 (2002).
373. Watson, M. J. *et al.* Metabolic support of tumour-infiltrating regulatory T cells by lactic acid. *Nature* **591,** 645–651 (2021).
374. Xu, S. *et al.* Uptake of oxidized lipids by the scavenger receptor CD36 promotes lipid peroxidation and dysfunction in CD8+ T cells in tumors. *Immunity* **54,** 1561–1577 (2021).
375. Binnewies, M. *et al.* Understanding the tumor immune microenvironment (TIME) for effective therapy. *Nature medicine* **24,** 541–550 (2018).
376. Bengsch, B. *et al.* Bioenergetic insufficiencies due to metabolic alterations regulated by the inhibitory receptor PD-1 are an early driver of CD8+ T cell exhaustion. *Immunity* **45,** 358–373 (2016).
377. Scharping, N. E. *et al.* The tumor microenvironment represses T cell mitochondrial biogenesis to drive intratumoral T cell metabolic insufficiency and dysfunction. *Immunity* **45,** 374–388 (2016).
378. Schurich, A. *et al.* Distinct metabolic requirements of exhausted and functional virus-specific CD8 T cells in the same host. *Cell reports* **16,** 1243–1252 (2016).
379. Scharping, N. E. *et al.* Mitochondrial stress induced by continuous stimulation under hypoxia rapidly drives T cell exhaustion. *Nature immunology* **22,** 205–215 (2021).
380. Vardhana, S. A. *et al.* Impaired mitochondrial oxidative phosphorylation limits the self-renewal of T cells exposed to persistent antigen. *Nature immunology* **21,** 1022–1033 (2020).
381. Oestreich, K. J., Yoon, H., Ahmed, R. & Boss, J. M. NFATc1 regulates PD-1 expression upon T cell activation. *The Journal of Immunology* **181,** 4832–4839 (2008).
382. Martinez, G. J. *et al.* The transcription factor NFAT promotes exhaustion of activated CD8+ T cells. *Immunity* **42,** 265–278 (2015).
383. Wolf, Y., Anderson, A. C. & Kuchroo, V. K. TIM3 comes of age as an inhibitory receptor. *Nature Reviews Immunology* **20,** 173–185 (2020).
384. Guy, C. *et al.* LAG3 associates with TCR–CD3 complexes and suppresses signaling by driving co-receptor–Lck dissociation. *Nature Immunology* **23,** 757–767 (2022).
385. Yao, C. *et al.* Single-cell RNA-seq reveals TOX as a key regulator of CD8+ T cell persistence in chronic infection. *Nature immunology* **20,** 890–901 (2019).
386. Scott, A. C. *et al.* TOX is a critical regulator of tumour-specific T cell differentiation. *Nature* **571,** 270–274 (2019).
387. Khan, O. *et al.* TOX transcriptionally and epigenetically programs CD8+ T cell exhaustion. *Nature* **571,** 211–218 (2019).
388. Alfei, F. *et al.* TOX reinforces the phenotype and longevity of exhausted T cells in chronic viral infection. *Nature* **571,** 265–269 (2019).
389. Angelosanto, J. M., Blackburn, S. D., Crawford, A. & Wherry, E. J. Progressive loss of memory T cell potential and commitment to exhaustion during chronic viral infection. *Journal of virology* **86,** 8161–8170 (2012).
390. Wherry, E. J., Barber, D. L., Kaech, S. M., Blattman, J. N. & Ahmed, R. Antigen-independent memory CD8 T cells do not develop during chronic viral infection. *Proceedings of the National Academy of Sciences* **101,** 16004–16009 (2004).
391. Blackburn, S. D., Shin, H., Freeman, G. J. & Wherry, E. J. Selective expansion of a subset of exhausted CD8 T cells by αPD-L1 blockade. *Proceedings of the National Academy of Sciences* **105,** 15016–15021 (2008).

392. Paley, M. A. *et al.* Progenitor and terminal subsets of CD8+ T cells cooperate to contain chronic viral infection. *Science* **338,** 1220–1225 (2012).
393. Im, S. J. *et al.* Defining CD8+ T cells that provide the proliferative burst after PD-1 therapy. *Nature* **537,** 417–421 (2016).
394. Beltra, J.-C. *et al.* Developmental relationships of four exhausted CD8+ T cell subsets reveals underlying transcriptional and epigenetic landscape control mechanisms. *Immunity* **52,** 825–841 (2020).
395. He, R. *et al.* Follicular CXCR5-expressing CD8+ T cells curtail chronic viral infection. *Nature* **537,** 412–416 (2016).
396. Siddiqui, I. *et al.* Intratumoral Tcf1+ PD-1+ CD8+ T cells with stem-like properties promote tumor control in response to vaccination and checkpoint blockade immunotherapy. *Immunity* **50,** 195–211 (2019).
397. Im, S. J., Konieczny, B. T., Hudson, W. H., Masopust, D. & Ahmed, R. PD-1+ stemlike CD8 T cells are resident in lymphoid tissues during persistent LCMV infection. *Proceedings of the National Academy of Sciences* **117,** 4292–4299 (2020).
398. Connolly, K. A. *et al.* A reservoir of stem-like CD8+ T cells in the tumor-draining lymph node preserves the ongoing antitumor immune response. *Science immunology* **6,** eabg7836 (2021).
399. Hudson, W. H. *et al.* Proliferating transitory T cells with an effector-like transcriptional signature emerge from PD-1+ stem-like CD8+ T cells during chronic infection. *Immunity* **51,** 1043–1058 (2019).
400. Kanev, K. *et al.* Proliferation-competent Tcf1+ CD8 T cells in dysfunctional populations are CD4 T cell help independent. *Proceedings of the National Academy of Sciences* **116,** 20070–20076 (2019).
401. Zander, R. *et al.* Tfh-cell-derived interleukin 21 sustains effector CD8+ T cell responses during chronic viral infection. *Immunity* **55,** 475–493 (2022).
402. Chen, Z. *et al.* TCF-1-centered transcriptional network drives an effector versus exhausted CD8 T cell-fate decision. *Immunity* **51,** 840–855 (2019).
403. Vodnala, S. K. *et al.* T cell stemness and dysfunction in tumors are triggered by a common mechanism. *Science* **363,** eaau0135 (2019).
404. Odorizzi, P. M., Pauken, K. E., Paley, M. A., Sharpe, A. & Wherry, E. J. Genetic absence of PD-1 promotes accumulation of terminally differentiated exhausted CD8+ T cells. *Journal of Experimental Medicine* **212,** 1125–1137 (2015).
405. Burnet, M. Cancer—a biological approach: III. Viruses associated with neoplastic conditions. IV. Practical applications. *British medical journal* **1,** 841 (1957).
406. Thomas, L. & Lawrence, H. Cellular and humoral aspects of the hypersensitive states. *New York: Hoeber-Harper,* 529–32 (1959).
407. Shankaran, V. *et al.* IFNγ and lymphocytes prevent primary tumour development and shape tumour immunogenicity. *Nature* **410,** 1107–1111 (2001).
408. Schreiber, R. D., Old, L. J. & Smyth, M. J. Cancer immunoediting: integrating immunity's roles in cancer suppression and promotion. *Science* **331,** 1565–1570 (2011).
409. Waldman, A. D., Fritz, J. M. & Lenardo, M. J. A guide to cancer immunotherapy: from T cell basic science to clinical practice. *Nature Reviews Immunology* **20,** 651–668 (2020).
410. Leach, D. R., Krummel, M. F. & Allison, J. P. Enhancement of antitumor immunity by CTLA-4 blockade. *Science* **271,** 1734–1736 (1996).
411. Hodi, F. S. *et al.* Biologic activity of cytotoxic T lymphocyte-associated antigen 4 antibody blockade in previously vaccinated metastatic melanoma and ovarian carcinoma patients. *Proceedings of the National Academy of Sciences* **100,** 4712–4717 (2003).
412. Hodi, F. S. *et al.* Improved survival with ipilimumab in patients with metastatic melanoma. *New England Journal of Medicine* **363,** 711–723 (2010).

413. Schadendorf, D. *et al.* Pooled analysis of long-term survival data from phase II and phase III trials of ipilimumab in unresectable or metastatic melanoma. *Journal of clinical oncology* **33,** 1889 (2015).
414. Vaddepally, R. K., Kharel, P., Pandey, R., Garje, R. & Chandra, A. B. Review of indications of FDA-approved immune checkpoint inhibitors per NCCN guidelines with the level of evidence. *Cancers* **12,** 738 (2020).
415. Van Elsas, A., Hurwitz, A. A. & Allison, J. P. Combination immunotherapy of B16 melanoma using anti–cytotoxic T lymphocyte–associated antigen 4 (CTLA-4) and granulocyte/macrophage colony-stimulating factor (GM-CSF)-producing vaccines induces rejection of subcutaneous and metastatic tumors accompanied by autoimmune depigmentation. *The Journal of experimental medicine* **190,** 355–366 (1999).
416. Simpson, T. R. *et al.* Fc-dependent depletion of tumor-infiltrating regulatory T cells co-defines the efficacy of anti–CTLA-4 therapy against melanoma. *Journal of Experimental Medicine* **210,** 1695–1710 (2013).
417. Sharma, A. *et al.* Anti-CTLA-4 Immunotherapy Does Not Deplete FOXP3+ Regulatory T Cells (Tregs) in Human CancersAnti-CTLA-4 Therapy Does Not Deplete FOXP3+ Cells. *Clinical Cancer Research* **25,** 1233–1238 (2019).
418. Wherry, E. J. & Kurachi, M. Molecular and cellular insights into T cell exhaustion. *Nature Reviews Immunology* **15,** 486–499 (2015).
419. Blank, C. *et al.* PD-L1/B7H-1 inhibits the effector phase of tumor rejection by T cell receptor (TCR) transgenic CD8+ T cells. *Cancer research* **64,** 1140–1145 (2004).
420. Iwai, Y. *et al.* Involvement of PD-L1 on tumor cells in the escape from host immune system and tumor immunotherapy by PD-L1 blockade. *Proceedings of the National Academy of Sciences* **99,** 12293–12297 (2002).
421. Juneja, V. R. *et al.* PD-L1 on tumor cells is sufficient for immune evasion in immunogenic tumors and inhibits CD8 T cell cytotoxicity. *Journal of Experimental Medicine* **214,** 895–904 (2017).
422. Curiel, T. J. *et al.* Blockade of B7-H1 improves myeloid dendritic cell–mediated antitumor immunity. *Nature medicine* **9,** 562–567 (2003).
423. Lau, J. *et al.* Tumour and host cell PD-L1 is required to mediate suppression of anti-tumour immunity in mice. *Nature communications* **8,** 1–11 (2017).
424. Hirano, F. *et al.* Blockade of B7-H1 and PD-1 by monoclonal antibodies potentiates cancer therapeutic immunity. *Cancer research* **65,** 1089–1096 (2005).
425. Robert, C. *et al.* Nivolumab in previously untreated melanoma without BRAF mutation. *New England journal of medicine* **372,** 320–330 (2015).
426. Robert, C. *et al.* Pembrolizumab versus ipilimumab in advanced melanoma. *New England Journal of Medicine* **372,** 2521–2532 (2015).
427. Weber, J. *et al.* Adjuvant nivolumab versus ipilimumab in resected stage III or IV melanoma. *New England Journal of Medicine* **377,** 1824–1835 (2017).
428. Miller, B. C. *et al.* Subsets of exhausted CD8+ T cells differentially mediate tumor control and respond to checkpoint blockade. *Nature immunology* **20,** 326–336 (2019).
429. Huang, A. C. *et al.* T-cell invigoration to tumour burden ratio associated with anti-PD-1 response. *Nature* **545,** 60–65 (2017).
430. Yost, K. E. *et al.* Clonal replacement of tumor-specific T cells following PD-1 blockade. *Nature medicine* **25,** 1251–1259 (2019).
431. Marin-Acevedo, J. A., Kimbrough, E. O. & Lou, Y. Next generation of immune checkpoint inhibitors and beyond. *Journal of hematology & oncology* **14,** 1–29 (2021).
432. Rosenberg, S. A. & Restifo, N. P. Adoptive cell transfer as personalized immunotherapy for human cancer. *Science* **348,** 62–68 (2015).
433. Weiden, P. L. *et al.* Antileukemic effect of graft-versus-host disease in human recipients of allogeneic-marrow grafts. *New England Journal of Medicine* **300,** 1068–1073 (1979).

434. Rosenberg, S. A. *et al.* Observations on the systemic administration of autologous lymphokine-activated killer cells and recombinant interleukin-2 to patients with metastatic cancer. *New England journal of medicine* **313,** 1485–1492 (1985).
435. Rosenberg, S. A., Spiess, P. & Lafreniere, R. A new approach to the adoptive immunotherapy of cancer with tumor-infiltrating lymphocytes. *Science* **233,** 1318–1321 (1986).
436. Rosenberg, S. A. *et al.* Use of tumor-infiltrating lymphocytes and interleukin-2 in the immunotherapy of patients with metastatic melanoma. *New England Journal of Medicine* **319,** 1676–1680 (1988).
437. Zacharakis, N. *et al.* Immune recognition of somatic mutations leading to complete durable regression in metastatic breast cancer. *Nature medicine* **24,** 724–730 (2018).
438. Morgan, R. A. *et al.* Cancer regression in patients after transfer of genetically engineered lymphocytes. *Science* **314,** 126–129 (2006).
439. Gross, G., Waks, T. & Eshhar, Z. Expression of immunoglobulin-T-cell receptor chimeric molecules as functional receptors with antibody-type specificity. *Proceedings of the National Academy of Sciences* **86,** 10024–10028 (1989).
440. Maher, J., Brentjens, R. J., Gunset, G., Rivière, I. & Sadelain, M. Human T-lymphocyte cytotoxicity and proliferation directed by a single chimeric TCRζ/CD28 receptor. *Nature biotechnology* **20,** 70–75 (2002).
441. Imai, C. *et al.* Chimeric receptors with 4-1BB signaling capacity provoke potent cytotoxicity against acute lymphoblastic leukemia. *Leukemia* **18,** 676–684 (2004).
442. Song, D.-G. *et al.* In Vivo Persistence, Tumor Localization, and Antitumor Activity of CAR-Engineered T Cells Is Enhanced by Costimulatory Signaling through CD137 (4-1BB) Costimulated FRα-Specific CAR Therapy of Cancer. *Cancer research* **71,** 4617–4627 (2011).
443. Krishna, S. *et al.* Stem-like CD8 T cells mediate response of adoptive cell immunotherapy against human cancer. *Science* **370,** 1328–1334 (2020).
444. Porter, D. L. *et al.* Chimeric antigen receptor T cells persist and induce sustained remissions in relapsed refractory chronic lymphocytic leukemia. *Science translational medicine* **7,** 303ra139–303ra139 (2015).
445. Chan, J. D. *et al.* Cellular networks controlling T cell persistence in adoptive cell therapy. *Nature Reviews Immunology* **21,** 769–784 (2021).
446. Sinclair, L. V. *et al.* Control of amino-acid transport by antigen receptors coordinates the metabolic reprogramming essential for T cell differentiation. *Nature immunology* **14,** 500–508 (2013).
447. Cornish, G. H., Sinclair, L. V. & Cantrell, D. A. Differential regulation of T-cell growth by IL-2 and IL-15. *Blood* **108,** 600–608 (2006).
448. Alizadeh, D. *et al.* IL15 Enhances CAR-T Cell Antitumor Activity by Reducing mTORC1 Activity and Preserving Their Stem Cell Memory PhenotypeSuperior Antitumor Activity of CAR-T Cells Cultured in IL15. *Cancer immunology research* **7,** 759–772 (2019).
449. Giuffrida, L. *et al.* IL-15 preconditioning augments CAR T cell responses to checkpoint blockade for improved treatment of solid tumors. *Molecular Therapy* **28,** 2379–2393 (2020).
450. Gattinoni, L. *et al.* Acquisition of full effector function in vitro paradoxically impairs the in vivo antitumor efficacy of adoptively transferred CD8+ T cells. *The Journal of clinical investigation* **115,** 1616–1626 (2005).
451. Klebanoff, C. A. *et al.* IL-15 enhances the in vivo antitumor activity of tumor-reactive CD8+ T cells. *Proceedings of the National Academy of Sciences* **101,** 1969–1974 (2004).
452. Philip, M. *et al.* Chromatin states define tumour-specific T cell dysfunction and reprogramming. *Nature* **545,** 452–456 (2017).
453. Das, S. & Johnson, D. B. Immune-related adverse events and anti-tumor efficacy of immune checkpoint inhibitors. *Journal for immunotherapy of cancer* **7,** 1–11 (2019).
454. Pircher, H., Bürki, K., Lang, R., Hengartner, H. & Zinkernagel, R. M. Tolerance induction in double specific T-cell receptor transgenic mice varies with antigen. *Nature* **342,** 559–561 (1989).

455. Lee, P. P. *et al.* A critical role for Dnmt1 and DNA methylation in T cell development, function, and survival. *Immunity* **15,** 763–774 (2001).
456. Rubtsov, Y. P. *et al.* Regulatory T cell-derived interleukin-10 limits inflammation at environmental interfaces. *Immunity* **28,** 546–558 (2008).
457. Brüning, J. C. *et al.* A muscle-specific insulin receptor knockout exhibits features of the metabolic syndrome of NIDDM without altering glucose tolerance. *Molecular cell* **2,** 559–569 (1998).
458. Schwenk, F., Baron, U. & Rajewsky, K. A cre-transgenic mouse strain for the ubiquitous deletion of loxP-flanked gene segments including deletion in germ cells. *Nucleic acids research* **23,** 5080 (1995).
459. Kaplan, M. H., Schindler, U., Smiley, S. T. & Grusby, M. J. Stat6 is required for mediating responses to IL-4 and for the development of Th2 cells. *Immunity* **4,** 313–319 (1996).
460. Voehringer, D., Wu, D., Liang, H.-E. & Locksley, R. M. Efficient generation of long-distance conditional alleles using recombineering and a dual selection strategy in replicate plates. *BMC biotechnology* **9,** 1–7 (2009).
461. Clausen, B., Burkhardt, C., Reith, W., Renkawitz, R. & Förster, I. Conditional gene targeting in macrophages and granulocytes using LysMcre mice. *Transgenic research* **8,** 265–277 (1999).
462. Dutko, F. J. & Oldstone, M. B. Genomic and biological variation among commonly used lymphocytic choriomeningitis virus strains. *Journal of General Virology* **64,** 1689–1698 (1983).
463. Ahmed, R., Salmi, A., Butler, L. D., Chiller, J. M. & Oldstone, M. Selection of genetic variants of lymphocytic choriomeningitis virus in spleens of persistently infected mice. Role in suppression of cytotoxic T lymphocyte response and viral persistence. *The Journal of experimental medicine* **160,** 521–540 (1984).
464. Mueller, S. N. *et al.* Qualitatively different memory CD8+ T cells are generated after lymphocytic choriomeningitis virus and influenza virus infections. *The Journal of Immunology* **185,** 2182–2190 (2010).
465. Dagley, M. J. & McConville, M. J. DExSI: a new tool for the rapid quantitation of 13C-labelled metabolites detected by GC-MS. *Bioinformatics* **34,** 1957–1958 (2018).
466. Milner, J. J. *et al.* Runx3 programs CD8+ T cell residency in non-lymphoid tissues and tumours. *Nature* **552,** 253–257 (2017).
467. Garg, G. *et al.* Blimp1 prevents methylation of Foxp3 and loss of regulatory T cell identity at sites of inflammation. *Cell reports* **26,** 1854–1868 (2019).
468. Mognol, G. P. *et al.* Exhaustion-associated regulatory regions in CD8+ tumor-infiltrating T cells. *Proceedings of the National Academy of Sciences* **114,** E2776–E2785 (2017).
469. Yu, T. *et al.* Modulation of M2 macrophage polarization by the crosstalk between Stat6 and Trim24. *Nature communications* **10,** 1–15 (2019).
470. Cheuk, S. *et al.* CD49a expression defines tissue-resident CD8+ T cells poised for cytotoxic function in human skin. *Immunity* **46,** 287–300 (2017).
471. Ganesan, A.-P. *et al.* Tissue-resident memory features are linked to the magnitude of cytotoxic T cell responses in human lung cancer. *Nature immunology* **18,** 940–950 (2017).
472. Kumar, B. V. *et al.* Human tissue-resident memory T cells are defined by core transcriptional and functional signatures in lymphoid and mucosal sites. *Cell reports* **20,** 2921–2934 (2017).
473. Sade-Feldman, M. *et al.* Defining T cell states associated with response to checkpoint immunotherapy in melanoma. *Cell* **175,** 998–1013 (2018).
474. Luo, Y. *et al.* Single-cell transcriptomic analysis reveals disparate effector differentiation pathways in human Treg compartment. *Nature communications* **12,** 1–14 (2021).
475. Ricardo-Gonzalez, R. R. *et al.* Tissue signals imprint ILC2 identity with anticipatory function. *Nature immunology* **19,** 1093–1099 (2018).
476. Niethamer, T. K. *et al.* Defining the role of pulmonary endothelial cell heterogeneity in the response to acute lung injury. *Elife* **9,** e53072 (2020).
477. Kurd, N. S. *et al.* Early precursors and molecular determinants of tissue-resident memory CD8+ T lymphocytes revealed by single-cell RNA sequencing. *Science immunology* **5,** eaaz6894 (2020).

478. Zakharov, P. N., Hu, H., Wan, X. & Unanue, E. R. Single-cell RNA sequencing of murine islets shows high cellular complexity at all stages of autoimmune diabetes. *Journal of Experimental Medicine* **217** (2020).
479. Milner, J. J. *et al.* Heterogenous populations of tissue-resident CD8+ T cells are generated in response to infection and malignancy. *Immunity* **52,** 808–824 (2020).
480. R Core Team. *R: A Language and Environment for Statistical Computing* R Foundation for Statistical Computing (Vienna, Austria, 2020). https://www.R-project.org/.
481. Van Rossum, G. & Drake, F. L. *Python 3 Reference Manual* ISBN: 1441412697 (CreateSpace, Scotts Valley, CA, 2009).
482. Irizarry, R. A. *et al. affy: Methods for Affymetrix Oligonucleotide Arrays* R package version 1.64.0 (2019).
483. Gentleman, R. *annotate: Annotation for microarrays* R package version 1.64.0 (2019).
484. Aibar, S., of Computational Biology. VIB-KU Leuven Center for Brain Disease Research. Leuven, S. A. L. & Belgium. *AUCell: Analysis of gene set activity in single-cell RNA-seq data (e.g. identify cells with specific gene signatures)* R package version 1.10.0 (2020). http://scenic.aertslab.org.
485. Morgan, M. *BiocManager: Access the Bioconductor Project Package Repository* R package version 1.30.10 (2019). https://CRAN.R-project.org/package=BiocManager.
486. Durinck, S. & Huber, W. *biomaRt: Interface to BioMart databases (i.e. Ensembl)* R package version 2.42.1 (2020).
487. Bryan, J. *cellranger: Translate Spreadsheet Cell Ranges to Rows and Columns* R package version 1.1.0 (2016). https://github.com/rsheets/cellranger.
488. Wickham, H., François, R., Henry, L. & Müller, K. *dplyr: A Grammar of Data Manipulation* R package version 1.0.2 (2020). https://CRAN.R-project.org/package=dplyr.
489. Chen, Y. *et al. edgeR: Empirical Analysis of Digital Gene Expression Data in R* R package version 3.28.1 (2020). http://bioinf.wehi.edu.au/edgeR.
490. Korotkevich, G., Sukhov, V. & Sergushichev, A. *fgsea: Fast Gene Set Enrichment Analysis* R package version 1.12.0 (2019). https://github.com/ctlab/fgsea/.
491. Gentleman, R., Carey, V., Huber, W. & Hahne, F. *genefilter: methods for filtering genes from high-throughput experiments* R package version 1.68.0 (2019).
492. Davis, S. *GEOquery: Get data from NCBI Gene Expression Omnibus (GEO)* R package version 2.54.1 (2019). https://github.com/seandavi/GEOquery.
493. Wickham, H. *et al. ggplot2: Create Elegant Data Visualisations Using the Grammar of Graphics* R package version 3.3.3 (2020). https://CRAN.R-project.org/package=ggplot2.
494. Smyth, G. *et al. limma: Linear Models for Microarray Data* R package version 3.42.2 (2020). http://bioinf.wehi.edu.au/limma.
495. Bates, D. & Maechler, M. *Matrix: Sparse and Dense Matrix Classes and Methods* R package version 1.2-18 (2019). http://Matrix.R-forge.R-project.org/.
496. Dolgalev, I. *msigdbr: MSigDB Gene Sets for Multiple Organisms in a Tidy Data Format* R package version 7.1.1 (2020). https://github.com/igordot/msigdbr.
497. Carlson, M. *org.Hs.eg.db: Genome wide annotation for Human* R package version 3.10.0 (2019).
498. Carlson, M. *org.Mm.eg.db: Genome wide annotation for Mouse* R package version 3.10.0 (2019).
499. Kolde, R. *pheatmap: Pretty Heatmaps* R package version 1.0.12 (2019). https://CRAN.R-project.org/package=pheatmap.
500. Neuwirth, E. *RColorBrewer: ColorBrewer Palettes* R package version 1.1-2 (2014). https://CRAN.R-project.org/package=RColorBrewer.
501. Wickham, H. & Hester, J. *readr: Read Rectangular Text Data* R package version 1.4.0 (2020). https://CRAN.R-project.org/package=readr.
502. Wickham, H. & Bryan, J. *readxl: Read Excel Files* R package version 1.3.1 (2019). https://CRAN.R-project.org/package=readxl.

503. Hoffman, P. *Seurat: Tools for Single Cell Genomics* R package version 4.0.4 (2021). https://CRAN.R-project.org/package=Seurat.
504. Wickham, H. *stringr: Simple, Consistent Wrappers for Common String Operations* R package version 1.4.0 (2019). https://CRAN.R-project.org/package=stringr.
505. Wickham, H. *tidyr: Tidy Messy Data* R package version 1.1.2 (2020). https://CRAN.R-project.org/package=tidyr.
506. Hunter, J. D. Matplotlib: A 2D graphics environment. *Computing in Science & Engineering* **9,** 90–95 (2007).
507. Harris, C. R. *et al.* Array programming with NumPy. *Nature* **585,** 357–362. https://doi.org/10.1038/s41586-020-2649-2 (Sept. 2020).
508. McKinney, W. *Data Structures for Statistical Computing in Python* in *Proceedings of the 9th Python in Science Conference* (eds van der Walt, S. & Millman, J.) (2010), 56–61.
509. Wolf, F. A., Angerer, P. & Theis, F. J. SCANPY: large-scale single-cell gene expression data analysis. *Genome biology* **19,** 1–5 (2018).
510. Corces, M. R. *et al.* An improved ATAC-seq protocol reduces background and enables interrogation of frozen tissues. *Nature methods* **14,** 959–962 (2017).
511. Martin, M. Cutadapt removes adapter sequences from high-throughput sequencing reads. *EMBnet. journal* **17,** 10–12 (2011).
512. Langmead, B. & Salzberg, S. L. Fast gapped-read alignment with Bowtie 2. *Nature methods* **9,** 357–359 (2012).
513. Li, H. *et al.* The sequence alignment/map format and SAMtools. *Bioinformatics* **25,** 2078–2079 (2009).
514. Quinlan, A. R. & Hall, I. M. BEDTools: a flexible suite of utilities for comparing genomic features. *Bioinformatics* **26,** 841–842 (2010).
515. Zhang, Y. *et al.* Model-based analysis of ChIP-Seq (MACS). *Genome biology* **9,** 1–9 (2008).
516. Pohl, A. & Beato, M. bwtool: a tool for bigWig files. *Bioinformatics* **30,** 1618–1619 (2014).
517. Kao, C., Daniels, M. A. & Jameson, S. C. Loss of CD8 and TCR binding to Class I MHC ligands following T cell activation. *International immunology* **17,** 1607–1617 (2005).
518. Haluszczak, C. *et al.* The antigen-specific CD8+ T cell repertoire in unimmunized mice includes memory phenotype cells bearing markers of homeostatic expansion. *Journal of Experimental Medicine* **206,** 435–448 (2009).
519. Herndler-Brandstetter, D. *et al.* KLRG1+ effector CD8+ T cells lose KLRG1, differentiate into all memory T cell lineages, and convey enhanced protective immunity. *Immunity* **48,** 716–729 (2018).
520. Grayson, J. M., Zajac, A. J., Altman, J. D. & Ahmed, R. Cutting edge: increased expression of Bcl-2 in antigen-specific memory CD8+ T cells. *The Journal of Immunology* **164,** 3950–3954 (2000).
521. Norment, A. M., Salter, R. D., Parham, P., Engelhard, V. H. & Littman, D. R. Cell-cell adhesion mediated by CD8 and MHC class I molecules. *Nature* **336,** 79–81 (1988).
522. Bushkin, Y., Demaria, S., Le, J. & Schwab, R. Physical association between the CD8 and HLA class I molecules on the surface of activated human T lymphocytes. *Proceedings of the National Academy of Sciences* **85,** 3985–3989 (1988).
523. Blue, M.-L., Craig, K. A., Anderson, P., Branton Jr, K. R. & Schlossman, S. F. Evidence for specific association between class I major histocompatibility antigens and the CD8 molecules of human suppressor/cytotoxic cells. *Cell* **54,** 413–421 (1988).
524. Rosenstein, Y., Ratnofsky, S., Burakoff, S. & Herrmann, S. Direct evidence for binding of CD8 to HLA class I antigens. *The Journal of experimental medicine* **169,** 149–160 (1989).
525. Ross, J. O. *et al.* Distinct phases in the positive selection of CD8+ T cells distinguished by intrathymic migration and T-cell receptor signaling patterns. *Proceedings of the National Academy of Sciences* **111,** E2550–E2558 (2014).
526. Hogquist, K. A. *et al.* T cell receptor antagonist peptides induce positive selection. *Cell* **76,** 17–27 (1994).

527. Veillette, A., Zúñiga-Pflücker, J., Bolen, J. B. & Kruisbeek, A. Engagement of CD4 and CD8 expressed on immature thymocytes induces activation of intracellular tyrosine phosphorylation pathways. *The Journal of experimental medicine* **170,** 1671–1680 (1989).
528. Clement, M. *et al.* Anti-CD8 antibodies can trigger CD8+ T cell effector function in the absence of TCR engagement and improve peptide–MHCI tetramer staining. *The Journal of Immunology* **187,** 654–663 (2011).
529. Brownlie, R. J. & Zamoyska, R. T cell receptor signalling networks: branched, diversified and bounded. *Nature Reviews Immunology* **13,** 257–269 (2013).
530. Zenke, S. *et al.* Quorum regulation via nested antagonistic feedback circuits mediated by the receptors CD28 and CTLA-4 confers robustness to T cell population dynamics. *Immunity* **52,** 313–327 (2020).
531. Leone, R. D. *et al.* Glutamine blockade induces divergent metabolic programs to overcome tumor immune evasion. *Science* **366,** 1013–1021 (2019).
532. Tolnay, M., Bazin, H. & Medgyesi, G. A. Rat IgG subclasses mediating binding and phagocytosis of target cells by homologous macrophages. *Molecular immunology* **30,** 1273–1278 (1993).
533. Sandu, I., Cerletti, D., Claassen, M. & Oxenius, A. Exhausted CD8+ T cells exhibit low and strongly inhibited TCR signaling during chronic LCMV infection. *Nature communications* **11,** 1–11 (2020).
534. Makino, S. *et al.* Breeding of a non-obese, diabetic strain of mice. *Experimental Animals* **29,** 1–13 (1980).
535. Miyazaki, A. *et al.* Predominance of T lymphocytes in pancreatic islets and spleen of pre-diabetic non-obese diabetic (NOD) mice: a longitudinal study. *Clinical and experimental immunology* **60,** 622 (1985).
536. Carrero, J. A., Calderon, B., Towfic, F., Artyomov, M. N. & Unanue, E. R. Defining the transcriptional and cellular landscape of type 1 diabetes in the NOD mouse. *PloS one* **8,** e59701 (2013).
537. Gorini, G., Medgyesi, G. & Doria, G. Heterogeneity of mouse myeloma γG globulins as revealed by enzymatic proteolysis. *The Journal of Immunology* **103,** 1132–1142 (1969).
538. Vlasak, J. & Ionescu, R. *Fragmentation of monoclonal antibodies* in *MAbs* **3** (2011), 253–263.
539. Pauken, K. E. *et al.* Single-cell analyses identify circulating anti-tumor CD8 T cells and markers for their enrichment. *Journal of Experimental Medicine* **218** (2021).
540. Adachi, K. & Davis, M. M. T-cell receptor ligation induces distinct signaling pathways in naive vs. antigen-experienced T cells. *Proceedings of the National Academy of Sciences* **108,** 1549–1554 (2011).
541. Fahmy, T. M., Bieler, J. G., Edidin, M. & Schneck, J. P. Increased TCR avidity after T cell activation: a mechanism for sensing low-density antigen. *Immunity* **14,** 135–143 (2001).
542. Shinzawa, M. *et al.* Reversal of the T cell immune system reveals the molecular basis for T cell lineage fate determination in the thymus. *Nature immunology* **23,** 731–742 (2022).
543. Singer, A., Adoro, S. & Park, J.-H. Lineage fate and intense debate: myths, models and mechanisms of CD4-versus CD8-lineage choice. *Nature Reviews Immunology* **8,** 788–801 (2008).
544. Wiehagen, K. R. *et al.* Loss of tonic T-cell receptor signals alters the generation but not the persistence of CD8+ memory T cells. *Blood, The Journal of the American Society of Hematology* **116,** 5560–5570 (2010).
545. Maile, R. *et al.* Peripheral "CD8 tuning" dynamically modulates the size and responsiveness of an antigen-specific T cell pool in vivo. *The Journal of Immunology* **174,** 619–627 (2005).
546. Holler, P. D. & Kranz, D. M. Quantitative analysis of the contribution of TCR/pepMHC affinity and CD8 to T cell activation. *Immunity* **18,** 255–264 (2003).
547. Zhong, S. *et al.* T-cell receptor affinity and avidity defines antitumor response and autoimmunity in T-cell immunotherapy. *Proceedings of the National Academy of Sciences* **110,** 6973–6978 (2013).
548. Wooldridge, L. *et al.* CD8 controls T cell cross-reactivity. *The Journal of Immunology* **185,** 4625–4632 (2010).

549. Schulien, I. *et al.* Characterization of pre-existing and induced SARS-CoV-2-specific CD8+ T cells. *Nature medicine* **27,** 78–85 (2021).
550. Lee, C. H. *et al.* Potential CD8+ T cell cross-reactivity against SARS-CoV-2 conferred by other coronavirus strains. *Frontiers in immunology* **11,** 579480 (2020).
551. Lineburg, K. E. *et al.* CD8+ T cells specific for an immunodominant SARS-CoV-2 nucleocapsid epitope cross-react with selective seasonal coronaviruses. *Immunity* **54,** 1055–1065 (2021).
552. Zheng, L. *et al.* The CD8α–PILRα interaction maintains CD8+ T cell quiescence. *Science* **376,** 996–1001 (2022).
553. Martin, A. J. *et al.* Anti-coreceptor therapy drives selective T cell egress by suppressing inflammation-dependent chemotactic cues. *JCI insight* **1** (2016).
554. Yi, Z. *et al.* Long-term remission of diabetes in NOD mice is induced by nondepleting anti-CD4 and anti-CD8 antibodies. *Diabetes* **61,** 2871–2880 (2012).
555. Benjamin, R. J. & Waldmann, H. Induction of tolerance by monoclonal antibody therapy. *Nature* **320,** 449–451 (1986).
556. Qin, S. *et al.* " Infectious" transplantation tolerance. *Science* **259,** 974–977 (1993).
557. Cobbold, S. P. *et al.* Induction of foxP3+ regulatory T cells in the periphery of T cell receptor transgenic mice tolerized to transplants. *The Journal of Immunology* **172,** 6003–6010 (2004).
558. Dossa, R. G. *et al.* Development of T-cell immunotherapy for hematopoietic stem cell transplantation recipients at risk of leukemia relapse. *Blood, The Journal of the American Society of Hematology* **131,** 108–120 (2018).
559. Morris, E. C., Tsallios, A., Bendle, G. M., Xue, S.-a. & Stauss, H. J. A critical role of T cell antigen receptor-transduced MHC class I-restricted helper T cells in tumor protection. *Proceedings of the National Academy of Sciences* **102,** 7934–7939 (2005).
560. Shakiba, M. *et al.* TCR signal strength defines distinct mechanisms of T cell dysfunction and cancer evasion. *Journal of Experimental Medicine* **219,** e20201966 (2021).
561. Rath, J. A. *et al.* Single-cell transcriptomics identifies multiple pathways underlying antitumor function of TCR-and CD8$\alpha\beta$-engineered human CD4+ T cells. *Science advances* **6,** eaaz7809 (2020).
562. Tomonari, K. & Spencer, S. Epitope-specific binding of CD8 regulates activation of T cells and induction of cytotoxicity. *International Immunology* **2,** 1189–1194 (1990).
563. Luescher, I. F. *et al.* CD8 modulation of T-cell antigen receptor–ligand interactions on living cytotoxic T lymphocytes. *Nature* **373,** 353–356 (1995).
564. Mo, F. *et al.* An engineered IL-2 partial agonist promotes CD8+ T cell stemness. *Nature* **597,** 544–548 (2021).
565. Blagih, J. *et al.* The energy sensor AMPK regulates T cell metabolic adaptation and effector responses in vivo. *Immunity* **42,** 41–54 (2015).
566. Newton, R. H. *et al.* Maintenance of CD4 T cell fitness through regulation of Foxo1. *Nature immunology* **19,** 838–848 (2018).
567. Sinclair, L. V. *et al.* Phosphatidylinositol-3-OH kinase and nutrient-sensing mTOR pathways control T lymphocyte trafficking. *Nature immunology* **9,** 513–521 (2008).
568. Zou, C., Wang, Y. & Shen, Z. 2-NBDG as a fluorescent indicator for direct glucose uptake measurement. *Journal of biochemical and biophysical methods* **64,** 207–215 (2005).
569. Sinclair, L. V., Barthelemy, C. & Cantrell, D. A. Single cell glucose uptake assays: a cautionary tale. *Immunometabolism* **2** (2020).
570. D'Souza, L. J., Wright, S. H. & Bhattacharya, D. Genetic evidence that uptake of the fluorescent analog 2NBDG occurs independently of known glucose transporters. *PloS one* **17,** e0261801 (2022).
571. Chen, X. *et al.* Succinate dehydrogenase/complex II is critical for metabolic and epigenetic regulation of T cell proliferation and inflammation. *Science Immunology* **7,** eabm8161 (2022).
572. Klysz, D. *et al.* Glutamine-dependent α-ketoglutarate production regulates the balance between T helper 1 cell and regulatory T cell generation. *Science signaling* **8,** ra97–ra97 (2015).

573. Matias, M. I. *et al.* Regulatory T cell differentiation is controlled by αKG-induced alterations in mitochondrial metabolism and lipid homeostasis. *Cell reports* **37,** 109911 (2021).
574. Schofield, C. J. & Zhang, Z. Structural and mechanistic studies on 2-oxoglutarate-dependent oxygenases and related enzymes. *Current opinion in structural biology* **9,** 722–731 (1999).
575. McDonough, M. A., Loenarz, C., Chowdhury, R., Clifton, I. J. & Schofield, C. J. Structural studies on human 2-oxoglutarate dependent oxygenases. *Current opinion in structural biology* **20,** 659–672 (2010).
576. Tulsawani, R. *et al.* Effect of sub-acute oral cyanide administration in rats: protective efficacy of alpha-ketoglutarate and sodium thiosulfate. *Chemico-biological interactions* **156,** 1–12 (2005).
577. Johnson, K. A. & Goody, R. S. The original Michaelis constant: translation of the 1913 Michaelis–Menten paper. *Biochemistry* **50,** 8264–8269 (2011).
578. Ho, P.-C. *et al.* Phosphoenolpyruvate is a metabolic checkpoint of anti-tumor T cell responses. *Cell* **162,** 1217–1228 (2015).
579. Klein Geltink, R. I. *et al.* Metabolic conditioning of CD8+ effector T cells for adoptive cell therapy. *Nature Metabolism* **2,** 703–716 (2020).
580. Swamy, M. *et al.* Glucose and glutamine fuel protein O-GlcNAcylation to control T cell self-renewal and malignancy. *Nature immunology* **17,** 712–720 (2016).
581. Hart, G. W., Housley, M. P. & Slawson, C. Cycling of O-linked β-N-acetylglucosamine on nucleocytoplasmic proteins. *Nature* **446,** 1017–1022 (2007).
582. Asano, T. *et al.* The role of N-glycosylation in the targeting and stability of GLUT1 glucose transporter. *FEBS letters* **324,** 258–261 (1993).
583. Asano, T. *et al.* The role of N-glycosylation of GLUT1 for glucose transport activity. *Journal of biological chemistry* **266,** 24632–24636 (1991).
584. Jandl, J. H., Inman, J. K., Simmons, R. L., Allen, D. W. *et al.* Transfer of iron from serum iron-binding protein to human reticulocytes. *The Journal of clinical investigation* **38,** 161–185 (1959).
585. Aisen, P. Transferrin receptor 1. *The international journal of biochemistry & cell biology* **36,** 2137–2143 (2004).
586. Netz, D. J. *et al.* Eukaryotic DNA polymerases require an iron-sulfur cluster for the formation of active complexes. *Nature chemical biology* **8,** 125–132 (2012).
587. Wu, Y. & Brosh Jr, R. M. DNA helicase and helicase–nuclease enzymes with a conserved iron–sulfur cluster. *Nucleic acids research* **40,** 4247–4260 (2012).
588. Read, A. D., Bentley, R. E., Archer, S. L. & Dunham-Snary, K. J. Mitochondrial iron–sulfur clusters: Structure, function, and an emerging role in vascular biology. *Redox Biology* **47,** 102164 (2021).
589. Murali-Krishna, K. & Ahmed, R. Cutting edge: naive T cells masquerading as memory cells. *The Journal of Immunology* **165,** 1733–1737 (2000).
590. Fan, K. *et al.* Magnetoferritin nanoparticles for targeting and visualizing tumour tissues. *Nature nanotechnology* **7,** 459–464 (2012).
591. Motamedi, M., Xu, L. & Elahi, S. Correlation of transferrin receptor (CD71) with Ki67 expression on stimulated human and mouse T cells: The kinetics of expression of T cell activation markers. *Journal of immunological methods* **437,** 43–52 (2016).
592. Gammella, E., Buratti, P., Cairo, G. & Recalcati, S. The transferrin receptor: the cellular iron gate. *Metallomics* **9,** 1367–1375 (2017).
593. Zheng, Y. *et al.* A role for mammalian target of rapamycin in regulating T cell activation versus anergy. *The Journal of Immunology* **178,** 2163–2170 (2007).
594. Feng, H. *et al.* Transferrin receptor is a specific ferroptosis marker. *Cell reports* **30,** 3411–3423 (2020).
595. Dixon, S. J. *et al.* Ferroptosis: an iron-dependent form of nonapoptotic cell death. *Cell* **149,** 1060–1072 (2012).
596. Stockwell, B. R. *et al.* Ferroptosis: a regulated cell death nexus linking metabolism, redox biology, and disease. *Cell* **171,** 273–285 (2017).

597. Xu, C. *et al.* The glutathione peroxidase Gpx4 prevents lipid peroxidation and ferroptosis to sustain Treg cell activation and suppression of antitumor immunity. *Cell reports* **35,** 109235 (2021).
598. Jackson, S. H., Devadas, S., Kwon, J., Pinto, L. A. & Williams, M. S. T cells express a phagocyte-type NADPH oxidase that is activated after T cell receptor stimulation. *Nature immunology* **5,** 818–827 (2004).
599. Mak, T. W. *et al.* Glutathione primes T cell metabolism for inflammation. *Immunity* **46,** 675–689 (2017).
600. Lee, H. *et al.* Energy-stress-mediated AMPK activation inhibits ferroptosis. *Nature cell biology* **22,** 225–234 (2020).
601. Robbins, P. F. *et al.* Cutting edge: persistence of transferred lymphocyte clonotypes correlates with cancer regression in patients receiving cell transfer therapy. *The Journal of Immunology* **173,** 7125–7130 (2004).
602. Ku, C. C., Murakami, M., Sakamoto, A., Kappler, J. & Marrack, P. Control of homeostasis of CD8+ memory T cells by opposing cytokines. *Science* **288,** 675–678 (2000).
603. Loschinski, R. *et al.* IL-21 modulates memory and exhaustion phenotype of T-cells in a fatty acid oxidation-dependent manner. *Oncotarget* **9,** 13125 (2018).
604. Hinrichs, C. S. *et al.* IL-2 and IL-21 confer opposing differentiation programs to CD8+ T cells for adoptive immunotherapy. *Blood, The Journal of the American Society of Hematology* **111,** 5326–5333 (2008).
605. Hermans, D. *et al.* Lactate dehydrogenase inhibition synergizes with IL-21 to promote CD8+ T cell stemness and antitumor immunity. *Proceedings of the National Academy of Sciences* **117,** 6047–6055 (2020).
606. Sukumar, M. *et al.* Inhibiting glycolytic metabolism enhances CD8+ T cell memory and antitumor function. *The Journal of clinical investigation* **123,** 4479–4488 (2013).
607. Bruhns, P. Properties of mouse and human IgG receptors and their contribution to disease models. *Blood, The Journal of the American Society of Hematology* **119,** 5640–5649 (2012).
608. Nimmerjahn, F. & Ravetch, J. V. Divergent immunoglobulin g subclass activity through selective Fc receptor binding. *Science* **310,** 1510–1512 (2005).
609. Cross, E. W., Blain, T. J., Mathew, D. & Kedl, R. M. Anti-CD8 monoclonal antibody-mediated depletion alters the phenotype and behavior of surviving CD8+ T cells. *Plos one* **14,** e0211446 (2019).
610. Dahan, R. *et al.* FcγRs modulate the anti-tumor activity of antibodies targeting the PD-1/PD-L1 axis. *Cancer cell* **28,** 285–295 (2015).
611. Salter, R. D. *et al.* Polymorphism in the α3 domain of HLA-A molecules affects binding to CD8. *Nature* **338,** 345–347 (1989).
612. Robinson, M.-P. *et al.* Efficient expression of full-length antibodies in the cytoplasm of engineered bacteria. *Nature communications* **6,** 1–9 (2015).
613. Moritz, B. & Stracke, J. O. Assessment of disulfide and hinge modifications in monoclonal antibodies. *Electrophoresis* **38,** 769–785 (2017).
614. Neergaard, M. S., Nielsen, A. D., Parshad, H. & Van De Weert, M. Stability of monoclonal antibodies at high-concentration: head-to-head comparison of the IgG1 and IgG4 subclass. *Journal of pharmaceutical sciences* **103,** 115–127 (2014).
615. Sun, Y. *et al.* PILRα negatively regulates mouse inflammatory arthritis. *The Journal of Immunology* **193,** 860–870 (2014).
616. Yu, X. *et al.* The surface protein TIGIT suppresses T cell activation by promoting the generation of mature immunoregulatory dendritic cells. *Nature immunology* **10,** 48–57 (2009).
617. Joller, N. *et al.* Cutting edge: TIGIT has T cell-intrinsic inhibitory functions. *The Journal of Immunology* **186,** 1338–1342 (2011).
618. He, W. *et al.* CD155T/TIGIT Signaling Regulates CD8+ T-cell Metabolism and Promotes Tumor Progression in Human Gastric CancerCD155/TIGIT Regulates T-cell Metabolism in Gastric Cancer. *Cancer research* **77,** 6375–6388 (2017).

619. Davern, M. *et al.* PD-1 and TIGIT blockade differentially affect tumour cell survival under hypoxia and glucose deprived conditions in oesophageal adenocarcinoma; implications for overcoming resistance to PD-1 blockade in hypoxic tumours. *Translational oncology* **19,** 101381 (2022).
620. Aksoy, P., White, T. A., Thompson, M. & Chini, E. N. Regulation of intracellular levels of NAD: a novel role for CD38. *Biochemical and biophysical research communications* **345,** 1386–1392 (2006).
621. Hogan, K. A., Chini, C. C. & Chini, E. N. The multi-faceted ecto-enzyme CD38: roles in immunomodulation, cancer, aging, and metabolic diseases. *Frontiers in immunology* **10,** 1187 (2019).
622. Chen, P.-M. *et al.* CD38 reduces mitochondrial fitness and cytotoxic T cell response against viral infection in lupus patients by suppressing mitophagy. *Science Advances* **8,** eabo4271 (2022).
623. Chatterjee, S. *et al.* CD38-NAD+ axis regulates immunotherapeutic anti-tumor T cell response. *Cell metabolism* **27,** 85–100 (2018).
624. Sim, M. J. *et al.* High-affinity oligoclonal TCRs define effective adoptive T cell therapy targeting mutant KRAS-G12D. *Proceedings of the National Academy of Sciences* **117,** 12826–12835 (2020).
625. Schober, K. *et al.* Reverse TCR repertoire evolution toward dominant low-affinity clones during chronic CMV infection. *Nature immunology* **21,** 434–441 (2020).
626. Feucht, J. *et al.* Calibration of CAR activation potential directs alternative T cell fates and therapeutic potency. *Nature medicine* **25,** 82–88 (2019).
627. Jansen, C. S. *et al.* An intra-tumoral niche maintains and differentiates stem-like CD8 T cells. *Nature* **576,** 465–470 (2019).
628. Moran, A. E. *et al.* T cell receptor signal strength in Treg and iNKT cell development demonstrated by a novel fluorescent reporter mouse. *Journal of Experimental Medicine* **208,** 1279–1289 (2011).
629. Kaech, S. M. & Cui, W. Transcriptional control of effector and memory CD8+ T cell differentiation. *Nature Reviews Immunology* **12,** 749–761 (2012).
630. Giri, J. G. *et al.* Identification and cloning of a novel IL-15 binding protein that is structurally related to the alpha chain of the IL-2 receptor. *The EMBO journal* **14,** 3654–3663 (1995).
631. Soudja, S. M., Ruiz, A. L., Marie, J. C. & Lauvau, G. Inflammatory monocytes activate memory CD8+ T and innate NK lymphocytes independent of cognate antigen during microbial pathogen invasion. *Immunity* **37,** 549–562 (2012).
632. Richer, M. J. *et al.* Inflammatory IL-15 is required for optimal memory T cell responses. *The Journal of clinical investigation* **125,** 3477–3490 (2015).
633. Nolz, J. C., Harty, J. T. *et al.* IL-15 regulates memory CD8+ T cell O-glycan synthesis and affects trafficking. *The Journal of clinical investigation* **124,** 1013–1026 (2014).
634. Grabstein, K. H. *et al.* Cloning of a T cell growth factor that interacts with the β chain of the interleukin-2 receptor. *Science* **264,** 965–968 (1994).
635. Ring, A. M. *et al.* Mechanistic and structural insight into the functional dichotomy between IL-2 and IL-15. *Nature immunology* **13,** 1187–1195 (2012).
636. Mitchell, D. M., Ravkov, E. V. & Williams, M. A. Distinct roles for IL-2 and IL-15 in the differentiation and survival of CD8+ effector and memory T cells. *The Journal of Immunology* **184,** 6719–6730 (2010).
637. Ikemizu, S., Chirifu, M. & Davis, S. J. IL-2 and IL-15 signaling complexes: different but the same. *Nature immunology* **13,** 1141–1142 (2012).
638. Colpitts, S. L. *et al.* Cutting edge: the role of IFN-α receptor and MyD88 signaling in induction of IL-15 expression in vivo. *The Journal of Immunology* **188,** 2483–2487 (2012).
639. Wu, J. *et al.* Skeletal muscle antagonizes antiviral CD8+ T cell exhaustion. *Science advances* **6,** eaba3458 (2020).
640. Mortier, E. *et al.* Macrophage-and dendritic-cell-derived interleukin-15 receptor alpha supports homeostasis of distinct CD8+ T cell subsets. *Immunity* **31,** 811–822 (2009).

641. Cepero-Donates, Y. *et al.* Homeostasis of IL-15 dependent lymphocyte subsets in the liver. *Cytokine* **82,** 95–101 (2016).
642. Leach, S. M. *et al.* Human and mouse transcriptome profiling identifies cross-species homology in pulmonary and lymph node mononuclear phagocytes. *Cell reports* **33,** 108337 (2020).
643. Rubtsov, Y. P. *et al.* Regulatory T cell-derived interleukin-10 limits inflammation at environmental interfaces. *Immunity* **28,** 546–558 (2008).
644. Bamford, R. N., Battiata, A. P., Burton, J. D., Sharma, H. & Waldmann, T. A. Interleukin (IL) 15/IL-T production by the adult T-cell leukemia cell line HuT-102 is associated with a human T-cell lymphotrophic virus type I region/IL-15 fusion message that lacks many upstream AUGs that normally attenuates IL-15 mRNA translation. *Proceedings of the National Academy of Sciences* **93,** 2897–2902 (1996).
645. Onu, A., Pohl, T., Krause, H. & Bulfone-Paus, S. Regulation of IL-15 secretion via the leader peptide of two IL-15 isoforms. *The Journal of Immunology* **158,** 255–262 (1997).
646. Tosiek, M. J., Fiette, L., El Daker, S., Eberl, G. & Freitas, A. A. IL-15-dependent balance between Foxp3 and RORγt expression impacts inflammatory bowel disease. *Nature communications* **7,** 1–11 (2016).
647. Perna, S. K. *et al.* Interleukin 15 Provides Relief to CTLs from Regulatory T Cell–Mediated Inhibition: Implications for Adoptive T Cell–Based Therapies for Lymphoma. *Clinical Cancer Research* **19,** 106–117 (2013).
648. Brüning, J. C. *et al.* A muscle-specific insulin receptor knockout exhibits features of the metabolic syndrome of NIDDM without altering glucose tolerance. *Molecular cell* **2,** 559–569 (1998).
649. Clausen, B., Burkhardt, C., Reith, W., Renkawitz, R. & Förster, I. Conditional gene targeting in macrophages and granulocytes using LysMcre mice. *Transgenic research* **8,** 265–277 (1999).
650. Hamilton, S. E. & Jameson, S. C. CD8 T cell memory: it takes all kinds. *Frontiers in immunology* **3,** 353 (2012).
651. Maynard, C. L. *et al.* Regulatory T cells expressing interleukin 10 develop from Foxp3+ and Foxp3- precursor cells in the absence of interleukin 10. *Nature immunology* **8,** 931–941 (2007).
652. Sosinowski, T. *et al.* CD8α+ dendritic cell trans presentation of IL-15 to naive CD8+ T cells produces antigen-inexperienced T cells in the periphery with memory phenotype and function. *The Journal of Immunology* **190,** 1936–1947 (2013).
653. Kok, L., Masopust, D. & Schumacher, T. N. The precursors of CD8+ tissue resident memory T cells: from lymphoid organs to infected tissues. *Nature Reviews Immunology* **22,** 283–293 (2022).
654. Yu, B. *et al.* Epigenetic landscapes reveal transcription factors that regulate CD8+ T cell differentiation. *Nature immunology* **18,** 573–582 (2017).
655. Crowl, J. T. *et al.* Tissue-resident memory CD8+ T cells possess unique transcriptional, epigenetic and functional adaptations to different tissue environments. *Nature Immunology* **23,** 1121–1131 (2022).
656. Dijkgraaf, F. E. *et al.* Tissue patrol by resident memory CD8+ T cells in human skin. *Nature immunology* **20,** 756–764 (2019).
657. Wakim, L., Smith, J., Caminschi, I., Lahoud, M. H. & Villadangos, J. A. Antibody-targeted vaccination to lung dendritic cells generates tissue-resident memory CD8 T cells that are highly protective against influenza virus infection. *Mucosal immunology* **8,** 1060–1071 (2015).
658. Christo, S. N. *et al.* Discrete tissue microenvironments instruct diversity in resident memory T cell function and plasticity. *Nature immunology* **22,** 1140–1151 (2021).
659. Shiohara, T. Fixed drug eruption: pathogenesis and diagnostic tests. *Current opinion in allergy and clinical immunology* **9,** 316–321 (2009).
660. Suárez-Fariñas, M., Fuentes-Duculan, J., Lowes, M. A. & Krueger, J. G. Resolved psoriasis lesions retain expression of a subset of disease-related genes. *Journal of Investigative Dermatology* **131,** 391–400 (2011).
661. Gaide, O. *et al.* Common clonal origin of central and resident memory T cells following skin immunization. *Nature medicine* **21,** 647–653 (2015).

662. Dudek, M. *et al.* Auto-aggressive CXCR6+ CD8 T cells cause liver immune pathology in NASH. *Nature* **592,** 444–449 (2021).
663. Pfister, D. *et al.* NASH limits anti-tumour surveillance in immunotherapy-treated HCC. *Nature* **592,** 450–456 (2021).
664. Liang, S., Mozdzanowska, K., Palladino, G. & Gerhard, W. Heterosubtypic immunity to influenza type A virus in mice. Effector mechanisms and their longevity. *The Journal of Immunology* **152,** 1653–1661 (1994).
665. Sridhar, S. *et al.* Cellular immune correlates of protection against symptomatic pandemic influenza. *Nature medicine* **19,** 1305–1312 (2013).
666. Wu, T. *et al.* Lung-resident memory CD8 T cells (TRM) are indispensable for optimal cross-protection against pulmonary virus infection. *Journal of leukocyte biology* **95,** 215–224 (2014).
667. Slütter, B. *et al.* Dynamics of influenza-induced lung-resident memory T cells underlie waning heterosubtypic immunity. *Science immunology* **2,** eaag2031 (2017).
668. Hirai, T. *et al.* Competition for active TGFβ cytokine allows for selective retention of antigen-specific tissue-resident memory T cells in the epidermal niche. *Immunity* **54,** 84–98 (2021).
669. Gomez Perdiguero, E. *et al.* Tissue-resident macrophages originate from yolk-sac-derived erythro-myeloid progenitors. *Nature* **518,** 547–551 (2015).
670. Slütter, B., Pewe, L. L., Kaech, S. M. & Harty, J. T. Lung airway-surveilling CXCR3hi memory CD8+ T cells are critical for protection against influenza A virus. *Immunity* **39,** 939–948 (2013).
671. Mehta, D. S., Wurster, A. L. & Grusby, M. J. Biology of IL-21 and the IL-21 receptor. *Immunological reviews* **202,** 84–95 (2004).
672. Hou, J. *et al.* An interleukin-4-induced transcription factor: IL-4 Stat. *Science* **265,** 1701–1706 (1994).
673. Shuai, K. & Liu, B. Regulation of JAK–STAT signalling in the immune system. *Nature Reviews Immunology* **3,** 900–911 (2003).
674. Sutherland, A. P. *et al.* IL-21 promotes CD8+ CTL activity via the transcription factor T-bet. *The Journal of Immunology* **190,** 3977–3984 (2013).
675. Mueller, S. N. *et al.* Qualitatively different memory CD8+ T cells are generated after lymphocytic choriomeningitis virus and influenza virus infections. *The Journal of Immunology* **185,** 2182–2190 (2010).
676. Anderson, K. G. *et al.* Cutting edge: intravascular staining redefines lung CD8 T cell responses. *The Journal of Immunology* **189,** 2702–2706 (2012).
677. Morrot, A., Hafalla, J. C., Cockburn, I. A., Carvalho, L. H. & Zavala, F. IL-4 receptor expression on CD8+ T cells is required for the development of protective memory responses against liver stages of malaria parasites. *The Journal of experimental medicine* **202,** 551–560 (2005).
678. Ricardo-Gonzalez, R. R. *et al.* IL-4/STAT6 immune axis regulates peripheral nutrient metabolism and insulin sensitivity. *Proceedings of the National Academy of Sciences* **107,** 22617–22622 (2010).
679. Kaplan, M. H., Schindler, U., Smiley, S. T. & Grusby, M. J. Stat6 is required for mediating responses to IL-4 and for the development of Th2 cells. *Immunity* **4,** 313–319 (1996).
680. Bot, A. *et al.* Local IL-4 expression in the lung reduces pulmonary influenza-virus-specific secondary cytotoxic T cell responses. *Virology* **269,** 66–77 (2000).
681. Huber, S., Hoffmann, R., Muskens, F. & Voehringer, D. Alternatively activated macrophages inhibit T-cell proliferation by Stat6-dependent expression of PD-L2. *Blood, The Journal of the American Society of Hematology* **116,** 3311–3320 (2010).
682. Kälin, S. *et al.* A Stat6/Pten axis links regulatory T cells with adipose tissue function. *Cell metabolism* **26,** 475–492 (2017).
683. Minutti, C. M. *et al.* Local amplifiers of IL-4Rα–mediated macrophage activation promote repair in lung and liver. *Science* **356,** 1076–1080 (2017).
684. Goplen, N. P. *et al.* Tissue-resident CD8+ T cells drive age-associated chronic lung sequelae after viral pneumonia. *Science immunology* **5,** eabc4557 (2020).

685. Galkina, E. *et al.* Preferential migration of effector CD8+ T cells into the interstitium of the normal lung. *The Journal of clinical investigation* **115,** 3473–3483 (2005).
686. Takamura, S. *et al.* Interstitial-resident memory CD8+ T cells sustain frontline epithelial memory in the lung. *Journal of Experimental Medicine* **216,** 2736–2747 (2019).
687. Wein, A. N. *et al.* CXCR6 regulates localization of tissue-resident memory CD8 T cells to the airways. *Journal of Experimental Medicine* **216,** 2748–2762 (2019).
688. Day, C., Patel, R., Guillen, C. & Wardlaw, A. J. The chemokine CXCL16 is highly and constitutively expressed by human bronchial epithelial cells. *Experimental lung research* **35,** 272–283 (2009).
689. Kotanides, H. & Reich, N. C. Interleukin-4-induced STAT6 recognizes and activates a target site in the promoter of the interleukin-4 receptor gene. *Journal of Biological Chemistry* **271,** 25555–25561 (1996).
690. Daniel, C., Salvekar, A. & Schindler, U. A gain-of-function mutation in STAT6. *Journal of Biological Chemistry* **275,** 14255–14259 (2000).
691. Idzerda, R. L. *et al.* Human interleukin 4 receptor confers biological responsiveness and defines a novel receptor superfamily. *The Journal of experimental medicine* **171,** 861–873 (1990).
692. Kondo, M. *et al.* Sharing of the interleukin-2 (IL-2) receptor γ chain between receptors for IL-2 and IL-4. *Science* **262,** 1874–1877 (1993).
693. Obiri, N. I., Debinski, W., Leonard, W. J. & Puri, R. K. Receptor for interleukin 13: interaction with interleukin 4 by a mechanism that does not involve the common γ chain shared by receptors for interleukins 2, 4, 7, 9, and 15. *Journal of Biological Chemistry* **270,** 8797–8804 (1995).
694. Murata, T., Taguchi, J., Puri, R. & Mohri, H. Sharing of receptor subunits and signal transduction pathway between the IL-4 and IL-13 receptor system. *International journal of hematology* **69,** 13–20 (1999).
695. Chang, Y.-J. *et al.* Innate lymphoid cells mediate influenza-induced airway hyper-reactivity independently of adaptive immunity. *Nature immunology* **12,** 631–638 (2011).
696. Li, B. W. *et al.* T cells and ILC2s are major effector cells in influenza-induced exacerbation of allergic airway inflammation in mice. *European Journal of Immunology* **49,** 144–156 (2019).
697. Bao, K. & Reinhardt, R. L. The differential expression of IL-4 and IL-13 and its impact on type-2 immunity. *Cytokine* **75,** 25–37 (2015).
698. Voehringer, D., Shinkai, K. & Locksley, R. M. Type 2 immunity reflects orchestrated recruitment of cells committed to IL-4 production. *Immunity* **20,** 267–277 (2004).
699. Oliphant, C. J. *et al.* MHCII-mediated dialog between group 2 innate lymphoid cells and CD4+ T cells potentiates type 2 immunity and promotes parasitic helminth expulsion. *Immunity* **41,** 283–295 (2014).
700. Wang, Z. *et al.* PD-1hi CD8+ resident memory T cells balance immunity and fibrotic sequelae. *Science immunology* **4,** eaaw1217 (2019).